MULTIFUNCTIONAL HYBRID NETWORKS BASED ON SELF ASSEMBLING PEPTIDE SEQUENCES

by

Sameer Sathaye

A dissertation submitted to the Faculty of the University of Delaware in partial fulfillment of the requirements for the Doctor of Philosophy in Materials Science and Engineering

Spring 2014

ProQuest LLC.
789 East Eisenhower Parkway
P.O. Box 1346
Ann Arbor, MI 48106 - 1346

MULTIFUNCTIONAL HYBRID NETWORKS BASED ON SELF ASSEMBLING PEPTIDE SEQUENCES

by

Sameer Sathaye

Approved: _____
David C.Martin, Ph.D.
Chair of the Department of Materials Science and Engineering

Approved: _____
Babatunde A. Ogunnaike, Ph.D.
Dean of the College of Engineering

Approved: _____
James G. Richards, Ph.D.
Vice Provost for Graduate and Professional Education

I certify that I have read this dissertation and that in my opinion it meets the academic and professional standard required by the University as a dissertation for the degree of Doctor of Philosophy.

Signed: _____

Darrin J.Pochan, Ph.D.
Professor in Charge of Dissertation

I certify that I have read this dissertation and that in my opinion it meets the academic and professional standard required by the University as a dissertation for the degree of Doctor of Philosophy.

Signed: _____

Kristi L.Kiick, Ph.D.
Member of Dissertation Committee

I certify that I have read this dissertation and that in my opinion it meets the academic and professional standard required by the University as a dissertation for the degree of Doctor of Philosophy.

Signed: _____

Michael E.Mackay, Ph.D.
Member of Dissertation Committee

I certify that I have read this dissertation and that in my opinion it meets the academic and professional standard required by the University as a dissertation for the degree of Doctor of Philosophy.

Signed: _____

Millicent O.Sullivan, Ph.D.
Member of Dissertation Committee

ACKNOWLEDGEMENTS

It was a great pleasure to conduct my PhD research under the supervision of my advisor Professor Darrin J. Pochan. I am grateful for his guidance, encouragement and support throughout the course of this work.

I would like to thank the members of my thesis committee, Prof. Kristi Kiick, Prof. Michael Mackay and Prof. Millicent O.Sullivan for their guidance and time. I would like to thank Dr. Chaoying Ni and Frank Kriss for their expertise and help in electron microscopy and sample preparation.

I would like to thank Dr.Joel Schneider and Cem Sonmez at the National Institutes of Health National Cancer Institute, Frederick, MD for help with peptide synthesis and purification.

I also express my thanks to all past and present Pochan group members. In particular, I am thankful to Dr. Nikhil Sharma, Dr. Aysegul Altunbas and Jiahua Zhu for their friendship and expertise in self-assembly of peptides and polymers.

Finally, I thank my family – my mother, Prof.Sadhana Sathaye, my late grandparents and Priyanka for all their support and love.

TABLE OF CONTENTS

LIST OF FIGURES

LIST OF TABLES

LIST OF SCHEMES

ABSTRACT

The overall aim of this dissertation is to achieve a comprehensive correlation between the molecular level changes in primary amino acid sequences of amphiphilic β-hairpin peptides and their consequent solution-assembly properties and bulk network hydrogel behavior. This has been accomplished using two broad approaches.

In the first approach, amino acid substitutions were made to peptide sequence MAX1 such that the hydrophobic surfaces of the folded β-hairpins from the peptides demonstrate shape specificity in hydrophobic interactions with other β-hairpins during the assembly process, thereby causing changes to the peptide nanostructure and bulk rheological properties of hydrogels formed from the peptides. Steric lock and key complementary hydrophobic interactions were designed to occur between two β-hairpin molecules of a single molecule, LNK1 during β–sheet fibrillar assembly of LNK1. Experimental results from circular dichroism, transmission electron microscopy and oscillatory rheology collectively indicate that the molecular design of the LNK1 peptide can be assigned the cause of the drastically different behavior of the networks relative to MAX1. The results indicate elimination or significant reduction of fibrillar branching due to steric complementarity in LNK1 that does not exist in MAX1, thus supporting the original hypothesis. As an extension of the designed steric lock and key complementarity between two β-hairpin molecules of the same peptide molecule

LNK1, three new pairs of peptide molecules LP1-KP1, LP2-KP2 and LP3-KP3 that resemble complementary 'wedge' and 'trough' shapes when folded into β-hairpins were designed and studied. All six peptides individually and when blended with their corresponding shape complement formed fibrillar nanostructures with non-uniform thickness values. Loose packing in the assembled structures was observed in all the new peptides as compared to the uniform tight packing in MAX1 by SANS analysis. This loose packing can be attributed to the designed wedge and trough shapes of the peptides disturbing formation of a uniform bilayer type structure proposed in the case of MAX1 with each hairpin having a flat hydrophobic surface. Although designed changes in hydrophobic shape of the peptide nanofibril core in the new peptides were found to significantly influence the self-assembled nanostructure and network rheological behavior, a lack of direct morphological and rheological evidence to prove shape specific hydrophobic interactions between wedge and trough shaped β-hairpins was encountered.

In the second approach, peptides with established differences in assembly kinetics and bulk mechanical properties of assembled peptide hydrogels were used to develop composite materials with diverse morphological and mechanical properties by blending with the biopolymer hyaluronic acid. The diverse properties of the composites have been correlated to the specific peptide hydrogels used to develop the composite and the different stages of peptide assembly at which blending with hyaluronic acid was carried out.

Finally along with overall conclusions, the new area of co-assembly of peptides in solution has been explored and discussed as potential future work following the research discussed in this dissertation. Strategies such as construction of composite hydrogels from blends of MAX1/MAX8 peptide hydrogels and biologically important anionic species such as heparin biopolymer and DNA have been discussed. Another area of future work discussed is the design and study of peptides that can incorporate chemically crosslinkable functional groups in their hydrophobic amino acid side chains that can be covalently crosslinked after peptide assembly into fibrils. Such covalent crosslinking can potentially lead to stiffer individual peptide fibrils due to additional bond formation at the fibrillar core and therefore much stiffer hydrogels due to a synergistic effect. These enhanced stiffness values can render these new hydrogels excellent candidates for applications like development of extracellular mimetic materials and substrates with easily tunable stiffness values for stem cell differentiation studies.

Chapter 1

INTRODUCTION

"Hydrogel" is a general term used for water swollen, porous materials of polymeric, protein, peptidic, colloidal, surfactant or lipid origin. Hydrogels are a mainstay in the food and pharmaceutical industries and are also increasingly finding applications in areas such as biosensing[1,2], microfluidics[3-6], drug delivery[7-10] and tissue engineering[7,9,11,12]. A broad classification of hydrogels based on the type of crosslinking is commonly made, e.g. chemically (covalently) crosslinked or physically crosslinked (based on secondary interactions such as hydrogen bonding, hydrophobic and electrostatic interactions). The highly hydrated and porous nature of hydrogels in general can be leveraged for their utility as encapsulating agents and delivery devices for therapeutic agents such as cells[13-18], growth factors[19-21], DNA[22-25], peptides and proteins [26-29] and drugs[30,31].

Physically crosslinked hydrogels are networks held together by topological interactions that include entanglement, branching and/or secondary interactions. Secondary interactions consist of, but are not limited to, hydrogen bonding, hydrophobic interactions, electrostatic interactions and π-π interactions. These interactions can be finely controlled by changes in solution environment, such as temperature, pH, ionic strength, presence of specific solutes; consequently, the formation of physical hydrogels may be reversible. Traditional synthetic methods, such as crosslinking copolymerization, crosslinking of

polymeric precursors and polymer–polymer crosslinking, have afforded numerous hydrogel materials with excellent properties[32,33]. However, crosslinking via traditional synthetic approaches can seldom afford precise control over the nanoscale and microscale morphology of the crosslinked network. In contrast, self- assembly of macromolecules into physical hydrogels has the potential to produce precisely defined, hierarchical, 3D structures[34-37]. In nature, or with proper synthetic design, molecules such as peptides, polypeptides, proteins and DNA readily undergo self-assembly. Self-assembly of peptides and proteins is encountered in most structural and functional biological systems, such as actin filaments in the cytoskeleton or microtubules and the fibrous protein components of the extracellular matrix. The distinctive features of peptide/protein self-assembly are: (a) high specificity, mediated by molecular recognition and binding among polypeptide building blocks; (b) self assembly cues needed for the folding and function of a polypeptide that are usually pre-determined by the primary structure; and (c) precise dynamic control of the material's structure and properties due to the reversibility of the assembly and disassembly processes. The simplicity, specificity and controllability of the self-assembly processes observed in nature and synthetic peptide/protein systems has inspired the work discussed in this dissertation. Amphiphilic β-hairpin peptides based on the parent sequence MAX1 [VKVKVKVK-(V^{D}PPT)-KVKVKVKV-NH_2], undergo hierarchical self-assembly into β-sheet nanofibrils upon being subject to appropriate aqueous solution conditions[38,39]. The nanofibrils undergo physical crosslinking via defect

induced branching[40] and entanglement to yield solid hydrogels with unique shear-thinning and rehealing properties[41]. This work involves the design of amphiphilic peptide sequences based on an established platform of self-assembling β-hairpin peptides for constructing hydrogel materials with diverse functionalities.

1.1. Motivation

The central motivation of this dissertation is to explore structure-property relationships between newly designed β-hairpin peptide primary structure, the corresponding solution assembly pathways of the new peptides, and bulk network behavior of hydrogels formed from the peptides. This work has been broadly classified into two parts. In the first part, effects of shape complementary interactions designed into the self-assembling β-hairpins on the peptide assembly and the resulting hydrogel properties are studied. The second approach discussed in this dissertation is that of constructing multicomponent hybrid hydrogel materials by blending the structurally and biologically important biopolymer hyaluronic acid and the hydrogels from the β-hairpin peptide MAX8 [VKVKVKVK-(V^{D}PPT)-KVEVKVKV-NH_2].

Specific molecular recognition interactions between complimentary peptide and protein molecules have been used for designing smart responsive hydrogel materials. Examples of such efforts include materials based on specific interactions between coiled coil polypeptide domains such as leucine zipper domains[42-45], interactions between di-tryptophan (WW) and proline rich

domains[46] and tetratricopeptide repeat (TPR)-peptide interaction[47]. A specific type of protein-protein interaction, named the 'Lock and Key' mechanism, involves recognition between molecules with complementary steric binding domains. Specific steric packing in ligand-receptor interactions[48,49], protein-DNA binding[50] and designed colloidal particles[51] has been studied but not toward designed materials development. The lock and key analogy was first put forward by Emil Fischer more than 100 years ago to describe specificity in enzyme-substrate interactions. One of the most widely studied shape dependent lock and key type interactions is the ligand protein interaction between the vitamin biotin and the egg white glycoprotein avidin, which is of tremendous interest in biotechnological applications[52]. Similarly, Holzinger et al. have reported complexation between biotin and β-cyclodextrin as a representation of a new bioreceptor immobilization affinity system[53]. Also widely reported shape-dependent recognition patterns involving proteins are interactions between proteins and DNA based on DNA local shape variations (individual base pair & minor double helix region) and DNA global shape variations (various helical topologies and deformations)[54]. The motivation towards introducing steric specificity to hydrophobic interactions in β-hairpin peptides is to explore whether designed changes to the shape of each β-hairpin molecule have a large effect on the overall self assembly properties and resulting hydrogel mechanical properties formed from the hairpins.

The biopolymer, hyaluronic acid, or hyaluronan (HA) (a term used to

describe both the acidic form of the polymer and the salt of hyaluronic acid) is a promising material for biomaterial applications[55]. HA is a non-sulfated glycosaminoglycan (GAG) in the extracellular matrix (ECM) of many soft connective tissues, composed of alternating units of D-glucuronic acid and N-acetyl-D-glucosamine, linked together via alternating β-1,4 and β-1,3 glycosidic bonds[56]. β-hairpin peptide hydrogels from the MAX8 peptide function as injectable solids that can be delivered using a common device such as a syringe[57]. They have also been shown to be biocompatible matrices for 3D encapsulation of cells such as mesenchymal stem cells[58] and MG63 progenitor osteoblasts[57]. Synthesized in the cell membrane[59] HA is extruded out of the cell into the native ECM, where it provides mechanical support[60]. Owing to its copious negative charges, HA has a high (1000 X) water absorbent capacity and thus acts as a space filler, lubricant and osmotic buffer in the native ECM[61]. The high water absorptive capacity of HA renders it an ideal matrix for solute and nutrient delivery to wounded tissue. In addition to these prominent structural attributes, HA interacts with its cell surface receptors (CD44 or RHAMM) and activates various cell signaling pathways[62,63]. These signaling pathways direct various cell functions, including cell adhesion, cytoskeletal rearrangement, cell migration, cell proliferation and differentiation[62-64]. Given the potential biomedical applications of the MAX8 β-hairpin-based hydrogels and HA individually, construction of multicomponent, hybrid hydrogels based upon these two types of materials is a step toward developing smarter biomaterials with designed material and

biological properties.

1.2. Objectives and Organization of Thesis

One of the two main objectives of this dissertation is to achieve a comprehensive correlation between the changes in peptide β-hairpin shapes brought about by molecular level changes in primary amino acid sequences of amphiphilic β-hairpin peptides and potential changes in rheological behavior of the networks formed from the new peptides. The other objective is the construction of hybrid, multicomponent hydrogel materials by making simple blends of β-hairpin peptide hydrogels with established mechanical properties with the structurally and biologically important biopolmer, hyaluronic acid.

The organization of the thesis and topics covered are as follows. Chapter 1 discusses the motivation, objective and organization of the thesis. The studied hydrogel networks are based purely on physical crosslinking and demonstrate application potential in areas such as drug delivery and tissue engineering. Thus, Chapter 1 provides a review of literature focusing on rheological characterization of hydrogels formed from solution assembly of peptide, polypeptide and protein systems. The hydrogels formed from molecules reviewed in Chapter 1 are purely physically crosslinked networks, similar to the networks being discussed in the rest of the dissertation. Some of the networks also demonstrate unique shear-thinning and rehealing abilities as exhibited by some peptides discussed herein. The experimental methods used throughout the thesis will be discussed in Chapter 2. Hydrogels based on β-hairpin peptide MAX1 [VKVKVKVK-(V^{D}PPT)-

KVKVKVKV-NH_2] and its derivatives demonstrate yield-stress material properties. A brief introduction to the self-assembly and hydrogel properties of MAX1 and its derivatives is provided in Chapter 3. A unique property exhibited by these yield-stress hydrogels is that of shear-thinning and rehealing. When a MAX1 (or MAX8) network hydrogel is subject to shear using a rheometer or syringe injection, the network yields and flows under the shear but immediately reheals into a solid network upon removal of shear. Such shear-thinning and rehealing properties have been reported for many other solution assembled peptide hydrogels as discussed in Chapter 1. Thus, fundamental exploration of the shear-thinning and rehealing behavior of a MAX8 hydrogel by simultaneous visual observation using confocal microscopy and in-situ under-shear behavior of the hydrogel using a rheometer has been discussed in Chapter 3. This work using a compound rheometer-confocal microscope assembly was carried out in collaboration with the laboratory of Prof. Daniel Blair at Georgetown University, Washington D.C. Chapter 3 provides experimental evidence of bulk fracture demonstrated by MAX8 hydrogels that is a manifestation of their yield-stress material properties. Chapter 4 investigates the introduction of significant changes in the hydrogel network behavior of β-hairpin peptide-based hydrogels by introduction of steric lock and key specificity to critical hydrophobic interactions at the core of the fibrils formed by a single peptide, LNK1. In Chapter 5, shape complementary hydrophobic interactions between other designs of steric pairs of peptides and the resultant nanostructures and hydrogel properties are

discussed. Three pairs of peptides with increasing gradient of a 'wedge' and a 'trough' shape respectively are designed and assembly behavior of the individual peptides and their 1:1 (w/w) blends were studied. Chapter 6 focuses on discussion of development and characterization of morphologically and rheologically diverse hybrid networks based on hydrogel blends of β-hairpin peptide MAX8 and the biopolymer hyaluronic acid. Overall conclusions will be made in the last chapter.

1.3. Rheological Characterization of Physically crosslinked Peptide and Protein Hydrogels

Study of self-assembly pathways of peptides/proteins and morphological characteristics of the assembled nanostructure is essential for comprehensively understanding self-assembled peptide/protein based materials. Applications of these systems as functional materials like drug delivery systems, cell culture substrates and 3D scaffolds for tissue engineering compels thorough characterization and fine control of mechanical properties and morphologies of hydrogels. Thus, rheological characterization has become an increasingly important tool to obtain more information about the viscoelastic and flow properties of *de-novo* hydrogels based on proteins and peptides. Common rheological studies conducted on hydrogel materials include measurement of shear storage modulus (G'), loss modulus (G") and loss factor (tan (δ)) measured as functions of time, oscillatory frequency and oscillatory strain. Such studies can

provide an insight about gelation kinetics, linear viscoelastic regions and relaxation time scales relevant to the studied hydrogels. Mechanical properties of solid hydrogels are most commonly measured using rheometric measurements. Anseth[65] and Yan[41] have presented comprehensive reviews pertaining to measurement of mechanical and viscoelastic properties of hydrogels. Fundamental principles of rheological measurements have been provided in texts such as those by Macosko[66] and Mezger[67]. In the next section, recent rheological characterization on physically crosslinked hydrogels reported in the literature discussing applications of self-assembled hydrogels from peptides and proteins as functional materials is discussed.

1.3.1. Hydrogels based on β-sheet structures

Hydrogels constructed using the β-hairpin peptides are networks of entangled and branched β-sheet structures. Hydrogels based on β-sheet secondary structures formed by peptide, polypeptide and protein molecules of different architectures have been investigated extensively. A majority of these hydrogels are obtained from solution-assembled peptides and proteins, and some can exhibit shear-thinning and rehealing abilities as shown by the β-hairpin hydrogels studied in the Pochan laboratory. For example, Aulisia et al.[68] have reported on shear-thinning and rehealing hydrogels based on multidomain peptides; a) $K_2(QL)_6K_2$ b) $E(QL)_6E$ c) $K_2(SL)_6K_2$ d) $E(SL)_6E$ e) $E(CLSL)_3E$. These multi-domain peptides have an ABA structure with the middle B domain

containing alternating hydrophilic and hydrophobic amino acids. The A block at the end contains charged amino acids that at neutral pH counter the tendency of the central block to associate. These peptides are shown to form nanofibers that form viscoelastic hydrogels. These gels display varying abilities of rehealing on removal of shear treatment. Upon formation, the charged nanofibers are cross-linked ionically with either phosphate or magnesium ions, similar to some of the modified β-hairpin sequences based on MAX1 that can be solution assembled in the presence of zinc and other heavy metal ions [69,70]. Fibers formed by peptides containing serine as compared to glutamine in their central blocks were reported to form much longer and more entangled fibers leading to stiffer hydrogels. The nanofibers from peptides containing the negatively charged serines were reported to show a much larger rise in storage modulus when crosslinked with an oppositely charged cross linker ($Mg+^{2}$ ions) as compared to those containing positively charged glutamines crosslinked with phosphate ions. The hydrogels from serine containing peptides were shown to demonstrate an increased propensity to reheal after being subjected to shear treatment by flowing through a narrow bore syringe. When the nanofibers containing cystine residues were oxidized using hydrogen peroxide forming covalent disulphide bonds along or normal to the fiber axis, the stiffness of the hydrogels formed thereupon was dramatically increased (~60X). This increase was reported to be larger than that obtained when the nanofibers were crosslinked with Mg^{+2} ions. As suggested by the authors, this approach shows the versatility of the multi-domain peptide

hydrogel mechanical properties as a function of the peptide sequence.

Further work by Bakota et al.[26] employed extensive rheological strain sweep and time sweep measurements to demonstrate the enzymatic crosslinking of nanofibers from multi domain peptides. The results reported in this study suggest that nanofibers formed from lysine-containing multidomain peptides will undergo oxidative crosslinking in standard mammalian cell culture conditions in presence of fetal bovine serum. This phenomenon of exogenous, enzymatic oxidative crosslinking has been suggested as a facile strategy for tuning nanofibrillar hydrogel stiffness from multidomain peptides. Multidomain peptides containing the cell attaching peptide sequence RGD have also been reported by the same group to form mechanically stable nanofibrous shear-thinning and rehealing hydrogels, which makes their syringe delivery possible.

Bowerman et al.[71] have studied the relative importance of hydrophobicity of the non-aromatic versus aromatic amino acids in the $(XEXE)_2$ peptides during their amyloid like self assembly into fibrils. The authors have correlated the hydrogelation properties through rheological behavior of a set of peptides relative to the hydrophobic character of the individual amino acids (Alanine, Valine, Leucine, Phenylalanine and Cyclohexylalanine) in the 'X' position of $(XEXE)_2$. Results from the rheological characterization of the hydrogels constructed using these peptides indicate that increasing the generic hydrophobicity, and not aromaticity, contributes to the non-covalent supramolecular cross linking of the fibrils. The introduction of aromatic as well as non-aromatic hydrophobic side

chain amino acid residues in newly designed β-hairpin peptide molecules in order to confer specific lock and key, wedge or trough shapes to them has been an important design strategy discussed later in this thesis. The Nilsson group also reports on the construction of β-sheet peptide hydrogels based on a reductive trigger that induces a conformational change from a peptide macrocycle to a β-sheet[72].

An example of investigation of self-assembly and hydrogelation behavior of blends of synthetic peptides, which is one the main objectives of this thesis, to obtain smarter and more tunable materials has been provided by Ramchandran et al. Ramachandran et al.[73,74] report on co-assembly of amphiphilic peptides into hydrogels with potential biomedical applications. The authors discuss peptides KAW10, KAW15, EAW10 and EAW15. Peptide molecules having the same charged residue (lysine or glutamic acid) do not undergo self-assembly with each other but do so when blended with molecules containing an opposite charge (glutamic acid or lysine, correspondingly). The assembly strategy discussed by the authors involved making hydrogels by blending pairs of peptides from the four peptides generating four pairs, two with sticky ends (with unmatched lengths of amino acids in peptide pair) and two with blunt (with exactly matched lengths of amino acids in peptide pair) ends. All four pairs were reported to undergo co-assembly with very different kinetics but form shear-thinning and rehealing hydrogels. The KAW:EAW blunt end pair was found to form the most stable hydrogels post cessation of shear, negating the importance of the sticky ends for

stiffer network formation. Such examples of hydrogels based on specific peptide designs (blunt ended versus sticky ended peptides) serve as an inspiration to explore new design strategies such as peptide-peptide shape specific interactions that are described in this dissertation.

Guilbaud et al.[75] have reported on the correlation between enzyme concentration, hydrogel morphology and properties of enzymatically triggered β-sheet forming tetrapeptide hydrogels. They have shown formation of heterogeneous hydrogel morphology due to denser hydrogel domains in the vicinity of the enzyme, which act as a reinforcement phase for the hydrogels as determined by rheometeric experiments. Peptide hydrogels based on mussel inspired iron crosslinking and formation of shear-thinning and rehealing hydrogels has been reported by Ceylan et al.[76]

1.3.2. Hydrogel Materials based on specific molecular recognition

Specific interactions between peptide, protein and polymer molecules have been used widely for designing smart responsive materials. A special type of specific molecular recognition interaction, the 'lock and key' interaction, has been a frequently used design motif employed in the work addressing the first main objective of this dissertations. Apart from the β-sheet secondary structure, α-helix is the second main type of secondary structure adopted by peptides and proteins and as such is a widely used tool in design of self-assembling peptide, and protein based materials.

Coiled coils are formed from peptide and protein domains in an α-helical secondary structure. The Tirrell group put forward one of the first accounts of hydrogel materials based on coiled coil formation. These materials are multi domain proteins with a water-soluble polyelectrolyte block flanked on both ends by leucine zipper domains, which formed coiled coil dimers due to interhelical hydrophobic intreractions. These dimers act as cross-link junctions, which are shown to help in formation of transient hydrogels[42]. The Kopecek group and other groups have used the strategy of incorporating leucine zipper domains[77-81]. Susceptibility of these leucine zipper domains to denaturation at high pH or high temperature leads to reversal of these gels into solutions. A similar reversibility of hydrogel network properties is exhibited by MAX1 and other β-hairpin peptide hydrogels upon reversal of solution conditions necessary for self-assembly. The stiffness of hydrogels formed as a function of concentration, pH and ionic strength were studied using rheological measurements and was attributed to network topology[82]. Another study from the same group shows that the pH dependent viscosity transition of such networks can be attributed to the dynamic properties of the networks[83]. Further, disulfide covalent bonding due to cysteine incorporation in the leucine zipper domain has been reported to show enhancement of rheological properties from the hydrogels formed from the cysteine containing peptides[43,84]. Xu and Kopecek have presented coiled-coil-containing block copolypeptides, in which the gelation process was monitored by microrheology[79]. The authors report a reversible sol–gel transition observed on

addition or removal of guanidine hydrochloride that denatures the coiled-coil domains. Hybrid hydrogels based on β-sheet peptides grafted onto HPMA copolymers specifically for the purpose of nucleation of hydroxyapetite, ultimately intended for bone regeneration, have been reported by Wu et al.[80] The bulk mechanical properties of the hybrid gels were shown to be dependent on the peptide concentration and incubation time. Woolfson and colleagues discuss development of hybrid peptides by incorporating characteristics of α-helix and β-hairpin into one peptide sequence that could transform from an α-helix into a β-hairpin upon heating. Such a fibrous gel could be reversed into a solution at lower pH values, indicating behavior similar to β-hairpin hydrogels discussed in this work[85]. The same group has reported on an α-helical peptide-based fibrillar hydrogel based on the fundamental coiled-coil interactions, with the exception of the amino acids at certain positions on coiled-coil surfaces replaced with three alanine residues for enhanced intermolecular interaction. Mixing of complementary peptides under chilled conditions or room temperature was reported to form self-supporting thermally stable physical gels[86,87]. Deming et al.[88-90] have reported the study of hydrogel formation from polypeptide diblock copolymers comprised of a hydrophilic polyelectrolyte charged segment and a hydrophobic segment. The charged polyelectrolyte block was shown to determine the sol–gel transition. The equilibrium storage modulus of the hydrogel was dependent on hydrophilic to hydrophobic ratio and block length. Two factors, the conformational differences in the hydrophobic segment in the diblock and

solution ionic strength were shown to affect the critical gelling concentration. These hydrogels demonstrated shear-thinning and rehealing properties (~80-90% of their pre shear rigidity value). Grove at al.[47,91] have described the fabrication of ionic-strength-responsive hydrogels by using modular bottom-up protein design based on the 34 amino acid tetratricopeptide (TPR) repeat. Specific, noncovalent interactions between repeat protein modules and their partner peptide PEG ligands act as cross-link junctions for these hydrogels. The authors discuss the potential of hydrogels based on these modular protein designs for tissue engineering applications. Foo et al.[46] have reported a similar simple mixing strategy to induce sol-gel phase transition without any extensive changes in environmental conditions by using molecular recognition interactions between proline rich and di-tryptophan (WW) rich domains in engineered protein materials. The transient physical cross link junctions in such gels yield relatively weak (~50 Pa) gels (as studied by microrheology), but provide them a shear - thinning and rehealing nature, which makes them appropriate for injectable therapeutic applications. Lu et al.[18] report on a 'Dock and Lock' physically crosslinked hydrogel, in which the crosslink junctions are the interactions between the Docking and Dimerization Domain (DDD) of cAMP dependent protein kinase A (PKA) and the anchoring domain (AD) of A-kinase anchoring proteins (AKAP). These hydrogels were found to be relatively stiff (G' ~1000 Pa) as compared to similar protein based molecular recognition gels and demonstrated shear-thinning and immediate rehealing properties due to inherently

expedited kinetics of the DDD and AD binding. Extensive oscillatory time, frequency and strain sweep measurements were carried out to characterize these gels rheologically. The experimental reports by Foo and Lu as described above also serve as an inspiration for the work discussed in this dissertation involving peptide-peptide and peptide-polymer blends. The blends of the negatively charged hyaluronic acid biopolymer and positively charged β-hairpin peptide fibrils are hypothesized to yield electrostatically complexed, hybrid materials with enhanced mechanical and biological functionalities. Liu et al.[92] report on a physically crosslinked hydrogel based on thiol containing polypeptide macromer assembled via coiled coil interactions. These coiled coil interactions act as points of physical crosslinking, imparting a physically crosslinked nature to the hydrogel network formed from these macromers. These polypeptide macromers are covalently bound to vinyl sulfone containing PEG molecules through a biologically benign Michael type addition reaction. These unique gels were also shown to be benign towards epithelial cells encapsulated within them.

1.3.3. Elastin and related hydrogels

Elastin, the natural protein is found abundantly in elastic tissues in the human body. Elasticity and the mechanical reversible character of elastin allow tissues such as arteries, skin and vocal folds to extend upon stress addition and recover upon stress removal. The elastomeric properties of this protein provide major motivation for mimetic molecules (elastin like polypeptides (ELP)) to be

based of this protein[93]. The pentapeptide repeat unit valine-proline-glycine-X-glycine (where X is any residue but proline) is the signature sequence of elastin. The critical temperature of inverse phase transition, above which ELP solubility decreases and ELP hydrogelation occurs, can be varied by changing the 'X' amino acid[94,95]. Thermal reversible gelling hydrogels for cartilage repair were developed using the thermal reversibility of the elastin molecule[96,97]. Cytocompatible ELP coacervates, which have hydrogel-like properties but mechanically do not measure up to natural connective tissue, have been reported[96-99]. A step up from these coacervates, crosslinked ELP hydrogels that displayed enhanced mechanical properties over ELP coacervates have been reported[99-103]. ELP hydrogels with improved mechanical properties developed by controlling the phase separation characteristics in ELP solutions have also been reported[101,102,104-106]. These efforts demonstrate control of hydrogel mechanical properties by variation in polypeptide sequence and ionic strength. Hybrid ELPs obtained by incorporation of silk residue repeat sequences into ELP sequences for drug and DNA delivery have also been reported[107,108]. These proteins, with temperature-controlled kinetics of gelation have been be used for in-situ gelation application after syringe injection. Cysteine-containing elastin like proteins, which undergo thermal as well as oxidative gelation and their rheological characterization has been reported by the Chilkoti group[109,110].

1.3.4. Gelatin Gels

Gelatin gels find applications in biomedical applications such as protein delivery due to their biocompatibility and temperature sensitive gelation[111,112]. Gelatin is produced by denaturation of naturally derived collagen in solution through an acidic or alkaline process, which leads to separation of the triple-helical tropocollagen into three single-strand gelatin molecules. These single stranded molecules undergo a coil–helix transformation when cooled in aqueous solutions[113,114]. Above a critical protein concentration thermoreversible gelation takes place from the helices[113-115]. Dependence of gel equilibrium modulus and gel melting temperature on gelatin concentration and molecular weight experimentally and theoretically has been reported by Gilsenan at al[116,117]. Creep and creep recovery measurements used to observe long-term viscoelastic behavior of gelatin gels was also reported by the same authors[118]. Comparison of creep compliance with the inverse of the equilibrium gel modulus, which provided potential proof of elastic solid like behavior of gelatin gels, has also been reported. According to the authors, an observed non-recovery of the deformation at the end of the recovery phase provides an indication of viscoelastic behavior of gelatin gels.

1.3.5. Globular protein hydrogels

'Globular proteins' constitute another class of proteins that demonstrate gel-forming capabilities. Gels from globular proteins are not only relevant

industrially for commercial applications in foods, but have also shown great promise in emerging areas such as tissue engineering e.g. Lysozome based gels[119-121]. Unfolding of globular proteins at higher temperatures allows aggregation of individual protein molecules above a certain critical gelation concentration. This aggregation has been attributed to secondary interactions such as hydrogen bonding and hydrophobic effects. Depending upon whether solution pH of the proteins is closer or further from the pI, globular proteins can undergo aggregation to form particulate or fine stranded hydrogels. Extensive rheological studies focused on gels from globular proteins such as bovine serum albumin, β-lactoglobulin and ovalbumin and the correlation of their mechanical properties with their structural and molecular characteristics have been reported in the literature[122-126]. Theoretical modeling has also been reported for better understanding of the gelation mechanisms. These models attempt to explain the dependence of gelation time, critical gelation concentration and equilibrium gel modulus on variables such as protein concentration, pH, temperature and ionic strength. In a series of publications, Ross-Murphy et al.[107,122-124,127] have reported on several models to describe the gelation behavior of fibrillar β-lactoglobulin gels formed at both acidic and basic pH. Van der Linden et al.[128-131] have described an adjusted random contact model that correlates the critical percolation concentration and ionic strength for fine-stranded gels. Studies focused on developments of theoretical models that use parameters obtained from data on the aggregation process, hydrogel rheology and complementary

techniques such as light scattering have also been reported[132-137]. Miller et al[97]. have reported on thermoreversible lysozyme gels formed in mixtures of water and dithiothreitol as solvents. The lysozyme gelation was reported to be achieved by heating the protein solution up to 85° C and then slowly cooling back to room temperature, resulting into denaturation of the lysozyme proteins and formation of entangled β-sheet-rich fibrils forming a gel network. Dynamic oscillatory measurements were reported to probe the gelation behavior and mechanical properties[120]. The plateau elastic modulus of the gels was reported to be dependent on lysozyme concentration in a power law relation.

1.3.6. Fibrous protein hydrogels

Silks form a class of highly studied fibrous proteins whose fibers have mechanical properties (Young's modulus and tensile strength[138,139]) unsurpassed by almost any other polymer of biological or synthetic origin. The biocompatible and degradable silk proteins[140-142] serve as motivation for various studies to explore silk gels as tissue engineering scaffolds[143-145] and drug delivery agents when blended with gelatin. Silk fibroin is mainly found in protein from natural silkworm fibers[146]. Above a critical concentration silk fibroin assembles in solution leading to a physical hydrogel of β-sheet-rich fibrils. Cytocompatibility and biodegradability of silk fibroin has been established by various accounts in the literature[144,145,147-151]. These fibers are distinct from self-assembled fibrillar nanostructures from β-sheet peptides in terms of dimensions of fibrillar structures

formed. The hydrogels formed from silk proteins are composed of micron-scale macromolecular clusters of β-sheets[152] as compared to the well-defined nanosized β-sheets fibrillar structures from the β-hairpin peptides investigated in this dissertation.

Kang et al[153]. and Yoo et al[154]. report that the stability and rigidity of silk fibroin hydrogel were affected by the amount of the polymer, poloxamer 407. Wang et al[155,156]. have reported on expediting gelation kinetics of silk fibroin under physiological conditions facilitating homogeneous 3D encapsulation of living mesenchymal stem cells . Yucel et al[152]. report mechanical stimuli provided by vortexing as a means of expediting gelation kinetics of fibroin protein solution. Moreover, these mechanically stimulated silk hydrogels were also shown to be capable of shear-thinning by injection and rehealing to pre-shear rigidity immediately after shear cessation. Vollrath et al[157]. discuss pH dependent gelation of spidroin proteins at lower pH (~ 5.5) and reversal to solution at pH 7. Fibrillar networks from synthetic spidroins stabilized by chemical or physical crosslinks have also been reported. The physical spidroin hydrogels were reported to be easily disrupted due to the purely topological fibrillar entanglement acting as crosslinks, in contrast to much stiffer chemically crosslinked gels with elastic moduli up to around 1000 Pa[158-160].

Fibrin is another natural, fibrous protein with potential biomaterial applications for wound healing and growth factor delivery[161]. Fibrinogen is covalently crosslinked by thrombin, in the event of an injury forms fibrin. When

further crosslinked by factor XIII, fibrin forms a clot that is a blood-coagulating network[154]. Fukada[162] and Kaibara[163-165] provide early reports on various techniques to study dynamic rheological properties of fibrin clots along with mechanism of blood coagulation. Ryan et al[166,167] have reported a structure property relationship study relating rheological behavior of fibrin clots to their structural characteristics. They suggest a direct dependence of mechanical rigidity of fibrin clots on the concentration of thrombin, calcium, and fibrinogen and network cross link densities.

1.3.7. Hydrogels based on peptide amphiphiles:

Peptide amphiphiles (PA) are an interesting family of functionally diverse molecules whose assembly properties have been extensively studied both fundamentally and with respect to biomedical applications[168-179]. Some applications targeted for assembled structures from PAs are biomineralization, scaffolding for therapeutic delivery and tissue regeneration. Some of the first studies of PA self-assembly were put forward by Hartgerink et al[174,175]. A PA molecule is a hydrophilic peptide sequence covalently bonded to a hydrophobic aliphatic segment. PAs are particularly suited to tissue repair and the controlled therapeutic release since they offer flexibility of design. For e.g, a biological ligand can be used as a head group of the peptide sequence of an individual PA molecule for biofunctionalization[168]. Additionally, kinetics of PA self-assembly and the assembled nanostructure can be controlled by controlling

the individual amino acid sequences in the peptide sequence[173]. Such dependence of assembly and hydrogelation properties on peptide primary sequence has also been observed in β-hairpin peptides. The most significant example is that of MAX8, which is a derivative of MAX1 with one negatively charged side chain amino acid (glutamic acid) obtained by replacing a positively charged side chain amino acid (lysine) in MAX1. The electrostatic interactions within MAX8 molecules expedite the assembly kinetics of MAX8 as compared to the assembly kinetics of MAX1[180,181]. Molecular amphiphilicity leads PAs to self-assemble into nanofibers[169,174,175] or nanobelts[173] and further into fibrillar networks above certain concentrations. Although the assembled structures from PAs are fibrillar in morphology, the size scales of these fibrils are larger than those observed for fibrils from β-hairpin peptides due to larger PA molecules. Niece and colleagues[176] demonstrated that the sol–gel transition was triggered on mixing acidic and basic PAs at physiological pH. With the cell-binding ligand IKVAV as the head group, a PA solution mixed with neural cells when injected in vivo of a rat, a solid gel was shown to be formed[48]. The authors also discuss the gelation behavior and viscoelastic properties of PA-based gels as studied via dynamic oscillatory measurements. Stendahl et al[169]. performed a detailed investigation on effects of pH, ionic strength and type of metal ions on mechanical stiffness of PA gels. Mechanical stiffness of PA-based hydrogels as a function of increasing calcium concentration in the solution environment has been reported by Jun et al[182]. The authors have attributed the decrease of storage modulus after a

threshold value of calcium concentration to possible phase separation that occurs within the gel. In a separate study, it was found that stability and mechanical strength of PA-based hydrogels were dependent on the number and position of glycine residue that can hydrogen bond[68]. Pashuck et al[183]. Have reported the control of mechanical properties of nanofibrillar peptide amphiphile hydrogels based on number and positions of hydrophobic amino acid residues in the peptide amphiphiles. Greenfield et al[184]. have reported tunability of rheological properties such as stiffness and strain response of self-assembled fibrillar peptide amphiphile networks due to changes in the types of interfibrillar interactions such as hydrogen bonding and ionic bridges. Toksoz et al[185]. report on the self- assembly and gelation properties of PA molecules, specifically upon isolation and neutralization of ionic charges on the molecules. Charge neutralization was reported by the not only by the use of counter-ions like calcium but also macromolecules such as heparin and DNA.

1.3.8. Hydrogels based on low molecular weight peptidic gelators

In addition to peptides and polypeptides from amino acids, oligopeptides of low molecular weight, such as fluorenylmethoxycarbonyl (Fmoc)-protected amino acids, can self-assemble into supramolecular hydrogels that can be studied using oscillatory rheology measurements. Biological studies have demonstrated potential biomedical applications for these hydrogels such as tissue regeneration[186-188] and drug delivery[189-191]. These short peptides form hydrogels

when using pH[186,190,192-194] and temperature as a gelation trigger or in the presence of a natural enzyme[190-195].

The Ulijn group has reported hydrogelation of Fmoc-functionalized amino acids initiated under physiological conditions. Fmoc– diphenylalanine (Fmoc–F_2) molecules were reported to undergo self-assembly into fibrous hydrogels that support 3D cell culture of living cells[186-188]. Functionalization of the network with different chemical moieties has been explored as an approach to tune mechanical rigidity of Fmoc–F_2 gels[187]. The resulting gel networks were shown to display optimized compatibility with various cells. Xu and coworkers have presented a series of Fmoc–dipeptides, which show a reversible sol–gel transition in response to shift in temperature and pH[192,193]. In addition, the same group reported hydrogelation in response to the binding of vancomycin where gel stiffness was observed to increase significantly. Mahler et al[196]. have demonstrated sol–gel transition from Fmoc–F_2 solution in water at an appropriate concentration, leading to shear-thinning Fmoc–F_2 gels. Recently, Adams et al[197]. have reported the gelation of Fmoc–dipeptides induced by hydrolysis of glucono-d-lactone. The resulting hydrogels were homogeneous with reproducible mechanical properties irrespective of the pre-shear history experienced by the hydrogels. Several groups have also studied enzyme-induced gelation of low molecular weight peptides. Specifically, the Ulijn group has discussed the hydrogelation of Fmoc–tyrosine–OH triggered under physiological conditions by the presence of alkaline phosphatase. The concentration of alkaline phosphatase was crucial in

determining the gelation kinetics and stiffness of hydrogels formed[198]. Xu and coworkers discuss hydrogelation of Fmoc– tyrosine at 37° C at pH 6.0 and pH 9.6 induced by alkaline phosphate[192,193]. The final gels were reversed to a solution with kinase. Other enzymes like thermolysin[195], β-lactamase[199] and MMP-9[200] have been used to trigger hydrogelation of various hydrogelators.

The literature focusing on solution assembly and hydrogel forming characteristics of synthetic and naturally occurring peptide, polypeptide and protein systems discussed in Section 1.3 provides an introduction to this relatively new area of biomaterial research. Efforts towards thorough physical characterization of hitherto studied systems and development of derivative systems based on current ones are underway in academia. The use of chemically non-complex strategies such as assembly of blends of peptide molecules and development of multicomponent hybrid materials from peptide-biopolymer systems based purely on secondary interactions as described in this dissertation constitute a step forward in unlocking the full potential of peptide and protein based materials.

REFERENCES

(1) Buenger, D.; Topuz, F.; Groll, J. *Progress in Polymer Science* **2012**, *37*, 1678.

(2) Miyata, T.; Uragami, T.; Nakamae, K. *Advanced Drug Delivery Reviews* **2002**, *54*, 79.

(3) Bassetti, M. J.; Chatterjee, A. N.; Aluru, N. R.; Beebe, D. J. *Journal of Microelectromechanical Systems* **2005**, *14*, 1198.

(4) Burdick, J. A.; Khademhosseini, A.; Langer, R. *Langmuir* **2004**, *20*, 5153.

(5) Domachuk, P.; Tsioris, K.; Omenetto, F. G.; Kaplan, D. L. *Advanced Materials* **2010**, *22*, 249.

(6) Dong, L.; Jiang, H. *Soft Matter* **2007**, *3*, 1223.

(7) Hoffman, A. S. *Advanced Drug Delivery Reviews* **2002**, *54*, 3.

(8) Peppas, N. A.; Bures, P.; Leobandung, W.; Ichikawa, H. *European Journal of Pharmaceutics and Biopharmaceutics* **2000**, *50*, 27.

(9) Peppas, N. A.; Hilt, J. Z.; Khademhosseini, A.; Langer, R. *Advanced Materials* **2006**, *18*, 1345.

(10) Qiu, Y.; Park, K. *Advanced Drug Delivery Reviews* **2001**, *53*, 321.

(11) Langer, R.; Tirrell, D. A. *Nature* **2004**, *428*, 487.

(12) Lee, K. Y.; Mooney, D. J. *Chemical Reviews* **2001**, *101*, 1869.

(13) Kloxin, A. M.; Kasko, A. M.; Salinas, C. N.; Anseth, K. S. *Science* **2009**, *324*, 59.

(14) Godier-Furnemont, A. F. G.; Martens, T. P.; Koeckert, M. S.; Wan, L.; Parks, J.; Arai, K.; Zhang, G.; Hudson, B.; Homma, S.; Vunjak-Novakovic, G. *Proceedings of the National Academy of Sciences of the United States of America* **2011**, *108*, 7974.

(15) Su, J.; Hu, B.-H.; Lowe, W. L., Jr.; Kaufman, D. B.; Messersmith, P. B. *Biomaterials* **2010**, *31*, 308.

(16) Olsen, B. D.; Kornfield, J. A.; Tirrell, D. A. *Macromolecules* **2010**, *43*, 9094.

(17) Aguado, B. A.; Mulyasasmita, W.; Su, J.; Lampe, K. J.; Heilshorn, S. C. *Tissue Engineering Part A* **2012**, *18*, 806.

(18) Lu, H. D.; Charati, M. B.; Kim, I. L.; Burdick, J. A. *Biomaterials* **2012**, *33*, 2145.

(19) Borselli, C.; Storrie, H.; Benesch-Lee, F.; Shvartsman, D.; Cezar, C.; Lichtman, J. W.; Vandenburgh, H. H.; Mooney, D. J. *Proceedings of the National Academy of Sciences of the United States of America* **2010**, *107*, 3287.

(20) McCall, J. D.; Lin, C.-C.; Anseth, K. S. *Biomacromolecules* **2011**, *12*, 1051.
(21) Vulic, K.; Shoichet, M. S. *J. Am. Chem. Soc.* **2012**, *134*, 882.
(22) Segura, T.; Chung, P. H.; Shea, L. D. *Biomaterials* **2005**, *26*, 1575.
(23) Ma, D.; Zhang, H.-B.; Chen, D.-H.; Zhang, L.-M. *Journal of Colloid and Interface Science* **2011**, *364*, 566.
(24) Shepard, J. A.; Wesson, P. J.; Wang, C. E.; Stevans, A. C.; Holland, S. J.; Shikanov, A.; Grzybowski, B. A.; Shea, L. D. *Biomaterials* **2011**, *32*, 5092.
(25) Dadsetan, M.; Szatkowski, J. P.; Shogren, K. L.; Yaszemski, M. J.; Maran, A. *Journal of Biomedical Materials Research Part A* **2009**, *91A*, 1170.
(26) Bakota, E. L.; Aulisa, L.; Galler, K. M.; Hartgerink, J. D. *Biomacromolecules* **2011**, *12*, 82.
(27) Branco, M. C.; Pochan, D. J.; Wagner, N. J.; Schneider, J. P. *Biomaterials* **2010**, *31*, 9527.
(28) Aimetti, A. A.; Machen, A. J.; Anseth, K. S. *Biomaterials* **2009**, *30*, 6048.
(29) Branco, M. C.; Pochan, D. J.; Wagner, N. J.; Schneider, J. P. *Biomaterials* **2009**, *30*, 1339.
(30) Altunbas, A.; Lee, S. J.; Rajasekaran, S. A.; Schneider, J. P.; Pochan, D. J. *Biomaterials* **2011**, *32*, 5906.
(31) Branco, M. C.; Schneider, J. P. *Acta Biomaterialia* **2009**, *5*, 817.
(32) Hennink, W. E.; van Nostrum, C. F. *Advanced Drug Delivery Reviews* **2002**, *54*, 13.
(33) Kopecek, J.; Yang, J. Y. *Polym. Int.* **2007**, *56*, 1078.
(34) Zhang, S. G.; Marini, D. M.; Hwang, W.; Santoso, S. *Current Opinion in Chemical Biology* **2002**, *6*, 865.
(35) Barnes, C. P.; Sell, S. A.; Boland, E. D.; Simpson, D. G.; Bowlin, G. L. *Advanced Drug Delivery Reviews* **2007**, *59*, 1413.
(36) Ulijn, R. V.; Smith, A. M. *Chemical Society Reviews* **2008**, *37*, 664.
(37) Rajagopal, K.; Schneider, J. P. *Current Opinion in Structural Biology* **2004**, *14*, 480.
(38) Schneider, J. P.; Pochan, D. J.; Ozbas, B.; Rajagopal, K.; Pakstis, L.; Kretsinger, J. *J. Am. Chem. Soc.* **2002**, *124*, 15030.
(39) Ozbas, B.; Rajagopal, K.; Schneider, J. P.; Pochan, D. J. *Physical Review Letters* **2004**, *93*.
(40) Yucel, T.; Micklitsch, C. M.; Schneider, J. P.; Pochan, D. J. *Macromolecules* **2008**, *41*, 5763.
(41) Yan, C. Q.; Pochan, D. J. *Chemical Society Reviews* **2010**, *39*, 3528.
(42) Petka, W. A.; Harden, J. L.; McGrath, K. P.; Wirtz, D.; Tirrell, D. A. *Science* **1998**, *281*, 389.
(43) Shen, W.; Lammertink, R. G. H.; Sakata, J. K.; Kornfield, J. A.; Tirrell, D. A. *Macromolecules* **2005**, *38*, 3909.

(44) Papapostolou, D.; Smith, A. M.; Atkins, E. D. T.; Oliver, S. J.; Ryadnov, M. G.; Serpell, L. C.; Woolfson, D. N. *Proceedings of the National Academy of Sciences of the United States of America* **2007**, *104*, 10853.

(45) Jing, P.; Rudra, J. S.; Herr, A. B.; Collier, J. H. *Biomacromolecules* **2008**, *9*, 2438.

(46) Foo, C.; Lee, J. S.; Mulyasasmita, W.; Parisi-Amon, A.; Heilshorn, S. C. *Proceedings of the National Academy of Sciences of the United States of America* **2009**, *106*, 22067.

(47) Grove, T. Z.; Osuji, C. O.; Forster, J. D.; Dufresne, E. R.; Regan, L. *J. Am. Chem. Soc.* **2010**, *132*, 14024.

(48) Schwyzer, R. *Biopolymers* **1995**, *37*, 5.

(49) Helm, C. A.; Knoll, W.; Israelachvili, J. N. *Proceedings of the National Academy of Sciences of the United States of America* **1991**, *88*, 8169.

(50) Sprules, T.; Green, N.; Featherstone, M.; Gehring, K. *Journal of Biological Chemistry* **2003**, *278*, 1053.

(51) Sacanna, S.; Irvine, W. T. M.; Chaikin, P. M.; Pine, D. J. *Nature* **2010**, *464*, 575.

(52) Wilchek, M.; Bayer, E. A. *Anal. Biochem.* **1988**, *171*, 1.

(53) Holzinger, M.; Singh, M.; Cosnier, S. *Langmuir* **2012**, *28*, 12569.

(54) Rohs, R.; Jin, X. S.; West, S. M.; Joshi, R.; Honig, B.; Mann, R. S. In *Annual Review of Biochemistry, Vol 79*; Kornberg, R. D., Raetz, C. R. H., Rothman, J. E., Thorner, J. W., Eds.; Annual Reviews: Palo Alto, 2010; Vol. 79, p 233.

(55) Necas, J.; Bartosikova, L.; Brauner, P.; Kolar, J. *Veterinarni Medicina* **2008**, *53*, 397.

(56) Hales, H. G. G. a. C. A. *Chemistry and Biology of Hyaluronan*; Elsevier Ltd.: Oxford, 2004.

(57) Yan, C. Q.; Mackay, M. E.; Czymmek, K.; Nagarkar, R. P.; Schneider, J. P.; Pochan, D. J. *Langmuir* **2012**, *28*, 6076.

(58) Haines-Butterick, L.; Rajagopal, K.; Branco, M.; Salick, D.; Rughani, R.; Pilarz, M.; Lamm, M. S.; Pochan, D. J.; Schneider, J. P. *Proceedings of the National Academy of Sciences of the United States of America* **2007**, *104*, 7791.

(59) Prehm, P. *Biochemical Journal* **1984**, *220*, 597.

(60) Weigel, P. H.; Hascall, V. C.; Tammi, M. *Journal of Biological Chemistry* **1997**, *272*, 13997.

(61) T.C.Laurent; Fraser, J. R. E. *FASEB Journal* **1992**, *6*, 2397.

(62) Turley, E. A.; Austen, L.; Vandeligt, K.; Clary, C. *Journal of Cell Biology* **1991**, *112*, 1041.

(63) E.A.Turley, P. W. N. a. L. Y. W. B. *Journal of Biological Chemistry* **2002**, *277*, 4589.

(64) Knudson, C. B.; Knudson, W. *Faseb Journal* **1993**, *7*, 1233.

(65) Anseth, K. S.; Bowman, C. N.; BrannonPeppas, L. *Biomaterials* **1996**, *17*, 1647.
(66) C.W.Macosko *Rheology: Principles, Measurements and Applications*; Wiley-VCH, Inc.: New York, N.Y, 1994.
(67) T.G.Mezger *The Rheology Handbook: For Users of Rotational and Oscillatory Rheometers*; 2nd ed. Hannover, 2006.
(68) Aulisa, L.; Dong, H.; Hartgerink, J. D. *Biomacromolecules* **2009**, *10*, 2694.
(69) Knerr, P. J.; Branco, M. C.; Nagarkar, R.; Pochan, D. J.; Schneider, J. P. *Journal of Materials Chemistry* **2012**, *22*, 1352.
(70) Micklitsch, C. M.; Knerr, P. J.; Branco, M. C.; Nagarkar, R.; Pochan, D. J.; Schneider, J. P. *Angew. Chem.-Int. Edit.* **2011**, *50*, 1577.
(71) Bowerman, C. J.; Ryan, D. M.; Nissan, D. A.; Nilsson, B. L. *Molecular Biosystems* **2009**, *5*, 1058.
(72) Bowerman, C. J.; Nilsson, B. L. *J. Am. Chem. Soc.* **2010**, *132*, 9526.
(73) Ramachandran, S.; Flynn, P.; Tseng, Y.; Yu, Y. B. *Chemistry of Materials* **2005**, *17*, 6583.
(74) Ramachandran, S.; Trewhella, J.; Tseng, Y.; Yu, Y. B. *Chemistry of Materials* **2006**, *18*, 6157.
(75) Guilbaud, J. B.; Rochas, C.; Miller, A. F.; Saiani, A. *Biomacromolecules* **2013**, *14*, 1403.
(76) Ceylan, H.; Urel, M.; Erkal, T. S.; Tekinay, A. B.; Dana, A.; Guler, M. O. *Advanced Functional Materials* **2013**, *23*, 2081.
(77) Wang, C.; Stewart, R. J.; Kopecek, J. *Nature* **1999**, *397*, 417.
(78) Wang, C.; Kopecek, J.; Stewart, R. J. *Biomacromolecules* **2001**, *2*, 912.
(79) Xu, C.; Kopecek, J. *Pharmaceutical Research* **2008**, *25*, 674.
(80) Wu, L. C.; Yang, J. Y.; Kopecek, J. *Biomaterials* **2011**, *32*, 5341.
(81) Klok, H.-A. *Macromolecules* **2009**, *42*, 7990.
(82) Shen, W.; Zhang, K. C.; Kornfield, J. A.; Tirrell, D. A. *Nature Materials* **2006**, *5*, 153.
(83) Shen, W.; Kornfield, J. A.; Tirrell, D. A. *Macromolecules* **2007**, *40*, 689.
(84) Shen, W.; Kornfield, J. A.; Tirrell, D. A. *Soft Matter* **2007**, *3*, 99.
(85) Ciani, B.; Hutchinson, E. G.; Sessions, R. B.; Woolfson, D. N. *Journal of Biological Chemistry* **2002**, *277*, 10150.
(86) Pandya, M. J.; Spooner, G. M.; Sunde, M.; Thorpe, J. R.; Rodger, A.; Woolfson, D. N. *Biochemistry* **2000**, *39*, 8728.
(87) Banwell, E. F.; Abelardo, E. S.; Adams, D. J.; Birchall, M. A.; Corrigan, A.; Donald, A. M.; Kirkland, M.; Serpell, L. C.; Butler, M. F.; Woolfson, D. N. *Nature Materials* **2009**, *8*, 596.

(88) Nowak, A. P.; Breedveld, V.; Pakstis, L.; Ozbas, B.; Pine, D. J.; Pochan, D.; Deming, T. J. *Nature* **2002**, *417*, 424.
(89) Pochan, D. J.; Pakstis, L.; Ozbas, B.; Nowak, A. P.; Deming, T. J. *Macromolecules* **2002**, *35*, 5358.
(90) Breedveld, V.; Nowak, A. P.; Sato, J.; Deming, T. J.; Pine, D. J. *Macromolecules* **2004**, *37*, 3943.
(91) Grove, T. Z.; Forster, J.; Pimienta, G.; Dufresne, E.; Regan, L. *Biopolymers* **2012**, *97*, 508.
(92) Liu, Y.; Liu, B.; Riesberg, J. J.; Shen, W. *Macromolecular Bioscience* **2011**, *11*, 1325.
(93) Jia, X.; Kiick, K. L. *Macromolecular Bioscience* **2009**, *9*, 140.
(94) Urry, D. W. *Journal of Physical Chemistry B* **1997**, *101*, 11007.
(95) Meyer, D. E.; Chilkoti, A. *Biomacromolecules* **2004**, *5*, 846.
(96) Betre, H.; Setton, L. A.; Meyer, D. E.; Chilkoti, A. *Biomacromolecules* **2002**, *3*, 910.
(97) Betre, H.; Ong, S. R.; Guilak, F.; Chilkoti, A.; Fermor, B.; Setton, L. A. *Biomaterials* **2006**, *27*, 91.
(98) Setton, L. A.; Mow, V. C.; Howell, D. S. *Journal of Orthopaedic Research* **1995**, *13*, 473.
(99) McHale, M. K.; Setton, L. A.; Chilkoti, A. *Tissue Engineering* **2005**, *11*, 1768.
(100) Annabi, N.; Mithieux, S. M.; Boughton, E. A.; Ruys, A. J.; Weiss, A. S.; Dehghani, F. *Biomaterials* **2009**, *30*, 4550.
(101) Lee, J.; Macosko, C. W.; Urry, D. W. *Macromolecules* **2001**, *34*, 5968.
(102) Lim, D. W.; Nettles, D. L.; Setton, L. A.; Chilkoti, A. *Biomacromolecules* **2007**, *8*, 1463.
(103) Trabbic-Carlson, K.; Setton, L. A.; Chilkoti, A. *Biomacromolecules* **2003**, *4*, 572.
(104) Chow, D.; Nunalee, M. L.; Lim, D. W.; Simnick, A. J.; Chilkoti, A. *Materials Science & Engineering R-Reports* **2008**, *62*, 125.
(105) Nagapudi, K.; Brinkman, W. T.; Thomas, B. S.; Park, J. O.; Srinivasarao, M.; Wright, E.; Conticello, V. P.; Chaikof, E. L. *Biomaterials* **2005**, *26*, 4695.
(106) Wright, E. R.; McMillan, R. A.; Cooper, A.; Apkarian, R. P.; Conticello, V. P. *Advanced Functional Materials* **2002**, *12*, 149.
(107) Dinerman, A. A.; Cappello, J.; Ghandehari, H.; Hoag, S. W. *Journal of Controlled Release* **2002**, *82*, 277.
(108) Megeed, Z.; Haider, M.; Li, D. Q.; O'Malley, B. W.; Cappello, J.; Ghandehari, H. *Journal of Controlled Release* **2004**, *94*, 433.
(109) Asai, D.; Xu, D. H.; Liu, W. G.; Quiroz, F. G.; Callahan, D. J.; Zalutsky, M. R.; Craig, S. L.; Chilkoti, A. *Biomaterials* **2012**, *33*, 5451.

(110) Xu, D. H.; Asai, D.; Chilkoti, A.; Craig, S. L. *Biomacromolecules* **2012**, *13*, 2315.
(111) Yamamoto, M.; Tabata, Y.; Ikada, Y. *Journal of Bioactive and Compatible Polymers* **1999**, *14*, 474.
(112) Young, S.; Wong, M.; Tabata, Y.; Mikos, A. G. *Journal of Controlled Release* **2005**, *109*, 256.
(113) Nijenhuis, K. t. *Polymer Bulletin* **2007**, *58*, 27.
(114) Rossmurphy, S. B. *Polymer* **1992**, *33*, 2622.
(115) Clark, A. H.; Rossmurphy, S. B. *Advances in Polymer Science* **1987**, *83*, 57.
(116) Gilsenan, P. M.; Ross-Murphy, S. B. *Food Hydrocolloids* **2000**, *14*, 191.
(117) Gilsenan, P. M.; Ross-Murphy, S. B. *Journal of Rheology* **2000**, *44*, 871.
(118) Gilsenan, P. M.; Ross-Murphy, S. B. *International Journal of Biological Macromolecules* **2001**, *29*, 53.
(119) Foegeding, E. A. *Food Biophysics* **2006**, *1*, 41.
(120) Yan, H.; Frielinghaus, H.; Nykanen, A.; Ruokolainen, J.; Saiani, A.; Miller, A. F. *Soft Matter* **2008**, *4*, 1313.
(121) Yan, H.; Saiani, A.; Gough, J. E.; Miller, A. F. *Biomacromolecules* **2006**, *7*, 2776.
(122) Gosal, W. S.; Clark, A. H.; Pudney, P. D. A.; Ross-Murphy, S. B. *Langmuir* **2002**, *18*, 7174.
(123) Gosal, W. S.; Clark, A. H.; Ross-Murphy, S. B. *Biomacromolecules* **2004**, *5*, 2420.
(124) Gosal, W. S.; Clark, A. H.; Ross-Murphy, S. B. *Biomacromolecules* **2004**, *5*, 2430.
(125) Gosal, W. S.; Ross-Murphy, S. B. *Current Opinion in Colloid & Interface Science* **2000**, *5*, 188.
(126) Totosaus, A.; Montejano, J. G.; Salazar, J. A.; Guerrero, I. *International Journal of Food Science and Technology* **2002**, *37*, 589.
(127) Tobitani, A.; RossMurphy, S. B. *Macromolecules* **1997**, *30*, 4855.
(128) Sagis, L. M. C.; Veerman, C.; van der Linden, E. *Langmuir* **2004**, *20*, 924.
(129) Veerman, C.; de Schiffart, G.; Sagis, L. M. C.; van der Linden, E. *International Journal of Biological Macromolecules* **2003**, *33*, 121.
(130) Veerman, C.; Ruis, H.; Sagis, L. M. C.; van der Linden, E. *Biomacromolecules* **2002**, *3*, 869.
(131) Veerman, C.; Sagis, L. M. C.; Heck, J.; van der Linden, E. *International Journal of Biological Macromolecules* **2003**, *31*, 139.
(132) Durand, D.; Gimel, J. C.; Nicolai, T. *Physica a-Statistical Mechanics and Its Applications* **2002**, *304*, 253.
(133) Mehalebi, S.; Nicolai, T.; Durand, D. *Soft Matter* **2008**, *4*, 893.

(134) Mehalebi, S.; Nicolai, T.; Durand, D. *International Journal of Biological Macromolecules* **2008**, *43*, 129.
(135) Pouzot, M.; Benyahia, L.; Nicolai, T. *Journal of Rheology* **2004**, *48*, 1123.
(136) Pouzot, M.; Durand, D.; Nicolai, T. *Macromolecules* **2004**, *37*, 8703.
(137) Pouzot, M.; Nicolai, T.; Durand, D.; Benyahia, L. *Macromolecules* **2004**, *37*, 614.
(138) Perez-Gonzalez, J.; Lopez-Duran, J. J.; Marin-Santibanez, B. M.; Rodriguez-Gonzalez, F. *Rheologica Acta* **2012**, *51*, 937.
(139) Pins, G. D.; Christiansen, D. L.; Patel, R.; Silver, F. H. *Biophysical Journal* **1997**, *73*, 2164.
(140) Arai, T.; Freddi, G.; Innocenti, R.; Tsukada, M. *Journal of Applied Polymer Science* **2004**, *91*, 2383.
(141) Dal Pra, I.; Freddi, G.; Minic, J.; Chiarini, A.; Armato, U. *Biomaterials* **2005**, *26*, 1987.
(142) Meinel, L.; Hofmann, S.; Karageorgiou, V.; Kirker-Head, C.; McCool, J.; Gronowicz, G.; Zichner, L.; Langer, R.; Vunjak-Novakovic, G.; Kaplan, D. L. *Biomaterials* **2005**, *26*, 147.
(143) Aoki, H.; Tomita, N.; Morita, Y.; Hattori, K.; Harada, Y.; Sonobe, M.; Wakitani, S.; Tamada, Y. *Bio-Medical Materials and Engineering* **2003**, *13*, 309.
(144) Fini, M.; Motta, A.; Torricelli, P.; Glavaresi, G.; Aldini, N. N.; Tschon, M.; Giardino, R.; Migliaresi, C. *Biomaterials* **2005**, *26*, 3527.
(145) Motta, A.; Migliaresi, C.; Faccioni, F.; Torricelli, P.; Fini, M.; Giardino, R. *Journal of Biomaterials Science-Polymer Edition* **2004**, *15*, 851.
(146) Inoue, S.; Tanaka, K.; Arisaka, F.; Kimura, S.; Ohtomo, K.; Mizuno, S. *Journal of Biological Chemistry* **2000**, *275*, 40517.
(147) Altman, G. H.; Diaz, F.; Jakuba, C.; Calabro, T.; Horan, R. L.; Chen, J. S.; Lu, H.; Richmond, J.; Kaplan, D. L. *Biomaterials* **2003**, *24*, 401.
(148) Horan, R. L.; Antle, K.; Collette, A. L.; Huang, Y. Z.; Huang, J.; Moreau, J. E.; Volloch, V.; Kaplan, D. L.; Altman, G. H. *Biomaterials* **2005**, *26*, 3385.
(149) Kim, U. J.; Park, J.; Kim, H. J.; Wada, M.; Kaplan, D. L. *Biomaterials* **2005**, *26*, 2775.
(150) Kim, U. J.; Park, J. Y.; Li, C. M.; Jin, H. J.; Valluzzi, R.; Kaplan, D. L. *Biomacromolecules* **2004**, *5*, 786.
(151) Nazarov, R.; Jin, H. J.; Kaplan, D. L. *Biomacromolecules* **2004**, *5*, 718.
(152) Yucel, T.; Cebe, P.; Kaplan, D. L. *Biophysical Journal* **2009**, *97*, 2044.
(153) Kang, G. D.; Nahm, J. H.; Park, J. S.; Moon, J. Y.; Cho, C. S.; Yeo, J. H. *Macromolecular Rapid Communications* **2000**, *21*, 788.

(154) Yoo, M. K.; Kweon, H. Y.; Lee, K. G.; Lee, H. C.; Cho, C. S. *International Journal of Biological Macromolecules* **2004**, *34*, 263.

(155) Wang, H.; Zhang, Y. P.; Shao, H. L.; Hu, X. C. *International Journal of Biological Macromolecules* **2005**, *36*, 66.

(156) Wang, X.; Kluge, J. A.; Leisk, G. G.; Kaplan, D. L. *Biomaterials* **2008**, *29*, 1054.

(157) Vollrath, F.; Knight, D. P.; Hu, X. W. *Proceedings of the Royal Society B-Biological Sciences* **1998**, *265*, 817.

(158) Huemmerich, D.; Scheibel, T.; Vollrath, F.; Cohen, S.; Gat, U.; Ittah, S. *Current Biology* **2004**, *14*, 2070.

(159) Rammensee, S.; Huemmerich, D.; Hermanson, K. D.; Scheibel, T.; Bausch, A. R. *Applied Physics a-Materials Science & Processing* **2006**, *82*, 261.

(160) Slotta, U.; Hess, S.; Spiess, K.; Stromer, T.; Serpell, L.; Scheibel, T. *Macromolecular Bioscience* **2007**, *7*, 183.

(161) Zisch, A. H.; Lutolf, M. P.; Hubbell, J. A. *Cardiovascular Pathology* **2003**, *12*, 295.

(162) Fukada, E.; Kaibara, M. *Thrombosis Research* **1976**, *8*, 49.

(163) Kaibara, M.; Date, M. *Biorheology* **1985**, *22*, 197.

(164) Kaibara, M.; Fukada, E. *Biochimica Et Biophysica Acta* **1977**, *499*, 352.

(165) Kaibara, M.; Fukada, E. *Biorheology* **1980**, *17*, 255.

(166) Ryan, E. A.; Mockros, L. F.; Stern, A. M.; Lorand, L. *Biophysical Journal* **1999**, *77*, 2827.

(167) Ryan, E. A.; Mockros, L. F.; Weisel, J. W.; Lorand, L. *Biophysical Journal* **1999**, *77*, 2813.

(168) Silva, G. A.; Czeisler, C.; Niece, K. L.; Beniash, E.; Harrington, D. A.; Kessler, J. A.; Stupp, S. I. *Science* **2004**, *303*, 1352.

(169) Stendahl, J. C.; Rao, M. S.; Guler, M. O.; Stupp, S. I. *Advanced Functional Materials* **2006**, *16*, 499.

(170) Behanna, H. A.; Donners, J.; Gordon, A. C.; Stupp, S. I. *J. Am. Chem. Soc.* **2005**, *127*, 1193.

(171) Beniash, E.; Hartgerink, J. D.; Storrie, H.; Stendahl, J. C.; Stupp, S. I. *Acta Biomaterialia* **2005**, *1*, 387.

(172) Bull, S. R.; Guler, M. O.; Bras, R. E.; Meade, T. J.; Stupp, S. I. *Nano Letters* **2005**, *5*, 1.

(173) Cui, H.; Muraoka, T.; Cheetham, A. G.; Stupp, S. I. *Nano Letters* **2009**, *9*, 945.

(174) Hartgerink, J. D.; Beniash, E.; Stupp, S. I. *Science* **2001**, *294*, 1684.

(175) Hartgerink, J. D.; Beniash, E.; Stupp, S. I. *Proceedings of the National Academy of Sciences of the United States of America* **2002**, *99*, 5133.

(176) Niece, K. L.; Hartgerink, J. D.; Donners, J.; Stupp, S. I. *J. Am. Chem. Soc.* **2003**, *125*, 7146.

(177) Rajangam, K.; Arnold, M. S.; Rocco, M. A.; Stupp, S. I. *Biomaterials* **2008**, *29*, 3298.

(178) Tysseling-Mattiace, V. M.; Sahni, V.; Niece, K. L.; Birch, D.; Czeisler, C.; Fehlings, M. G.; Stupp, S. I.; Kessler, J. A. *Journal of Neuroscience* **2008**, *28*, 3814.

(179) Webber, M. J.; Tongers, J.; Renault, M.-A.; Roncalli, J. G.; Losordo, D. W.; Stupp, S. I. *Acta Biomaterialia* **2010**, *6*, 3.

(180) Haines-Butterick, L. A.; Rajagopal, K.; Lamm, M.; Pochan, D. J.; Schnieder, J. P. *Biopolymers* **2007**, *88*, 518.

(181) Rajagopal, K.; Lamm, M. S.; Haines-Butterick, L. A.; Pochan, D. J.; Schneider, J. P. *Biomacromolecules* **2009**, *10*, 2619.

(182) Jun, H. W.; Yuwono, V.; Paramonov, S. E.; Hartgerink, J. D. *Advanced Materials* **2005**, *17*, 2612.

(183) Olmsted, P. D. *Rheol. Acta* **2008**, *47*, 283.

(184) Greenfield, M. A.; Hoffman, J. R.; de la Cruz, M. O.; Stupp, S. I. *Langmuir* **2010**, *26*, 3641.

(185) Toksoz, S.; Mammadov, R.; Tekinay, A. B.; Guler, M. O. *Journal of Colloid and Interface Science* **2011**, *356*, 131.

(186) Jayawarna, V.; Ali, M.; Jowitt, T. A.; Miller, A. E.; Saiani, A.; Gough, J. E.; Ulijn, R. V. *Advanced Materials* **2006**, *18*, 611.

(187) Jayawarna, V.; Richardson, S. M.; Hirst, A. R.; Hodson, N. W.; Saiani, A.; Gough, J. E.; Ulijn, R. V. *Acta Biomaterialia* **2009**, *5*, 934.

(188) Zhou, M.; Smith, A. M.; Das, A. K.; Hodson, N. W.; Collins, R. F.; Ulijn, R. V.; Gough, J. E. *Biomaterials* **2009**, *30*, 2523.

(189) Yang, Z. M.; Xu, K. M.; Wang, L.; Gu, H. W.; Wei, H.; Zhang, M. J.; Xu, B. *Chem. Commun.* **2005**, 4414.

(190) Yang, Z.; Liang, G.; Ma, M.; Gao, Y.; Xu, B. *Small* **2007**, *3*, 558.

(191) Sutton, S.; Campbell, N. L.; Cooper, A. I.; Kirkland, M.; Frith, W. J.; Adams, D. J. *Langmuir* **2009**, *25*, 10285.

(192) Yang, Z. M.; Gu, H. W.; Fu, D. G.; Gao, P.; Lam, J. K.; Xu, B. *Advanced Materials* **2004**, *16*, 1440.

(193) Yang, Z. M.; Liang, G. L.; Wang, L.; Xu, B. *J. Am. Chem. Soc.* **2006**, *128*, 3038.

(194) Smith, A. M.; Williams, R. J.; Tang, C.; Coppo, P.; Collins, R. F.; Turner, M. L.; Saiani, A.; Ulijn, R. V. *Advanced Materials* **2008**, *20*, 37.

(195) Toledano, S.; Williams, R. J.; Jayawarna, V.; Ulijn, R. V. *J. Am. Chem. Soc.* **2006**, *128*, 1070.

(196) Mahler, A.; Reches, M.; Rechter, M.; Cohen, S.; Gazit, E. *Advanced Materials* **2006**, *18*, 1365.

(197) Adams, D. J.; Butler, M. F.; Frith, W. J.; Kirkland, M.; Mullen, L.; Sanderson, P. *Soft Matter* **2009**, *5*, 1856.

(198) Thornton, K.; Smith, A. M.; Merry, C. L. R.; Ulijn, R. V. *Biochemical Society Transactions* **2009**, *37*, 660.
(199) Yang, Z.; Ho, P.-L.; Liang, G.; Chow, K. H.; Wang, Q.; Cao, Y.; Guo, Z.; Xu, B. *J. Am. Chem. Soc.* **2007**, *129*, 266.
(200) Yang, Z.; Ma, M.; Xu, B. *Soft Matter* **2009**, *5*, 2546.

Chapter 2

MATERIALS AND METHODS

This chapter presents the materials used, synthesis of peptides and experimental techniques used in characterizing peptide solutions and hydrogels. The experimental details common to all the experiments in general have been presented here. Specific details of experiments related to individual studies have been discussed in the chapters covering the respective studies.

2.1. Synthesis of β-hairpin Peptides

The peptides LNK1, MAX1, LP1, KP1, LP2, KP2, LP3 and KP3 were purchased from New England Peptide, LLC (Gardener, MA, USA). The LNK1 peptide is the first hydrophobically modified peptide that incorporates shape specific interactions to potentially eliminate fibrillar branching. Comparisons of self-assembly pathways and hydrogel rheological properties of LNK1 and MAX1 peptides have been discussed in Chapter 4. LP1-KP1, LP2-KP2 and LP3-KP3 are pairs of hydrophobically modified peptides which resemble wedge (LP1, LP2 and LP3) and trough shapes (KP1, KP2 and KP3) when folded into β-hairpins. Self-assembly and hydrogel network properties of these peptides individually and when blended in pairs (LP1-KP1, LP2-KP2 and LP3-KP3) 1:1 (w/w) to study potential shape complementary interactions between the pairs have been discussed in Chapter 5. Hydrogels constructed using the MAX8 peptide have been

used to construct composite materials by blending hydrogels with hyaluronic acid, as discussed in Chapter 5. Self-assembly and hydrogel rheological properties of gels formed from blends of MAX1 and P5 peptides are discussed briefly in Chapter 7. The MAX1, MAX8 and P5 peptides were synthesized at the Chemical Biology Laboratory, National Cancer Institute, National Institute of Health, Frederick, MD in collaboration with the group of Dr.Joel P.Schneider. All peptides were prepared using Fmoc-based solid phase peptide synthesis as described by a standard protocol[1]. For the three peptides, an automated ABI 433A peptide synthesizer (Applied Biosystems, Life Technologies, Grand Island, NY, USA) was used to synthesize the peptides. Fmoc-based solid peptide chemistry with HCTU activation was performed. A trifluoroacetic acid: thioanisole: 1,2-ethanedithiol: anisole (90:5:3:2) cocktail under Argon atmosphere for 2 h was used to cleave the dried resin-bound peptides from the resin and for simultaneous side-chain deprotection. Precipitation by cold diethyl ether and lyophilization of crude peptides were followed by peptide purification that was carried out by reverse phase-HPLC equipped with a semi-preparative Vydac C18 column. HPLC solvents A and B were 0.1% TFA in water and 0.1% TFA in 9:1 acetonitrile: water, respectively. Linear gradients were employed as 0% solvent B over 2 min, 0-17% solvent B over 10 min and then 17-100% solvent B over 166 min for MAX8. For MAX1 the gradients employed were 0-15% solvent B over 10 min and then 15-100% solvent B over 170 min. For P5, the gradients were as 0% solvent B over 2 min, 0-11% solvent B over 7 min and then 11-100% solvent

B over 178 min. Analytical HPLC and electrospray ionization (ESI-positive mode) were performed to verify the purity of the lyophilized peptides.

2.2. Peptide Assembly and Hydrogel Preparation

The procedure to produce a 0.5 % (w/v) hydrogel from a peptide is described. A 1 mg aqueous solution of a given peptide (MAX1, LNK1, LP1, KP1, LP2, KP2, LP3, KP3) or 1:1 blend by weight of pairs of peptides LP1: KP1, LP2:KP2, LP3:KP3, in 100 μL of deionized chilled water (5°C) is prepared leading to a 1% (w/v) aqueous solution. An equal amount of chilled (5°C) buffer solution is added to the aqueous solution to give buffered solution of the peptide. The buffer solution used depends upon the peptide or pair of peptides to be assembled. Then the peptide assembly is triggered by quickly raising the temperature of the solution to 30°C. The temperature is ramped up at a rate of 10°C/ min. All peptides assemble into hydrogels of varying mechanical properties at 0.5% (w/v) concentration depending on their sequence. Buffer solutions used for hydrogel assembly throughout the thesis are 250 mM boric acid and 20 mM NaCl to ultimately yield pH 9 (125 mM boric acid, 10 mM NaCl) or 100 mM BTP and 300 mM NaCl or 100 mM NaCl, respectively, to yield solution conditions pH 7 (50 mM BTP, 150 mM NaCl) or pH 7 (50 mM BTP, 50 mM NaCl). In case of MAX8, chilled (5°C) 50mM HEPES buffer (pH 7.4) is used to dissolve the peptide and Dulbeccos Modified Eagle Medium (DMEM) with 25mM HEPES (pH 7.4) was used as the buffer solution. Details of preparation of

individual types of hybrid networks by blending MAX8 and hyaluronic acid have been discussed in the Experimental Section of Chapter 6.

2.3. Circular Dichroism (CD)

CD spectra were collected using either a Jasco J-810 spectropolarimeter (Jasco Inc. Easton, MD, USA) or an Aviv Model 420 spectropolarimeter (Aviv Biomedical Inc., Lakewood, NJ, USA). 150 μM solutions of the given peptide solution were prepared by adding equal volumes of chilled (5° C) buffer solution to 300 μM de-ionized peptide solution.. The random coil to β-hairpin folding transition temperatures were determined by scanning temperatures from 5°C to 80°C varying the wavelength between a window 190 nm to 250 nm at each temperature. Mean residue ellipticity [θ] was calculated from the equation, $[\theta] = \theta_{obs}/(10 \text{ X } l \text{ X } c \text{ X } n)$ where θ_{obs} is the measured ellipticity (millidegrees), l is the path length of the cell (cm), c is the peptide concentration (molar), and n is the number of residues on the peptide sequence. Temperature scans were performed with 2 °C increments and 5 min equilibration time at each temperature. Temperature of transition from random coil conformation to β-sheet conformation is determined by studying the dependence of MRE values at 218 nm as a function of temperature. 218 nm is chosen since it lies well within the signature wavelength range (216 nm -222nm) for a β-sheet to exhibit a minimum in MRE values.

2.4. Negative Staining Cast Film Transmission Electron Microscopy (Cast-film TEM)

Transmission Electron Microscopy was carried out on a 120kV Tecnai-12 Electron Microscope (FEI Company, Hillsboro, OR, USA). A hydrogel was prepared from a given peptide at 0.5% (w/v). To observe the fibrillar width, particularly the local nanostructure from the peptide self-assembly, 10 μL of gel was diluted to a concentration of 0.1% (w/v), and a drop was placed on a 300 mesh copper-coated grids (Electron Microscopy Sciences, Hatfield, PA, USA) held by a pair of tweezers. Excess fluid was blotted off with a filter paper. Then immediately 3 μL of a 1 % (w/v) of uranyl acetate solution in water was placed on the grid and blotted off after 40 sec. The gird was left to dry for an hour and used for imaging.

For the preparation of the sample for MAX1 and LNK1 networks after being subject to a shear treatment as described in Chapter 4, a small piece of the treated hydrogel without dilution was placed on a 300 mesh copper-coated grid and excess volume of gel was blotted off. 3 μL of a 1 % (w/v) of uranyl acetate solution in water was placed on the grid and blotted off after 40 sec for staining the sample. This method was applied to the networks after injection shear treatment samples to capture their morphology without dilution and additional mixing effects.

2.5. Cryogenic Transmission Electron Microscopy

Cryogenic transmission electron microscopy was performed on a MAX1 hydrogel sample (Chapter 3) using a Tecnai G2-12 Twin Transmission Electron Microscope (FEI Inc., Hillsboro, OR, USA) operating at voltage of 120 kV located in the W.M.Keck Electron Microscopy Facility at the University of Delaware. For sample preparation, a copper TEM grid, 300 mesh pre-coated with lacey carbon film (Ted Pella, Redding, CA, USA). A droplet of 2 μL diluted hydrogel solution was placed onto the copper grid loaded in an FEI Vitrobot. Each grid was blotted twice in order to obtain suitable specimen thickness for imaging. The blotting time was set as two seconds. The sample was quickly plunged into liquefied ethane (~90 K) cooled by a reservoir of liquid nitrogen to ensure the vitrification of water. The vitrified samples were transferred to a single tilt cryo transfer holder in a cryo transfer stage immersed in liquid nitrogen. During the imaging, the cryo-holder was kept below -170 °C to prevent sublimation of vitreous solvent.

2.6. Small Angle Neutron Scattering (SANS)

SANS experiments were performed on the 30 m instrument (NG-3) at the NIST Center for Neutron Research (NCNR), National Institute of Standards and Technology (NIST), Gaithersburg, MD. Gel samples were prepared by mixing the desired peptide(s) and buffer solutions both prepared in D_2O to enable adequate contrast between the hydrogen-rich gel matrix and the deuterated solvent. MAX1

hydrogel sample at pH 9 (125 mM boric acid, 10 mM NaCl) was prepared at 0.5 % (w/v). LP1, KP1, LP2, KP2, LP3, KP3, LP1-KP1 1:1 (w/w), LP2:KP2 1:1 (w/w) and LP3:KP3 1:1 (w/w) were all maintained at 1% (w/v) concentration. Solutions pre-equilibrated at 5° C were mixed in a vial and transferred immediately to titanium sample cells with 25 mm diameter quartz windows and a 1 mm path length. All samples were incubated at room temperature for 3 hours prior to scattering measurements. A monochromated neutron beam (λ = 6 Å) with a wavelength spread ($\delta I/I$) of 0.12 was incident on the sample. The scattered neutrons were captured on a 64 cm X 64 cm 2D detector. Varying sample-to-detector distances of 1.33, 4.5 and 13.17 m were used to the study of the scattering wavevector q in the range 0.004 $Å^{-1} < q < 0.4$ $Å^{-1}$, defined by $q = (4\pi/\lambda) \sin(\theta/2)$, where λ is the neutron wavelength and θ is the scattering angle. Raw data were corrected for background electronic noise and radiation, detector inhomogeneity and sensitivity, empty cell scattering and scattering from each buffer used to prepare the hydrogels. Intensities were normalized to an absolute scale relative to main beam transmission measurements through the sample and were reduced according to published protocol[2]. SANS data were analyzed using the cylindrical form factor model that are available from the NCNR at NIST. The models used were 'Cylinders with Monodisperse values of radius' for analysis of MAX1 and 'Cylinders with polydisperse values of radius' for the analyses of the wedge and trough shaped peptides. The error bars of the data points for all SANS plots are within the limits of the symbols. The reduction of data and fitting to

cylinder form factor with both monodisperse and polydisperse values of radii was performed by a software (a module that operates within IGOR) supplied by NCNR.

For the cylinder form factor fits with monodisperse values of radii, the following function was used as calculated by the software:

$$P(q) = (scale/V_{cyl}) * \int_0^{\pi/2} F^2(q,\alpha) \sin\alpha d\alpha \ldots \text{Equation 1.}$$

For the cylinder form factor fits with polydisperse values of radii, the following function was used as calculated by the software:

$$P(q) = (scale/V_{poly}) * \int_0^{x} f(r)dr \int_0^{\pi/2} F^2(q,\alpha) \sin\alpha d\alpha \ldots \text{Equation 2.}$$

q: Wavevector

α: Angle between the cylinder orientation and wave vector

The scattering amplitude F is given by

$$F(q,\alpha) = 2V_{cyl}(\rho_{cyl} - \rho_{solv})\ j_0(qH\cos\alpha)\frac{J_1(qr\sin\alpha)}{(qr\sin\alpha)} \quad \ldots \text{Equation 3.}$$

The polydispersity is included by integrating the form factor $P(q)$ over the Schulz distribution of the cylinder radius:

$$P(q) = \int_0^{\pi/2} F^2(q,\alpha) \sin\alpha d\alpha \ldots \text{Equation 4.}$$

The normalized Schulz distribution is

$$f(R) = (z+1)^{z+1} x^{z} \frac{\exp[-(z+1)x]}{R_{avg}\Gamma(z+1)}$$ …Equation 5.

R_{avg} = Mean radius input while fitting data

x= R/R_{avg}

$p = \sigma / R_{avg}$; p: polydispersity of radius values; σ^2: variance of the distribution

$z = [1/(p^2)] - 1$

The integration has been normalized by the second moment of the radius distribution, leading to the equation

$$V_{poly} = \pi r^2 L\left(\frac{z+2}{z+1}\right)$$ ... Equation 6.

from the original equation, which describes the Nth moment of the size distribution

$$\langle R^N \rangle = \frac{R_{avg}^N}{(z+1)^N} \frac{(z+N)!}{z!}$$ …Equation 7.

Performing fits to SANS data using the above described model returns values for the polydispersity 'p' in the radius values of the cylindrical nanostructures as well as the most frequent value of the cylinder radius.

The SANS data from each sample were also fitted in a low-q regime and a high-q regime, as a function $I = (A/q^n)$ at low q and $I = (B/q^m)$ at high q respectively using a data analysis package provided by NCNR that operates within IGOR. The specific q range windows for which fitting was carried out

have been mentioned in Chapter 5. Additionally, another model, the correlation length model which calculates the scattering intensity as

$I(q) = (A/q^n) + C/(1 + (qL)^m) + B$ …Equation 8.

This model was originally designed for fitting to clustered networks of polymer chains in which the 'n' defines scattering from polymer clusters at low-q and 'm' defines scattering from polymer chains[3,4]. B is the incoherent background, A and C are multiplicative factors for low and high q regimes of the SANS data. 'n' and 'm' are exponents used as fitting parameters and L is the correlation length for polymer chains. This model used to fit SANS data from assembled networks of peptides can potentially provide information about local and global network characteristics formed from the peptides. Details about values of parameters 'n' and 'm' obtained using the fits and their interpretation for understanding network behavior has been explained in detail in Chapter 5.

2.7. Oscillatory Rheology

In a common oscillatory rheological measurement, the storage modulus, G', and loss modulus, G", are the most common parameters that are measured for a hydrogel. G' (Pa) and G" (Pa) are usually monitored as a function of time, applied angular frequency and applied oscillatory stress. In a viscous sol state, G" is greater than G'. Therefore, for a solid, physical gel the storage modulus is greater than the loss modulus (G'>>G"). Oscillatory rheology measurements for the study of peptide gelation were performed on ARG2 rheometer (TA

Instruments, New Castle, DE, USA) using 20mm diameter stainless steel parallel plate geometry. Buffered peptide solutions 0.5%, 1% or 2% (w/v) were prepared in ice-chilled solutions by adding 100 μL of chilled (5° C) buffer to 100 μL of 1%, 2% or 4% (w/v) of the given peptide solution in chilled (5° C) deionized water. The chilled (5° C) buffered peptide solution was quickly transferred to the Peltier plate of the ARG2 rheometer equilibrated at 5°C, and the upper plate was lowered to a gap height of 500 μm. The upper plate and the Peltier plate were equilibrated to 30°C (or 35°C in case of LNK1 and MAX1 hydrogels) prior to carrying out the rheological experiments. For the shear-thinning and rehealing experiments, oscillatory time sweep measurement steps carried out for 90 minutes each, before and after subjecting the hydrogel networks to a steady state shear of 1000/s for 120 sec were carried out for all samples. For these oscillatory time sweep measurements, oscillatory frequency was maintained at 6 rad/s and oscillatory strain at 1%. The gap height was maintained at 500 μm for all the experiments.

Measurement of the moduli as a function of frequency shows behavior of a hydrogel at short vs. long time scales. The frequency dependence of the moduli is a feature critical to hydrogel characterization. At high frequencies (fast time scales) a viscoelastic liquid system can appear solid-like (G'>>G"), while at lower frequencies or longer time scales the same material will exhibit liquid-like responses (G">>G') and easily flow. Oscillatory frequency sweep measurements have been carried out on the hydrogels in Chapter 4, to study network properties

of hydrogels before and after intense shear treatment. For these measurements, oscillatory strain was maintained at 1%. By monitoring the moduli vs. strain, the linear viscoelastic regime (LVR) for a given material can be determined. The LVR is a window of applied strain values within which G' and G'' are independent of applied strain. Oscillatory strain sweep measurements as discussed for MAX1 in Chapter 3and that have been carried out on the hydrogels prepared using peptides discussed in this dissertation, with applied oscillatory frequency values maintained at 6 rad/s.

REFERENCES

(1) Nagarkar, R.; Schneider, J. P. *Methods in Molecular Biology* **2008**, *474*, 61.

(2) Kline, S. R. *Journal of Applied Crystallography* **2006**, *39*, 895.

(3) Hammouda, B.; Ho, D. L.; Kline, S. *Macromolecules* **2004**, *37*, 6932.

(4) Hammouda, B.; Horkay, F.; Becker, M. L. *Macromolecules* **2005**, *38*, 2019.

Chapter 3

INTRODUCTION TO β-HAIRPIN SELF-ASSEMBLY AND HYDROGEL YIELD STRESS MATERIAL-LIKE PROPERTIES

3.1. Introduction to β-hairpin Peptide Self-Assembly

The Pochan laboratory and the Schneider laboratory (National Cancer Institute, National Institutes of Health, Frederick, MD) have studied extensively the 'MAX' family of peptides that is based on a parent sequence MAX1[1-4]. MAX1 is a twenty amino acid residue amphiphilic peptide sequence VKVKVKVK-(V^DPPT)-KVKVKVKV-NH_2, with alternating hydrophobic valine (V) and hydrophilic lysine (K) residues[1]. This section serves to introduce the basic design characteristics of the base sequence MAX1 and its solution assembly and network characteristics.

In MAX1, the type II' turn sequence -V^DPPT- in the center is responsible for β-hairpin formation (Figure 3.1b) at elevated pH, ionic strength and temperature solution conditions from a random coil conformation in aqueous solution of low to neutral pH (Figure 3.1a). Higher pH serves to deprotonate the lysine side chain amino group and higher ionic strength serves to screen the positive charges on the lysine side chains, both leading to β-hairpin formation. The β-hairpin conformation has the two amphiphilic arms of MAX1 parallel to each stabilized by intramolecular hydrogen bonding. An increase in temperature emphasizes hydrophobic interactions between the valine side chains and serves as

another factor promoting the peptide folding and self-assembly. Facial hydrophobic interactions (Figure 3.1c) at the valine face between two β-hairpins form the core of the growing fibrils[5]. Lateral intermolecular hydrophobic interactions (Figure 3.1d) along the axis of the growing fibrils, along with the facial hydrophobic interactions, lead to hierarchical assembly of these β-hairpins into uniform fibrils (Figure 3.1e)[4]. Lateral intermolecular hydrogen bonding interactions also play a significant role in the assembly. Sometimes, during the facial hydrophobic collapse, two hairpins undergo an incomplete burial of the hydrophobic face. This incomplete burial manifests itself as a defect, which is responsible for nucleation of two fibrils emanating from the defect junction. Thus, these junctions of fibrils act as branching points and contribute to physical crosslinking of the fibrils in addition to fibrillar entanglement leading to formation of self-standing, solid hydrogels[6]. The cryogenic transmission electron micrograph (Figure 3.1f) shows the uniform fibrillar structure of the MAX1 network. The fibrils have a uniform thickness ~ 3 nm, corresponding to the strand length of each β-hairpin of MAX1.

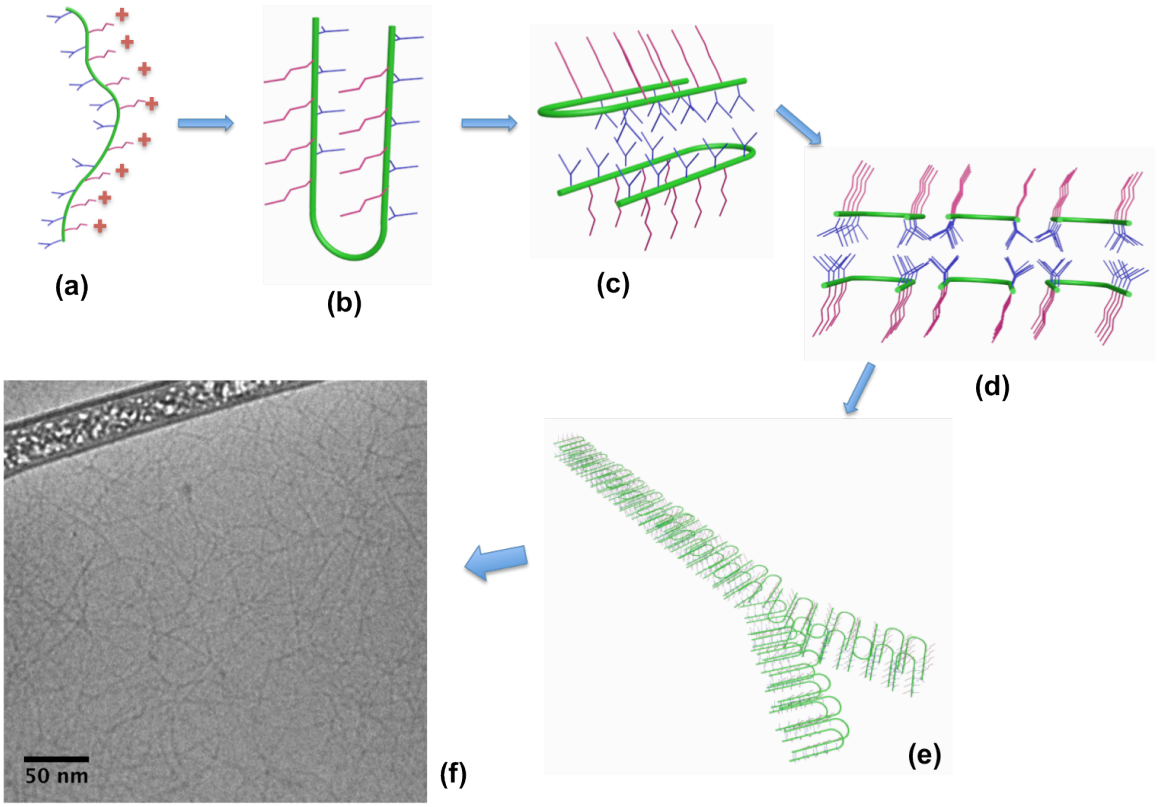

Figure 3.1. Schematic of MAX1 self-assembly (a) MAX1 Random coil conformation at low to neutral pH and low temperature (b) β-hairpin conformation (c) Facial hydrophobic collapse of two hairpins leading to formation of a bilayer type structure (d) Direction of lateral hydrophobic interactions among multiple bilayer type structures (e) hierarchically assembled branched fibril of MAX1 (f) Cryogenic Transmission Electron Microscopy showing fibrillar structure of MAX1.

3.2. Solution assembly behavior of β-hairpin peptide derivatives of MAX1

This section discusses the various peptide sequences obtained by making modifications to the primary amino acid structure of MAX1. MAX1 derivatives show diverse assembly characteristics such as responsiveness to different stimuli like UV light, enzymes, heavy metal ions, tunable assembly kinetics and corresponding hydrogel mechanical behavior. In case of MAX1

derivatives with slightly different primary structures, the specific pH, ionic strength and temperature conditions, or suitable combination of these solution parameters, are dependent on the specific peptide primary sequence used for assembly and hydrogel formation. As an example, the peptide MAX8 is obtained by point substitution of a positively charged lysine residue in MAX1 with a glutamic acid residue with a negative charge. At the same peptide concentration and solution conditions, MAX8 demonstrates faster assembly kinetics due to less overall positive charge (+7 as compared to +9 in case of MAX1) and additional attractive electrostatic interactions between the added glutamic acid and lysine residues[7,8]. MAX8 peptides can undergo self-assembly to form hydrogel materials under physiological pH (~7.4)[8], salt content[9] (~160mM Salt) and temperature conditions (37°C)[9-11]. MAX8 allows uniform 3D living mesenchymal cell or drug payload encapsulation due to the fast gelation time (~ 1 min v/s ~ 30 min for MAX1) at physiological solution conditions[10]. This expedited gelation leading to ultimately stiffer hydrogels from MAX8 as compared to those from MAX1 at the same peptide concentration and solution conditions has been shown clearly by oscillatory rheological measurements[12]. Thus, MAX8 has particular relevance to homogeneous 3D cell encapsulation and potential tissue engineering applications. Leonard et al.[13] have provided solid-state NMR spectroscopy evidence of the β-hairpin conformation being the dominant conformation within assembled fibrils of MAX8 peptide. MAX8 also has been shown to have a very similar fibrillar nanostructure as MAX1 in terms of fibril width (~3.2 nm)[6]. Due to faster gelation

kinetics than MAX1, MAX8 fibrils form networks with smaller pore sizes indicating more crosslink density of MAX8 fibrils as compared to MAX1 as evidenced by cryogenic transmission electron microscopy (cryo-TEM) and small angle neutron scattering (SANS) [14]. Hydrogels based on MAX1 and MAX8 have demonstrated cytocompatibility[15], non-inflammatory properties[10] and in some cases biologically effective properties such as antibacterial activity (MAX1[16] and MARG1[17], which is a gel forming MAX1 derivative). These biocompatible, self-assembling peptide systems provide flexibility of peptide structure by allowing introduction of specific biochemical functionalities such as post self-assembly chemical crosslinking to yield stiffer hydrogels[18]. Macromolecule self-diffusion and bulk release studies with MAX1 and MAX8 hydrogels have shown macromolecule mobility within, and release out of, the gels[19,20]. This demonstrates the ability of the porous ß-hairpin peptide hydrogels with tunable mesh sizes as viable candidates for tissue engineering and drug delivery scaffolds since they allow transport of nutrients and metabolites. Thus, due to the favorable therapeutic encapsulation and, biocompatibility and, in some cases, bioactivity, hydrogels from MAX1 and MAX8 demonstrate significant potential for their use in biomedical applications, particularly in light of the injectable solid attributes displayed as discussed below.

The MAX3 peptide is obtained by substituting two hydrophobic side chain valine residues with hydrophilic side chain threonine residues. Due to these point substitutions, the MAX3 peptide under the same solution conditions as MAX1

forms hydrogels only at a much higher temperature (~70°C) than MAX1 at the same solution conditions (~30°C). When cooled to temperatures significantly below 70°C (~5°C), gelation and assembly is reversed and the material becomes a low viscosity solution[5]. MAX3 hydrogels can undergo multiple cycles of sol to gel and gel to sol transitions. Such reversibility of hydrogel like properties is observed in case of MAX1 also, when temperature is used as the dominant stimulus for self-assembly along with pH/ionic strength solution conditions weaker than the pH 9, 10mM NaCl solution condition. Other examples of MAX1 derivatives include peptides with varying properties such as twisted fibrils, non-twisted and laminated fibrils all forming stiff, shear-thinning and rehealing hydrogels[21-23]. Due to the designs of the appropriately named 'strand swapping peptides' SSP1, SSP2, SSP3 undergo β-hairpin formation and bilayer type structure formation as observed in case of MAX1. But, instead of two hairpins forming a bilayer in case of MAX1, four hairpins are required to form a bilyer structure by burial of valine side chains in the SSP peptides. Thus, effectively twice the concentration of peptides was required to form fibrils and hydrogels with SSP peptides as compared to MAX1 as shown via rheology. Although different nanostructures are formed from SSP1 (singular twisted fibrillar), SSP2 (singular non-twisted fibrillar) and SSP3 (laminated non-twisted fibrillar), the basic assembly mechanism of these peptides is similar to that of MAX1.

Rheological measurements were used to probe the controlled biodegradation of peptide hydrogels based on a series of Degrading Peptides (DP)

through interaction metalloproteinase-13 (MMP-13)[24]. Oscillatory rheological characterization was used to measure stiffness values of hydrogels as they were subject to degradation using MMP-13 and thus helped directly validate that the enzymes were degrading the peptide fibrils that constituted the hydrogel. Hydrogel based on enantiomeric mixtures of self-assembling β-hairpins (MAX1 and D-MAX1) showing nonadditive, synergistic, enhancement in material rigidity compared to gels prepared from either pure enantiomer, have been reported by Nagy et al.[25] The fibrillar morphology of the hydrogel formed from the enantiomeric mixture is negligibly different from that based on either pure enantiomer. Non-additive mechanical synergistic effects were reported when peptide enantiomers are mixed. Similar to β-hairpin peptides shear-thinning and rehealing hydrogels from self- assembled amphiphilic non β-turn peptides forming hydrogels based on tapes and laminates have been reported.[26] The next section offers a detailed perspective on the hydrogel mechanical properties of MAX1 hydrogels as characterized by oscillatory rheology.

3.3. Rheological Properties of Hydrogels Constructed from β-hairpin Peptides

This section describes the hydrogel mechanical properties as investigated using oscillatory rheological characterization, the yield-stress material-like nature of these hydrogels and their unique ability of shear-thinning and rehealing. The shear-thinning and rehealing ability of these hydrogels confers upon them the

capacity to be injected as solids using a simple device like a syringe or a catheter. A well-defined linear viscoelastic region and yield strain value (~10-40%) dependent upon the specific peptide sequence and solution conditions used to trigger self-assembly is demonstrated by these hydrogels when subject to a strain sweep measurement at a constant frequency[1,3-6,27,28].

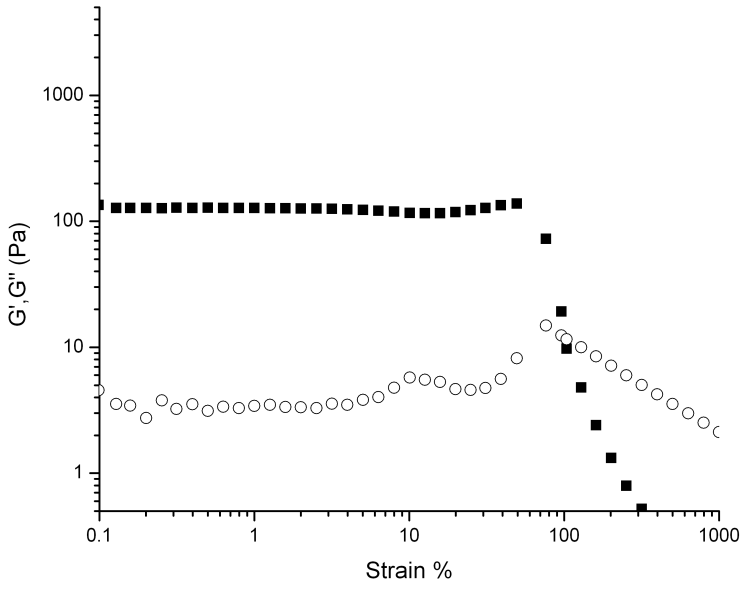

Figure 3.2. Oscillatory strain sweep measurement of a 0.5% (w/v) hydrogel at pH 9 (125mM Boric Acid 10mM NaCl), indicating a linear viscoelastic regime (LVR) ~ 60% oscillatory strain demonstrating yielding behavior of the hydrogel above 60% oscillatory strain. G' (Pa) indicated by solid squares, G" (Pa) indicated by hollow circles (G'>>G")

Figure 3.2 shows an oscillatory strain sweep measurement conducted on a 0.5% (w/v) hydrogel of MAX1 at solution conditions pH 9 (125mM Boric Acid,

10 mM NaCl) that demonstrates a well defined LVR ~ 60 %. During a frequency sweep measurement at constant small amplitude strain within the LVR, the hydrogels display an elastic modulus, G', almost independent to applied angular frequency (0.1-100 1/s) over several decades of applied angular frequency as shown in Figure 3.3 and discussed in other reports[1-3,5,6,9,27].

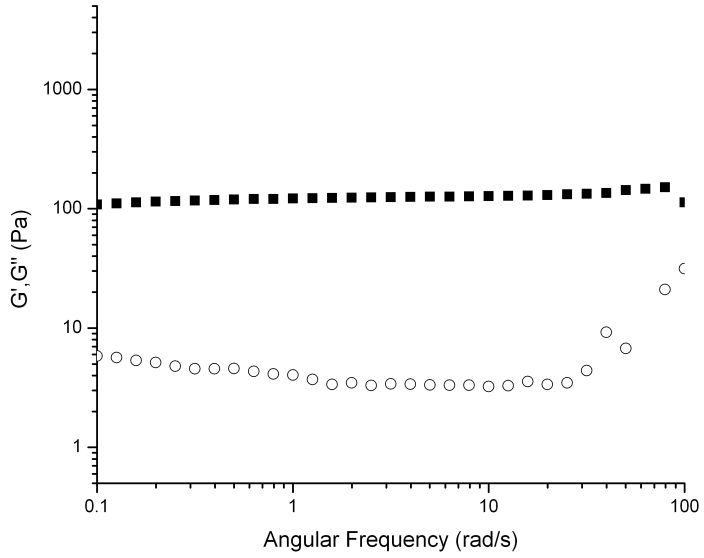

Figure 3.3. Oscillatory frequency sweep measurement of a 0.5% (w/v) hydrogel at pH 9 (125mM Boric Acid 10mM NaCl), showing relative independence of G' (Pa) to applied angular frequency (rad/s) indicating solid like character of MAX1 0.5% (w/v) hydrogel. G' (Pa) indicated by solid squares, G" (Pa) indicated by hollow circles (G'>>G")

The solid injectable gel behavior is characterized by studying evolution of storage modulus of a fully formed hydrogel after subjecting it to a steady state

shear using a bench-top rheometer. Figure 3.4 shows the shear-thinning and rehealing behavior of a 2% (w/v) hydrogel of MAX1 subject to steady state shear of 1000/s for 2 min (indicated by dotted line).

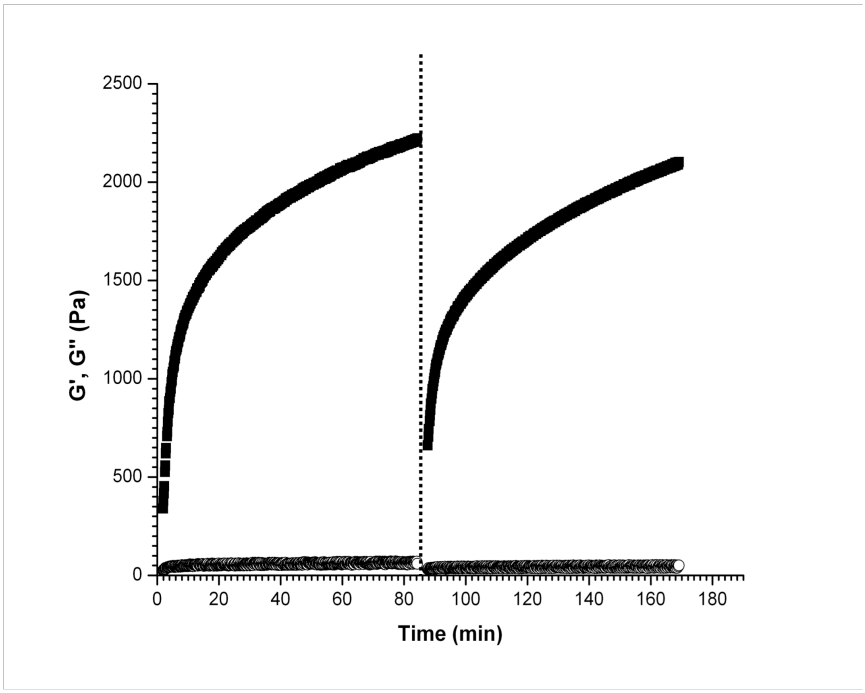

Figure 3.4. Oscillatory time sweep measurement showing evolution of storage modulus of 2% (w/v) pH 9 (125mM Boric Acid 10mM NaCl) to ~ 2200 Pa followed by steady state shear of amplitude 1000/s for 2 min indicated by the dotted line. The shear step is followed by an oscillatory time sweep measurement probing rehealing of the hydrogel to G' value close to the initial G' value. G' (Pa) indicated by solid squares, G" (Pa) indicated by hollow circles (G'>>G").

As discussed by Yan et al.[27], MAX1 and MAX8 hydrogels, as well as other MAX1 derivatives, undergo shear-thinning behavior when subject to

rheometer-induced shear and immediately form a solid on cessation of shear, leading to a value of stiffness modulus G' ~ 600 Pa, G'>>G" (immediately after the dotted line in Figure 3.4). When allowed to age, these hydrogels heal into networks with stiffness modulus G' (Pa) comparable to that of the network pre-shear. The rheological characterization of the MAX1/MAX8 hydrogels demonstrate the utility of these materials as preformed solid hydrogels that can retain their solid nature when injected in-vivo. This shear-thinning and rehealing behavior will be discussed in more detail in the next section.

3.4. Rheological Characterization of the Shear-Thinning and Rehealing Behavior of β-hairpin Hydrogels

As discussed in Section 3.3, rheological conditions employing small amplitude oscillatory strain conditions have been used to determine various mechanical attributes of hydrogels based on MAX1, MAX8 and derivative peptide sequences. Results from rheological measurements help in understanding various properties like hydrogel stiffness, linear viscoelastic region windows and yield stress values of these hydrogels. These properties help establish the utility of the hydrogels as biomaterials. An important property of MAX1, MAX8 and derivative peptide-based hydrogels is their shear-thinning and rehealing behavior that confers the ability of being injectable as solids onto the hydrogels. Solid injectable hydrogels of these peptides offer significant promise as delivery vehicles for drugs, cells and macromolecules such as proteins and polysaccharides. This section discusses fundamental investigation of the unique

shear- thinning and rehealing behavior of MAX8 hydrogels using the visual technique of confocal microscopy in simultaneous use with a bench top rheometer, which is responsible for subjecting the hydrogels to steady state shear treatment.

The behavior of MAX1 and MAX8 β-hairpin peptide hydrogels during and after steady state shear-induced flow has been explored by Yan et al. in order to fundamentally understand the mechanisms of the shear-thinning and rehealing behavior. In order to subject the hydrogels to steady state shear, a bench top rheometer equipped with parallel plate geometry was used. Even though this set-up offers appropriate rheometric characterization of the shear response of the hydrogel, it cannot offer information about any structural change exhibited by the hydrogel during simultaneously shear-induced flow. Furthermore, as reported by Yan et al., β-hairpin hydrogels underwent plug flow upon injection through a capillary in a scenario mimicking syringe injections. Apart from the portion of the gel directly in contact with the capillary wall where significant shearing took place, the gel across the majority of the capillary bore maintained a constant velocity and is subject to negligible shear. This flow profile result obtained by using a capillary device would not have been observed if the measurements were carried out solely using a conventional parallel plate or cone and plate geometry in a bench top rheometer. A negligible gradient in the velocity profile over the bulk of the hydrogel used to deliver the cells is observed in comparison to a laminar velocity profile for cells suspended in buffer solution injected using the

same capillary. The observation of no shear within the bulk of the gel during capillary flow led to observations of cells encapsulated within the hydrogel also experiencing minimal shear during flow with significant cell viability within the hydrogel network after the shear injection process.

Two other recent reports in the literature show the utility of confocal microscopy during hydrogel capillary flow for insight into the specific plug flow behavior of injectable, physically crosslinked gels. A very recent account from Aguado and Heilshorn[29] shows a similar plug flow regime as essential for protection of cells from deformation and shear while being injected as encapsulated within physically crosslinked alginate hydrogels. Olsen et al.[30] report a physically crosslinked injectable telechelic hydrogel that demonstrates extreme shear-thinning and rapid rehealing properties. Flow visualization and large amplitude oscillatory strain results demonstrate the formation of zones of non-homogenous shear within the hydrogel. Visualization of the velocity profile in capillary flow of a PC10P hydrogel labeled with fluorescent microsphere tracers shows that the portion of the gel closest to the capillary wall undergoes yielding indicating a plug flow profile for the gel in a capillary geometry[30].

In order to obtain information of any potential structural change exhibited by the β-hairpin hydrogels while being subject to steady state shear-induced flow, Yan et al.[27] have used the combination of rheology and material flow with the concurrent study of material nanostructure through small angle scattering. One combination was the use of rheo-SANS a concentric cylinder rheometer tool and

an incident neutron beam for small-angle scattering. The other combination technique was to flow the hydrogel through a capillary while observing the scattering of an incident x-ray beam. In both these techniques, the neutron or x-ray beam is directed normal to the direction of shear induced by the rotating cylinder tool/injection through capillary such that the incident neutrons or x-rays can scan a cross section of a hydrogel sample representing the entire hydrogel sample affected by the shear. Rheo-SANS is a compound technique that facilitates the study of structural change of a soft matter system while simultaneously monitoring changes in rheological properties of the system. An extensive review of Rheo-SANS study of soft matter systems has been provided by Eberle et al[31]. The construction of a modified commercial rheometer used to conduct rheometric measurements while simultaneously being able to monitor structural changes has been discussed by Porcar et al.[32] Small Angle Neutron Scattering (SANS) and Small Angle X-ray Scattering (SAXS) data from the hydrogels under shear help in elucidation of any changes in hydrogel nanostructure during the process of rheometer-induced or capillary-induced shear. Results from the combination techniques demonstrate that there is no noticeable change in hydrogel morphology during rheometer-induced or capillary-induced shear. Based on these results and results from bench-top rheology of β-hairpin peptide (MAX1/MAX8) hydrogels, a model has been proposed to explain how the gel network is fractured into domains during shear-thinning and flow. The domains can flow during shear but can immediately re-percolate into a solid hydrogel when the shear is

stopped. Within the fractured domains exists the same nanostructure, same fibrillar thickness and same porosity as the original bulk network. The lack of changes in hydrogel nanostructure during rheometer or capillary induced shear may also point to bulk fracture within a certain thickness of the hydrogel sample away from the shearing surface as explained by Yan et al.[27]. Instead of fracturing into domains within the bulk of the gel thus allowing the material to flow, a hydrogel layer near the stationary rheometer tool may fracture from the bulk material and consequently flow. In this case, the bulk of the hydrogel would remain stationary and thus would appear as the original bulk network by scattering. Given the possibility of bulk fracture of the hydrogel throughout the sample cross-section or fracture limited to a certain layer of the hydrogel sample, obtaining visual evidence of the exact, possible fracture characteristics of the MAX1/MAX8 hydrogels via imaging techniques such as confocal microscopy is an important step forward in understanding the shear response from these solid injectable hydrogels.

Given the plug flow behavior of the injectable solid MAX1 or MAX8 hydrogels; one could expect limited-thickness fracture behavior from the hydrogels when they are subjected to shear treatment using a rotating upper plate of a bench top rheometer. Intuitively, it can be expected that the shear induced by the rheometer upper plate might be fracturing only a localized layer of the hydrogel very near the upper plate, while the bulk of the gel might be negligibly affected by shear. Thus, direct visualization of the flow pattern of the hydrogel

when subject to shear using a rheometer upper plate would reveal the exact flow patterns obtained using a bench top rheometer. Rehealing behavior of MAX1 or MAX8 hydrogels after being subject to steady state shear has already been observed to be affected by the differences in amplitude and duration of the applied shear[27]. For example, a hydrogel subject to 1000/s of steady state shear for 2 min has recovers to a lower value of stiffness modulus, G' (Pa) as compared to a hydrogel subject to 1000/s of steady state shear for 5 sec. Is this difference due to differences in bulk shear of the gels or to differences in the fractured layer experiencing shear? Thus, imaging during shear application would help verify hydrogel flow patterns and any fracture properties as functions of various parameters associated with the shear treatment such as applied stress amplitude, duration and shear history.

In the experiments reported herein, a confocal rheometer was used to obtain direct visualization of the structural response of β-hairpin hydrogel when subject to steady state shear using a bench-top parallel plate rheometer. Experimental details and the instrumental configuration have been described in Chapter 2. Carboxyl-functionalized, fluorescent microparticles were encapsulated within the MAX8 hydrogels used for the study. The fluorescent microparticles indicated the presence of the hydrogel across the gap height when imaged using the confocal microscope in the device. These data show a sheared hydrogel sample at various steady state shear rates while it is being viewed from the bottom of the hydrogel sample looking upwards at the rheometer upper plate as shown by

the schematic in Figure 3.5. Specifically, each video shows images of multiple layers of the hydrogels at increasing heights within the sample away from the rheometer lower plate. These increasing heights are indicated by an increasing z value in the videos while the constant x and y values that indicate the position of the layers relative to the lower plate remain the same. The total thickness of the hydrogel scanned (μm), thickness of fractured layers (μm), the corresponding amplitude values of steady shear (s^{-1}) and the thickness of the fractured layers as a percentage of the total hydrogel thickness scanned measured in triplicate has been reported in Table 3.1. The video data obtained on the MAX8 hydrogel at the different steady state shear amplitudes (5/s, 50/s, 250/s, 400/s, 1000/s) shows fractured layers of different thicknesses corresponding to the shear amplitudes. The range of the z variable for the shear amplitude 5/s is $0 < z < 414$, corresponding to a minimum thickness of 0 μm and maximum thickness scanned ~ 980 μm. For the shear amplitudes of 50/s, 250/s, 400/s and 1000/s, the range of the z variable is $0 < z < 333$, corresponding to a minimum thickness of 0 μm and maximum thickness scanned ~790 μm. Under steady state shear of 5/s, the bulk of the encapsulated microparticles, i.e. the bulk of the MAX8 hydrogel, undergoes zero or negligible flow. Only a layer of average thickness ~ 23 μm ($z = 400/414$) near the upper plate (at the top of the bulk hydrogel) shows flow of encapsulated microparticles. This result clearly shows evidence of bulk fracture of the physically assembled MAX8 hydrogel. When the same hydrogel is subject to a steady state shear of 50/s, the layer of microparticles undergoing flow stays

approximately the same at an average of 25 μm (z = 325/333). When the amplitude of steady state shear is increased to 250/s, the fracture between stationary and flowing gel next to the upper plate occurs at an average thickness of 307 μm (z = 125/333) from the upper plate. At a steady state shear of 400/s, the microparticles appear to be in motion at a z value of ~ 75/333, corresponding to an average thickness of fractured MAX8 hydrogel ~ 625 μm. At a steady state shear of 1000/s, which is the most widely used shear amplitude to apply rheometer induced shear in the literature, the microparticles appear to be in motion at a z value of ~ 53/333, corresponding to an average thickness of fractured MAX8 hydrogel ~ 650 μm. These results provide evidence of the bulk fracture and yielding behavior of the MAX8 hydrogel, that is commonly considered as a shear-thinning and rehealing material. The experimental results acquired using the rheometer-confocal microscope studying the MAX8 hydrogel clearly indicate shear rate dependent fracture of the hydrogel.

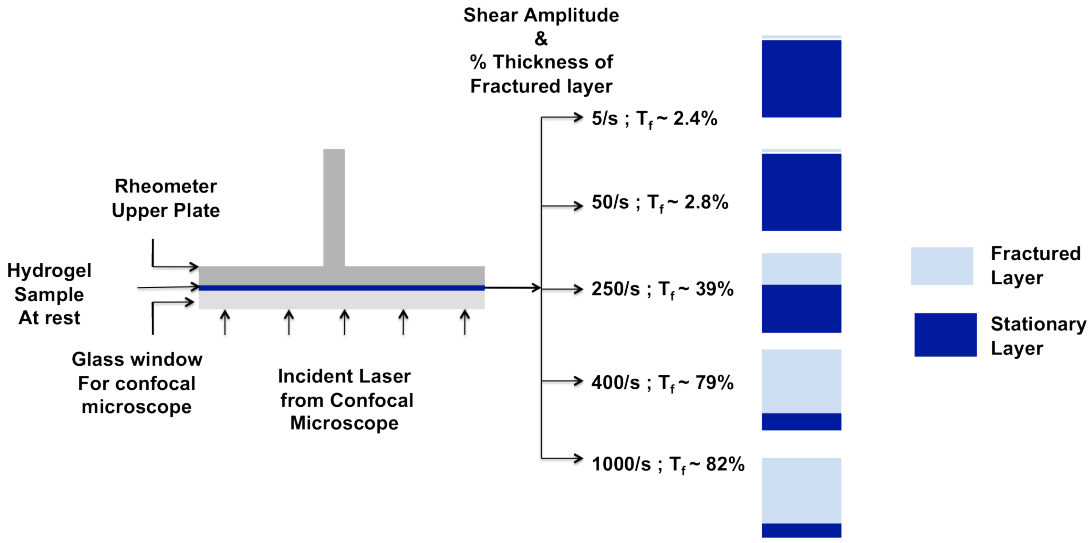

Figure 3.5. Schematic showing results obtained from rheometer-confocal microscope compound assembly. The hydrogel undergoes shear rate-dependent fracture in a layer of certain thickness away from the upper plate of the rheometer geometry, while the rest of the hydrogel undergoes no or negligible flow. The three squares indicate three small volumes across the cross-section of the hydrogel sample between the rheometer plates when the sample is subject to 5/s, 50/s, 250/s, 400/s and 1000/s amplitude steady state shear. The light blue and dark blue layers indicate the fractured and consequently flowing layer and stationary layers of the MAX8 hydrogel at steady state shear rates 5/s, 50/s, 250/s, 400/s and 1000/s respectively. T_f indicates the % thickness of the fractured layer.

Table 3.1. Results obtained from rheometer-confocal microscope compound assembly. The thickness of the hydrogel undergoing shear rate-dependent fracture away from the upper plate of the rheometer geometry is obtained by recording the z values from the videos at which the encapsulated microparticles start demnstarting motion. The z values are then converted to thickness of hydrogel layer in which negligible microparticle motion takes place by multiplying by the factor (2.37) fixed during the confocal microscopy measurement. The thickness of the fractured layer is obtained by subtracting the thickness of the stationary microparticle layer from the total hydrogel thickness.

Shear Rate (s^{-1})	**Total Thickness Gap height (μm)**	**Fractured Layer Thickness (μm)**	**% thickness Fractured**
5	980	23.3	2.4
50	790	25.3	2.8
250	790	307.0	38.8
400	790	624.6	79.0
1000	790	652.0	82.5

The results from the confocal rheometer assembly provide important direct visualization of the fracture and flow behavior of the β-hairpin hydrogels under commonly employed shear treatment using a rheometer. The data clearly show that the hydrogels demonstrate bulk fracture under steady-state shear in layers with thicknesses dependent on the shear rate. As shown in Table 3.1., the

thickness of the fractured layer increases directly with increased shear rate.

According to the model proposed by Yan et al.[27], MAX1/MAX8 hydrogels undergo fracture into smaller domains under shear indicated by yielding and flowing of the hydrogel within the shear field. Upon termination of rheometer or syringe induced shear, these fractured domains re-percolate to form a solid hydrogel network, indicated by bench top rheology with G'>G" (Pa). The bulk fracture indicated by the rheometer-confocal microscope compound assembly serves to reinforce the hydrogel fracture model proposed by Yan et al. The data from the compound assembly prove that yielding and flow of the MAX1 or MAX8 hydrogels take place within a defined layer parallel to the shearing plate of the rheometer. These data are also consistent with the yielding and shearing of MAX8 hydrogels in a layer close to the walls of a capillary during capillary flow of MAX8 hydrogels while the bulk of the material within the capillary flows as a plug and experiences no shear. Thus, a combination of a visual technique such as a confocal microscope and a rheometer helps elucidate the correlation between the structural changes and corresponding rheological behavior from physical hydrogels.

Rheological characterization of β-hairpin hydrogels as discussed in Section 3.1 and other assembled physical hydrogels as discussed in Chapter 1 has been carried out using a bench-top rheometer using parallel plate or cone and plate geometries. These oscillatory rheological measurements have been carried out with applied strain amplitudes within the Linear Viscoelastic Regime of the

hydrogels and correctly represent the hydrogel behavior. These results help in understanding parameters such as hydrogel stiffness and frequency dependence behavior from the hydrogels.

The experimental results from the capillary geometry and the compound rheometer-confocal microscope assembly clearly indicate shear rate dependent fracture exhibited by the β-hairpin peptide hydrogels. At higher amplitudes of steady state shear > 400/s, a significant majority of the hydrogel bulk away from the rheometer upper plate undergoes fracture and shear-thinning. Upon cessation of this shear, it also demonstrates rehealing behavior into a bulk solid hydrogel. Importantly, even if one is confined to use only of a bench-top rheometer, which does not yield a direct correlation between hydrogel structural changes under flow and the corresponding rheological shear response, the rheometer still faithfully represents shear-thinning and rehealing behavior. As long as a shear-fractured layer constitutes a significant thickness of a bulk physical hydrogel, the rheological behavior of the fractured layer can be considered qualitatively representative of that of the entire hydrogel sample when under shear. While difficult to determine what layer thickness is considered a "significant thickness", in all measurements performed herein, at least 20 mm of hydrogel experienced fracture and shear flow at the lowest shear rate of 5/s. Shear-thinning and immediate rehealing into a solid hydrogel upon cessation of shear has been observed when a hydrogel is subject to shear using a bench-top rheometer. Almost identical immediate rehealing behavior of a hydrogel when subject to

syringe injection-induced shear has been reported by Yan et al[27]. This observation also helps to validate the utility of pure rheometer-induced flow to study shear-thinning and rehealing behavior of β-hairpin peptide based hydrogels and other physical hydrogels that show this behavior. Thus, a combination of a visual technique such as a confocal microscope and a rheometer helps elucidate the correlation between the structural changes and corresponding rheological behavior from physical hydrogels.

This utility of a pure rheometer-induced flow can be reinforced by the use of simultaneous visual investigation of potential structural changes of hydrogels under flow. The compound rheometer-confocal microscope assembly is an example of an instrument with such reinforced utility. Efforts towards acquisition of a complete perspective about the structural as well as mechanical changes exhibited by various types of soft materials have been the focus of research well over a decade now. Visual confirmation of flow behavior of polymers solutions, melts and networks has been investigated using particle tracking in a variety of reports[33-36]. Wang et al. describe the development and implications of the method of Particle Tracking Velocimetry (PTV). This technique has been instrumental in direct visualization of flow behavior in case of rheological response from a variety materials such as DNA solutions[37-40], polymeric melts[38,41] and wormlike micelles[42] from surfactants. The principle of the PTV method is to optically track the fluorescing or diffracting particles embedded into the sample under study when illuminated by a laser. This method provides the visual proof of phenomena

such as wall slip and/or inhomogeneous shear in case of polymer melts and this method has been suggested by the authors as an "indispensable part of non-linear rheological studies of highly viscoelastic materials."[43]

3.5. Conclusion

Mechanical properties of hydrogels constructed using β-hairpin peptides MAX1 and MAX8 can be characterized by using small amplitude oscillatory rheological characterization. A bench top rheometer is a commonly used instrument used to investigate the mechanical properties and shear response of physically crosslinked hydrogel systems similar to the β-hairpin peptide hydrogels. When subject to steady state shear by using a bench-top rheometer or by injection through a syringe or catheter, MAX1/MAX8 hydrogels yield and flow under shear and immediately reheal into solid hydrogel networks upon cessation of shear, thus demonstrating shear-thinning and rehealing behavior. In a capillary flow scenario that mimics syringe injection, as demonstrated by Yan et al., apart from the portion of the gel directly in contact with the capillary wall where significant shearing took place, the gel across the majority of the capillary bore maintained a constant velocity and is subject to negligible shear. These results from Yan et al. have inspired the work discussed in this chapter and have led to more fundamental investigation of the shear-thinning and rehealing behavior of MAX1/MAX8 hydrogels when subject to a bench-top rheometer-induced shear. This chapter has discussed experimentally obtained visual evidence acquired by the use of a rheo-confocal microscope, of the fracture and

subsequent flow of physically crosslinked β-hairpin peptide hydrogels under steady state shear mimicking commonly conducted experimental conditions using bench top rheometers. The observed fracture demonstrates that the supposed bulk shear-thinning and rehealing behavior of physical gels can be limited to the yielding of a hydrogel layer close to the shearing surface with the bulk of the hydrogel below experiencing negligible shear.

REFERENCES

(1) Schneider, J. P.; Pochan, D. J.; Ozbas, B.; Rajagopal, K.; Pakstis, L.; Kretsinger, J. *J. Am. Chem. Soc.* **2002**, *124*, 15030.

(2) Pochan, D. J.; Schneider, J. P.; Kretsinger, J.; Ozbas, B.; Rajagopal, K.; Haines, L. *J. Am. Chem. Soc.* **2003**, *125*, 11802.

(3) Ozbas, B.; Kretsinger, J.; Rajagopal, K.; Schneider, J. P.; Pochan, D. J. *Macromolecules* **2004**, *37*, 7331.

(4) Rajagopal, K.; Ozbas, B.; Pochan, D. J.; Schneider, J. P. *European Biophysics Journal with Biophysics Letters* **2006**, *35*, 162.

(5) Ozbas, B.; Rajagopal, K.; Schneider, J. P.; Pochan, D. J. *Physical Review Letters* **2004**, *93*.

(6) Yucel, T.; Micklitsch, C. M.; Schneider, J. P.; Pochan, D. J. *Macromolecules* **2008**, *41*, 5763.

(7) Haines-Butterick, L.; Rajagopal, K.; Branco, M.; Salick, D.; Rughani, R.; Pilarz, M.; Lamm, M. S.; Pochan, D. J.; Schneider, J. P. *Proceedings of the National Academy of Sciences of the United States of America* **2007**, *104*, 7791.

(8) Rajagopal, K.; Lamm, M. S.; Haines-Butterick, L. A.; Pochan, D. J.; Schneider, J. P. *Biomacromolecules* **2009**, *10*, 2619.

(9) Altunbas, A.; Lee, S. J.; Rajasekaran, S. A.; Schneider, J. P.; Pochan, D. J. *Biomaterials* **2011**, *32*, 5906.

(10) Haines-Butterick, L. A.; Salick, D. A.; Pochan, D. J.; Schneider, J. P. *Biomaterials* **2008**, *29*, 4164.

(11) Yan, C. Q.; Mackay, M. E.; Czymmek, K.; Nagarkar, R. P.; Schneider, J. P.; Pochan, D. J. *Langmuir* **2012**, *28*, 6076.

(12) Haines-Butterick, L. A.; Rajagopal, K.; Lamm, M.; Pochan, D. J.; Schnieder, J. P. *Biopolymers* **2007**, *88*, 518.

(13) Leonard, S. R.; Cormier, A. R.; Pang, X. D.; Zimmerman, M. I.; Zhou, H. X.; Paravastu, A. K. *Biophysical Journal* **2013**, *105*, 222.

(14) Hule, R. A.; Nagarkar, R. P.; Altunbas, A.; Ramay, H. R.; Branco, M. C.; Schneider, J. P.; Pochan, D. J. *Faraday Discussions* **2008**, *139*, 251.

(15) Kretsinger, J. K.; Haines, L. A.; Ozbas, B.; Pochan, D. J.; Schneider, J. P. *Biomaterials* **2005**, *26*, 5177.

(16) Salick, D. A.; Kretsinger, J. K.; Pochan, D. J.; Schneider, J. P. *J. Am. Chem. Soc.* **2007**, *129*, 14793.

(17) Salick, D. A.; Pochan, D. J.; Schneider, J. P. *Advanced Materials* **2009**, *21*, 4120.

(18) Rughani, R. V.; Branco, M. C.; Pochan, D.; Schneider, J. P. *Macromolecules* **2010**, *43*, 7924.

(19) Branco, M. C.; Pochan, D. J.; Wagner, N. J.; Schneider, J. P. *Biomaterials* **2009**, *30*, 1339.

(20) Branco, M. C.; Pochan, D. J.; Wagner, N. J.; Schneider, J. P. *Biomaterials* **2010**, *31*, 9527.
(21) Nagarkar, R. P.; Hule, R. A.; Pochan, D. J.; Schneider, J. P. *Biopolymers* **2007**, *88*, 614.
(22) Hule, R. A.; Nagarkar, R. P.; Hammouda, B.; Schneider, J. P.; Pochan, D. J. *Macromolecules* **2009**, *42*, 7137.
(23) Nagarkar, R. P.; Hule, R. A.; Pochan, D. J.; Schneider, J. P. *J. Am. Chem. Soc.* **2008**, *130*, 4466.
(24) Giano, M. C.; Pochan, D. J.; Schneider, J. P. *Biomaterials* **2011**, *32*, 6471.
(25) Nagy, K. J.; Giano, M. C.; Jin, A.; Pochan, D. J.; Schneider, J. P. *J. Am. Chem. Soc.* **2011**, *133*, 14975.
(26) Geisler, I. M.; Schneider, J. P. *Advanced Functional Materials* **2012**, *22*, 529.
(27) Yan, C.; Altunbas, A.; Yucel, T.; Nagarkar, R. P.; Schneider, J. P.; Pochan, D. J. *Soft Matter* **2010**, *6*, 5143.
(28) Ozbas, B.; Rajagopal, K.; Haines-Butterick, L.; Schneider, J. P.; Pochan, D. J. *Journal of Physical Chemistry B* **2007**, *111*, 13901.
(29) Aguado, B. A.; Mulyasasmita, W.; Su, J.; Lampe, K. J.; Heilshorn, S. C. *Tissue Engineering Part A* **2012**, *18*, 806.
(30) Olsen, B. D.; Kornfield, J. A.; Tirrell, D. A. *Macromolecules* **2010**, *43*, 9094.
(31) Eberle, A. P. R.; Porcar, L. *Current Opinion in Colloid & Interface Science* **2012**, *17*, 33.
(32) Porcar, L.; Pozzo, D.; Langenbucher, G.; Moyer, J.; Butler, P. D. *Review of Scientific Instruments* **2011**, *82*.
(33) Adrian, R. J. *Experiments in Fluids* **2005**, *39*, 159.
(34) Cowen, E. A.; Monismith, S. G. *Experiments in Fluids* **1997**, *22*, 199.
(35) Maas, H. G.; Gruen, A.; Papantoniou, D. *Experiments in Fluids* **1993**, *15*, 133.
(36) Melling, A. *Measurement Science & Technology* **1997**, *8*, 1406.
(37) Boukany, P. E.; Hu, Y. T.; Wang, S. Q. *Macromolecules* **2008**, *41*, 2644.
(38) Boukany, P. E.; Wang, S. Q. *Soft Matter* **2009**, *5*, 780.
(39) Boukany, P. E.; Wang, S. Q. *Journal of Rheology* **2009**, *53*, 73.
(40) Hemminger, O. L.; Boukany, P. E.; Wang, S. Q.; Lee, L. J. *J. Non-Newton. Fluid Mech.* **2010**, *165*, 1613.
(41) Wang, S. Q.; Ravindranath, S.; Boukany, P.; Olechnowicz, M.; Quirk, R. P.; Halasa, A.; Mays, J. *Physical Review Letters* **2006**, *97*.
(42) Boukany, P. E.; Wang, S. Q. *Macromolecules* **2008**, *41*, 1455.
(43) Wang, S. Q.; Ravindranath, S.; Boukany, P. E. *Macromolecules* **2011**, *44*, 183.

Chapter 4

'LOCK AND KEY' HYDROPHOBIC SHAPE SPECIFIC INTERACTIONS DESIGNED INTO A SINGLE MODIFIED PEPTIDE MOLECULE 'LNK1'

4.1. Introduction

The hierarchical self-assembly of MAX1 β-hairpins into uniform fibrils can be attributed to several interactions. Facial hydrophobic interactions between the valine faces of two hairpins collapsed together form the cross-section of a growing fibril (Figure 4.1b). Additionally, lateral intermolecular hydrogen bonding and lateral hydrophobic interactions between folded hairpins define the axis of the growing fibrils[1]. After assembly, MAX1 forms self-standing hydrogel networks that are purely physically crosslinked. MAX1 has a relatively flat, uniform, hydrophobic face due to presence of only valine side chains. Due to this uniformity, the facial hydrophobic collapse at the core of the growing fibrils sometimes results in formation of a defect characterized by an incomplete burial of the hydrophobic valine side chains. Exposed valine face can lead to the nucleation of a branch point in the fibril growth leading to two daughter fibrils extending from the branch point. These branch points contribute to physical crosslinking of the hydrogel network in addition to fibrillar entanglement[2]. The defects in hydrophobic face packing of folded, opposing hairpins in a fibril, and the consequent branch point/new crosslink point that is formed, can be partially attributed to the lack of specificity in the facial hydrophobic interactions between

peptides due to the same steric volumes of the valine side chains. In this chapter, introduction of 'lock and key' type specificity in the facial hydrophobic interactions of the MAX1 peptide has been attempted with new peptide designs to limit the formation of branching crosslinks formed as a result of non-specific hydrophobic collapse.

Specific molecular recognition interactions between complimentary peptide and protein molecules have been used for designing smart responsive hydrogel materials. Examples of such efforts include materials based on specific interactions between coiled coil polypeptide domains such as leucine zipper domains[3-6], interactions between di-tryptophan (WW) and proline rich domains[7] and tetratricopeptide repeat (TPR)-peptide interaction[8]. A specific type of protein-protein interaction, named the 'Lock and Key' mechanism, involves recognition between molecules with complementary steric binding domains. Specific steric packing in ligand-receptor interactions[9,10], protein-DNA binding[11] and designed colloidal particles[12] has been studied but not toward designed materials development. The lock and key analogy was first put forward by Emil Fischer more than 100 years ago to describe specificity in enzyme-substrate interactions. One of the most widely studied shape dependent lock and key type interactions is the ligand protein interaction between the vitamin biotin and the egg white glycoprotein avidin, which is of tremendous interest in biotechnological applications[13]. Similarly, Holzinger et al. have reported complexation between biotin and β-cyclodextrin, as a representation of a new bioreceptor immobilization

affinity system[14]. Also widely reported shape-dependent recognition patterns involving proteins are interactions between proteins and DNA based on DNA local shape variations (individual base pair & minor double helix region) and DNA global shape variations (various helical topologies and deformations)[15]. The motivation towards introducing steric specificity to hydrophobic interactions in β-hairpin peptides is to explore whether designed changes to the shape of each β-hairpin molecule have a large effect on the overall self assembly properties and resulting hydrogel mechanical properties formed from the hairpins.

Several variants of MAX1 have been designed and studied previously. These variants have different primary sequences and have been developed to incorporate different functionalities such as faster gelation kinetics[16,17], photo-crosslinkable hydrophilic side chains[18], inherently anti-bacterial properties[19], swapped positions of hydrophobic and hydrophilic residues[1] etc. These functional variants have been designed by varying the hydrophilic side chains of MAX1. Each of these peptides has a non-specific valine hydrophobic face like MAX1. Thus, designed modifications to the hydrophobic face of MAX1 offer a new direction to the study of self-assembly and network behavior of the resulting peptides and have thus been attempted in the LNK1 peptide design.

4.2. Overview of the LNK1 Peptide Design

In the LNK1 peptide design (Nal)K(Nal)KAKAK-V^{D}PPT-KAKAK(Nal)K(Nal)-NH_2, the two end valine residues on each arm (Figure 4.1a)

of MAX1 (VKVKVKVK-V^{D}PPT-KVKVKVKV-NH_2) have been replaced by non-natural 2-napthylalanine (Nal) amino acid residues with a side chain of larger steric volume than valine (Figure 4.1d). The middle, non-turn valines of MAX1 have been replaced by alanine (A) residues with a side chain of smaller steric volume than valine (Figure 4.1e). Thus, two LNK1 hairpins can pack specifically into a lock and key type structure in the hydrophobic core (Figure 4.1f), disfavoring formation of branch points. This is in stark contrast to the possible incomplete burial of the valine side chains due to improper hydrophobic collapse in MAX1 leading to formation of a branch point[2] (Figure 4.1c). Thus, fibrils formed from LNK1 peptide self-assembly are intended to be unbranched (Figure 4.1g) as opposed to the branched fibrils of MAX1 (Figure 4.1c). We hypothesize that LNK1 fibrils form percolated networks only by fibril entanglement as opposed to the hydrogel networks of MAX1 that form a network due to fibril branching as well as entanglement. The local fibril nanostructure and ultimate hydrogel network structure, as characterized via a combination of physical characterization techniques such as circular dichroism (CD), transmission electron microscopy (TEM) and oscillatory rheological measurements, is discussed in the following section.

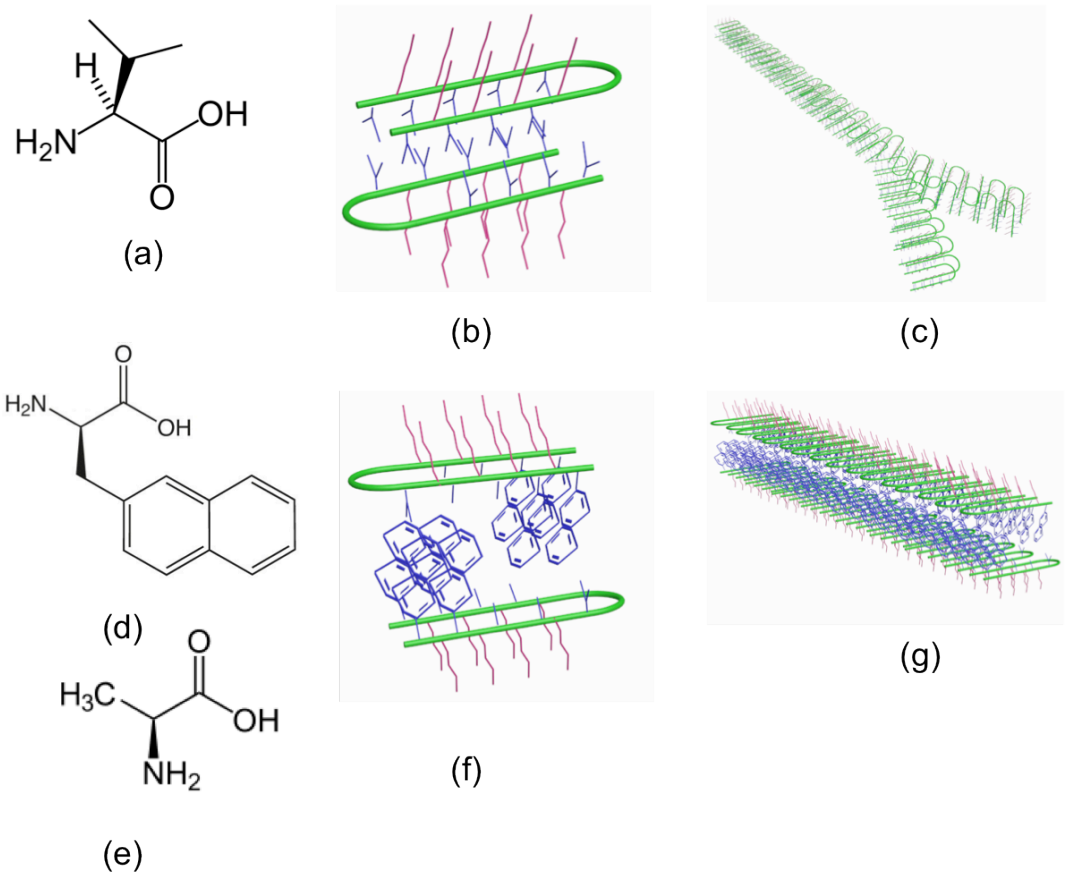

Figure 4.1. (a) Valine amino acids residue (b) Bilayer type fibril cross sectional structure from MAX1 (c) Defect-induced branch point in a MAX1 fibril (d) Napthylalanine amino acid residue (e) Alanine amino acid residue (f) Bilayer type structure from LNK1 (g) Homogenous unbranched LNK1 fibril.

4.3. Experimental Details of Rheological Characterization of MAX1 and LNK1 Hydrogels

Chapter 2 discusses experimental details of characterization techniques used to acquire data that have been discussed in this chapter. The paragraph below describes the advanced shear treatment applied to MAX1 and LNK1 network hydrogels to investigate potential differences in shear response of both the networks.

Characterization of network properties of both MAX1 and LNK1 networks was carried out using oscillatory frequency sweep measurements at a constant 1% strain. Prior to the frequency sweep measurements both hydrogel networks were allowed to assemble inside syringes by pulling buffered solutions (pH 9 125mM Boric Acid, 10mM NaCl) of both peptides into the syringes then maintained at 35°C. The hydrogels were then subjected to a multiple injection treatment that involved a sequential injection of MAX1 or LNK1 networks formed inside a syringe. Each gel was injected seven times through a 27-½ G needle. For future reference to this method within this chapter, it will be referenced to as the 'Injection Shear' treatment.

4.4. Results and Discussion

Peptides MAX1 and LNK1 were designed at the in the Pochan research group University of Delaware and synthesized and purifired by New England Peptide, LLC where mass spectrometry data confirming molecular weights of purified peptides were obtained.

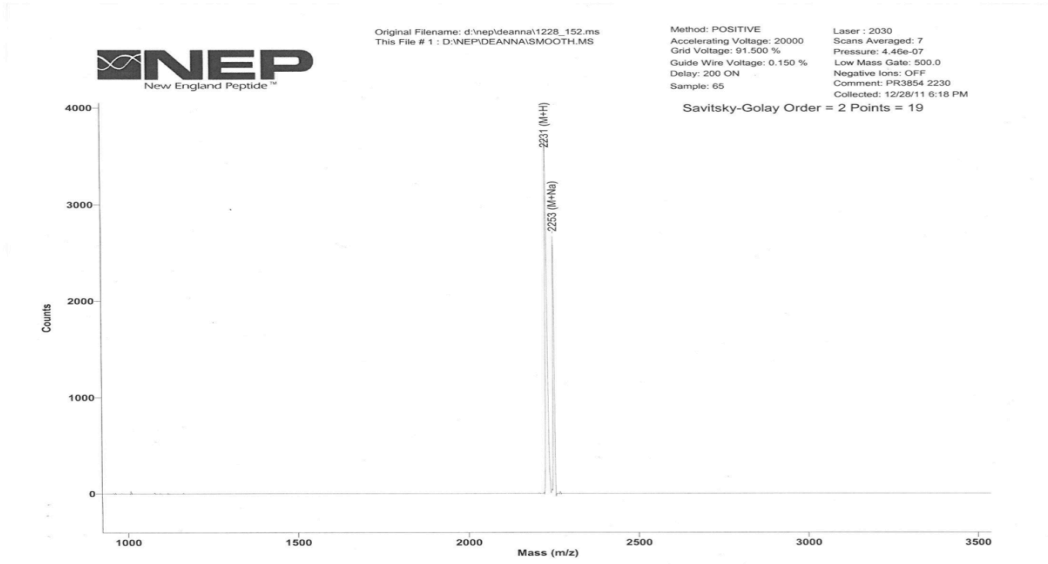

(a)

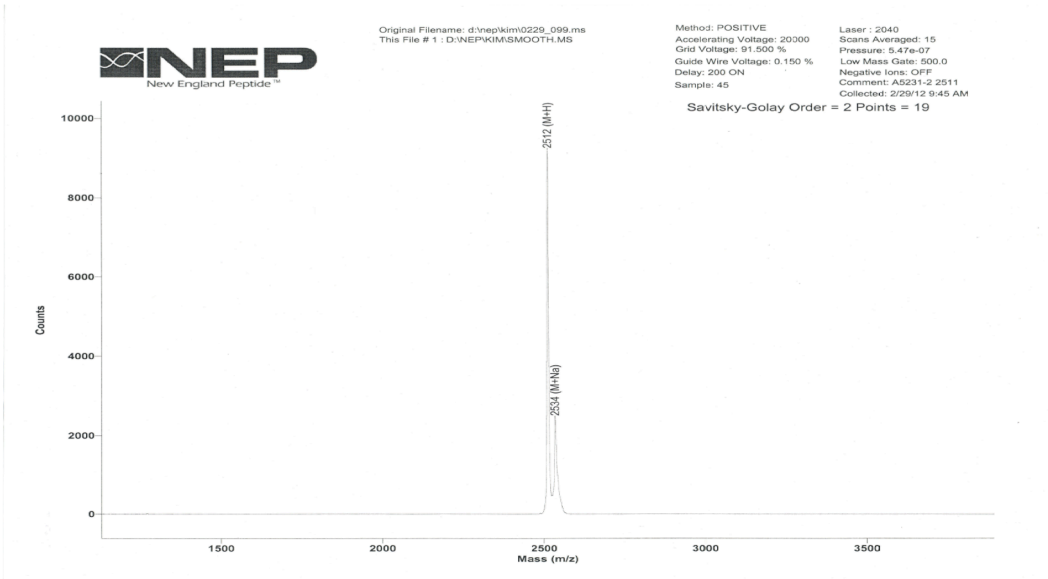

(b)

Figure 4.2. Matrix-assisted Laser Desorption Ionization Time of Flight (MALDI-TOF) Mass Spectral Analysis of peptides (a) MAX1 (b) LNK1 peptide used to confirm molecular weight of both peptide after purification. Data acquired by New England Peptide, LLC.

4.4.1. Circular Dichroism (CD)

CD data in Figure 4.4 show a similar folding transition temperature (~30°C) from random coil to β-sheet secondary conformation for both MAX1 and LNK1 under the same solution conditions (pH 9, 125mM Boric Acid, 10mM NaCl). These CD data are obtained by plotting mean residual ellipticity (MRE) at a fixed wavelength of 218 nm. This wavelength is chosen since this is the wavelength at which a minimum in the MRE values indicates formation of a β-sheet structure. Figure 4.3a shows variation of MRE as a function of wavelength for the MAX1 sample at different temperatures from 15°C to 60°C. Figure 4.3b shows the data collected in the same manner for the LNK1 sample. An unusual peak in the MRE values in the window of wavelengths from about 220 nm to 235 nm is observed in case of the LNK1 peptide but not for the MAX1 peptide. The presence of this peak in MRE values can be attributed to the contribution from the large aromatic groups of the napthylalanine side chain, which can potentially contribute to the scattering of incident radiation giving rise. The presence of such anomalous behavior in circular dichroism data from peptides containing large aromatic groups, phenylalanine in this particular case, has been reported by Lee et al[20]. The authors attribute this phenomenon to potential π-π stacking interactions between the aromatic groups. The similarity in folding temperature for both peptides offers evidence of β-sheet formation from LNK1 and hints at a possibly similar mechanism of folding and self-assembly of LNK1 compared to that of MAX1. In addition to having the same temperature as MAX1 of for folding of

into β-sheets, the CD data also indicate similarity in assembly kinetics of LNK1 compared to MAX1. Similar assembly kinetics for both peptides provides additional possibility of similar hydrogel network properties for LNK1 as those of MAX1.

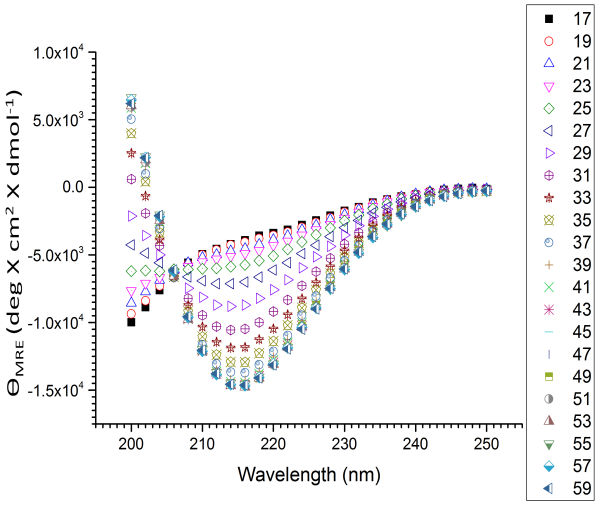

(a)

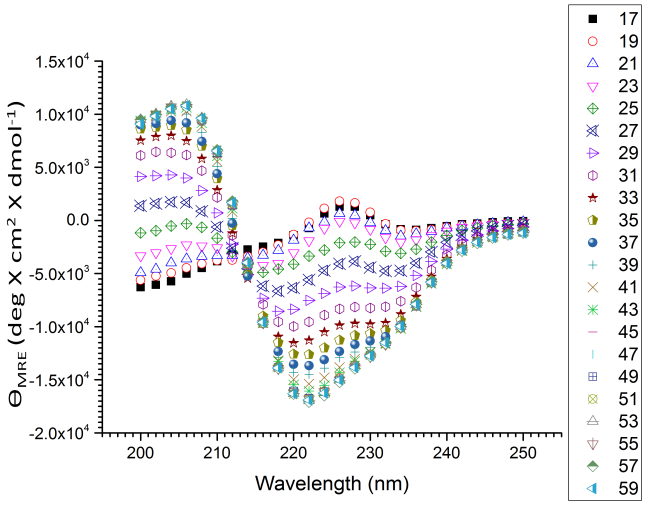

(b)

Figure 4.3. Mean residual ellipticity as a function of incident wavelength (200-250 nm) at different temperatures (°C), indicated in the column to the right for (a) MAX1 (b) LNK1 both at 150μM concentration in solution conditions pH 9 (125mM Boric Acid, 10mM NaCl)

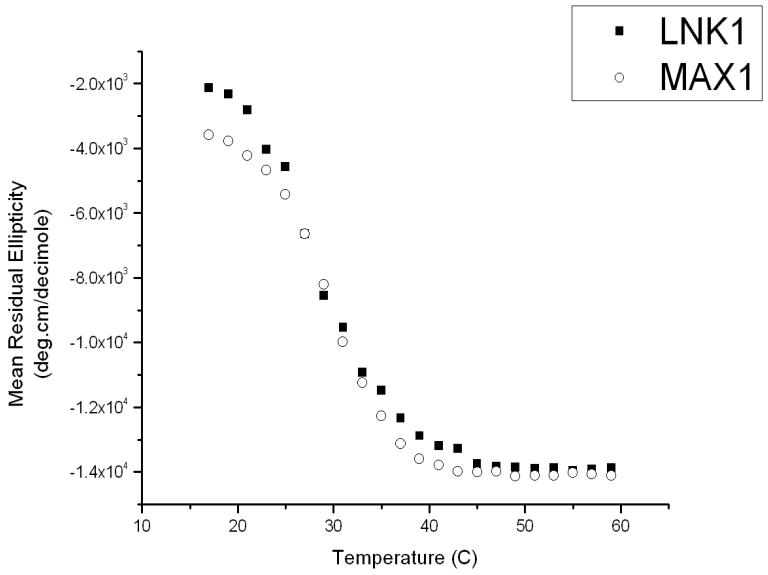

Figure 4.4. Circular Dichroism data (Mean Residual Ellipticity in deg.cm/decimole at 218 nm v/s Temperature °C) showing approximately same temperature of folding transition (~30°C) from random coil to β-sheet secondary conformation for both MAX1 and LNK1.

4.4.2. Transmission Electron Microscopy (TEM)

TEM characterization helps in comparing the nanostructures formed from the assembly of both peptides MAX1 and LNK1. The local nanostructure for both MAX1 and LNK1 is very similar, in particular the fibril thickness as observed by TEM (Figure 4.5a and 4.5b). Both peptides assemble into fibrils with uniform width of approximately 3 nm. The histograms accompanying the micrographs indicate frequency distributions of fibrillar thickness values of 15 fibrils from the corresponding micrograph. This similarity in the MAX1 and LNK1 fibril morphology indicates the two peptides assemble into similar fibrils with a two-peptide cross-section and hydrophobic core. Thus, the TEM data provide

additional evidence for the lock and key interactions working in LNK1 as hypothesized which ultimately form a nanostructure extremely similar to MAX1, in terms of fibrillar width.

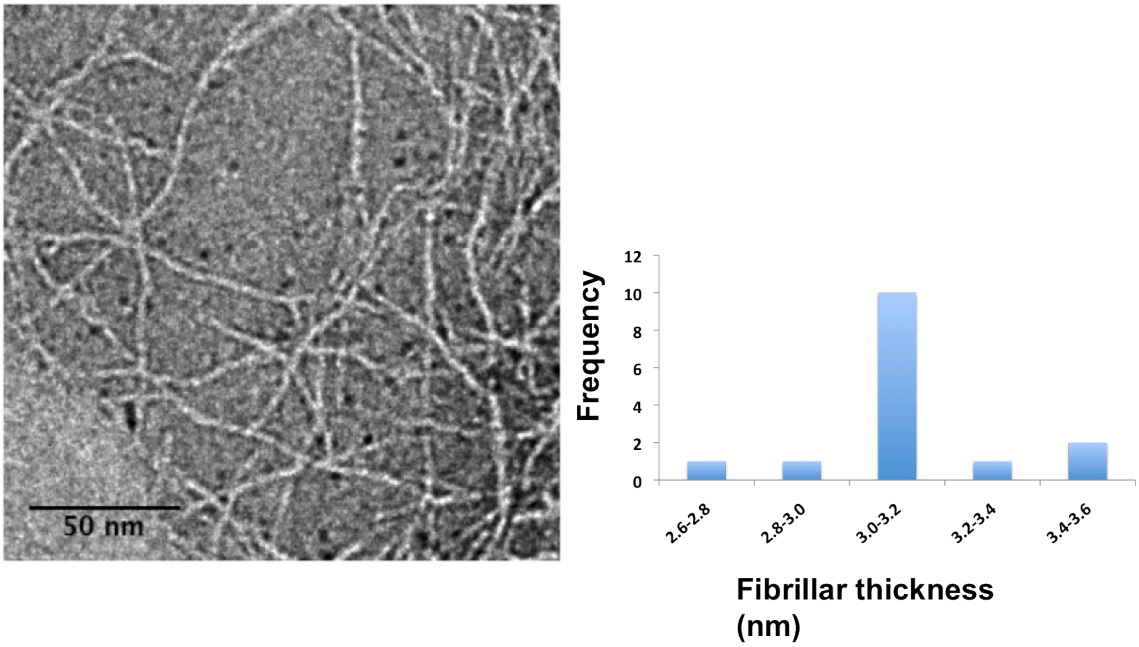

(a)

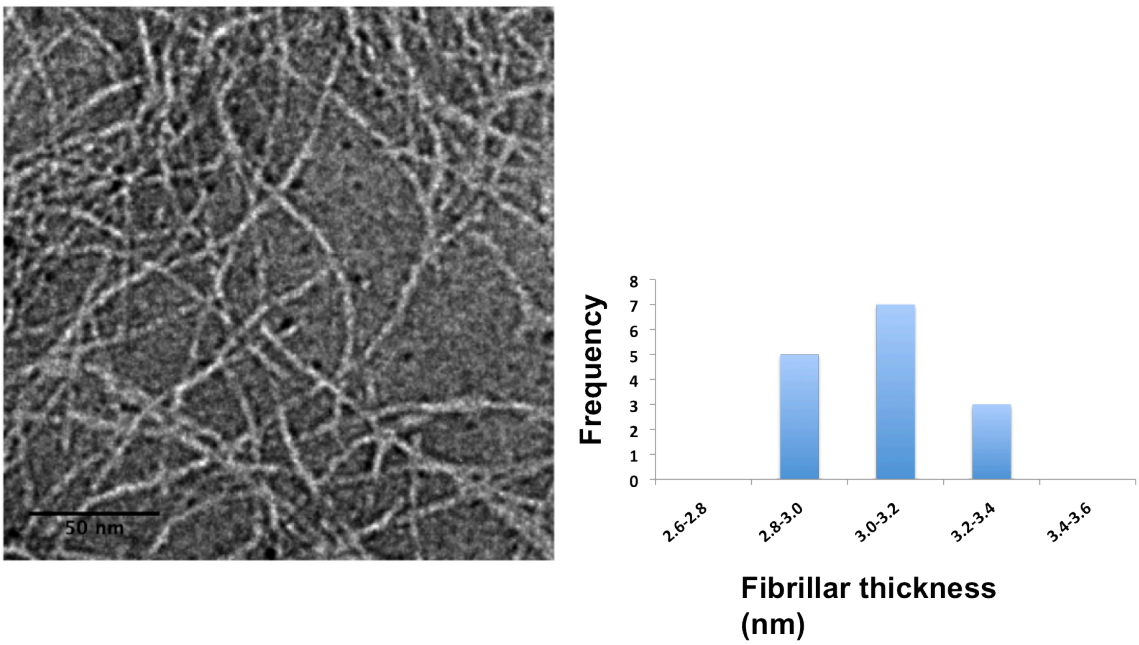

(b)

Figure 4.5: Transmission electron micrographs from (a) MAX1 and (b) LNK1 developed under the solution conditions pH 7 (50mM BTP, 150 mM NaCl) and negatively stained with 1 % (w/v) uranyl acetate solution in deionized water. Histograms accompanying the micrographs indicate frequency distributions of fibrillar thickness values of 15 fibrils from the corresponding micrograph.

Solid MAX1 hydrogels exhibit a unique property of undergoing shear thinning and flow under an applied shear stress (outside of the material linear viscoelastic regime) but immediately recovering into solid gels on cessation of shear. An earlier study by Yan et al.[21] exploring the hydrogel behavior during and after flow indicated the gel networks fracture into domains much larger than the length scale of individual fibrils in order to flow. The network morphology within gel domains during flow was structurally identical to the parent network at rest; the peptide fibrils displayed the same cross-section, the same physical

crosslinking points of fibrillar entanglement and branching and the same porosity. On cessation of shear, the large gel domains immediately percolate and form a bulk, hydrogel network. This shear-thinning and rehealing behavior of MAX1 would not exist if the network disintegrated into individual fibrils during flow since there would be no immediate mechanism for the fibrils to recrosslink (i.e. rebranch and reentangle) and percolate into a bulk network. The hypothesis is that the frequent fibrillar branching during MAX1 assembly is key to this shear-thinning but immediate network reformation behavior. If the network were composed of fibrils with only physical entanglements for crosslinks, the shear flow would disentangle the fibrils, thus obviating the network after shear. However, the branching causes the network to fracture into large domains of intact network structure in response to shear that does not allow the simple disentanglement of peptide fibril physical crosslinks during shear flow.

If the fibril branching in MAX1 is responsible for the observed shear thinning an immediate gel reformation behavior, then eliminating most fibril branching from the system should significantly affect the hydrogel flow properties. As mentioned earlier, the design of steric specificity in the hydrophobic core of the LNK1 fibrils was an attempt to produce lock and key type interactions and, ideally, preclude fibrillar branching. Thus, a very different shear response is expected when LNK1 hydrogel networks, presumably held together with physical entanglements as crosslinks, are subject to the exact same shear treatment as the MAX1 networks.

To explore the rheological response of MAX1 and LNK1 networks to shear and flow, self-assembled hydrogels from LNK1 or MAX1 were produced at a concentration of 0.5 % (w/v) at pH 9 (125mM Boric Acid, 10mM NaCl). Under these conditions both hydrogels show similar pre-shear behavior with G'>>G" (Pa). Figure 4.6a shows the shear thinning and recovery character of MAX1 hydrogels in which a MAX1 gel was subjected to intense steady state shear of 1000 rad/s for 120 sec. Upon cessation of shear, the hydrogel immediately showed solid gel properties (G' value of 75 Pa >>G") and quickly recovered to almost the same value of storage modulus (G', Pa) of the preshear, parent MAX1 network (~250 Pa) after several hours. In stark contrast, when an LNK1 network, formed with the same solution conditions as the MAX1 hydrogel network, was subject to the identical shear treatment, it immediately displayed very weak hydrogel network properties (G' of 5 Pa >G") and failed to recover to even 10% of its original modulus value after several hours (Figure 4.6b). The LNK1 design was meant to prevent branching of the peptide fibrils during assembly. Therefore, the shear treatment destroyed the physical entanglements between LNK1 fibrils that were unable to reform in any significant way on cessation of shear. This lack of rehealing upon cessation of shear is a very different shear response by the LNK1 hydrogel network that will be discussed later in this section.

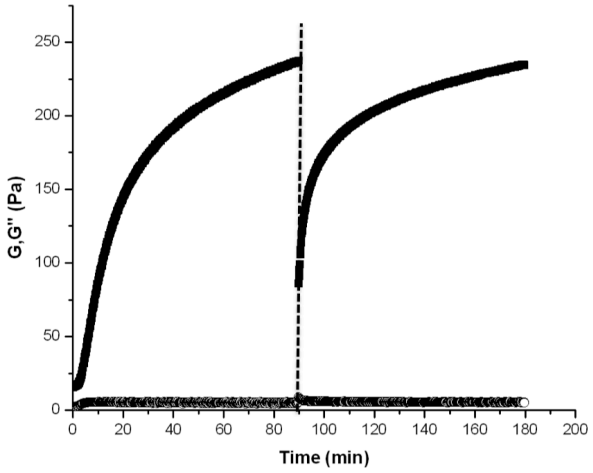

(a)

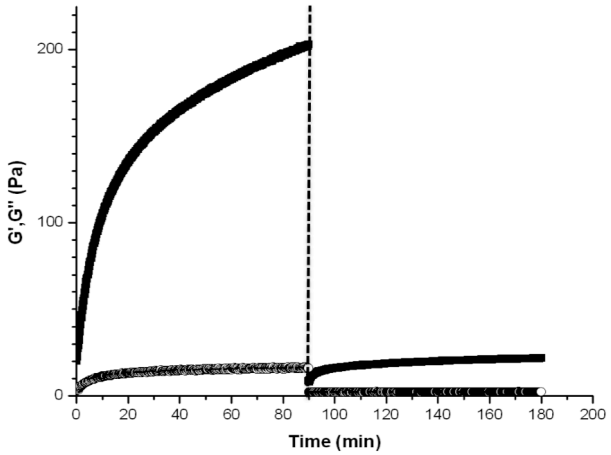

(b)

Figure 4.6. Oscillatory Time sweep measurements before and after application of steady state shear (1000/s for 120 sec, indicated by dotted line) on 0.5 % (w/v) (a) MAX1 (b) LNK1 networks under the same solution conditions (pH 9 125mM Boric Acid 10mM NaCl) (Solid squares indicate G' (Pa) and open circles G'' (Pa))

The data in Figure 4.6b indicate a significant reduction in the value of the storage modulus, G' (Pa), in case of the LNK1 networks after a simple steady shear treatment inside the rheometer showing a strong reduction of network like properties of the LNK1 networks. In order to more closely mimic conditions of potential clinical usage such as syringe or catheter injection, both LNK1 and MAX1 hydrogels were subject to the syringe injection shear treatment as described in the Experimental section in this chapter. The oscillatory frequency sweep data in Figure 4.7b reveals a complete elimination of hydrogel network properties of LNK1 networks, post injection shear treatment. The LNK1 samples show a greater value of the loss modulus, G", as compared to the storage modulus, G', with G">G' (Pa) at all frequencies. This is a clear signature of a material that is not a percolated hydrogel network but rather is a particulate suspension or molecular solution. In stark contrast, MAX1 materials retain hydrogel network properties even after the injection shear treatment with G'>>G" (Pa) at all frequencies. The transmission electron micrograph in Figure 4.7d shows the morphology of the LNK1 networks at the end of the injection shear treatment. Observed fibrillar bundle-like nanostructures are much wider (~10-15 nm) and non-uniform than the pre-shear treatment LNK1 fibrils shown in Figure 4.5b. The existence of these bundled structures can be attributed to fibrillar stacking in LNK1 samples as a result of the intense injection shear treatment that caused disentanglement of the original percolated LNK1 network. Once in these stacks, the fibrils no longer contribute to network properties and no longer form

physical crosslinks through entanglements. The MAX1 local nanostructure at the end of the exact same shear injection treatment (Figure 4.7c) is very similar to the MAX1 fibrils seen pre-treatment in Figure 4.5a. The oscillatory frequency sweep measurements carried out on the MAX1 networks clearly indicate a gel-like response from MAX1 networks post-shear injection treatment. MAX1, whose hydrophobic face is composed entirely of valine side chains that have the same side chain volume, demonstrates fibrillar branching and, thus, a bulk hydrogel network of MAX1 subject to shear treatment reheals into a fully percolated network when shear is stopped. Even the nanostructure of the MAX1 network before and after shear treatments is the same. In case of the LNK1 peptides with a designed specificity in the hydrophobic face, fibrillar branching is severely limited, and the rehealing properties of bulk LNK1 hydrogels subject to shear are completely eliminated. Even the nanostructure undergoes a significant change from individual fibrils to a bundled structure. Thus, designed hydrophobic specificity clearly affects the self-assembled hydrogel properties.

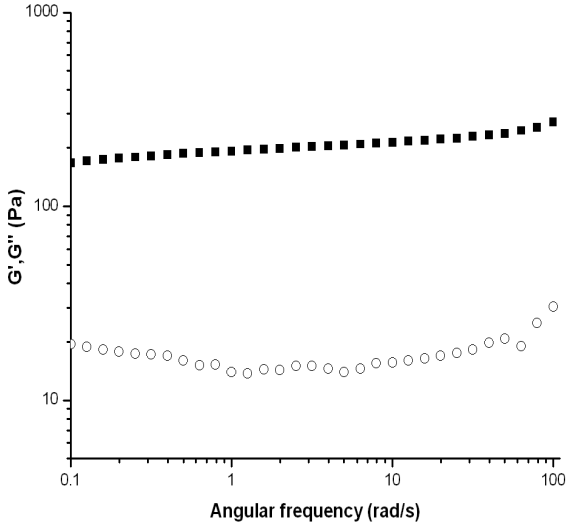

(a)

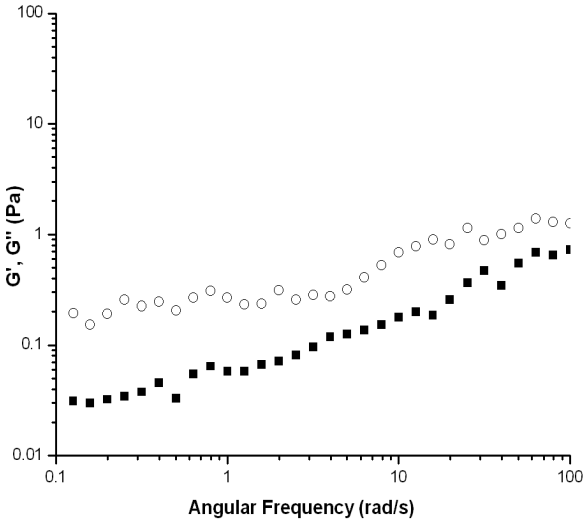

(b)

Figure 4.7. (cntd)

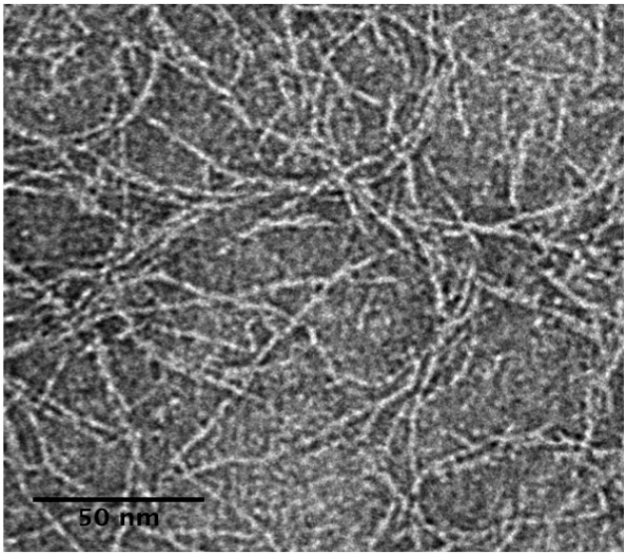

(c)

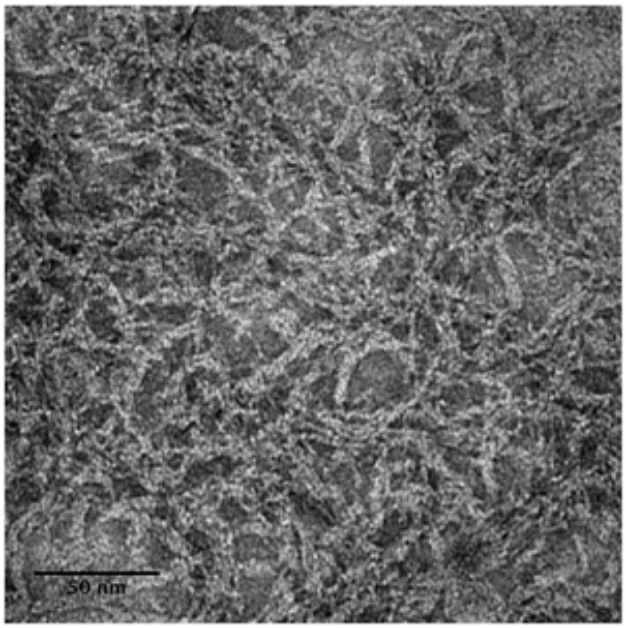

(d)

Figure 4.7. Oscillatory frequency sweep (a) MAX1 (b) LNK1 measurements after application of shear treatment to both networks formed under the same solution conditions (pH 9 125mM boric acid 10mM NaCl) (Solid squares indicate G' (Pa) and open circles G" (Pa)). Transmission electron micrographs (c) MAX1 (d) LNK1 post injection shear treatment

4.5. Conclusion

The LNK1 peptide design employs a steric lock and key specificity in the hydrophobic core of the β–sheet fibrils formed by the peptide. Experimentally, vast differences in the network properties of the hydrogels formed by the LNK1 peptide were observed as against those shown by the hydrogels formed from MAX1 peptide. The first prominent difference was the lack of recovery of storage modulus G' (Pa) values from the LNK1 network after the brief application and cessation of in-situ steady state shear. In addition to this, sequential multiple injections applied to the networks as a means of shear treatment were instrumental in complete elimination of network properties of the LNK1 networks. Experimental results from circular dichroism, transmission electron microscopy and oscillatory rheology help conclude that it is the molecular design of the LNK1 peptide that can be attributed to the drastically different behavior of the networks due to hydrophobic packing specificity and the consequent limitation of fibril branching.

REFERENCES

(1) Rajagopal, K.; Ozbas, B.; Pochan, D. J.; Schneider, J. P. *European Biophysics Journal with Biophysics Letters* **2006**, *35*, 162.

(2) Yucel, T.; Micklitsch, C. M.; Schneider, J. P.; Pochan, D. J. *Macromolecules* **2008**, *41*, 5763.

(3) Shen, W.; Lammertink, R. G. H.; Sakata, J. K.; Kornfield, J. A.; Tirrell, D. A. *Macromolecules* **2005**, *38*, 3909.

(4) Jing, P.; Rudra, J. S.; Herr, A. B.; Collier, J. H. *Biomacromolecules* **2008**, *9*, 2438.

(5) Papapostolou, D.; Smith, A. M.; Atkins, E. D. T.; Oliver, S. J.; Ryadnov, M. G.; Serpell, L. C.; Woolfson, D. N. *Proceedings of the National Academy of Sciences of the United States of America* **2007**, *104*, 10853.

(6) Petka, W. A.; Harden, J. L.; McGrath, K. P.; Wirtz, D.; Tirrell, D. A. *Science* **1998**, *281*, 389.

(7) Foo, C.; Lee, J. S.; Mulyasasmita, W.; Parisi-Amon, A.; Heilshorn, S. C. *Proceedings of the National Academy of Sciences of the United States of America* **2009**, *106*, 22067.

(8) Grove, T. Z.; Osuji, C. O.; Forster, J. D.; Dufresne, E. R.; Regan, L. *J. Am. Chem. Soc.* **2010**, *132*, 14024.

(9) Schwyzer, R. *Biopolymers* **1995**, *37*, 5.

(10) Helm, C. A.; Knoll, W.; Israelachvili, J. N. *Proceedings of the National Academy of Sciences of the United States of America* **1991**, *88*, 8169.

(11) Sprules, T.; Green, N.; Featherstone, M.; Gehring, K. *Journal of Biological Chemistry* **2003**, *278*, 1053.

(12) Sacanna, S.; Irvine, W. T. M.; Chaikin, P. M.; Pine, D. J. *Nature* **2010**, *464*, 575.

(13) Wilchek, M.; Bayer, E. A. *Anal. Biochem.* **1988**, *171*, 1.

(14) Holzinger, M.; Singh, M.; Cosnier, S. *Langmuir* **2012**, *28*, 12569.

(15) Rohs, R.; Jin, X. S.; West, S. M.; Joshi, R.; Honig, B.; Mann, R. S. In *Annual Review of Biochemistry, Vol 79*; Kornberg, R. D., Raetz, C. R. H., Rothman, J. E., Thorner, J. W., Eds.; Annual Reviews: Palo Alto, 2010; Vol. 79, p 233.

(16) Haines-Butterick, L.; Rajagopal, K.; Branco, M.; Salick, D.; Rughani, R.; Pilarz, M.; Lamm, M. S.; Pochan, D. J.; Schneider, J. P. *Proceedings of the National Academy of Sciences of the United States of America* **2007**, *104*, 7791.

(17) Rajagopal, K.; Lamm, M. S.; Haines-Butterick, L. A.; Pochan, D. J.; Schneider, J. P. *Biomacromolecules* **2009**, *10*, 2619.

(18) Rughani, R. V.; Branco, M. C.; Pochan, D.; Schneider, J. P. *Macromolecules* **2010**, *43*, 7924.

(19) Salick, D. A.; Kretsinger, J. K.; Pochan, D. J.; Schneider, J. P. *J. Am. Chem. Soc.* **2007**, *129*, 14793.
(20) Lee, N. R.; Bowerman, C. J.; Nilsson, B. L. *Biomacromolecules* **2013**, *14*, 3267.
(21) Yan, C. Q.; Pochan, D. J. *Chemical Society Reviews* **2010**, *39*, 3528.

Chapter 5

ANALYSIS OF SHAPE SPECIFIC HYDROPHOBIC INTERACTIONS IN BLENDS OF COMPLEMENTARY 'WEDGE' AND 'TROUGH' SHAPED β-HAIRPIN PEPTIDES

5.1. Introduction

The facial and lateral hydrophobic interactions have a profound influence on the self-assembly kinetics, fibrillar nanostructure and network rheological properties of the MAX1 peptide[1,2]. In the previous chapter it was discussed that design of shape specific interactions in the hydrophobic core of assembling β-hairpin peptides can be introduced by making suitable design changes to the primary structure of MAX1, yielding the LNK1 peptide sequence. This chapter discusses the effects of introducing shape specificity to the hydrophobic face of three newly designed pairs of β-hairpin peptides based on the original MAX1 sequence. The design idea is to study potential shape specific interactions in the hydrophobic face when complementarily shaped pairs of peptides are blended in an equal ratio by mass and allowed to co-assemble. The pairs of peptides LP1-KP1, LP2-KP2 and LP3-KP3 have an increasing gradient of local hydrophobic shape as shown in Figure 5.1, causing them to resemble a wedge shape (in case of LP1, LP2 and LP3) and a trough shape (in case of KP1, KP2 and KP3), which provide opportunities for shape complementary wedge-trough type of interaction as shown in Figure 5.1.

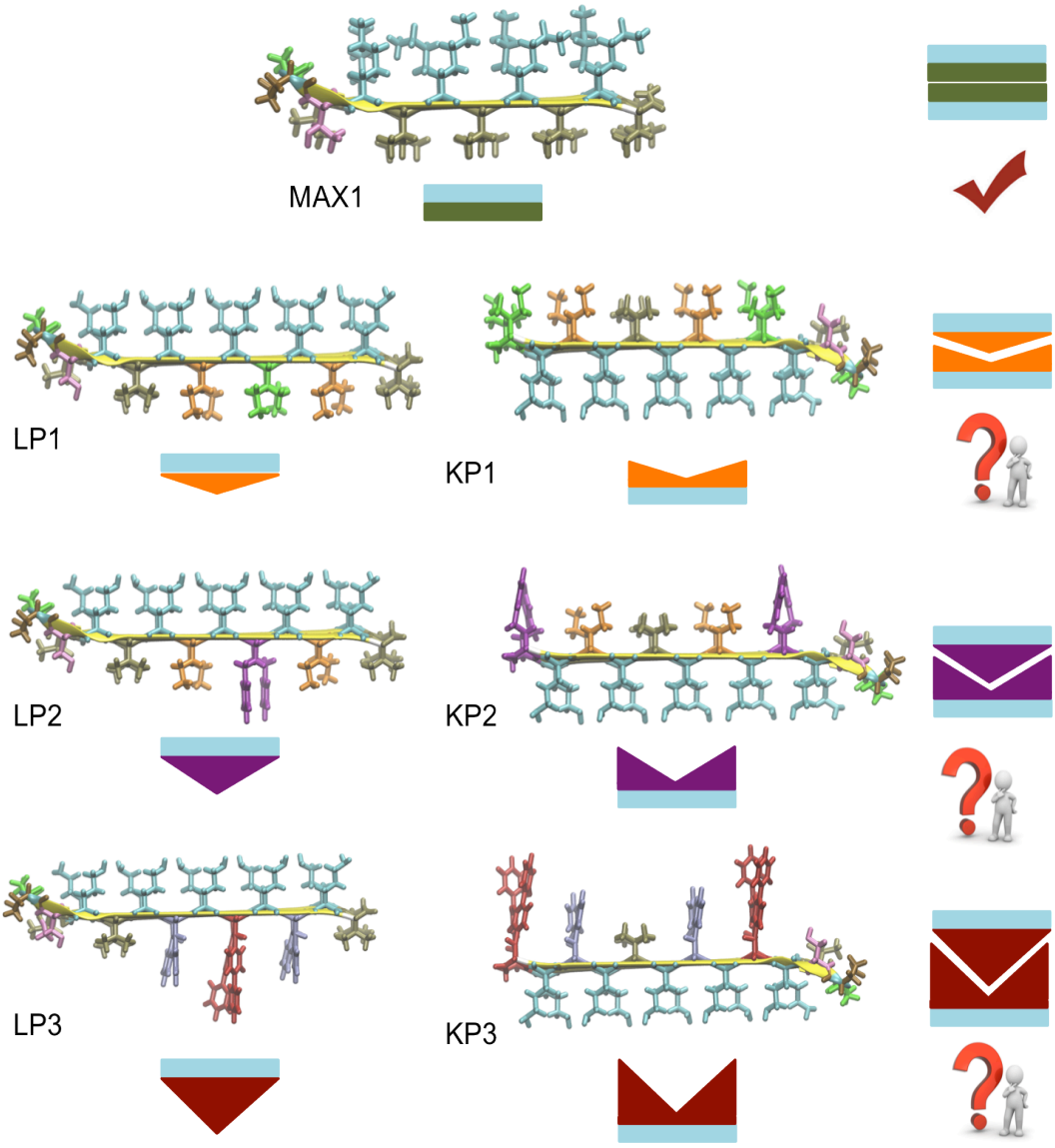

Figure 5.1. Schematic side-view (parallel with peptide backbone) representations of the peptides MAX1, LP1, KP1, LP2, KP2, LP3 and KP3 when folded into a ß-hairpin conformation and potential shape specific interactions, forming a bilayer-type fibril cross-section structure as shown on the right.

In order to achieve shape-specific patterns in the hydrophobic face, these peptides contain 24 residues (longer than the original MAX1 peptides consisting of 20 residues). The valine groups are selectively substituted with residues with sterically larger or smaller hydrophobic side chains on both arms of the hairpins flanking the $-V^{D}PPT-$ turn sequence. It is desired that the overall hydrophobic character of the designed peptides is similar to that of MAX1 for the purpose of having similar solution conditions for solution assembly, particularly close to room temperature assembly. The lysine residues on the hydrophilic face in MAX1 were replaced by ornithine residues that have slightly less hydrophobic side chains (3 side chain methylene groups as compared to 4 methylene groups) in lysine. This design change was intended to offset the higher hydrophobicity of the larger hydrophobic side chain residues replacing valine. Rajagopal[3] has discussed the effect of lysine replacement in MAX1 peptide by three different non-natural amino acids with decreasing number of methylene groups in the hydrophilic amino acid side chains. Replacement of lysine with ornithine does not significantly alter the solution conditions for β-sheet formation and self-assembly as compared to MAX1. The same report discusses that peptides that contain shorter hydrophilic side chains with none or one methylene group undergo self-assembly in much lower pH conditions as compared to MAX1 due to more entropic ease of the shorter side chains to find optimum positions for minimum electrostatic repulsion and β-hairpin formation. The sequences of the designed peptides are as shown in Scheme 5.1. Self-assembly of peptides with their entire

hydrophobic face replaced by non-natural amino acids some of which have been used in designing and synthesizing the new wedge and trough shaped peptides (norvaline and isolecuine) have been explored by Micklitsch[4]. The overall hydrophobicity of the peptides was reported to significantly influence solution conditions required for the peptide self-assembly, nanostructure and hydrogel mechanical properties from the peptides. Due to the hypothesized shape-specific interactions in the hydrophobic core of the fibrils assembled from a 1:1 (w/w) blend of the pairs of the peptides, the fibrils from these blends are expected to be unbranched as compared to the branched fibrils of MAX1, similar to the fibrils assembled from the LNK peptides discussed in Chapter 4. The hypothesis is that 1:1 blends of the new pairs of peptides would form fibrillar percolated networks only by fibril entanglement as opposed to the hydrogel networks of MAX1 that are formed due to fibril branching as well as entanglement. This chapter provides an insight to the assembly behavior of the newly designed peptides and their 1:1 blends, the assembled fibril nanostructure and ultimate hydrogel network structure via a combination of physical characterization techniques: circular dichroism (CD), cryogenic transmission electron microscopy (TEM), oscillatory rheological measurements, and small angle neutron scattering (SANS).

LP1: H2N-V(O)(Nva)(O)(I)(O)(Nva)(O)V(O)-V(dP)PT-(O)V(O)(Nva)(O)(I)(O)(Nva)(O)V-Am
KP1: H2N-(I)(O)(Nva)(O)(V)(O)(Nva)(O)(I)(O)-V(dP)PT-(O)(I)(O)(Nva)(O)(V)(O)(Nva)(O)(I)-Am

LP2: H2N-V(O)(Nva)(O)(hF)(O)(Nva)(O)V(O)-V (dP)PT-(O)V(O)(Nva)(O)(hF)(O)(Nva)(O)V-Am
KP2: H2N-(hF)(O)(Nva)(O)(V)(O)(Nva)(O)(hF)(O)-V (dP)PT-(O)(hF)(O)(Nva)(O)(V)(O)(Nva)(O)(hF)-Am

LP3: H2N-V(O)(hF)(O)(BiP)(O)(hF)(O)V(O)-V(dP)PT-(O)V(O)(hF)(O)(BiP)(O)(hF)(O)V-Am
KP3: H2N-(BiP)(O)(hF)(O)(V)(O)(hF)(O)(BiP)(O)-V(dP)PT-(O)(BiP)(O)(hF)(O)(V)(O)(hF)(O)(BiP)-Am

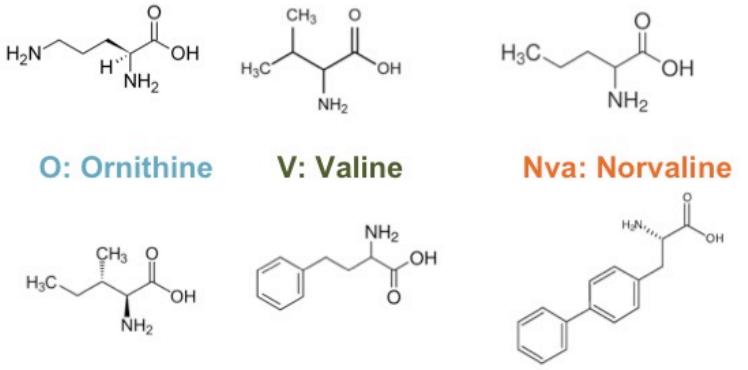

Scheme 5.1. Primary amino a cid sequences of the individual peptides LP1, KP1, LP2, KP2, LP3 and KP3.

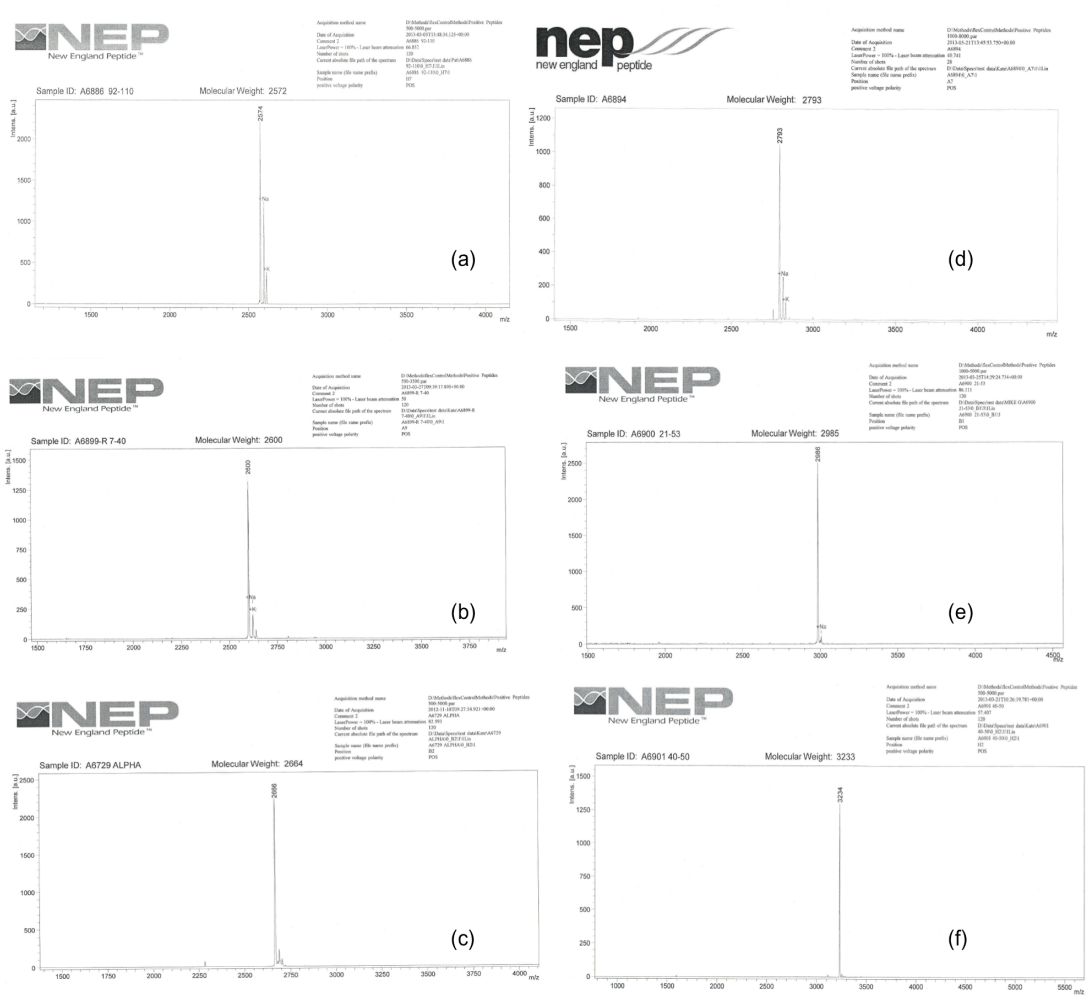

Figure 5.2. Matrix-assisted Laser Desorption Ionization Time of Flight (MALDI-TOF) Mass Spectral Analysis of peptides (a) LP1 (b) KP1 (c) LP2 (d) KP2 (e) LP3 (f) KP3 confirming appropriate molecular weight of the peptide synthesized by Solid Phase Peptide Synthesis.

5.2. Results and Discussion

5.2.1. Circular Dichrosim (CD)

Newly designed peptides are designed to have an increasingly steep gradient of the wedge shape (in the order LP1, LP2 and LP3) and trough shape (in the order KP1, KP2 and KP3) as shown in Figure 5.1. Molecular weights of the peptides synthesized using solid phase peptide synthesis were confirmed by Matrix-assisted Laser Desorption Ionization Time of Flight (MALDI-TOF) and are shown in Figure 5.2. The peptides were bought from New England Peptide LLC (Gardener, MA) where they obtained the MALDI-TOF data to confirm appropriate synthesis of designed peptides. CD experiments were performed to investigate folding, potential β-sheet formation and the corresponding solution conditions. β-sheet formation from a peptide or protein sample is indicated by presence of a minimum in the mean residue ellipticity (MRE) value in the range from 216 nm to 222 nm[5]. MRE values in deg·cm^2/decimole were measured in the window of wavelengths from 190 nm to 250 nm. An increase in ionic strength and pH serves to screen and deprotonate the primary amino groups on the ornithine side chains in the newly designed peptides, thus triggering folding of the peptides from a random coil conformation to a β-hairpin structure. Temperature serves as another mode of stimulus that aides the random coil-to-β-hairpin conformational change. Higher temperatures enhance hydrophobic interactions between the hydrophobic side chain containing amino acids, leading to faster folding and assembly of the peptides. Thus, peptides with greater overall

hydrophobic nature than others fold at comparatively lower temperatures under the same solution conditions. Mean residue ellipticity measurements at different temperatures help determine the exact folding temperatures of the newly designed peptides under the solution conditions chosen for assembly.

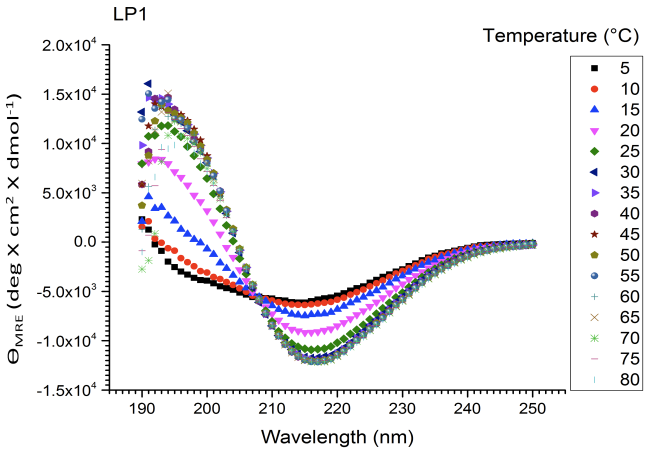

(a)

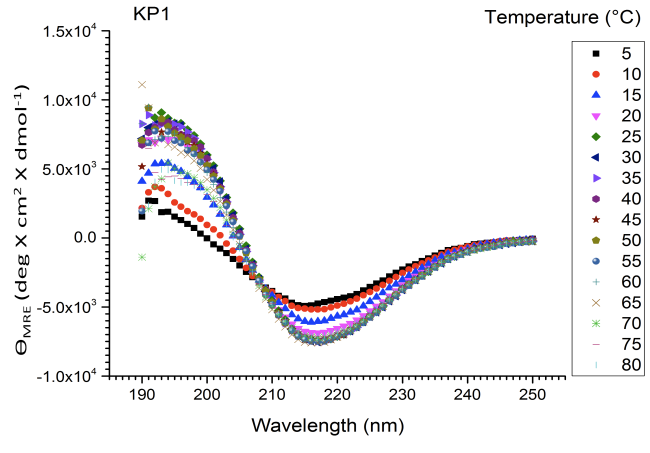

(b)

Figure 5.3 (cntd)

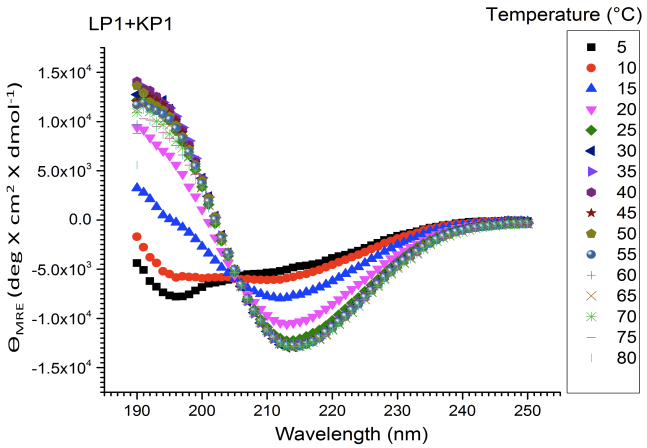

(c)

Figure 5.3. Circular dichroism data (mean residue ellipticity in deg.cm^2/decimole vs. wavelength (nm) (190 nm-250 nm) at different temperatures from 5°C to 80°C. showing changes in secondary structure from random coil to β-sheet secondary conformation at 150μM concentration overall at solution conditions pH 9 (125 mM boric acid, 10 mM NaCl) for (a) LP1 (b) KP1 (c) LP1:KP1 1:1 (w/w) blend.

Figures 5.3 shows the MRE values calculated across a window of wavelengths from 190 nm through 250 nm at increasing temperatures from 5°C through 80°C for the samples from peptides LP1, KP1 and LP1:KP1 1:1 blend. A minimum in the MRE values in the wavelength range of 216nm to 218 nm for LP1 and KP1 samples is obtained (Figure 5.3a and 5.3b). The minimum is obtained in case of the LP1:KP1 1:1 (w/w) blend in the range of 213 nm to 216 nm (Figure 5.3c).

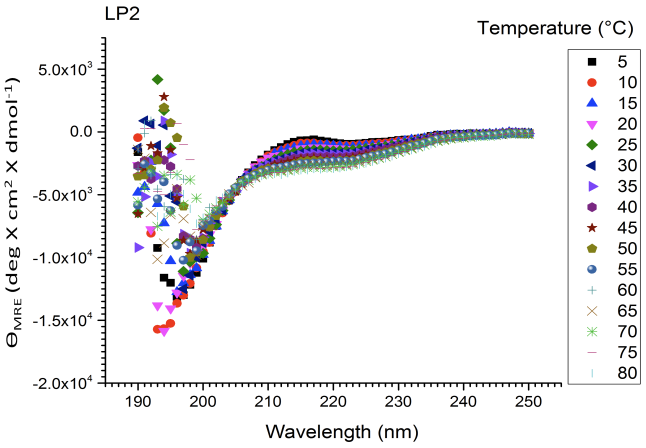

(a)

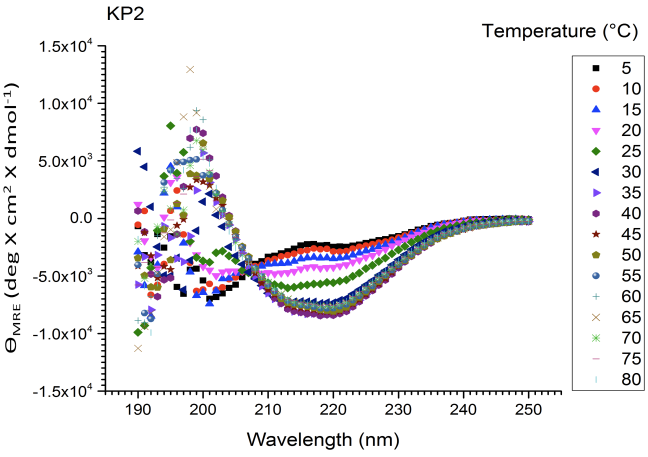

(b)

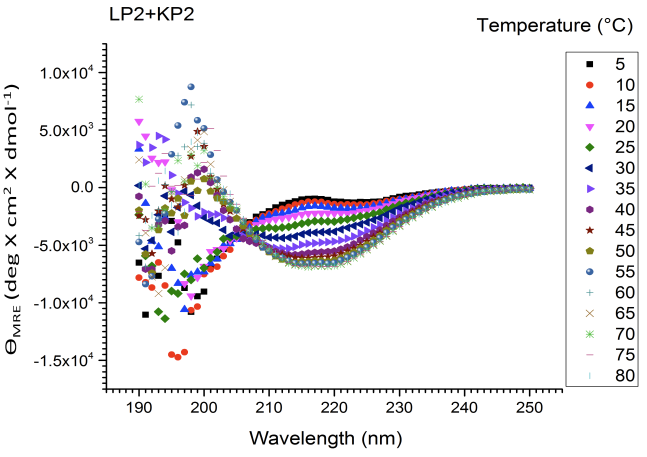

(c)

Figure 5.4 (cntd)

Figure 5.4. Circular dichroism data (mean residue ellipticity in deg.cm^2/decimole vs. wavelength (nm) (190 nm-250 nm) at different temperatures from 5°C to 80°C. showing changes in secondary structure from random coil to β-sheet secondary conformation at 150μM concentration overall at solution conditions pH 7 (50 mM BTP, 150 mM NaCl) for (a) LP2 (b) KP2 (c) LP2:KP2 1:1 (w/w) blend.

Figure 5.4. shows the data obtained from the group of samples LP2, KP2, LP2:KP2 1:1 (w/w) using the same experimental procedure. The solution conditions chosen for the samples LP1, KP1 and LP1: KP1 1:1 (w/w) are pH 9 (125 mM Boric Acid, 10 mM NaCl). The LP2 and KP2 peptides are more hydrophobic than the LP1 and KP1 peptides. Therefore, the solution conditions chosen for the samples LP2, KP2 and LP2: KP2 1:1 (w/w) are at the lower pH 7 (50 mM BTP, 150 mM NaCl). A lower pH presents a stimulus of a weaker magnitude for self-assembly as compared to the higher pH solution conditions chosen for the less hydrophobic LP1 and KP1 peptides. As seen in Figure 5.4b and Figure 5.4c minima in the MRE values in the wavelength range of 216nm to 218 nm are obtained for the samples KP2 and LP2:KP2 1:1 (w/w). A very weak minimum in the same wavelength range of 216 nm to 218 nm is obtained for the LP2 peptide in Figure 5.4a, indicating a very weak β-sheet structure formation in this peptide alone. This weak β-sheet structure formation from the LP2 peptide can be attributed to its overall lesser hydrophobicity as compared to the KP2 peptide. A sample of LP2:KP2 1:1 (w/w) blend shows β-sheet formation

comparable to that shown by the KP2 peptide, which is much stronger than that shown by the LP1 peptide.

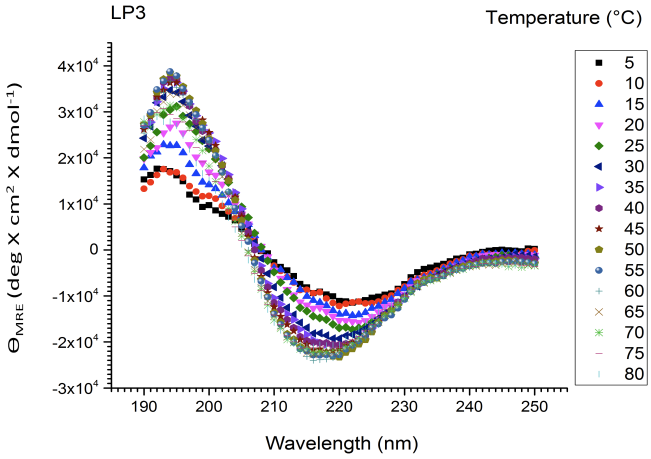

(a)

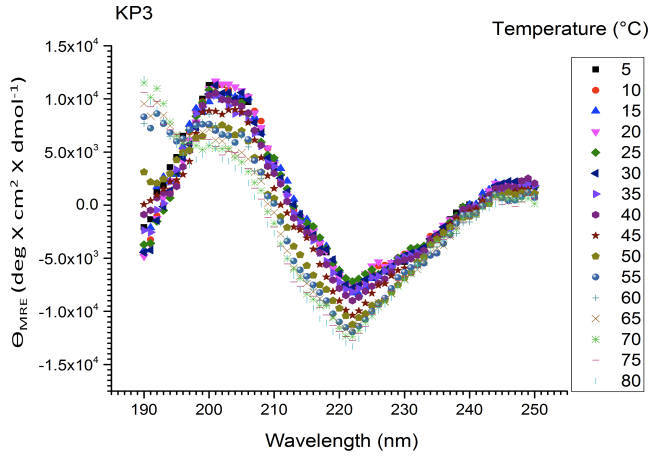

(b)

Figure 5.5 (cntd)

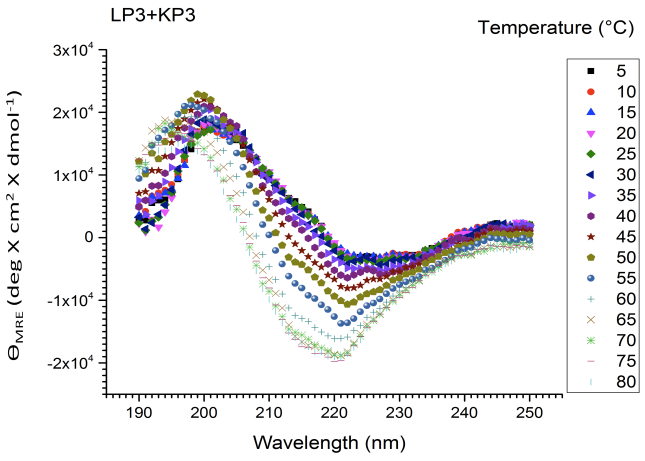

(c)

Figure 5.5. Circular dichroism data (mean residue ellipticity in deg.cm^2/decimole v/s wavelength (nm) (190 nm-250 nm) at different temperatures from 5°C to 80°C. showing changes in secondary structure from random coil to β-sheet secondary conformation at 150μM concentration overall at solution conditions pH 7 (50 mM BTP, 50 mM NaCl) for (a) LP3 (b) KP3 (c) LP3:KP3 1:1 (w/w) blend.

By virtue of having the steepest gradient of the wedge and trough shape, and thus containing the amino acids with the largest side chain volume, LP3 and KP3 peptides in terms of overall hydrophobic character are most hydrophobic in the series of the newly designed peptides. Figure 5.5 shows the CD data obtained from the group of samples LP3, KP3, LP3:KP3 1:1 (w/w) using the same experimental procedure. The solution conditions chosen for the samples LP3, KP3 and LP3: KP3 1:1 (w/w) are pH 7 (50 mM BTP, 50 mM NaCl) which present the weakest stimulus for assembly compared to the solution conditions chosen for the LP1, KP1 and LP2, KP2 peptides. For the LP3 peptide sample (Figure 5.5a) β-sheet structure formation is seen at 5°C, with a minimum at approximately 222

nm, which shifts towards 218 nm, with an increase in temperature up to 80°C. For the KP3 peptide sample (Figure 5.5b), β-sheet structure formation is seen at 5°C indicated by a minimum at 222 nm that remains stable throughout the range of temperature. In case of the LP3:KP3 1:1 (w/w) blend, similar behavior as the LP3 peptide is seen with a minimum at 5°C but at a much higher wavelength (230 nm) shifting towards 222 nm with an increase in temperature till 80°C. All three samples show the formation of β-sheet structure even at the lowest temperature (5°C) under the given solution conditions, with the extent of β-sheet structure increasing with an increase in temperature as evidenced by further decrease in the MRE values at the minimum. At lower temperatures (5°C to 50°C) in case of the LP3:KP3 1:1 (w/w) sample, the MRE versus wavelength curves exhibit minima at wavelength ~ 230 nm, which is out of the usual 216-222 nm range for β-sheet structures. A shift in minima of MRE values is also observed in the LP3 sample at low temperatures (5°C to 25°C), but this shift is within the expected range for β-sheet structure (216-222 nm). Such anomalous red shifting in MRE minimum values as a function of wavelength has not been observed for the MAX1, LP1, KP1, LP2 and KP2 peptides. The LP3 and KP3 peptides contain more amino acid residues with aromatic side chains that that are also larger in size and than the aromatic side chains of the LP1, KP1, LP2 and KP2 peptides. Aromatic groups have been reported to contribute to circular dichroism spectra in the near UV (320-260 nm) as well as the far UV (240-190 nm) regions in different proteins[6,7]. A possible explanation of the red shift can be the potential contribution from the

larger and more prolific aromatic side chain containing residues of the LP3 and KP3 peptides.

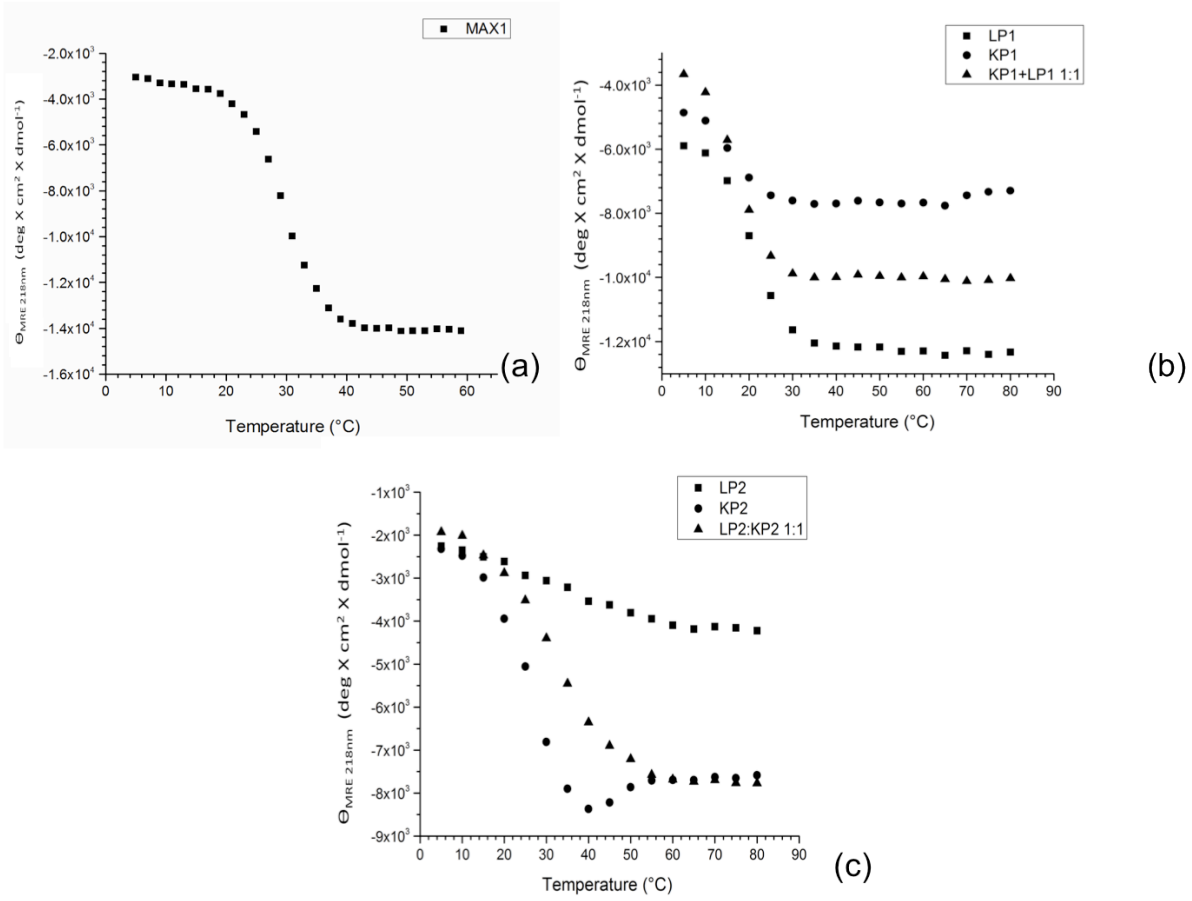

Figure 5.6. Circular dichroism data (mean residue ellipticity in deg·cm^2/decimole at 218 nm vs. temperature, °C) showing folding transition from random coil to β-sheet secondary conformation at 150μM concentration overall for (a) MAX1 at pH 9 (125 mM boric acid, 10 mM NaCl) (b) LP1, KP1, 1:1 (w/w) LP1:KP1; all at pH 9 (125 mM boric acid, 10 mM NaCl) (c) LP2, KP2, 1:1 (w/w) LP2:KP2 all at pH 7 (50 mM BTP, 150 mM NaCl). Solid squares indicate LP peptides, solid circles KP peptides and solid triangles 1:1 LP: KP blends.

For samples from the LP1-KP1 and LP2-KP2 pairs of peptides, MRE values at 218 nm as a function of temperature (°C) were plotted for each sample and a transition temperature from random coil to β-sheet conformation was determined for the sample at the given solution conditions. The wavelength 218 nm is chosen since it is well within the window of wavelengths in which a minimum in MRE is observed for a sample that shows a predominant β-sheet secondary structure. At solution conditions pH 9 (125mM boric acid, 10mM NaCl), MAX1 folds from a random coil conformation to a β-sheet structure at 30°C at 150μM concentration (Figure 5.6a), which has contributions from individual β-hairpins of MAX1 as well as the intermolecular β-sheet formation in the assembled fibrils. Folding behavior of MAX1 into β-sheet secondary structure has been discussed in Chapter 4 (Figure 4.3a). LP1 and KP1 peptides in terms of overall hydrophobic character are slightly more hydrophobic than MAX1 and, thus, undergo a conformational change from a random coil conformation to a β-sheet structure (Figure 5.6b) at the same solution conditions as MAX1, pH 9 (125 mM boric acid, 10 mM NaCl), although at a slightly lower temperature (~15°C) than 30°C in case of MAX1. LP2 and KP2 peptides are significantly more hydrophobic than MAX1 in terms of overall hydrophobicity. Thus, as shown by the CD data in Figure 5.6c, they undergo a conformational change from a random coil conformation to a β-sheet structure at solution conditions with a weaker

stimulus for self-assembly, i.e. pH 7 (50 mM BTP, 150 mM NaCl) as compared to MAX1, LP1 and LP2 at pH 9 (125 mM boric acid, 10 mM NaCl). The temperatures of self-assembly from the CD data can be considered to be approximately 40°C, 30°C and 30°C for the LP2, KP2 and LP2:KP2 1:1 (w/w) samples respectively. The higher temperature of folding for the LP2 as compared to the KP2 peptide and the blended sample, LP2:KP2 1:1 (w/w) is intuitively expected considering less overall hydrophobicity of the LP2 sample compared to the other two samples.

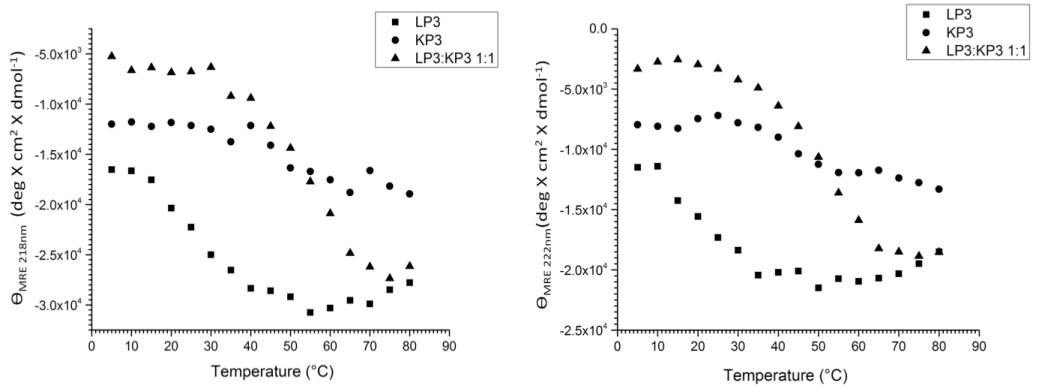

Figure 5.7. Circular dichroism data (mean residue ellipticity in deg·cm^2/decimole as a function of temperature, °C) showing folding transition from random coil to β-sheet secondary conformation at 150μM concentration overall for LP3, KP3, 1:1 (w/w) LP3:KP3 all at pH 7 (50 mM BTP, 50 mM NaCl) at (a) 218 nm (b) 222 nm. Solid squares indicate LP3 peptides, solid circles KP3 peptides and solid triangles 1:1 (w/w) LP3: KP3 blends.

In case of the LP3, KP3 and LP3:KP3 1:1 (w/w) blend, due to the shifting

in wavelength of MRE value minima, MRE values at both values of wavelength 218 nm and 222 nm were plotted as a function of temperature (°C) as shown in Figure 5.7. Intuitively, it is expected that the KP3 and the LP3:KP3 1:1 (w/w) samples would undergo β-sheet structure formation at lower temperatures than the LP3 sample under the same solution conditions due to higher overall hydrophobicity of the two samples as compared to LP3. In Figure 5.5, β-sheet structure is observed clearly in all LP3, KP3 and LP3:KP3 1:1 (w/w) samples at all temperatures starting from the lowest temperature (5°C). Thus, it is not possible to pick a single temperature value as the temperature of folding transition from random coil to β-sheet structure based on the MRE values at constant wavelengths (218 nm or 222 nm) as a function of temperature. However, the data in Figure 5.7a and Figure 5.7b do provide information of increase in the extent of β-sheet structure formation with an increase in temperature.

Results from the CD experiments help in determination of solution conditions that can be used for assembly of each respective peptide and their 1:1 (w/w) shape complementarity blends into a β-sheet secondary structure and consequent nanofibrils. The solution conditions used to conduct CD experiments on each group of samples (LP1, KP1 and 1:1 LP1:KP1 (w/w) blend), (LP2, KP2 and 1:1 LP2:KP2 (w/w) blend) and (LP3, KP3 and 1:1 LP3:KP3 (w/w) blend) have been chosen as the standard solution conditions for further study of self-assembled nanostructure and material properties from the above mentioned peptides and their blends. These solution conditions have been chosen since they

permit β-sheet secondary structure formation from a given pair of peptides individually and their blend to similar extents and at similar temperature values.

5.3. Cryogenic Transmission Electron Microscopy (cryo-TEM)

Cryo-TEM data were collected on the following samples from the wedge and trough shaped peptides; LP1, KP1, LP1:KP1 1:1 (w/w) blend, LP2, KP2, LP2:KP2 1:1 (w/w) blend and LP3, KP3, LP3:KP3 1:1 (w/w) blend. These data were collected by Hao-Jan Sun in the laboratory of Prof.Virgil Percec in the Department of Chemistry at the University of Pennsylvania. Cryo-TEM enables direct *in-situ* imaging of a particular sample immediately after vitrification of the sample without further processing steps such as drying and staining[8,9]. Thus, cryo-TEM helps in elimination of artifacts from various processing steps used in negative stain cast-film TEM like sample damage and flattening due to drying and generation of false contrasts due to uneven distribution of stain. A cryo-TEM image of an assembled structure from MAX1 shows a uniform fibrillar structure with ~3 nm thickness (Figure 5.8). This thickness corresponds to the strand length of a β-hairpin of MAX1 and a bilayer peptide cross section as described earlier in Chapter 3.

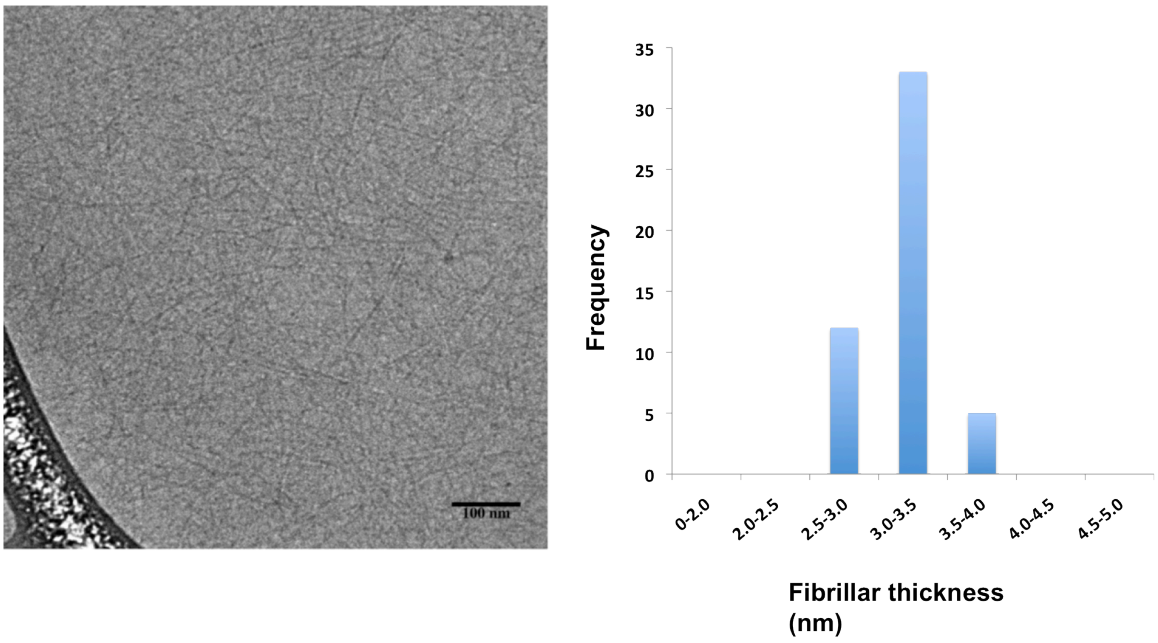

Figure 5.8. Cryogenic transmission electron micrograph for the MAX1 hydrogel sample, showing fibrils of uniform thickness values (~3 nm). The histogram accompanying the image shows a frequency distribution of thickness of the fibrillar structures formed by MAX1.

All of the new peptides LP1-KP1, LP2-KP2 and LP3-KP3 are marginally longer with 24 amino acid residues, as compared to the 20 amino acid residues of MAX1. Thus, the hypothesis is that if the new peptides undergo folding and self-assembly in a manner similar to MAX1, they would assemble into fibrillar nanostructures with slightly thicker average diameter than that of individual MAX1 fibrils corresponding to the increase in β-hairpin strand length over MAX1. According to this hypothesis, if the newly designed peptides underwent self-assembly in a manner similar to MAX1, they would form cylindrical-like

fibrils of ~3.8 nm. The hydrogel samples for the cryo-TEM experiments were prepared and aged for 48 hours prior to imaging. Figures 5.9, 5.10 and 5.11 show cryo-TEM data from the three pairs of peptides, LP1-KP1, LP2-KP2 and LP3-KP3 respectively, individually and their 1:1 (w/w) blends.

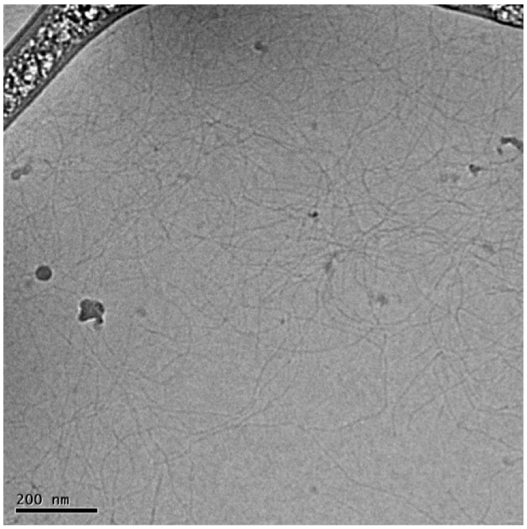

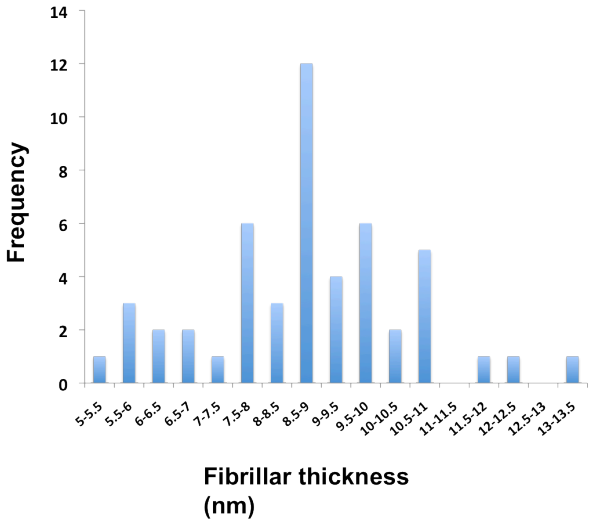

(a)

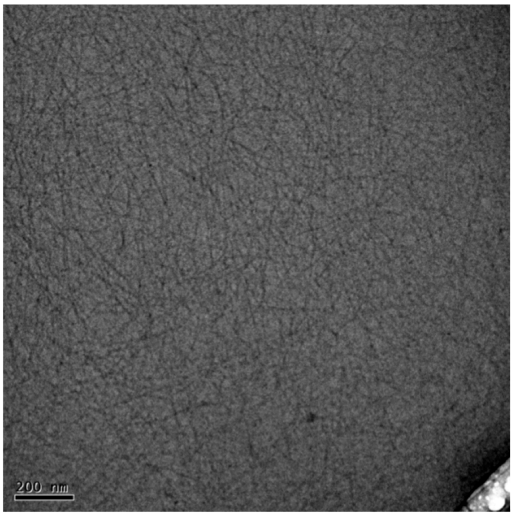

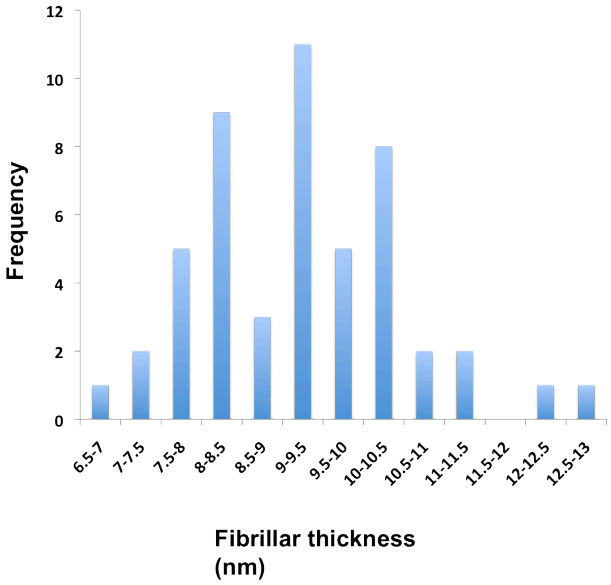

(b)

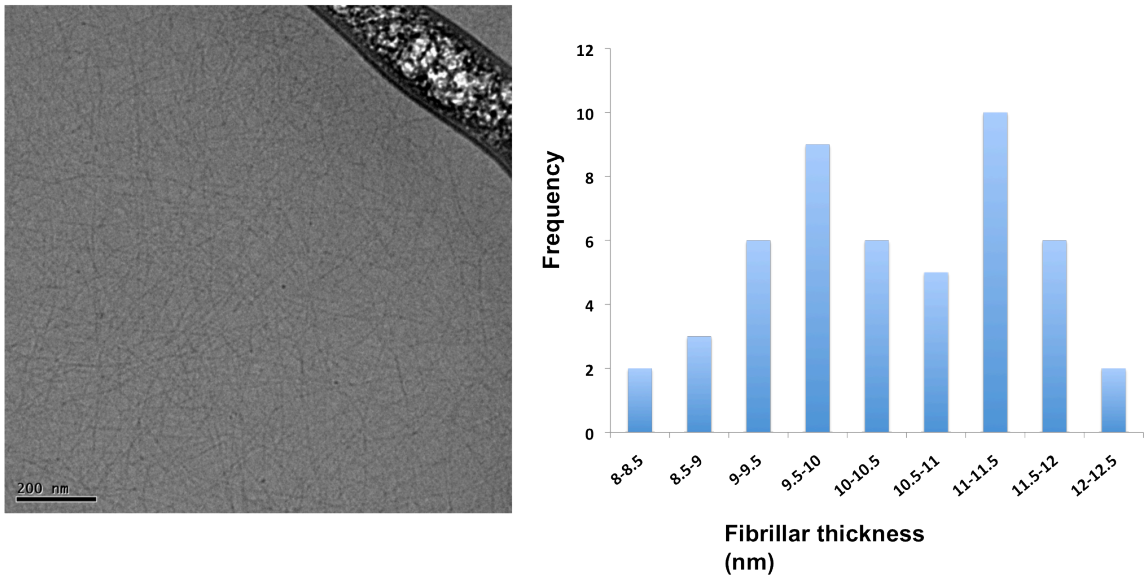

(c)

Figure 5.9. Cryogenic transmission electron micrograph for the (a) LP1 (b) KP1 (c) 1:1 (w/w) LP1:KP1 hydrogel samples, showing fibrillar nanostructures from the samples of varying thickness values. The histogram accompanying the image shows a frequency distribution of thickness of the fibrillar structures formed by the samples.

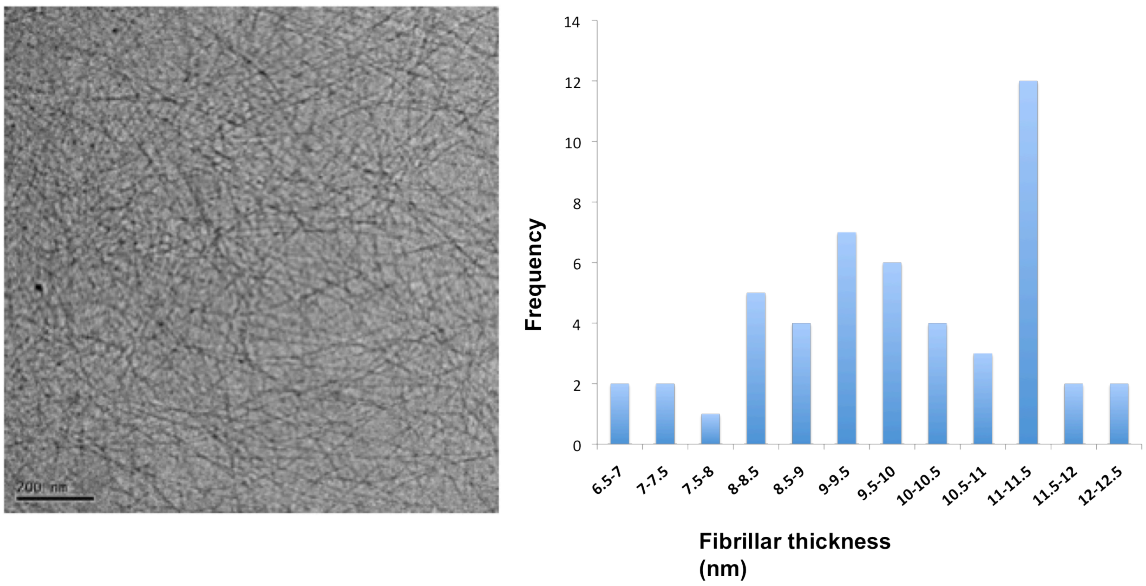

(a)

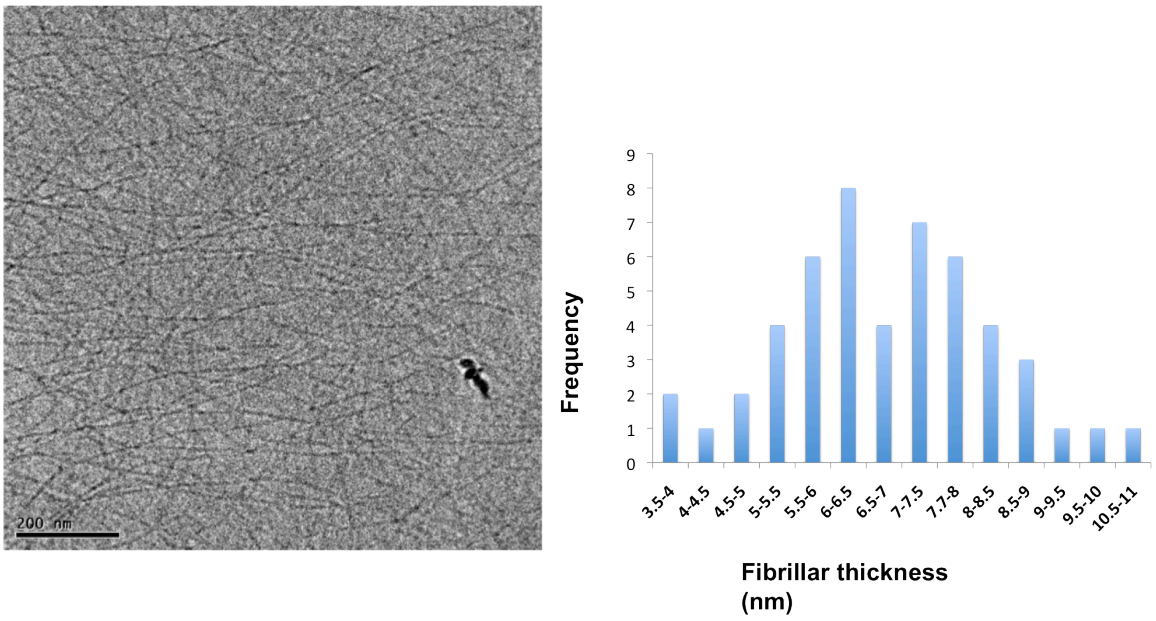

(b)

Figure 5.10 (cntd)

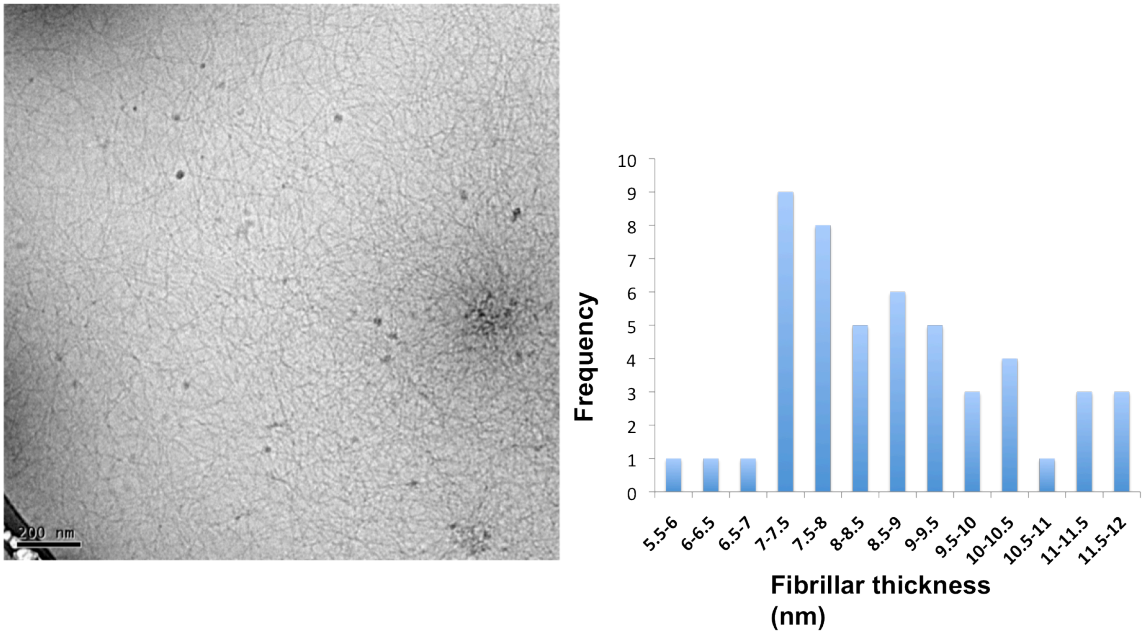

(c)

Figure 5.10. Cryogenic transmission electron micrograph for the (a) LP2 (b) KP2 (c) 1:1 (w/w) LP2:KP2 hydrogel samples, showing fibrillar nanostructures from the samples of varying thickness values. The histogram accompanying the image shows a frequency distribution of thickness of the fibrillar structures formed by the samples.

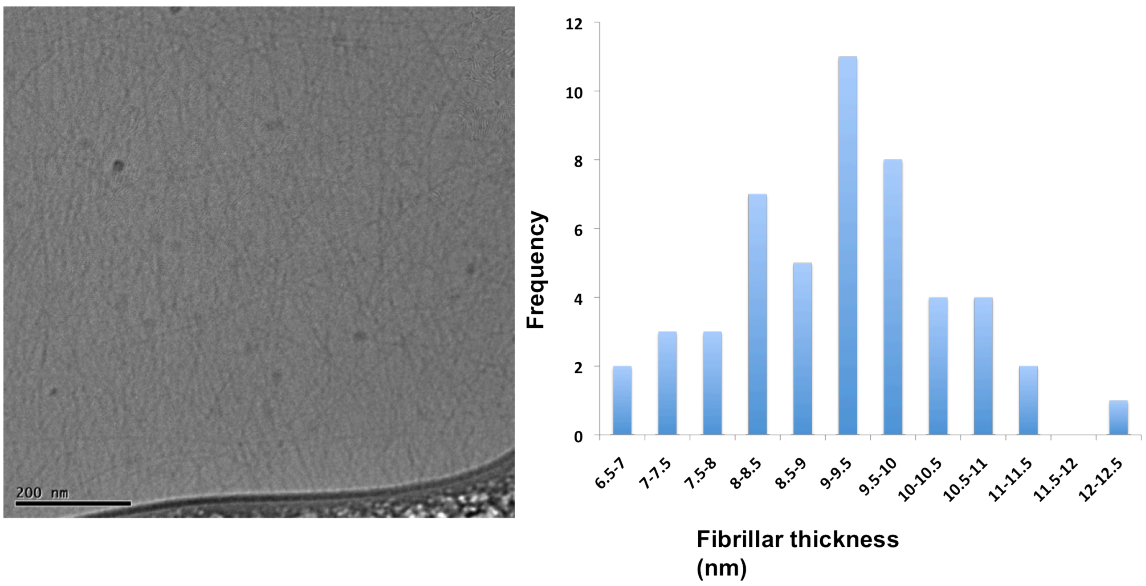

(a)

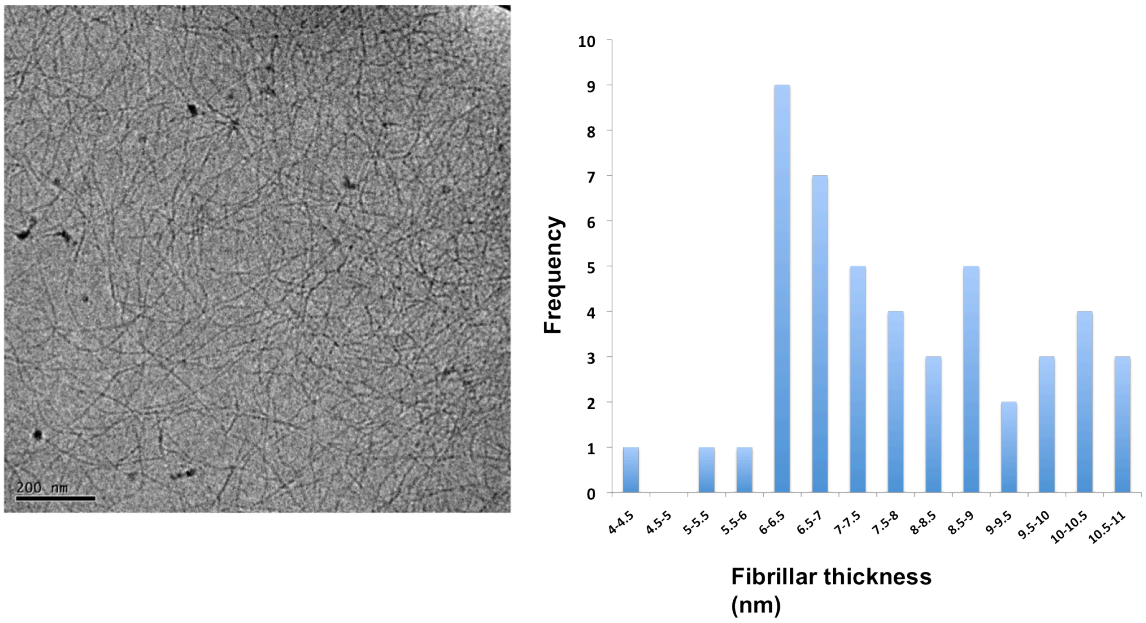

(b)

Figure 5.11 (cntd)

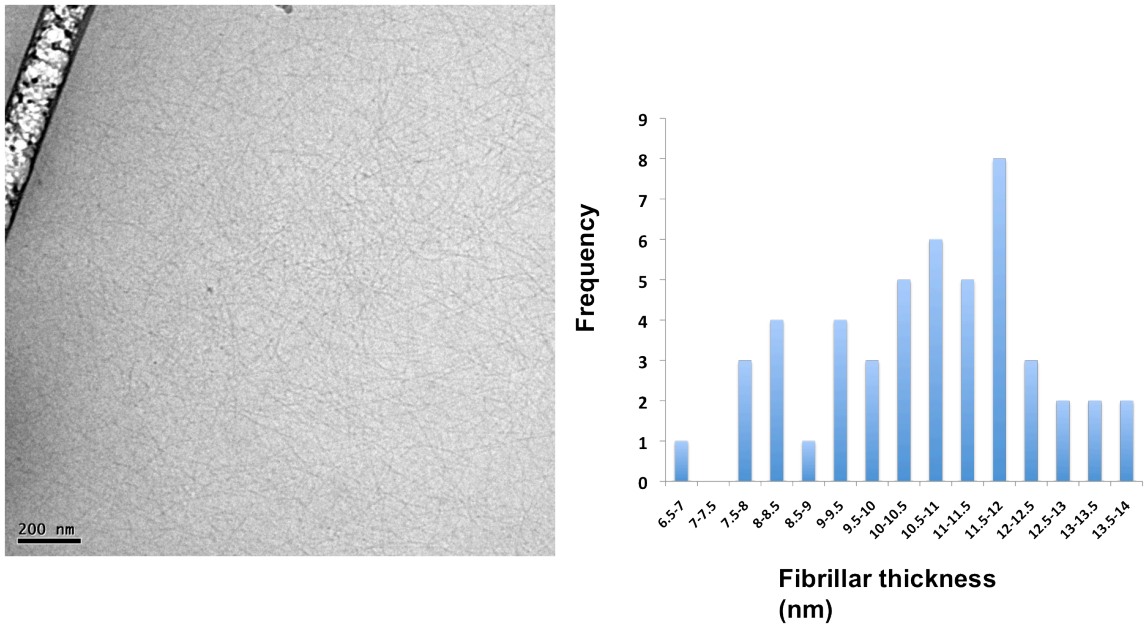

(c)

Figure 5.11. Cryogenic transmission electron micrograph for the (a) LP3 (b) KP3 (c) 1:1 (w/w) LP3:KP3 hydrogel samples, showing fibrillar nanostructures from the samples of varying thickness values. The histogram accompanying the image shows a frequency distribution of thickness of the fibrillar structures formed by the samples.

The nanostructures observed from the peptides LP1, KP1, LP2, KP, LP3 and KP3 and the 1:1 (w/w) blends of LP1:KP1, LP2:KP2 and LP3:KP3 show overall fibrillar morphology with values of fibrillar thickness much higher than the thickness values in case of MAX1. A detailed analysis of these images shows that the fibrillar nanostructures formed by each of the peptides or blends of peptides are highly non-uniform as indicated by the histograms associated with each image. The analyses of fibrillar thickness values of 50 fibrillar structures from each images was carried out using ImageJ, an image-processing program

available from the National Institutes of Health[10]. In each histogram, frequencies of occurrence of particular thickness values are represented on the Y-axis and the pertinent windows of thickness values on the X-axis.

The difference in nanostructure formed by the wedge and trough shaped peptides and their blends can be rationalized in the following manner. The uniform burial of the flat hydrophobic face exhibited by MAX1 peptides to yield uniformly thick cylindrical nanostructure is subject to disturbance due to the unique patterned hydrophobic surfaces in the wedge and trough shaped peptides. Due to this patterning there is a possibility of exposed hydrophobic surfaces due to the formation of a non-uniformly packed hydrophobic bilayer. These exposed hydrophobic surfaces can attempt to bury exposed hydrophobic surfaces from other growing nanostructures and lead to formation of assembled structures that are thicker than the individual and uniformly thick MAX1 fibrils. Another factor that might lead to deviation of the assembled nanostructure from the KP2 samples is the presence of hydrophobic side chain amino acids at the corners of the folded KP2 β-hairpin (Scheme 5.1). As discussed in Chapter 3, both lateral and facial hydrophobic interactions are fundamentally important secondary interactions that influence the self-assembly pathway and assembled nanostructure from β-hairpin peptides. The large hydrophobic side chains on a KP2 β-hairpin on the edge of a growing fibril could potentially undergo hydrophobic interactions with a KP2 β-hairpin from another growing fibril or from molecules still in solution, thus disturbing unidirectional fibrillar self-assembly of KP2 and leading to a wider,

more irregular cross-sectioned nanostructure.

5.4. Correlation between Assembled Nanostructure from Peptides, the Corresponding Network Structure and Network Mechanical Behavior

The last section discussed the presence of the overall fibrillar nanostructure formed by all the newly designed wedge and trough peptides with specific shapes of hydrophobic faces and also attempted to rationalize the formation of non-uniform, thicker structures from the new peptides as compared to MAX1. Thus, in order to discern any potential differences in the nanostructure at lower length scales (1-10 nm) and network morphology at higher length scales (10-200 nm), small angle neutron scattering characterization (SANS) was employed. This section presents an analysis and rationalization of the results acquired using small angle neutron scattering and oscillatory rheological characterization. The differences between the assembled nanostructure from peptides with varying hydrophobic face shapes and the hydrogel network morphology developed from the assembled nanostructure have been correlated with the mechanical properties of the networks, specifically the steady-state shear response of the networks. The discussion in this section has been presented in a three separate sections, each describing a wedge-trough pair and their 1:1 (w/w) blend.

5.4.1. Nanostructure-Network structure-shear response correlation for MAX1

Figure 5.8 shows a cryo-TEM image of hierarchically self-assembled fibrils from MAX1 which have a uniform ~3 nm cross-section. This fibrillar thickness is confirmed from SANS results obtained by fitting I (q) v/s q data to the monodisperse cylindrical form factor model available from NCNR as described in Chapter 2. The radius of the cylindrical structures as given by the model is ~1.5 nm, which is in agreement with the TEM data (Figure 5.8).

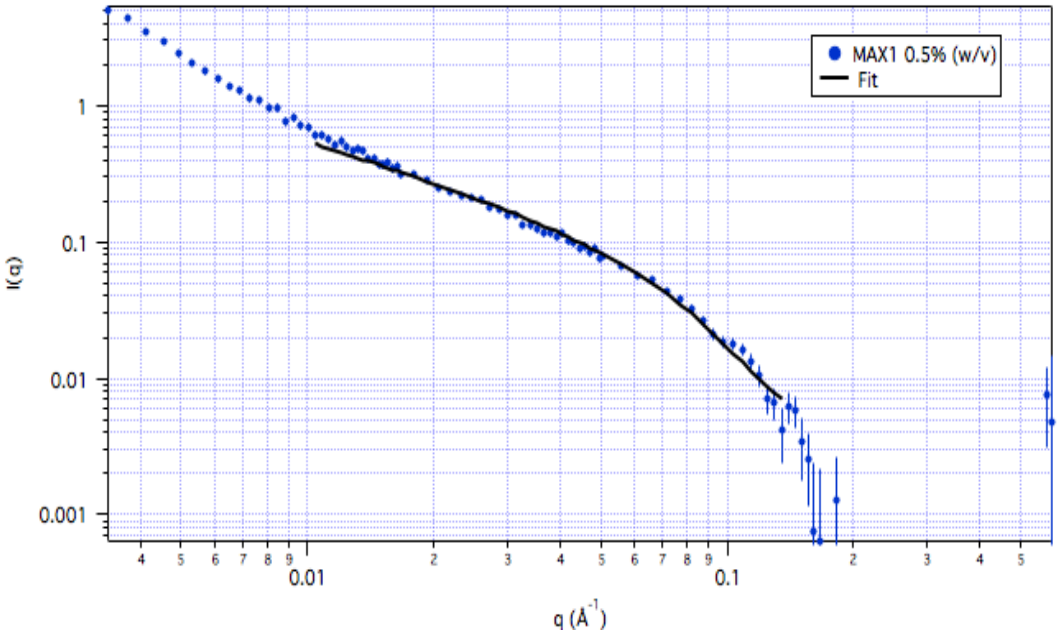

Figure 5.12. Fits of SANS I(q) v/s q data to monodisperse cylinder form factor for the MAX1.

The width of the MAX1 fibrils corresponds to the strand length of the folded peptide, which is approximately 3.2 nm[11,12]. Additionally, scattering

intensity in the intermediate q region can be expressed as I (q) ~ q^{-1} which indicates presence of rod-like objects at that length scale (Figure 5.13a). As shown in Table 5.1, the slope 'n' of the log (I) v/s log (q) from low-q range for MAX1 is ~ -1 indicating rod like or cylindrical assembled structures at length scales > 10s of nm. Log (I) v/s log (q) data obtained from MAX1 in the high q-range that probes the nanostructure in the length scale of the individual fibril surface, shows a dependence of I (q) ~ q^{-4}. Thus, slope 'm' of the log (I) v/s log (q) in the high q- range at the length scale of the surface of an individual MAX1 fibril is ~ -4, indicating a smooth surface for each individual fibril (Figure 5.13b). These data are consistent with the results indicating uniformly packed cylindrical self-assembled structure form MAX1 as shown by TEM (Figure 5.8).

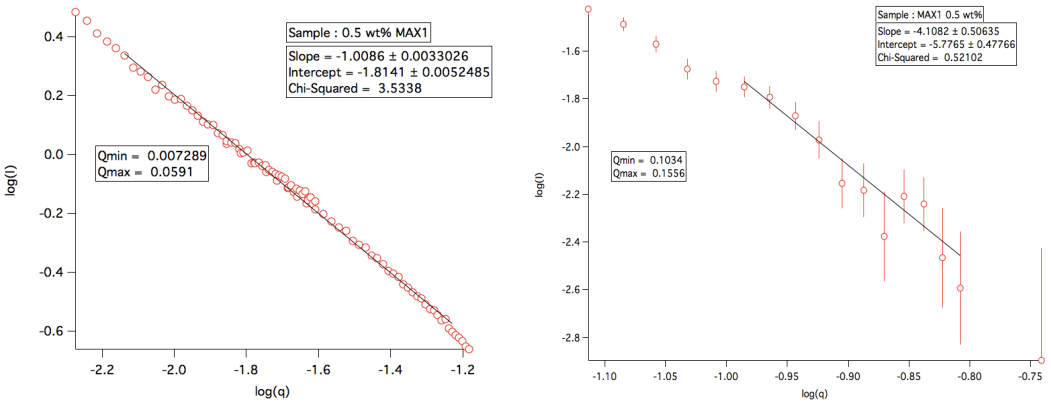

(a) (b)

Figure 5.13. Fits of SANS data log (I (q)) v/s log (q) at (a) low-q and (b) high-q windows for the MAX1 hydrogel

Table 5.1. Values of low-q exponent 'n' and high-q exponent 'm' obtained by fitting log (I(q)) v/s log (q) for the MAX1 sample

Sample	**Low-q 'n'**	**High-q 'm'**
MAX1	-1.00 *(0.007-0.06)*	-4.10 *(0.10-0.15)*

Solid MAX1 hydrogels exhibit a unique property of undergoing shear thinning and flow under large amplitude of applied shear stress but immediately recovering into solid gels on cessation of shear (Figure 5.14). An earlier study by Yan et al.,[13] which explored the hydrogel behavior during and after flow, indicated the gel networks fracture into domains much larger than the length scale of individual fibrils in order to flow. The network morphology within gel domains during flow was structurally identical to the parent network at rest; the peptide fibrils displayed the same cross-section, the same physical crosslinking points of fibrillar entanglement and branching and the same porosity. On cessation of shear, the smaller gel domains immediately percolate and form a bulk, hydrogel network. This shear-thinning and rehealing behavior of MAX1 would not exist if the network disintegrated into individual fibrils during flow since there would be no immediate mechanism for the fibrils to recrosslink and percolate into a bulk network. If the fibril branching in MAX1 is responsible for the observed shear thinning an immediate gel reformation behavior, then elimination of most fibril branching from the system should significantly affect the hydrogel flow properties. Thus, designed hydrophobic, shape-specific interactions in the blends

of appropriately designed LP and KP peptide pairs are hypothesized to significantly eliminate fibril branching in the networks and thus produce networks which display shear thinning behavior but not rehealing characteristics.

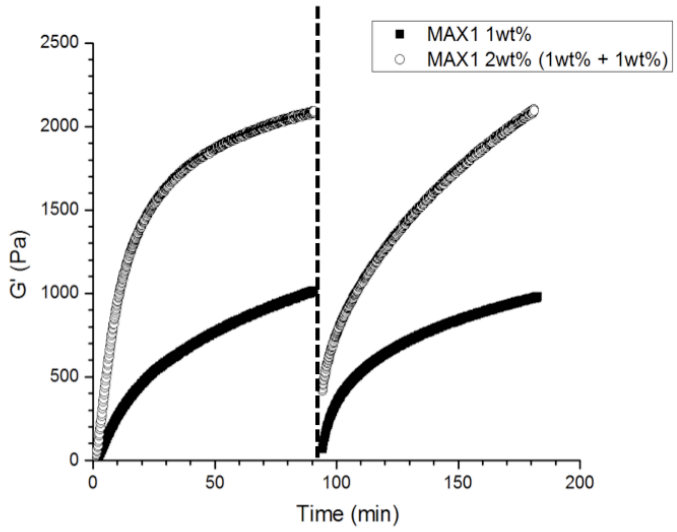

Figure 5.14. Steady state shear response of the MAX1 hydrogel at two concentrations 1% and 2% (w/v). Data shown are oscillatory time sweep measurement data (G'(Pa)) before and after application of steady state shear (1000/s for 120 sec, indicated by dotted line). For all data points G'>>G", indicating solid nature of the hydrogels.

Thus, considered together, results from the cryo-TEM, SANS characterization and oscillatory rheological characterization show MAX1 formed uniform fibrillar nanostructures that form a hydrogel network with branching.

5.4.2. Nanostructure-Network Structure-Shear Response Correlation for LP1, KP1 and LP1:KP1 blend

Figure 5.15 shows the results of the fitting performed for I(q) v/s q data to polydisperse radius cylinder form factor for the hydrogels constructed from LP1, KP1 and 1:1 (w/w) LP1:KP1. As described in Chapter 2, the polydisperse radius cylinder function provided by NCNR calculates the form factor for a cylindrical nanostructure with polydisperse values of cylinder radius. Fitting the data to this function yields the polydispersity in the radius values and also the average value of the cylindrical radius. As shown in figure 5.15, good fits of the data from all three samples to the model are obtained across all the q-ranges investigated by SANS.

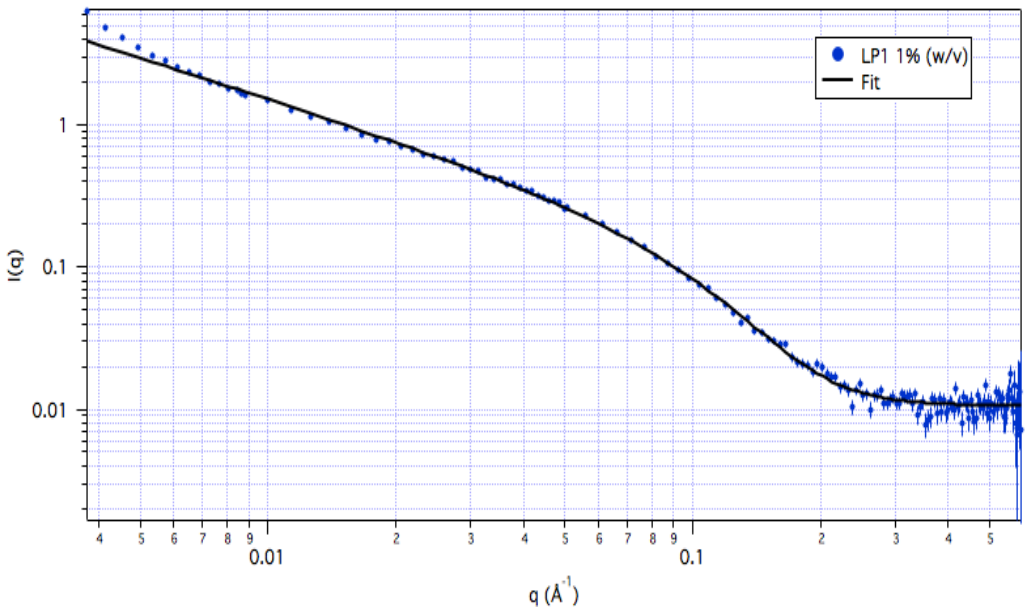

(a)

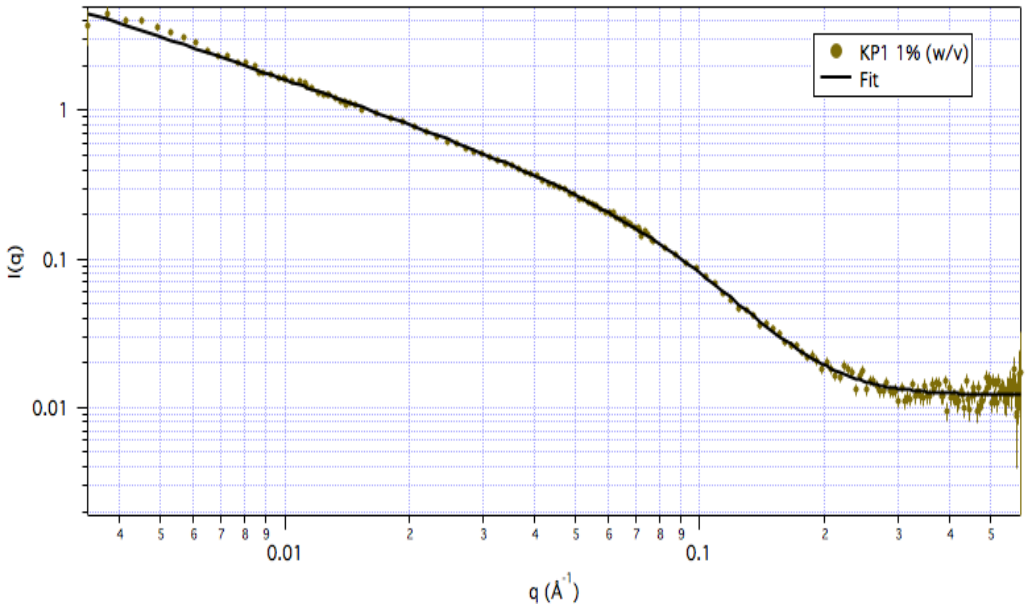

(b)

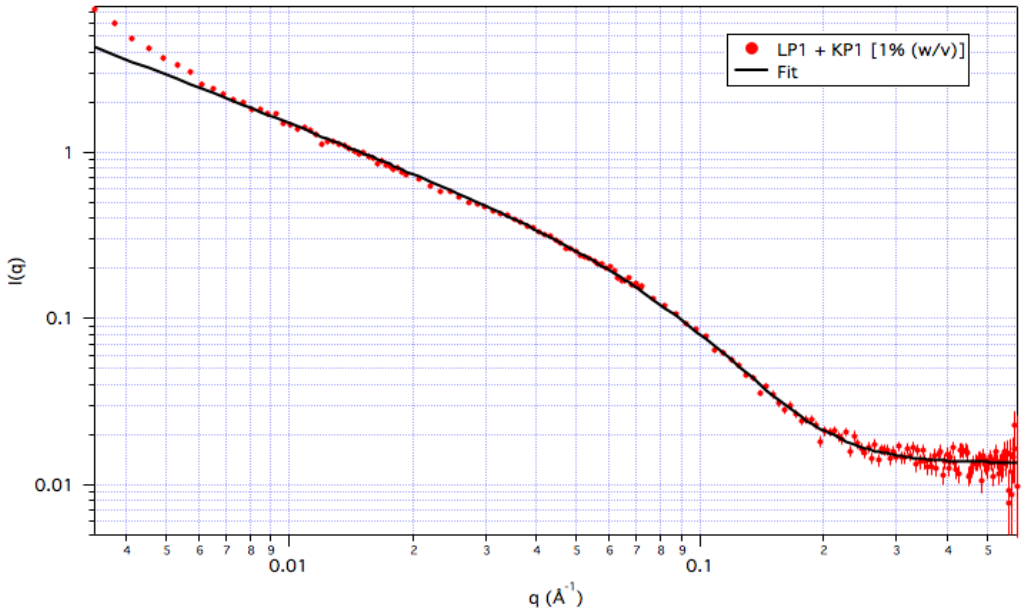

(c)

Figure 5.15. Fits of SANS I(q) v/s q data to polydisperse radius cylinder form factor for (a) LP1 (b) KP1 and (c) LP1:KP1 1:1 (w/w).

It was noticed that in the above SANS plots there seems to be significant scattering intensity at high q even after typical background (i.e. buffer solution) scattering intensity subtraction. In order to determine any impact of buffer scattering or of peptides that are not included in the fibrillar network that may contribute to the background scattering, the SANS signal with and without background scattering were compared as discussed below. The red curves in Figure 5.16 (a-c) indicate the I(q) v/s q plots for the LP1, KP1 and 1:1 (w/w) LP1:KP1 samples including scattering signal contribution from the buffer pH 9 125 mM boric Acid 10 mM NaCl. The black curve indicates scattering signal from the neat buffer pH 9 125 mM boric Acid 10 mM NaCl. The blue curves are scattering signal exclusively from the peptide nanostructure of LP1, KP1 and 1:1 (w/w) LP1:KP1 blend obtained by subtracting the buffer scattering (black curve) from the overall sample scattering signal (red curve). The blue curves indicate presence of weak but observable scattering signal in the q ranges between $0.2 < q < 0.5$ $A^{\circ -1}$. Such high-q scattering is not observed in case of the exclusively MAX1 peptide nanostructure scattering i.e. when the buffer scattering signal is subtracted from the MAX1 sample scattering signal. The presence of high-q scattering exclusively from the nanostructure of LP1, KP1 and 1:1 (w/w) LP1:KP1 peptides might indicate the presence of an extremely low concentration of peptides in solution that are not part of the network structure.

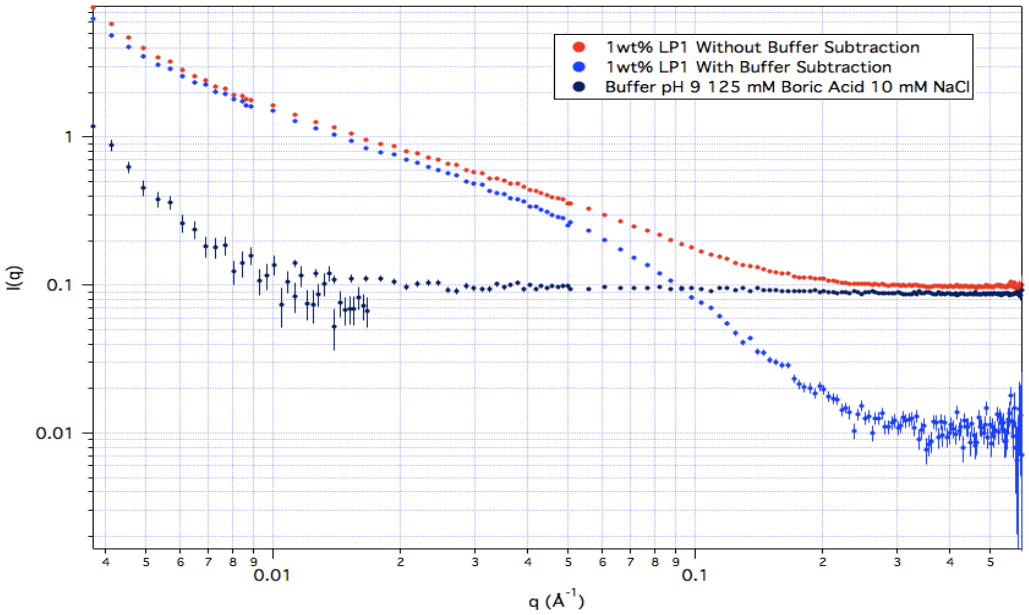

(a)

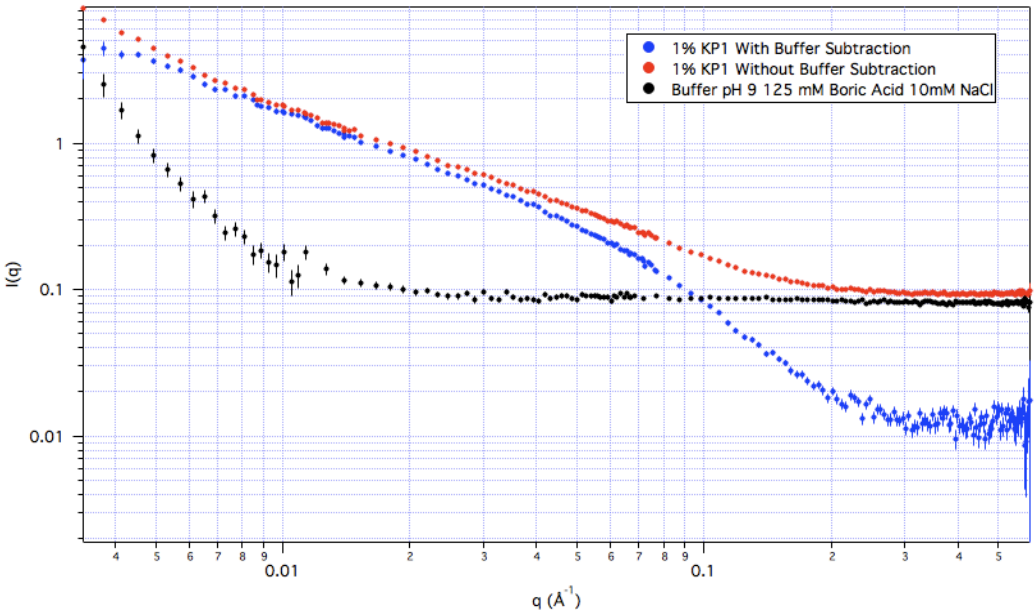

(b)

Figure 5.16 (cntd)

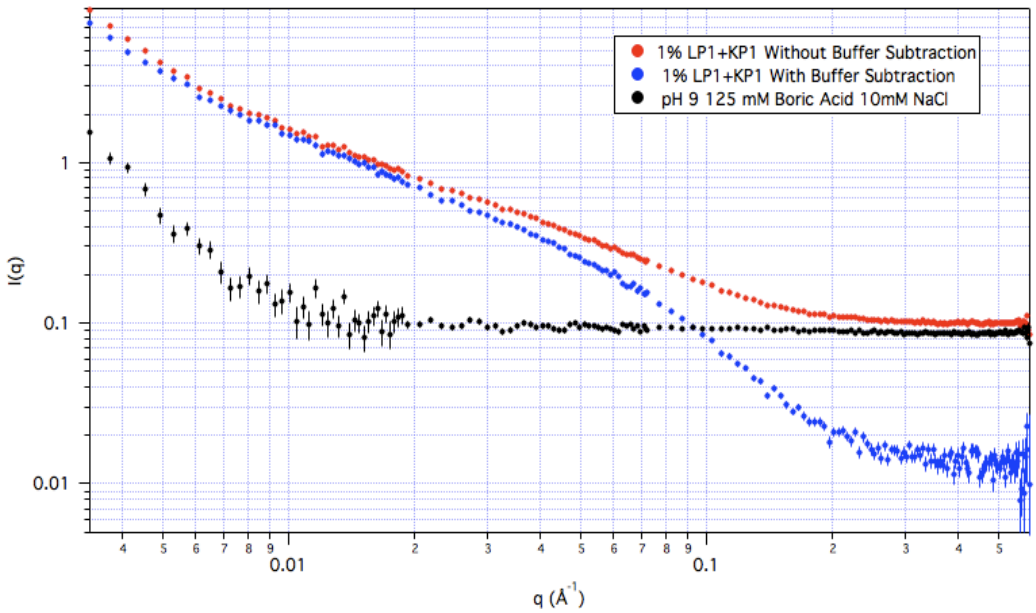

(c)

Figure 5.16. I (q) v/s q scattering signal from sample with scattering contribution from buffer retained (red) and subtracted (blue) and the buffer scattering itself (black) for (a) LP1 (b) KP1 and (c) 1:1 (w/w) LP1:KP1.

The values of the average radius and poydispersity in radius values for samples LP1, KP1 and 1:1 (w/w) LP1:KP1 are listed in Table 5.2. The good fits to the polydisperse radius cylinder model for these samples demonstrate the cylindrical morphology of the assembled structure obtained after assembly of the peptide samples, with the average radius values in the range of 0.7 to 1 nm. These samples also exhibit high polydispersity ($0.25 < p < 1$)[14,15] in radius values. These data indicate that although the nanostructures formed from the peptide samples are fibrillar with a cylinder-like morphology, they are starkly different from the uniformly thick cylindrical fibrillar nanostructures formed from MAX1 peptides which have cross sectional radius values ~1.6 nm from SANS. The existence of

polydispersity in radius values of cylinders assembled from the LP1, KP1 and 1:1 (w/w) LP1:KP1 peptides points to deviation in the peptide self-assembly process shown by MAX1. This deviation can be attributed to non-uniformity in shape of hydrophobic face in case of the LP1, KP1 peptides and their 1:1 blend.

Table 5.2. Values of average radius and polydispersity in radius values obtained by fitting I(q) v/s q for the samples LP1, KP1 and LP1:KP1 1:1 (w/w) with fit windows specified for each sample.

Sample	**Radius (nm)**	**Polydispersity** $p = \sigma / R_{avg}$ σ: Schulz distribution variance; R_{avg}: Average radius
LP1	0.99±0.05	0.43
KP1	0.77±0.06	0.60
1:1 (w/w) LP1+KP1	0.69±0.07	0.64

Among all the newly designed peptides, the LP1 and KP1 peptide designs have the shallowest shape gradient of the wedge and trough shapes respectively. The uniform burial of the flat hydrophobic face exhibited by MAX1 peptides to yield uniformly thick cylindrical nanostructure is subject to disturbance due to the unique patterned hydrophobic surfaces in the wedge and trough shaped peptides. As discussed in Section 5.3, due to this patterning there is a possibility of exposed

hydrophobic surfaces due to the formation of a non-uniformly packed hydrophobic bilayer as well as exposed hydrophobic chemistry on the edges of growing fibrils. These exposed hydrophobic surfaces can possibly lead to formation of assembled structures from LP1, KP1 and 1:1 (w/w) LP1:KP1 that are much less uniform than the individual and uniformly thick MAX1 fibrils.

Fits of the SANS data log (I (q)) v/s log (q) in two different q ranges (specified for each sample in Table 5.3.) were performed for each sample LP1, KP1 and 1:1 (w/w) LP1:KP1. As an example of the fitting data, Figure 5.17a and 5.17b shows the fits of log (I (q)) v/s log (q) for the sample LP1 at low-q and high-q windows respectively. Similar to MAX1, LP1, KP1 and 1:1 (w/w) LP1:KP1 also show an $I(q) \sim q^{-1}$ dependence in the low to mid q region, as shown by the value of exponent 'n' in Table 5.3 for the three samples. These data confirm the formation of cylindrical assembled structures for the three hydrogels. In the high-q region however, the scattering signal from all of the three gels looks very different from MAX1. At this length scale where the scattering signal is obtained at the surface of an individual fibril, an $I(q) \sim q^{m}$ dependence, with $2 < m < 3$ is observed. The scattered intensity due to surface fractal scattering scales as $I(q) \sim q^{-(6-D_s)}$[16,17]. Values of 'm' in the range $2 < m < 3$ lead to values of D_s in a range $3 < D_s < 4$. These values of D_s point to surface fractal scattering from the structure at that length scale. In the q range specified in Table 3, the length scale being investigated is that of the surface of each individual fibril. Thus, the values of 'm' (Table 5.3) indicate the presence of a rough surface for each individual

fibril. These data help infer that a slight change in shape of the hydrophobic face adversely influences the smooth packing of the peptide molecules into nanostructures during their self-assembly, but on larger length scales does not disturb formation of fibrillar structures from the peptide assembly. The presence of fibrillar nanostructures at larger length scales is confirmed from the cryogenic transmission electron microscopy measurements as discussed in section 5.3.

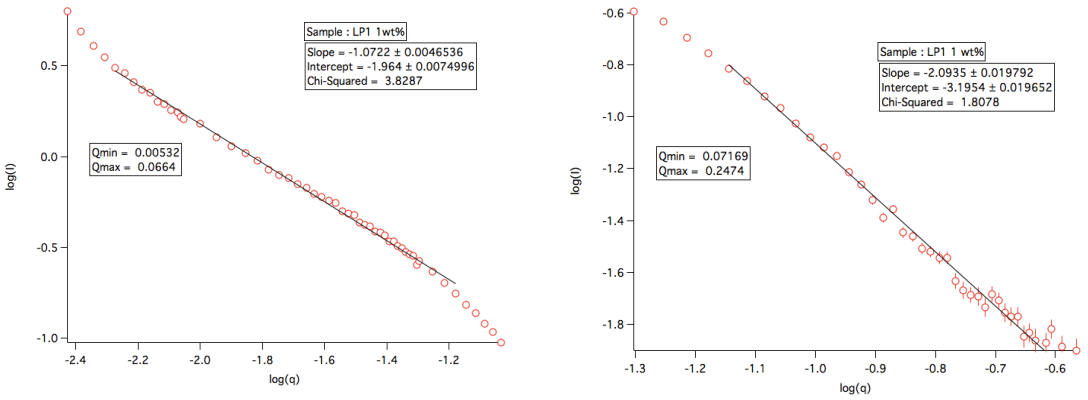

(a) **(b)**

Figure 5.17. Fits of SANS data log (I (q)) v/s log (q) at (a) low-q and (b) high-q windows for the LP1 hydrogel sample providing an example of how the fits were performed for all the samples.

Table 5.3. Values of low-q exponent 'n' and high-q exponent 'm' obtained by fitting log (I(q)) v/s log (q) for the samples LP1, KP1 and LP1:KP1 1:1 (w/w) with fit windows specified for each sample

Sample	**Low-q 'n'**	**High-q 'm'**
LP1	-1.07 *(0.005-0.066)*	-2.09 *(0.07-0.24)*
KP1	-1.13 *(0.005-0.069)*	-2.07 *(0.07-0.24)*
1:1 (w/w) LP1+KP1	-1.11 *(0.005-0.069)*	-2.01 *(0.07-0.17)*

In addition to the above fits, the scattering data obtained from the three samples has been fit to the correlation length model available from NCNR. This model calculates the scattering intensity as

$$I(q) = (A/q^{n1}) + C/(1 + (qL)^{m1}) + B$$

This model used to fit SANS data from assembled networks of peptides can potentially provide quantification of local and global network characteristics formed from the peptides. This model has been previously employed in order to study MAX8 networks[18]. In the above equation, network scattering in the low q regime can be described by the first term, A/q^{n1} and is qualitatively similar to Porod-like scattering[19]. High q scattering is expressed by the second term, $C/[1 + (QL)^{m1}]$. This is a Lorentzian function that has been used to characterize polymer/solvent interactions and chain solvation characteristics[20]. In this analysis, it can be used to identify the fibrillar morphology and the network structure on the

nanoscale. The multiplicative factors of the Porod and Lorentzian terms (A and C, respectively), the q-independent incoherent background scattering (B), the correlation length (L), and the low-q and high-q scattering exponents (n1 and m1, respectively) were obtained by fitting the SANS data to this model.

Scattering exponents in the low-q and high-q regimes (n1 and m1, respectively) can be interpreted to be representative of the network densities observed at these two distinct length scales. Model functions similar to the correlation length models that correlate the clustering and solvation characteristics of polymer solutions[21] and polyelectrolyte solutions[20] to the value of the high-q exponent 'm1' have been reported in the literature. From these studies, it can be inferred that values of 'm1' in a range $1< m1 <3$ can be attributed to mass fractal scattering from the studied samples at high-q length scales (~ 1-10 nm), with higher values of 'm1' representing higher network densities or higher clustering at this local length scale in the networks.

As an example of the good fits to this model of the data from the three samples, a fit to the model by the LP1 sample data is shown in Figure 5.18. The values of exponent 'm1' obtained from the fits to data from LP1, KP1 and 1:1 (w/w) LP1:KP1 are shown in Table 5.4. The values of 'm1' for LP1, KP1 and 1:1 (w/w) LP1:KP1 are in the range $1< m1< 3$ and are very similar for all the three samples, indicating very similar network densities at the length scales associated with high-q windows for all three samples.

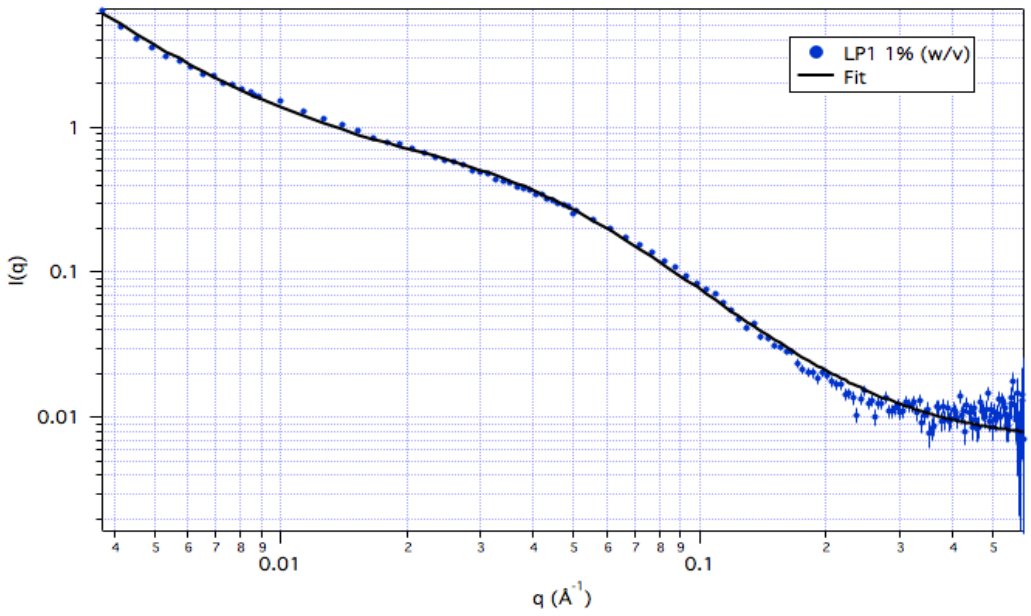

Figure 5.18. Fit of SANS I(q) v/s q data to the correlation length model for the LP1 hydrogel

Table 5.4. Values of high-q exponent 'm1' obtained by fitting I(q) v/s q for the samples LP1, KP1 and LP1:KP1 1:1 (w/w).

Sample	**High-q exponent 'm1'**
LP1	2.76
KP1	2.82
1:1 (w/w) LP1+KP1	2.90

As shown in Figure 5.19, stiff hydrogels are obtained from LP1 (~200 Pa), KP1 (~300 Pa) at 1% (w/v) and the 1:1 (w/w) LP1: KP1 (~400 Pa) sample at effectively 2% (w/v) under the same solution conditions. Additionally, all three hydrogels demonstrate shear thinning behavior when subject to high amplitude

(1000/s) steady state shear for a period of 2 min and rehealing to a substantial value of the original stiffness modulus upon removal of shear treatment and allowing to age for several hours. LP1 and KP1 have only slightly steeper gradients of the wedge and trough shapes as compared to the totally flat hydrophobic valine rich face of MAX1. Thus, the hydrophobic specificity in case of LP1 and KP1 might not be sufficient to cause a significant elimination of branching while fibril formation. This is evidenced by the shear thinning and substantial rehealing behavior demonstrated by all three hydrogel samples LP1, KP1 and 1:1 (w/w) LP1:KP1. The higher stiffness of the 1:1 (w/w) LP1:KP1 blend as compared to the LP1 and KP1 hydrogels individually can also be attributed to the overall 2% (w/v) hydrogel.

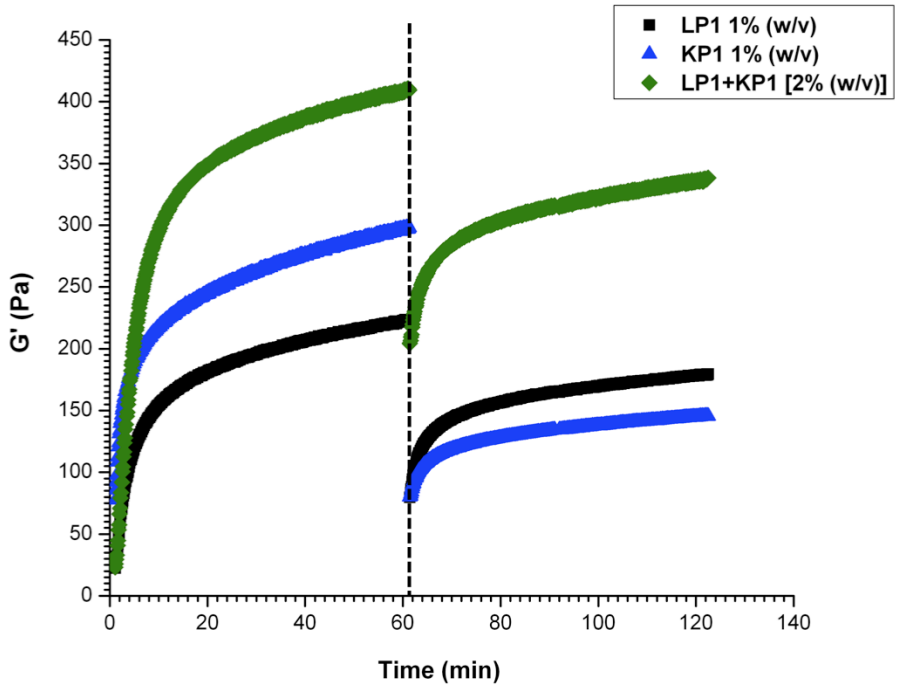

Figure 5.19. Steady state shear response of hydrogels from samples LP1 1% (w/v) , KP1 1% (w/v) and 1:1 (w/w) LP1:KP1 2% (w/v). Data shown are oscillatory time sweep measurement data (G'(Pa)) before and after application of steady state shear (1000/s for 120 sec, indicated by dotted line). For all data points G'>>G", indicating solid nature of the hydrogels.

Thus, considered together, results from the cryo-TEM, SANS characterization and the oscillatory rheological characterization indicate branched fibrillar structures formed from the LP1, KP1 and 1:1 (w/w) LP1:KP1 peptides, which have cylindrical morphologies. The analyses of results from these techniques do not indicate shape specific interactions between the complementary wedge and trough shaped β-hairpins of LP1 and KP1 and consequent elimination of fibrillar branching in the blended sample of LP1 and KP1 as previously hypothesized.

5.4.3. Nanostructure-Network structure-shear response correlation for LP2, KP2 and LP2:KP2 blend

Cryogenic TEM from all the three samples LP2, KP2 and 1:1 (w/w) LP2:KP2 indicated an overall fibrillar morphology with varying values of thickness (Figure 5.10), as discussed in Section 5.3.

SANS characterization performed on the three hydrogel samples helps decipher differences in the nanostructure formed from the differently shaped hairpin peptides. Figure 5.20 shows the results of the fitting performed for I(q) v/s q data to polydisperse radius cylinder form factor for the hydrogels constructed from LP2, KP2 and 1:1 (w/w) LP2:KP2. Data were fit to the polydisperse radius cylinder function as described in Chapter 2 to yield the polydispersity in the radius values and also the average value[22] of the cylindrical radius. As shown in figure 5.20, a good fit of the data to the model is obtained across all the q-ranges investigated by SANS for the sample LP2, but not the samples KP2 and 1:1 (w/w) LP2:KP2.

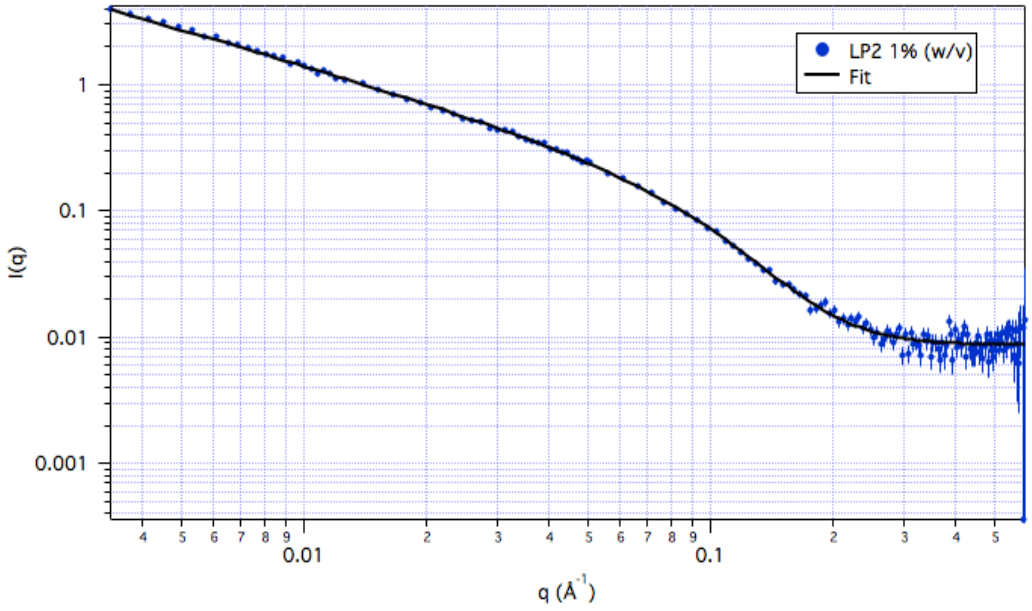

(a)

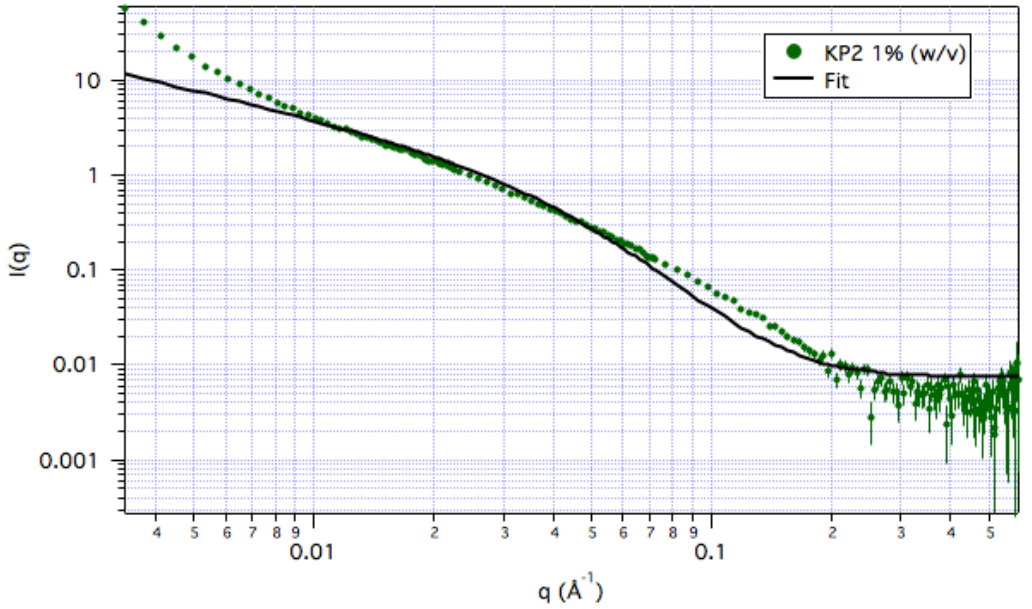

(b)

Figure 5.20 (cntd)

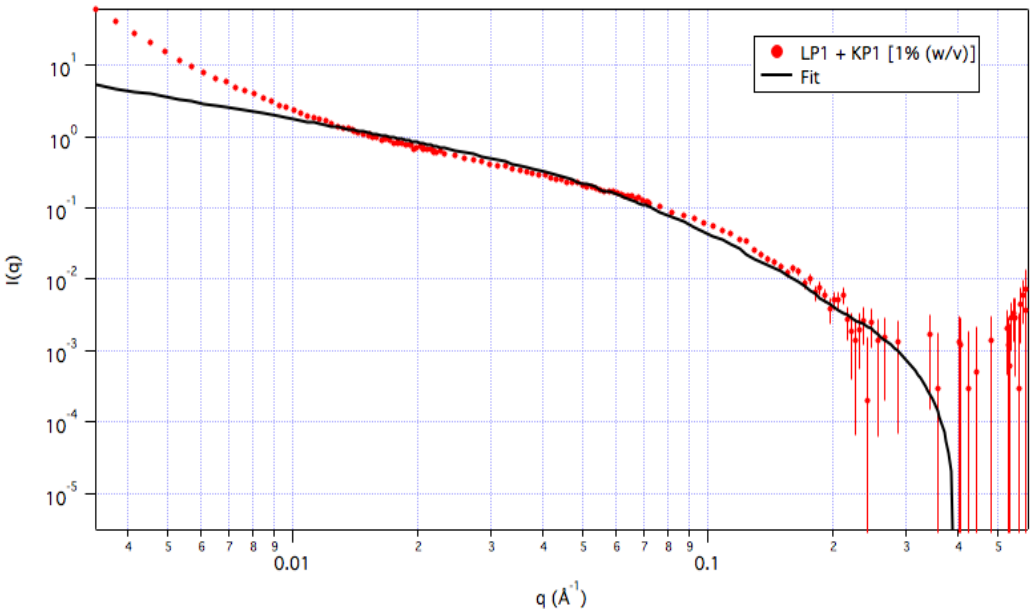

(c)

Figure 5.20. Fits of SANS I(q) v/s q data to polydisperse radius cylinder form factor for (a) LP2 (b) KP2 and (c) LP2:KP2 1:1 (w/w).

The red curves in Figure 5.21 (a-c) indicate the I(q) v/s q plots for the LP2, KP2 and 1:1 (w/w) LP2:KP2 samples including scattering signal contribution from the buffer pH 7 50 mM BTP 150 mM NaCl. The black curve indicates scattering signal from the neat buffer pH 7 50 mM BTP 150 mM NaCl. The blue curve is scattering signal exclusively from the peptide nanostructure of LP2, KP2 and 1:1 (w/w) LP2:KP2 blend and is obtained by subtracting the buffer scattering (black curve) from the overall sample scattering signal (red curve). The blue curves indicate presence of observable scattering signal in the q ranges between 0.2 <q< 0.5 $A^{\circ-1}$ for the LP2 and KP2 peptide nanostructures. The high-q scattering is significantly diminished in case of the 1:1 (w/w) LP2:KP2 sample as

compared to the LP2 and KP2 samples. Similar to the LP1, KP1 and 1:1 (w/w) LP1:KP1 blend, the presence of high-q scattering exclusively from the nanostructure of LP2 and KP2 might indicate the presence of a low concentration of peptides in solution that are not part of the network structure. It is important to note the diminished high-q scattering for the 1:1 (w/w) LP2:KP2 blend. This diminished scattering signal for the blend might indicate the peptide participating exclusively in the nanostructure or being retained in the network nanostructure without being broken away, as compared to the neat LP2 and KP2 peptide nanostructures.

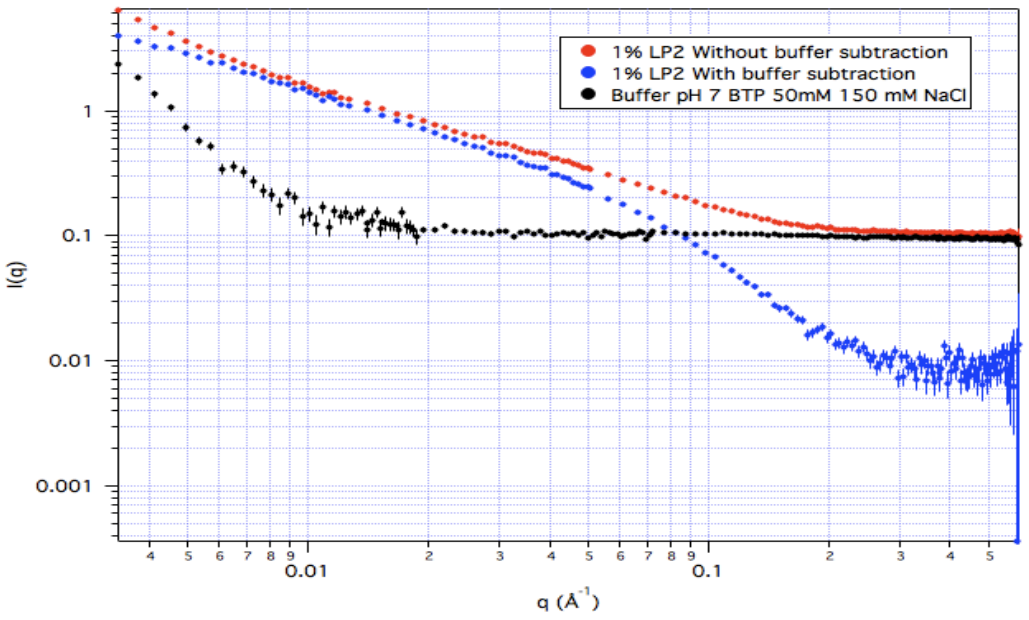

(a)

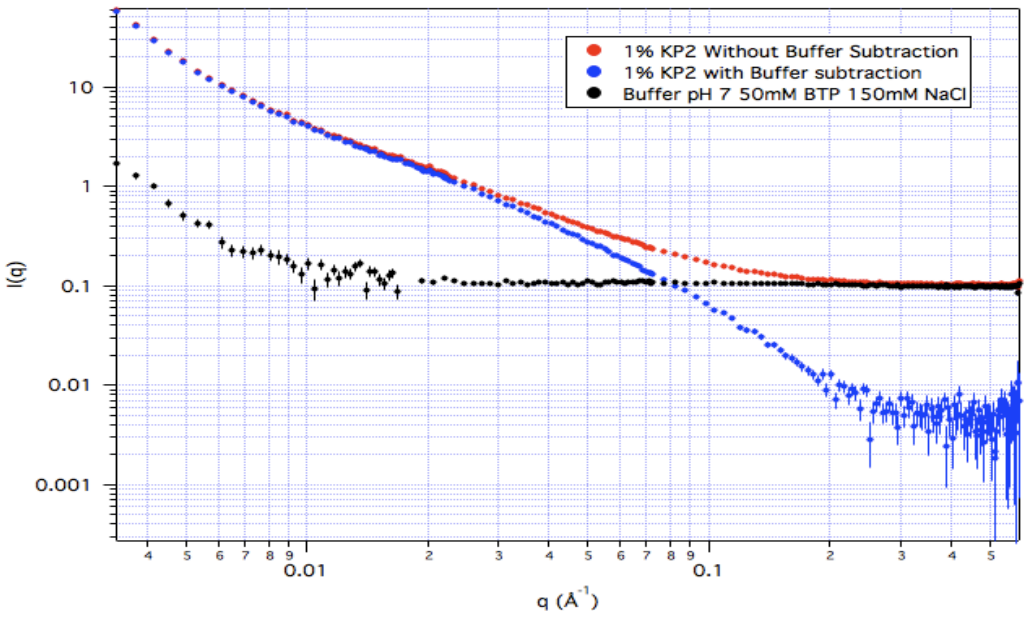

(b)

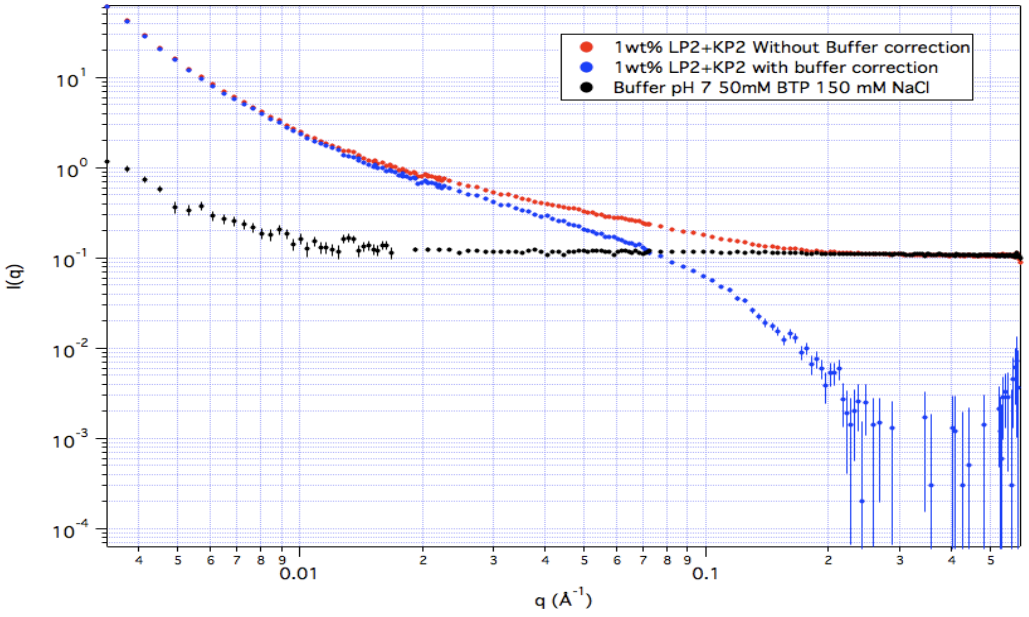

(c)

Figure 5.21. I (q) v/s q scattering signal from sample with scattering contribution from buffer retained (red) and subtracted (blue) and the buffer scattering itself (black) for (a) LP2 (b) KP2 and (c) 1:1 (w/w) LP2:KP2

The value of the average radius of the cylindrical nanostructures obtained for the sample LP2 are ~ 1 nm, with the polydispersity in the radius values ~ 0.5. This value is an average value of radii calculated by the software and can be considered to be within the range of expected radius values of the cylindrical nanostructure based on the strand lengths of the individual peptide hairpins and the radius values obtained from the cylindrical nanostructures formed by MAX1, LP1, KP1 and 1:1 (w/w) LP1:KP1. The data from the samples KP2 and 1:1 (w/w) LP2:KP2 cannot be fit to the polydisperse radius cylinder function and thus radius and polydispersity values obtained from the fit are not reliable. (Table 5.5) Values of the polydispersity in cylindrical radius values are not meaningful due to the expression of polydispersity given by $p = \sigma / R_{avg}$; $\sigma << R_{avg}$.

Table 5.5. Values of average radius and polydispersity in radius values obtained by fitting I(q) v/s q for the samples LP2, KP2 and LP2:KP2 1:1 (w/w) with fit windows specified for each sample.

Sample	**Radius (nm)**	**Polydispersity** $p = \sigma / R_{avg}$ σ: Schulz distribution variance; R_{avg}: Average radius
LP2	0.91±0.07	0.50

The LP2 and KP2 peptides have steeper wedge and trough shape gradients

compared to the LP1 and KP1 peptides. As shown in Figure 5.15, shapes of the I (q) v/s q curves obtained from all three samples LP2, KP2 and 1: 1 (w/w) LP2: KP2 are significantly different from one another, indicating an influence of the steeper shape gradients on the hierarchically assembled morphologies from the three samples. The value of the exponent 'n' obtained by plotting log (I) v/s log (q) is ~ -1 only for the LP2 assembled structure and deviates significantly from the -1 value in case of structures from KP2 (-1.66) and 1:1 (w/w) LP2:KP2 (-1.40) (Table 5.6).

The wedge shaped hydrophobic surface of LP2 does not appear to disturb assembly of the folded β-hairpins attempting to bury their hydrophobic surfaces and subsequently assembling into cylindrical nanostructures. The absence of strictly cylindrical morphology formed from the KP2 peptide can be attributed to the trough shaped hydrophobic surface of KP2. This non-uniform surface might offer more local surface area for hydrophobic packing leading to uneven burial of hydrophobic surfaces. The uneven packing of two trough-shaped folded β-hairpins may ultimately lead to an assembled structure distorted from a cylindrical morphology. Another factor that might lead to deviation of the assembled nanostructure from the KP2 samples is the presence of hydrophobic side chain amino acids at the corners of the folded KP2 β-hairpin as described in Section 5.3. As discussed before, both lateral and facial hydrophobic interactions are fundamentally important secondary interactions that influence the self-assembly pathway and assembled nanostructure from β-hairpin peptides. The large

hydrophobic side chains on a KP2 β-hairpin on the edges of growing fibrils could potentially undergo hydrophobic interactions with a KP2 β-hairpin from another growing fibril or with molecules in solution, thus disturbing any unidirectional fibrillar self-assembly of KP2, leading to a non-uniform nanostructure cross-section and overall morphology as observed by the scattering 'low-q' scattering exponent 'n' for KP2 which deviates significantly from the value ~ -1. It is important to note that such distortion from a cylindrical morphology is not observed in case of the trough shaped peptide KP1. This lack of distortion of KP1 from a cylindrical morphology can be attributed to the smaller size of its hydrophobic side chain amino acids (norvaline) in the corners of the folded β-hairpins as compared to the relatively larger hydrophobic side chain corner amino acids (phenylalanine) in case of KP2. It is important to note that the 'n' value for the nanostructure assembled from the 1:1 (w/w) blend of LP2:KP2 also deviates significantly from the ~ -1 value. This provides evidence that in case of a 1:1 (w/w) blend of LP2 and KP2, the nanostructure is dominated by the contribution from KP2, which leads to the distortion of the cylindrical morphology of the nanostructure.

From the log (I(q)) v/s log (q) analysis of the three samples in the high-q region, LP2, KP2 and 1:1 (w/w) LP2:KP2 look very similar to that from LP1, KP1 and 1:1 (w/w) LP1:KP1 gels, respectively, at the high-q length scale. At this length scale, where the scattering signal is obtained at the length scale of the surface of an individual fibril level, we find an $I(q) \sim q^m$ dependence, with $2 < m$

< 3. These values of 'm' (Table 5.6) indicate the presence of a very rough surface for each individual assembled nanostructural unit, be it a cylindrical structure in case of LP2 or more non-specific fibrillar structure for KP2 and the blend.

Table 5.6. Values of low-q exponent 'n' and high-q exponent 'm' obtained by fitting log (I(q)) v/s log (q) for the samples LP2, KP2 and LP2:KP2 1:1 (w/w) with fit q windows specified for each sample

Sample	**Low-q 'n'**	**High-q 'm'**
LP2	-1.10 *(0.007-0.066)*	-2.18 *(0.07-0.20)*
KP2	-1.66 *(0.005-0.069)*	-2.40 *(0.07-0.24)*
1:1 (w/w) LP2:KP2	-1.40 *(0.07-0.196)*	-2.54 *(0.07-0.17)*

The values of exponent 'm1' obtained from the fits to data from LP2, KP2 and 1:1 (w/w) LP2:KP2 are shown in Table 5.7. The values of 'm1' for LP2, KP2 and 1:1 (w/w) LP2:KP2 are in the range 1< m1< 3. As discussed earlier, values of 'm1' in a range 1< m1 < 3 can be attributed to mass fractal scattering from the studied samples at high-q length scales (~ 1-10 nm), with higher values of 'm1' representing higher network densities. It is important to note that the 'm1' value for the 1:1 (w/w) LP2:KP2 is significantly lesser than the 'm1' values for LP2 and KP2, potentially indicating a less dense or looser network structure for the blend as compared to the network structure from LP2 and KP2 individually. This morphological characteristic of the network from the blend of LP2 and KP2 is distinct from that of the blend LP1 and KP1 peptides, which is similar in

morphology to the networks from the individual peptides, LP1 and KP1.

Table 5.7. Values of high-q exponent 'm1' obtained by fitting I (q) v/s q for the samples LP2, KP2 and LP2:KP2 1:1 (w/w).

Sample	**High-q exponent 'm1'**
LP2	2.72
KP2	2.88
1:1 (w/w) LP2:KP2	2.16

As shown in Figure 5.21, a stiff (~ 800Pa) 1% (w/v) hydrogel is formed from the LP2 peptide. This hydrogel demonstrates shear thinning behavior when subject to high amplitude steady state shear (1000/s) for a period of 2 min as well as substantial rehealing (~ 50% of original modulus) behavior upon cessation of shear treatment and allowing to age. This shear thinning and rehealing behavior in case of LP2 hydrogels suggests branched fibril formation by LP2 peptides. The hydrogel prepared from the KP2 peptide under the same solution conditions and concentration 1% (w/v), is much less stiff as compared to the LP2 hydrogel (~ 60 Pa) and shows poor rehealing abilities post cessation of shear treatment and ageing for several hours. The properties of poor network formation and lack of rehealing after shear treatement exhibited by the KP2 hydrogels can be potentially attributed to the lack of the uniform cylindrical morphology of its nanostructure. A non-cylindrical fibrillar morphology demonstrated by assembled KP2 peptides

can also be largely unbranched as opposed to the branched cylindrical fibrillar morphology of the assembled LP2 peptides.

When a hydrogel is prepared from a 1:1 (w/w) blend of LP2 and KP2, it has a much lower stiffness value, G' ~220 Pa, as compared to the G' gel obtained from LP2 (~820 Pa) but much higher than the G' for a KP2 hydrogel (~60 Pa). This result obtained for 1:1 (w/w) LP2:KP2 blend, is significantly different to the 1:1 (w/w) LP1:KP1 2% (w/v) (~ 410 Pa) overall network which is stiffer than the pure LP1 1% (w/v) (~200 Pa) and KP1 1% (w/v) (~ 60 Pa) networks. The much lower stiffness of the hydrogel from the blend of 1:1 (w/w) LP2: KP2 indicates potential elimination of branching in the LP2:KP2 blend. The critical observation in case of the blend of LP2 and KP2 is that the hydrogel formed from the blend (~ 410 Pa) shear thins but fails to recover to even 10% of the original storage modulus of the original network (Figure 5.21 green curve). This lack of rehealing might indicate that a branched fibrillar nanostructure as seen in case of MAX1, LP1, KP1 and LP2 might not be present in case of 1:1 (w/w) LP2:KP2.

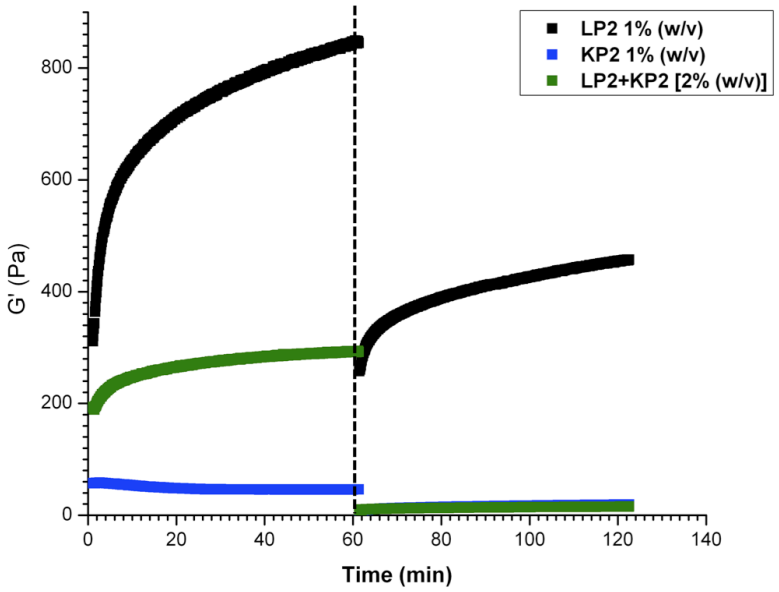

Figure 5.22. Steady state shear response of hydrogels from samples LP2 1% (w/v), KP2 1% (w/v) and 1:1 (w/w) LP2:KP2 2% (w/v). Data shown are oscillatory time sweep measurement data (G'(Pa)) before and after application of steady state shear (1000/s for 120 sec, indicated by dotted line). For all data points G'>>G", indicating solid nature of the hydrogels.

Considered together, results from the cryo-TEM, SANS characterization and the oscillatory rheological characterization indicate branched fibrillar structures formed from assembly of the LP2 peptide. On the other hand, the KP2 peptide and the 1:1 (w/w) LP2:KP2 demonstrate non-cylindrical, non-uniform fibrillar morphologies. The analyses of results from the nanostructural characterization techniques do not provide direct evidence to any shape specific interactions between the complementary wedge and trough shaped β-hairpins of LP2 and KP2. Results from rheological characterization indicate shear thinning but lack of rehealing behavior from hydrogels formed from 1:1 (w/w) blend of

LP2:KP2 suggesting significant decrease in the formation of branched fibrils in the blended sample of LP2 and KP2. The non-existence of branched fibrils in case of the LP2 and KP2 peptides can originate due to much more irregular and non-uniform assembled nanostructure from the assembly of the two samples. These irregularities can lead to disturbance in the formation of entanglements and branch points that are well defined in case of comparatively regular fibrillar structures. This disturbance can result in formation of networks with a much lesser degree of physical crosslinking and consequently poorer network mechanical properties. These poorer network properties can adversely affect the post shear rehealing abilities of the networks.

5.4.4. Nanostructure-Network structure-shear response correlation for LP3, KP3 and LP3:KP3 blend

Cryogenic TEM from all the three samples LP3, KP3 and 1:1 (w/w) LP3:KP3 indicated an overall fibrillar morphology with varying values of width (Figure 5.11), as discussed in Section 5.3. SANS characterization performed on the three hydrogel samples helps decipher differences in the nanostructure formed from the differently shaped hairpin peptides. Figure 5.22 shows the results of the fitting performed for I(q) v/s q data to polydisperse radius cylinder form factor for the hydrogels constructed from LP3, KP3 and 1:1 (w/w) LP3:KP3. Data were fit to the polydisperse radius cylinder function as described in Chapter 2 to yield the polydispersity in the radius values and also the average value of the cylindrical radius.

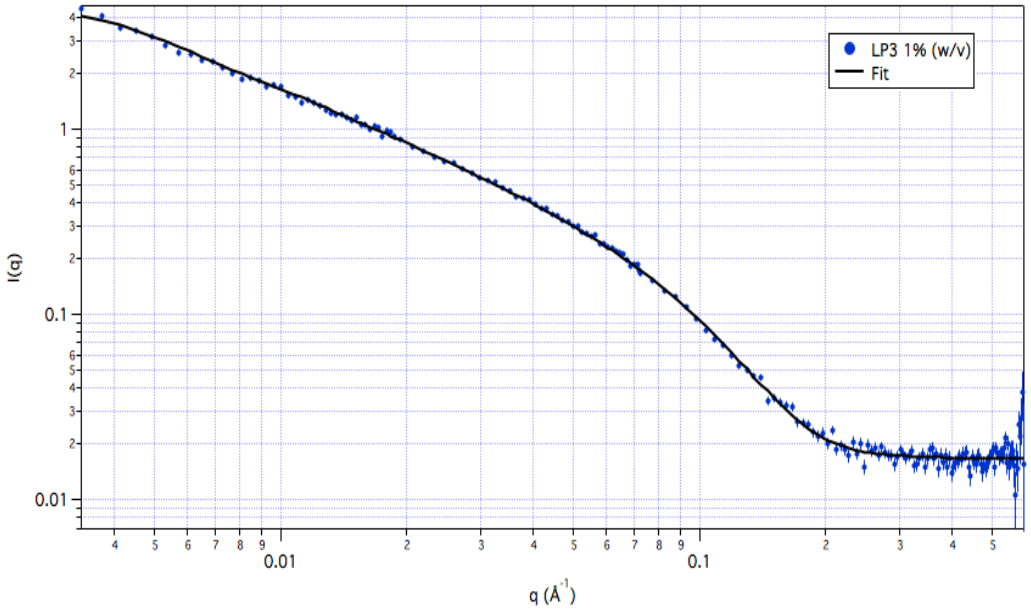

(a)

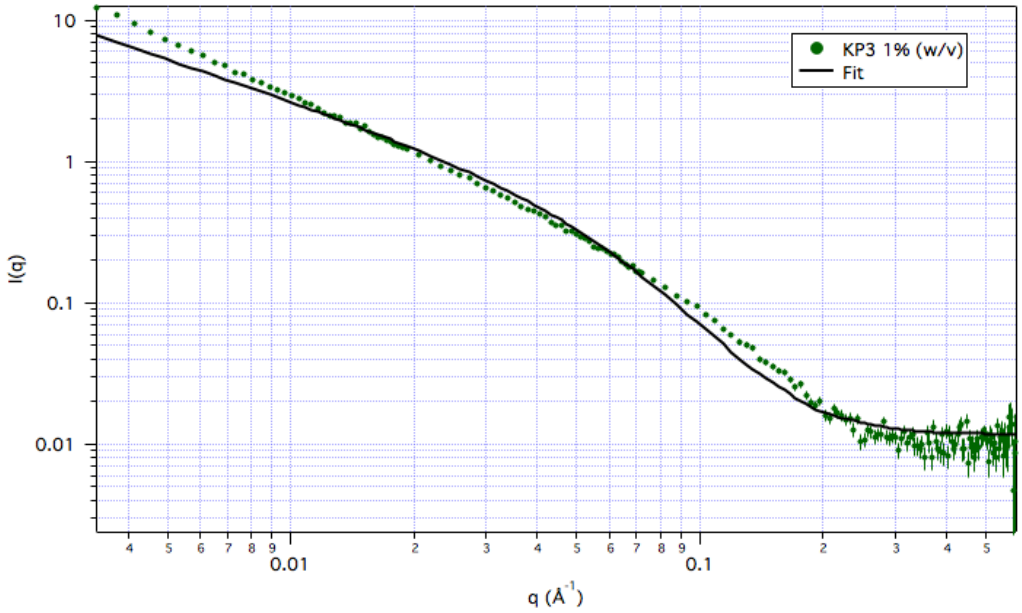

(b)

Figure 5.23 (cntd)

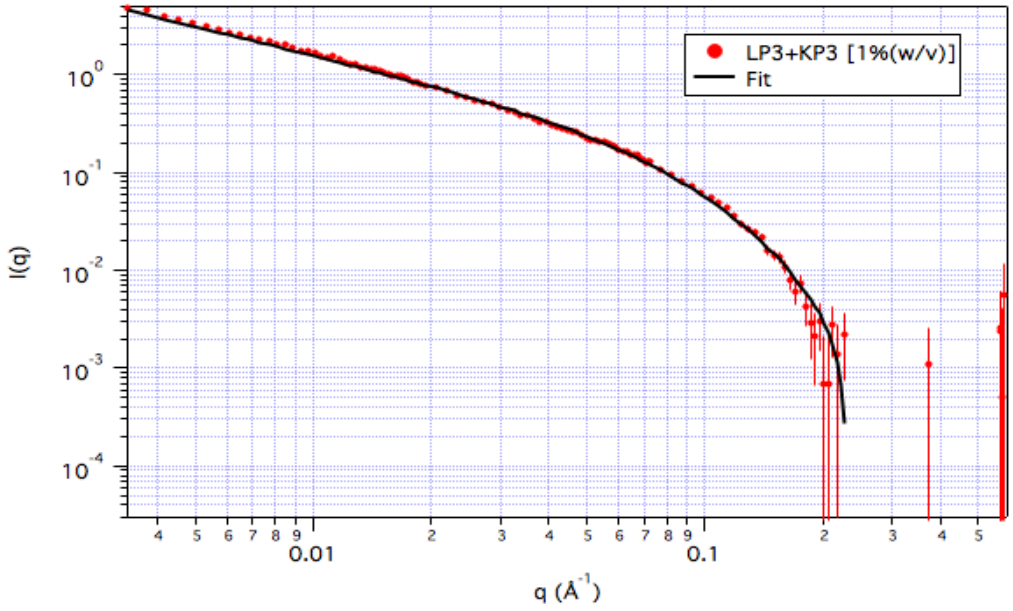

(c)

Figure 5.23. Fits of SANS I(q) v/s q data to polydisperse radius cylinder form factor for (a) LP3 (b) KP3 and (c) LP3:KP3 1:1 (w/w)

The red curves below in Figure 5.23 (a-c) indicate the I (q) v/s q plots for the LP3, KP3 and 1:1 (w/w) LP3:KP3 samples including scattering signal contribution from the buffer pH 7 50 mM BTP 50 mM NaCl. The black curve indicates scattering signal from the neat buffer pH 7 50 mM BTP 50 mM NaCl. Blue curves indicate scattering signal exclusively from the peptide nanostructure of LP3, KP3 and 1:1 (w/w) LP3:KP3 blend obtained after subtraction of the buffer scattering (black curve) from the overall sample scattering signal (red curve). The blue curves indicate presence of observable scattering signal in the q ranges between 0.2 <q< 0.5 A^{o-1} for the LP3 and KP3 peptide nanostructures. The high-q scattering is significantly diminished in case of the 1:1 (w/w) LP3:KP3

sample as compared to the LP3 and KP3 samples. Similar to earlier samples, the presence of weak high-q scattering intensity for LP3 and KP3 might indicate the presence of a low concentration of peptides in solution. It is important to note the diminished high-q scattering for the 1:1 (w/w) LP3:KP3 blend similar to the 1:1 (w/w) LP2:KP2 blend. This diminished scattering signal for the blend might indicate peptide participating exclusively in the nanostructure or being retained in the network nanostructure without being broken away, as compared to the neat LP3 and KP3 peptide nanostructures.

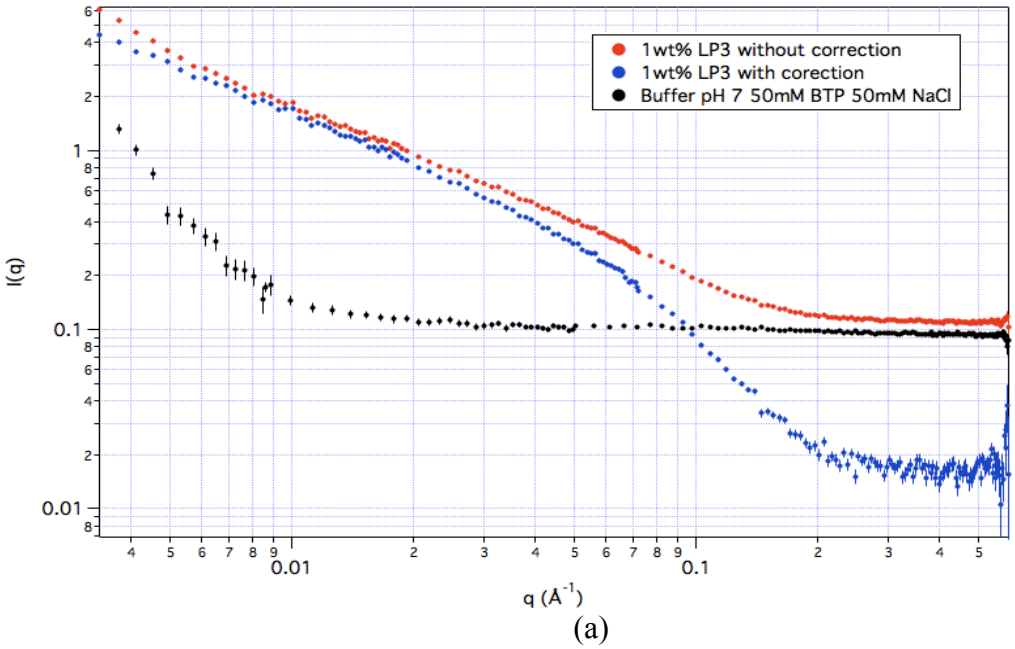

(a)

Figure 5.24 (cntd)

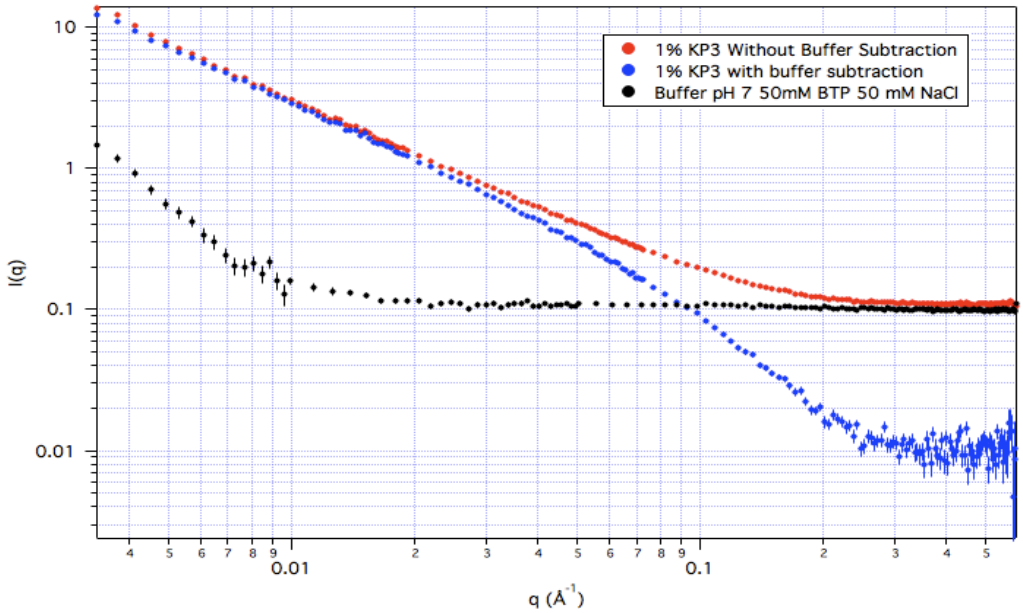

(b)

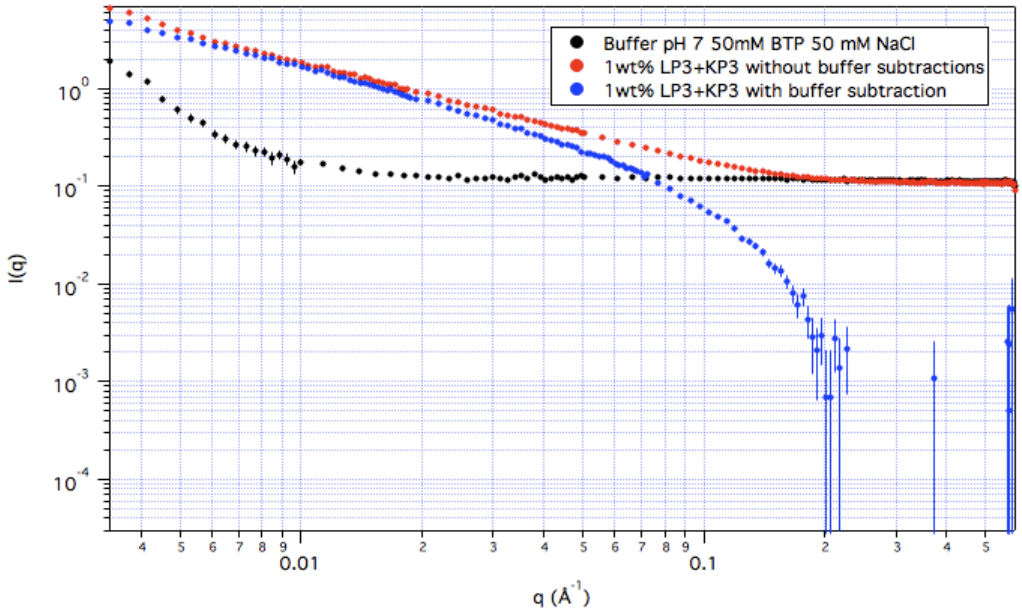

(c)

Figure 5.24. I (q) v/s q scattering signal from sample with scattering contribution from buffer retained (red) and subtracted (blue) and the buffer scattering itself (black) for (a) LP3 (b) KP3 and (c) LP3+KP3

As shown in figure 5.22, a good fit of the data to the model is obtained

across all the q-ranges investigated by SANS for the sample LP3, but not the sample KP3. In case of the 1:1 (w/w) LP3:KP3 sample, even if a least square fit of model to the SANS data is obtained, the values of the average radius and the polydispersity in the radius values are not in agreement with expected values. The value of average radius obtained ~ 0.2 nm which is much lower than the average radius value observed in case of other cylinder forming peptides like LP1, KP1, LP2 and LP3. The value of the polydispersity in radius values obtained (~1.3) is not theoretically possible (Table 5.8.). Thus, the nanostructure assembled from the 1:1 (w/w) LP3:KP3 blend cannot be considered to have a polydisperse cylindrical morphology as described by SANS.

Table 5.8. Values of average radius and polydispersity in radius values obtained by fitting I(q) v/s q for the samples LP2, KP2 and LP2:KP2 1:1 (w/w) with fit windows specified for each sample

Sample	**Radius (nm)**	**Polydispersity** $p = \sigma / R_{avg}$ σ: Schulz distribution variance; R_{avg}: Average radius
LP3	1.33±0.04	0.30

The LP3 and KP3 peptides have steeper wedge and trough shape gradients compared to the first two pairs of peptides. As shown in Figure 5.22, shapes of the I (q) v/s q curves obtained from all three samples LP3, KP3 and 1:1 (w/w) LP3:

KP3 are significantly different from one another, indicating an influence of the steep shape gradients on the hierarchically assembled morphologies from the three samples. The value of the exponent 'n' obtained by plotting log (I) v/s log (q) is ~ -1 for the LP3 assembled structure and deviates significantly from the -1 value in case of structures from KP3 (-1.40). In case of the blended sample, 1:1 (w/w) LP3:KP3, the deviation from the -1 value is observed (-1.24) (Table 5.9). Thus, considering only the value of 'n', it can be inferred that the assembled nanostructure of the 1:1 (w/w) blend of LP3 and KP3 deviates from a cylindrical morphology to something much more non-uniform along the length of the nanofibrils.

The wedge shaped hydrophobic surface of LP3 does not appear to disturb assembly of the folded β-hairpins attempting to bury their hydrophobic surfaces and subsequently assembling into polydisperse cylindrical nanostructures. The absence of strictly cylindrical morphology formed from the KP3 peptide can be attributed to the trough shaped hydrophobic surface of KP3, similar to the assembly of KP2. This non-uniform surface might offer more local surface area for hydrophobic packing leading to uneven burial of hydrophobic surfaces. The uneven packing of two trough-shaped folded β-hairpins may ultimately lead to an assembled structure distorted from a cylindrical morphology. Similar to KP2, the presence of hydrophobic side chain amino acids at the edges of the folded KP3 β-hairpin as described in Section 5.3 might possibly disturb uniform packing and cylindrical nanostructure formation by KP3. The large hydrophobic side chains on

a KP3 β-hairpin within a growing fibril could potentially undergo hydrophobic interactions with a KP2 β-hairpin from another growing fibril or with molecules in solution, thus disturbing any unidirectional fibrillar self-assembly of KP2, leading to a much less uniform nanostructure as observed by the scattering low-q scattering exponent 'n' for KP2 which deviates significantly from the value ~ -1. It is important to note that the 'n' value for the nanostructure assembled from the 1:1 (w/w) blend of LP3:KP3 also deviates from the ~ -1 value, but this deviation is not as pronounced as that for the pure KP3 sample. This deviation of the n value in case of 1:1 (w/w) LP3:KP3 points to the formation of a non-cylindrical nanostructure from the 1:1 (w/w) blend of LP3 and KP3.

From the log (I(q)) v/s log (q) analysis of the three samples in the high-q region, LP3, KP3 and 1:1 (w/w) LP3:KP3 look very similar to the samples from the first pairs LP1-KP1 and LP2-KP2. At this length scale, where the scattering signal is obtained at the length scale of the surface of an individual fibril level we find an $I(q) \sim q^m$ dependence, with $2 < m < 3$. These values of 'm' (Table 5.9) indicate the presence of a rough, nonuniform surface for each individual assembled nanostructural unit, be it a cylindrical structure in case of LP3 and the 1:1 (w/w) blend or irregular fibrillar structure for KP3.

Table 5.9. Values of low-q exponent 'n' and high-q exponent 'm' obtained by fitting log (I(q)) v/s log (q) for the samples LP3, KP3 and LP3:KP3 1:1 (w/w) with q fit windows specified for each sample

Sample	**Low-q 'n'**	**High-q 'm'**
LP3	-1.09 *(0.009-0.06)*	-2.19 *(0.08-0.19)*
KP3	-1.42 *(0.009-0.06)*	-2.09 *(0.07-0.24)*
1:1 (w/w) LP3:KP3	-1.24 *(0.007-0.06)*	-2.67 *(0.07-0.18)*

The values of exponent 'm1' obtained from the fits to data from LP3, KP3 and 1:1 (w/w) LP3:KP3 are shown in Table 5.10. The values of 'm1' for LP3, KP3 and 1:1 (w/w) LP3:KP3 are in the range $1< m1< 3$. As discussed earlier, values of 'm1' in a range $1< m1 < 3$ can be attributed to mass fractal scattering from the studied samples at high-q length scales (~ 1-10 nm), with higher values of 'm1' representing higher network densities. The 'm1' value for the three samples goes of progressively decreasing in the order of $m1_{LP3} > m1_{KP3} > m1_{LP3:KP3}$ indicating a decrease in network density or presence of a looser network structure for the KP3 sample and the blended sample compared to the LP3 sample. The trends in changes in morphological characteristics of the networks from LP3, KP3 and 1:1 LP3:KP3 blend are distinct from the trends in morphology changes in case of networks from the samples in the LP1-KP1 and LP2-KP2 groups of

samples.

Table 5.10. Values of high-q exponent 'm1' obtained by fitting I(q) v/s q for the samples LP3, KP3 and LP3:KP3 1:1 (w/w).

Sample	**High-q exponent 'm1'**
LP3	2.73
KP3	2.24
1:1 (w/w) LP3:KP3	2.08

An LP3 1% (w/v) hydrogel demonstrates shear thinning and rehealing behavior when studied using a steady state shear treatment and allowed recovery post shear cessation (Figure 5.24 black curve). The LP3 hydrogel is a stiff hydrogel (~ 200 Pa) with the shear-thinning and rehealing behavior suggesting a branched fibrillar structure. The KP3 hydrogel constructed at the same concentration and same solution conditions as the LP3 network is much less stiff (~80 Pa) and also shows poor rehealing abilities after being subject to shear treatment, indicative of both an irregular nanostructure and lack of branching. The hydrogel from the 1:1 (w/w) blend of LP3:KP3 (overall 2% (w/v)) is an order of magnitude stiffer (~1600 Pa) than the pure LP3 1% (w/v) gel (~200 Pa) and the pure KP3 1% (w/v) gel (~ 80 Pa). Thus, significant gel stiffness, much greater than that seen in case of the 1:1 (w/w) LP1:KP1 blend (Figure 5.19 green curve) or simply double the concentration MAX1 gel (Figure 5.14), is observed in case

of the 1:1 (w/w) LP3:KP3 blend. Due to the designed, steepest gradient of the hydrophobic wedge and trough shape, the LP3 and KP3 peptides contain the amino acids with the sterically largest side chains. The large side chains presumably offer much more surface area for hydrophobic collapse while undergoing assembly, thus leading to more instances of defect-induced branching. The reinforcement observed in the blended networks from LP3 and KP3 can be attributed to these presumed branching points. Additionally, these side chains are inherently more hydrophobic than the smaller hydrophobic side chains in KP1-LP1 and KP2-LP2 and can thus lead to formation of stiffer individual fibrils leading to stiffer overall networks. The hydrogel obtained from the blend of LP3 and KP3 demonstrates shear thinning and partial rehealing behavior, indicating formation of an extensively branched network structure.

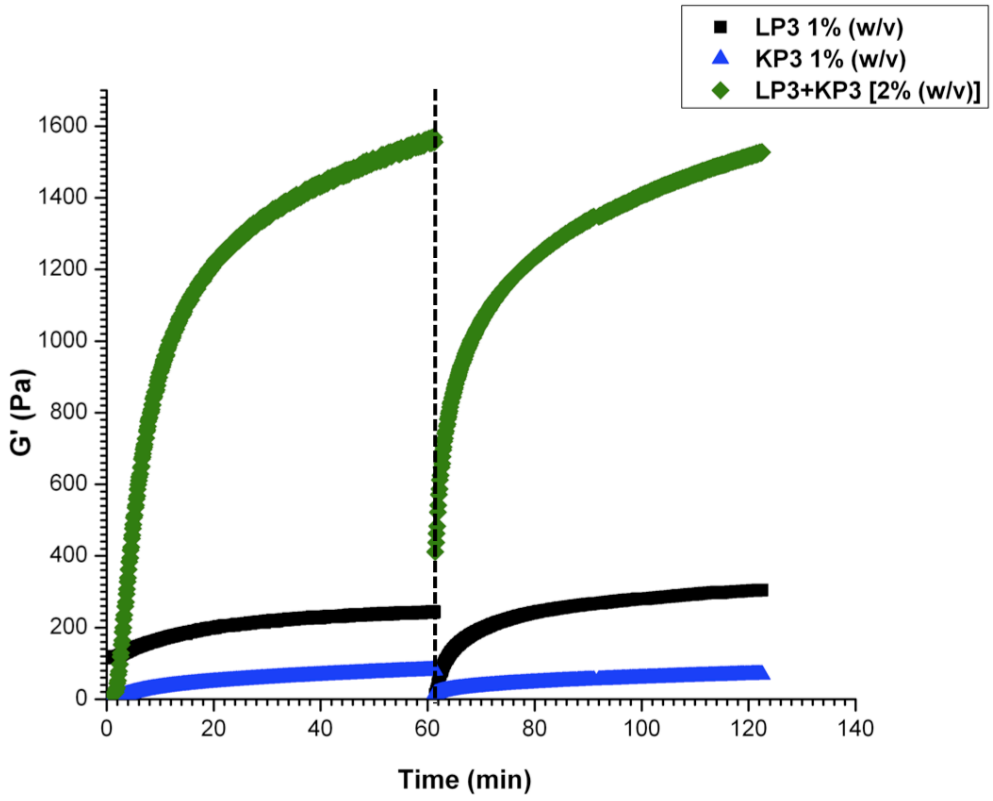

Figure 5.25. Steady state shear response of hydrogels from samples LP3 1% (w/v), KP3 1% (w/v) and 1:1 (w/w) LP3:KP3 2% (w/v) characterized using oscillatory rheology. Data shown are oscillatory time sweep measurement data (G'(Pa)) before and after application of steady state shear (1000/s for 120 sec, indicated by dotted line). For all data points G'>>G", indicating solid nature of the hydrogels.

Considered together, results from the cryo-TEM, SANS characterization and the oscillatory rheological characterization indicate branched cylindrical fibrillar structures formed from assembly of the LP3 peptide sample. On the other hand, the 1:1 (w/w) LP3:KP3 and KP3 peptide samples demonstrate non-uniform fibrillar morphologies. The analyses of results from the nanostructural characterization techniques as well as the rheological characterization techniques do not provide direct evidence to a any shape specific interactions between the

complementary wedge and trough shaped β-hairpins of LP3 and KP3 as originally designed.

5.5. Overall Analysis of the nanostructure-network structure-network mechanical behavior correlation for the wedge and trough peptides

The analysis of results from morphological and rheological characterization of self-assembled structures from the newly designed wedge and trough shaped β-hairpin peptides can be rationalized in the following manner. The first pair of peptides LP1 and KP1 is designed to demonstrate the shallowest gradients of the hydrophobic wedge and trough shapes, respectively, and these shapes gradients are only slightly steeper than the uniform hydrophobic face of MAX1. For the samples LP1, KP1 and 1:1 (w/w) LP1:KP1, fibrillar nanostructures are observed. These nanostructures can be considered to be cylindrical in morphology from SANS. It can also be inferred that the fibrillar cylindrical nanostructures are branched, since all three samples assemble into stiff, self-standing hydrogels that demonstrate shear thinning and rehealing behavior. The LP2 and KP2 peptides have been designed to demonstrate an intermediate gradient of the hydrophobic wedge and trough shape (as compared to LP1-KP1 and LP3-KP3 pairs) in the series of the newly designed peptides. The LP2 peptides form fibrillar, cylindrical nanostructures that can be inferred to be branched due to formation of stiff shear thinning and rehealing hydrogels. The KP2 peptide and the 1:1 LP2:KP2 sample both demonstrate fibrillar structures

that deviate from the cylindrical morphology. The hydrogel formed by the KP2 peptide is much less stiff as compared to the hydrogel from the LP2 peptide and is also sparingly rehealable after being subject to steady state shear. The hydrogel from the 1:1 blend of LP2 and KP2 is stiff and demonstrates shear thinning but lack of rehealing behavior after being subject to steady state shear. Thus, in case of pure KP2 and the 1:1 LP2:KP2 blend, a branched network of cylindrical fibrillar may not be observed as seen in case of MAX1, LP1, KP1 and 1:1 (w/w) LP1:KP1. The LP3 peptides form fibrillar, cylindrical nanostructures similar to LP1 and LP2 that can be considered as branched due to formation of stiff shear thinning and rehealing hydrogels from LP3. The KP3 peptide demonstrates fibrillar structures that deviate from the cylindrical morphology. The hydrogel formed by the KP3 peptide is much less stiff as compared to the hydrogel from the LP3 peptide and is also sparingly rehealable after being subject to steady state shear. The 1:1 (w/w) LP3:KP3 blend also demonstrates a non-uniform fibrillar morphology. The hydrogel formed from the blend 1:1 LP3:KP3 is synergistically an order of magnitude stiffer as compared to the hydrogels from LP3 and KP3 peptides individually. Thus, out of the new peptides with the steepest gradient in hydrophobic side chains, the LP3 sample formed the most cylindrical nanostructures that include branching whereas a fibrillar hydrogel network with branching that does display a non-uniform morphology is formed by the 1:1 (w/w) LP3:KP3 peptide sample.

Cryogenic Transmission Electron Microscopy data from all the samples of

the newly designed peptides demonstrate fibrillar nanostructures with non-uniform widths. These values of fibrillar width are much higher than the fibrillar widths quantified by the Small Angle Neutron Scattering data. The cryo-TEM data acquired on the samples show that the boundary between the fibrillar nanostructures and the solvents is not sharp. There exist areas of electronic contrast intermediate in magnitude between the contrast shown by the fibril and the solvent. These areas are not uniform, indicating an irregular and non-uniform nanostructure at the length scale of the individual fibril as confirmed by SANS data fitting at high-q. While performing image analysis on the cryo-TEM data fibrillar widths were counted by considering the areas of non-uniform electronic contrast. The SANS data quantifies the fibrillar thickness taking into account the neutron contrast between the most regular nanostructure and the solvent. The discrepancy between the fibrillar widths obtained by SANS and cryo-TEM techniques can be attributed to this difference in the way measurements of fibrillar thickness were performed by both techniques.

From the above analysis it is apparent that direct evidence to support the hypothesis of the wedge and trough shape specific interactions in the blends of the LP and KP peptides is not possible. In the 1:1 (w/w) blends of the LP and KP peptides, it is difficult to ensure that each wedge shaped LP hairpin will undergo shape specific hydrophobic collapse with one trough shaped KP hairpin. The lack of direct structural or rheological evidence of the shape specific wedge-trough interactions occurring in the blends of any LP and KP peptides can also be

attributed to the possibility of this 1:1 wedge-trough hydrophobic collapse not dominating the peptide assembly in the blends. Instead, there is clear possibility of wedge-wedge and trough-trough interactions, as well as other irregular aggregation, occurring during the assembly of the blends.

5.6. Conclusion

Samples from peptides LP1, KP1, LP2, KP2, LP3, KP3 and 1:1 (w/w) blends of LP1:KP1, LP2:KP2 and LP3:KP3 underwent random coil to β-sheet intramolecular folding in a manner similar to the parent sequence MAX1. Similar changes in solution conditions as observed in MAX1 were required for self-assembly depending upon overall hydrophobic nature of each of the peptides. The previous section discusses and rationalizes the observations from morphological characterization of the nanostructure and rheological characterization of the hydrogels relative to the assembled nanostructure from these samples. It can be concluded from the analyses discussed in Section 5.5 that direct morphological or rheological evidence of elimination or significant reduction in fibrillar branching has not been obtained using the discussed characterization techniques. In addition, clear complementarity of the wedge-trough hydrophobic face packing during assembly to produce clean, cylindrical nanostructures was not observed. The only indirect evidence regarding potential elimination of branching has been obtained in case of the shear thinning but non-rehealing hydrogel from the 1:1 (w/w) LP2:KP2 blend. Thus, although the

designed hydrophobic shape specificity or the lack of shape uniformity was found to significantly influence the self assembled nanostructure and network rheological behavior in newly designed self assembling β-hairpin peptides, no direct evidence of hydrophobic shape specificity has been obtained for the 1:1 blends of the peptides. This is most likely due to non-specific hydrophobic interactions between peptides due to the large hydrophobic side chains used in the design of the new peptides and the exposure of these hydrophobic side chains to the solution during the folding and assembly of the peptides causing non-specific aggregation. Non-specific aggregation during peptide assembly can be further investigated by acquisition of data on samples at different peptide concentrations and evaluation of potential structure factor contributions to the assembled nanostructure. Therefore, the design of new peptides incorporating a new set of hydrophobic side chain amino acids assembly of which can ensure proper shielding of hydrophobic side chains along the fibrillar edges to so as limit non-specific aggregation of peptides during solution assembly can be explored as a next step.

REFERENCES

(1) Rajagopal, K.; Ozbas, B.; Pochan, D. J.; Schneider, J. P. *European Biophysics Journal with Biophysics Letters* **2006**, *35*, 162.

(2) Yucel, T.; Micklitsch, C. M.; Schneider, J. P.; Pochan, D. J. *Macromolecules* **2008**, *41*, 5763.

(3) Rajagopal, K., University of Delaware, 2007.

(4) M.Micklitsch, C., University of Delaware, 2007.

(5) Kelly, S. M.; Price, N. C. *Current Protein & Peptide Science* **2000**, *1*, 349.

(6) Craig, S.; Pain, R. H.; Schmeissner, U.; Virden, R.; Wingfield, P. T. *International Journal of Peptide and Protein Research* **1989**, *33*, 256.

(7) Freskgard, P. O.; Martensson, L. G.; Jonasson, P.; Jonsson, B. H.; Carlsson, U. *Biochemistry* **1994**, *33*, 14281.

(8) Danino, D.; Bernheim-Groswasser, A.; Talmon, Y. *Colloids and Surfaces a-Physicochemical and Engineering Aspects* **2001**, *183*, 113.

(9) Bozolla J.J.; L.D., R. *Electron Microscopy*; Jones and Bartlett Publishers, Inc: Sudbury, MA, 1998.

(10) Schneider, C. A.; Rasband, W. S.; Eliceiri, K. W. *Nature Methods* **2012**, *9*, 671.

(11) Ozbas, B.; Rajagopal, K.; Schneider, J. P.; Pochan, D. J. *Physical Review Letters* **2004**, *93*.

(12) Schneider, J. P.; Pochan, D. J.; Ozbas, B.; Rajagopal, K.; Pakstis, L.; Kretsinger, J. *J. Am. Chem. Soc.* **2002**, *124*, 15030.

(13) Yan, C. Q.; Pochan, D. J. *Chemical Society Reviews* **2010**, *39*, 3528.

(14) Kotlarchyk, M.; Stephens, R. B.; Huang, J. S. *J. Phys. Chem.* **1988**, *92*, 1533.

(15) Lin, T. L.; Chen, S. H.; Gabriel, N. E.; Roberts, M. F. *J. Phys. Chem.* **1987**, *91*, 406.

(16) Bale, H. D.; Schmidt, P. W. *Physical Review Letters* **1984**, *53*, 596.

(17) Hammouda, B. Probing Nanoscale Structures- The SANS Toolbox.

(18) Hule, R. A.; Nagarkar, R. P.; Altunbas, A.; Ramay, H. R.; Branco, M. C.; Schneider, J. P.; Pochan, D. J. *Faraday Discussions* **2008**, *139*, 251.

(19) Porod, G. *Small-Angle X-ray Scattering*; Academic Press: London, 1982.

(20) Hammouda, B.; Horkay, F.; Becker, M. L. *Macromolecules* **2005**, *38*, 2019.

(21) Hammouda, B.; Ho, D. L.; Kline, S. *Macromolecules* **2004**, *37*, 6932.

(22) Jackson, A. J. Introduction to Small-Angle Neutron Scattering and Neutron Reflectometry **2008**.

Chapter 6

HYBRID MATERIALS BASED ON β-HAIRPIN PEPTIDE HYDROGELS AND HYALURONIC ACID

6.1. Introduction

Hybrid multicomponent hydrogels (HMH) can be defined as hydrogels that contain chemically, morphologically, and functionally diverse components[1] that are chemically or physically interconnected. Jia and Kiick[1] have provided an extensive review of efforts conducted towards developing HMH with superior mechanical properties and biological functionality as compared to their individual polymeric, peptidic or protein-based constituents. Hydrogels based on synthetic polypeptides and peptides, as discussed in the last several chapters of this thesis have potential biomedical applications such as drug delivery and tissue engineering[2,3]. However, hydrogels made from individual peptides, for example, do not have all of the desired properties needed for biomedical success (e.g. single material might need much higher stiffness and desired biological ligands than β-hairpins exhibit on their own). Therefore, instead of synthesizing new peptides with new function that must be incorporated into the peptide assembly mechanism, one can make a composite hydrogel by mixing peptide hydrogel with other biomolecules. Hydrogels based on various biopolymers such as chondroitin sulfate, alginate, cellulose derivatives, chitosan and hyaluronic acid have been comprehensively investigated for potential applications in tissue engineering and

studies based on these polymers including their specific biological properties have been reviewed extensively[4,5]. An interesting attribute of construction of HMHs by using peptide/protein based hydrogels and biopolymers offers an opportunity to develop modular biomaterials with synergistically enhanced properties by combining favorable mechanical, biological and morphological properties of their individual constituents.

MAX8 (VKVKVKVK-V^{D}PPT-KV**E**VKVKV-NH_2) is a peptide obtained by point substitution of the lysine group at position 15 in the MAX1 (VKVKVKVK-V^{D}PPT-KV**K**VKVKV-NH_2) sequence by a glutamic acid residue. Glutamic acid has a negatively charged side chain at moderate pH in contrast to the positively charged side chain of lysine. Thus, while undergoing folding and self-assembly MAX8 demonstrates additional electrostatic interactions as compared to MAX1 along with hydrophobic interactions and hydrogen bonding leading to expedited gelation kinetics and ultimately formation of stiffer hydrogels than MAX1 under the same solution conditions and peptide concentration[6]. MAX8 peptides can undergo self-assembly to form hydrogel materials under physiological pH (~7.4)[7,8], salt content[9] (~160mM Salt) and temperature conditions (37°C)[9-11]. MAX8 allows uniform 3D living mammalian cell or drug payload encapsulation due to quicker gelation time relative to MAX1 (~ 1 min v/s ~ 30 min for MAX1) at physiological solution conditions[10]. Thus, MAX8 has particular relevance to homogeneous 3D cell encapsulation and potential tissue engineering applications.

Hydrogels based on the β-hairpin forming peptides MAX1 and MAX8 demonstrate tunable material properties such as gel stiffness[12], mesh size[13] and gelation kinetics[7,14,15] that can be easily controlled by varying parameters like peptide concentration and solution conditions (pH and/or ionic strength[14] and temperature[16]). In addition to the stable and tunable nature of ß-hairpin peptide hydrogels from MAX1 and MAX8, these hydrogels function as injectable solids that can be delivered using a common device such as a syringe. These preformed, solid gels undergo shear thinning on exposure to syringe-induced stress and immediately self-heal into solids post-injection and eventually restore their original rigidity on removal of the stress[17]. Yan et al[11]. have shown that during syringe injection of a MAX8 hydrogel with encapsulated MG63 progenitor osteoblasts, only the gel portion at the walls of a syringe experience shear and eventual recovery while the bulk of MG63 cells encapsulated within the bulk of the MAX8 hydrogel experience negligible shear. This particular plug flow property of these gels protects the cells encapsulated within from syringe shear effects and does not adversely affect cell viability. Thus, hydrogels based on MAX1 and MAX8 are potential vectors for the injectable delivery of materials of therapeutic importance that include cells, drugs and proteins such as growth factors.

In addition to their structural utility, hydrogels based on β-hairpins have demonstrated biocompatibility (MAX1 and MAX8) [18,19], non-inflammatory properties (MAX1 and MAX8) [10] and in some cases biologically effective

properties such as antibacterial activity (MAX1[20] and MARG1[21], which is a gel forming MAX1 derivative). These biocompatible self-assembling peptide systems provide flexibility of peptide structure by allowing introduction of specific functionalities for materials and biochemical properties such as post self-assembly chemical crosslinking to yield stiffer hydrogels[22]. Macromolecule self-diffusion and bulk release studies with MAX1 and MAX8 hydrogels have shown macromolecule mobility within and release out of the gels[23,24]. This demonstrates the ability of the porous ß-hairpin peptide hydrogels with tunable mesh sizes as good candidates for tissue engineering and drug delivery scaffolds since they allow transport of nutrients and metabolites. Favorable structural, injectable, biocompatible and, in some cases, bioactive properties of hydrogels based on β-hairpin MAX1 and MAX8 hydrogels render them as attractive constituent materials for developing hybrid multicomponent hydrogels. Although it is possible to obtain fine control over the various properties like responsiveness to stimuli, gelation kinetics, pore size and hydrogel stiffness by modifying the peptide primary sequence, additional functionality may need to be imparted to β-hairpin peptide based hydrogels that can not be done by simple functionalization of the constituent peptides. Since the peptide hydrogels are physical and solution assembled, the simple process of mixing becomes a viable technique to add additional functionality to the network. Therefore, one may desire to add significant, additional functionality by simple construction of HMHs with these peptides and other molecules. The HMHs can be developed by incorporating

desired additional molecules ranging from polymeric (biopolymer, protein/peptide[23], DNA) molecules or small molecule drugs[9]. This chapter discusses the construction of HMHs with hyaluronic acid and self-assembled hydrogels based on MAX1 and MAX8 hydrogels.

The biopolymer, hyaluronic acid or hyaluronan (HA) (a term used to describe both the acidic form of the polymer and the salt of hyaluronic acid)[25] is a promising material for biomaterial applications. HA is a non-sulfated glycosaminoglycan (GAG) in the extracellular matrix (ECM) of many soft connective tissues, composed of alternating units of D-glucuronic acid and N-acetyl-D-glucosamine, linked together via alternating ß-1,4 and ß-1,3 glycosidic bonds[26]. Synthesized in the cell membrane[27], HA is extruded out of the cell into the native ECM, where it provides mechanical support[28]. Owing to its copious negative charges, HA has a high (1000 X) water absorbent capacity and thus acts as a space filler, lubricant and osmotic buffer in the native ECM[29]. The high water absorptive capacity of HA renders it an ideal matrix for solute and nutrient delivery to wounded tissue. Its ability to stimulate inflammatory signals for wound healing along with its ability to influence cell motility[30] and proliferation underscores its importance as a wound repair biomaterial[31,32]. The favorable wound healing properties of HA inspire its use as a potential tissue regeneration and repair material. Hydrated HA plays a prominent role in providing viscoelastic nature to cartilage[33], vitreous humor[34] and vocal folds[35]. In cartilage, HA forms large aggregates with aggrecan providing compressive resistance to the tissue

while in the vocal fold lamina propria, modulates tissue viscosity by providing shock-absorbing properties[36,37]. In addition to these prominent structural attributes, HA interacts with its cell surface receptors (CD44 or RHAMM) and activates various signaling pathways[38,39]. These signaling pathways direct various cell functions, including cell adhesion[40], cytoskeletal rearrangement, cell migration[41], cell proliferation and differentiation[38]. HA reacts with oxygen-derived free radicals thus demonstrating antioxidant effects[29]. HA plays an important role in mediating inflammation, as it is able to inhibit macrophage migration and aggregation. Additionally, tumor progression and angiogenesis depend on HA and hyaluronidase levels and the degradation profile of HA. Tumor invasion sites sometimes show high concentrations of HA and the HA coating around tumor cells effectively protects these cells against immune surveillance. The importance of HA in various biological functions presents it as a compelling biofunctional component in developing hybrid multicomponent hydrogels. Highly concentrated solutions of high molecular weight hyaluronic acid can form networks based on molecular entanglements but do not demonstrate mechanical integrity comparable to solid hydrogels required for biomedical applications[42,43]. Thus, to impart desired mechanical properties to hyaluronic acid based materials, chemical modification and crosslinking of HA molecules are necessary. The chemical modifications of hyaluronic acid that have been studied in order to develop hydrogels include thiolation, hydrazide functionalizaion and methacrylation of HA molecules[44]. These functional groups on the modified HA

polymers can be covalently crosslinked using suitable chemical crosslinking agents to yield solid hydrogels from hyaluronic acid. For the remainder of this chapter, hyaluronic acid in its native from i.e. without any chemical modification will be referred to as 'unmodified HA'. The use of unmodified HA eliminates the need for crosslinking agents and radical initiators to be employed in the development of HMHs based on these molecules. Crosslinking agents and radical initiators used for construction of hydrogels from modified HA can be potentially toxic to cells and tissues in contact with HMHs from modified HA that are used as biomaterials[45].

Given the tremendous potential biomedical applications of the injectable solid MAX1/MAX8 ß-hairpin hydrogels and HA individually, developing multicomponent hybrid hydrogels based upon these two types of materials is a step forward in development of smarter biomaterials. The construction of multicomponent hydrogels based on these two components has been inspired by nanocomposite materials that show synergistically enhanced functional properties like mechanical properties[46-49], flexural properties and heat stability[50], controlled gas permeability[51-53] and flammability[54-58] as compared to those of their individual components. An example of such materials is the class of polymer-layered clay silicates. Silicate layers stacked in a regular fashion with weak interatomic forces can be defined as clay silicates[59]. Clay silicates contain aluminosilicate layers with (30-150 nm thickness values) with a negative charge on their surfaces that are responsible for binding water and cations bound between them. When these

clay silicates are used as fillers in a polymeric matrix the large surface area offered by them after they are exfoliated into individual, dispersed layers leads to better adsorption of polymers, leading to greater interactions between the filler and the matrix phases, leading to synergistically enhanced properties[60]. The chief motivation of developing composite materials based on peptide fibrillar networks and hyaluronic acid is the combination of the favorable biological properties of hyaluronic acid with the versatile mechanical properties of peptide fibrillar networks by leveraging the specific electrostative interactions (peptide fibrils coated by positively charged lysine, HA a negatively charged polymer) between the HA polymers and peptide fibrils analogous to clay silicates and polymers. The methods of mixing these two materials described in this chapter are simple bench top processes that lead to physically interconnected hybrid networks. As stated, these networks are based on electrostatic interactions between the abundantly positively charged peptide nanofibrils and largely negatively charged HA biopolymer. The purely physical nature of the interactions between the two components eliminate the need of potentially cytotoxic residual crosslinking agents and initiators in the hybrid hydrogels which are typically a concern when chemically crosslinked hydrogels are developed for biomedical applications[61]. The simple mixing methods to construct the HMHs based on the physically crosslinked peptide hydrogels and HA also do not require development of new derivatives of either component by chemically modifications[44]. MAX1/MAX8 undergo a well defined hierarchical self-assembly pathway that involves peptide

folding into ß-hairpin structure, ß-sheet fibril formation, cluster formation from branched and entangled fibrils and finally formation of a percolated network from the clusters[62]. Each stage of assembly of either MAX1 or MAX8 β-hairpin peptide is characterized by the distinct morphology of the assembled structure (for example individual fibrils at early stages of assembly, clusters of fibrils at middle stages or a fully percolated network at late stages of assembly) and corresponding material physical state (for example, viscous solution at the fibril or cluster stage and solid hydrogel for fully percolated network). A peptide solution at different stages of assembly can be used as a component to mix with aqueous HA solution to develop HMHs with diverse mechanical and morphological properties. MAX1/MAX8 peptides both contain lysine residues with a primary amino group. Under aqueous solution conditions at high pH (~7-9) and ionic strength (~150-400mM), the primary amino groups undergo deprotonation and charge screening respectively, leading to β-hairpin formation from MAX1/MAX8. Even in these conditions, a number of lysine side chains are positively charged leading to positively charged fibrils of MAX1 /MAX8. Under similar solution conditions, HA molecules are largely negatively charged. One of the motivations behind developing HMHs from MAX1/MAX8 peptide hydrogels and HA biopolymers is to impart enhanced mechanical properties to the MAX1/MAX8 hydrogels by increasing interactions between them by introducing electrostatic interactions between positively charged peptide fibrils and negatively charged HA. Specifically the points of electrostatic interaction between HA and peptide fibrils

can act as extra points of intrafibrillar and interfibrillar physical crosslinking, leading to potentially stiffer individual fibrils, additional network crosslinks and thus stiffer overall networks than those made from exclusively peptides. Additionally, MAX1/MAX8 networks in various stages of self-assembly display varied mechanical properties as described above (i.e. early assembly stages exhibit viscous solution properties while later stages of assembly exhibit stiff gel properties due to fibril percolation). Thus, the introduction of HA molecules to MAX1/MAX8 networks at different stages of solution assembly is hypothesized to yield HMHs of widely varied mechanical properties . For example, accelerated assembly and network formation kinetics leads to enhanced stiffness in case of MAX1/MAX8 hydrogels[14,62]. Self-assembly and network formation kinetics is expected to be expedited in case of HA addition to the non-percolated fibrillar network due to enhanced electrostatic interactions. Thus, addition of HA molecules to a non-percolated but fibrillar MAX1/MAX8 network is hypothesized to yield a stiffer hydrogel as compared to a hydrogel obtained by addition of HA molecules to fully percolated MAX1/MAX8 hydrogel. This chapter discusses three different methods employed for construction of HMHs from MAX1/MAX8 networks and aqueous solutions of chemically unmodified HA and the resultant HMH properties.

6.2. Materials and Methods

6.2.1. Preparation of Hybrid Multicomponent Hydrogels

Three methods of construction of HMHs from MAX1/MAX8 β-hairpin peptide hydrogels and HA are discussed in this section. Method 1 describes the construction of composite networks with MAX8 fibrillar network functioning as the matrix and solid electrostatic complexes of MAX8 and unmodified HA functioning as the filler medium. Method 2 describes composite materials obtained by diffusion of unmodified HA molecules in a fully percolated MAX1 hydrogel network. Method 3 describes construction of composite HMHs by introduction of HA molecules in aqueous solution to a continuously sheared percolated MAX1 hydrogel. From this point onward in this chapter, the materials developed using the respective methods will be referred to by referencing the method of preparation. The first to be discussed are the composite networks prepared using solid electrostatic complexes of MAX8 and unmodified HA as fillers and MAX8 fibrils as matrix will be referred to as composite prepared using Method 1.

6.2.1.1 Method 1: Composite hydrogels with MAX8 fibrils as matrix and solid electrostatic complexes of MAX8 and unmodified HA as fillers

Hoare et al.[63] describe the 'plum pudding' analogy to describe drug delivery systems having a similar morphology to that achieved using this method. The drug delivery systems contain a dispersed phase of microparticles or nanoparticles in a hydrogel matrix, with therapeutic drugs encapsulated within the particles. The microparticle or nanoparticle encapsulation with a gel matrix can provide two different layers of encapsulation to provide an additional diffusion barrier to the encapsulated drugs thus leading to more control over release of drug from the system. Method 1 is useful in developing composite hydrogels that resemble the drug delivery systems described by the plum pudding model, with solid precipitates of MAX8 fibrils and HA being the fillers and a fibrillar network of MAX8 being the matrix (Figure 6.1). Hyaluronic acid polymers of different molecular weights (5 KDa, 35 KDa, 169 KDa, 419 KDa, 1 MDa and 2 MDa) were purchased from Lifecore Biomedical LLC (Chaska, MN, USA). Method 1 is a two-step process. In the first step a 1% (w/v) hydrogel of MAX8 was prepared. For this, 1 mg MAX8 peptide was dissolved in 50μL chilled (5°C) 50mM HEPES buffer (pH 7.4) (Life Technologies, Grand Island, NY, USA). Then 50μL chilled (5°C) Gibco® RPMI-1640 cell culture medium without Fetal Bovine Serum (FBS) (pH 7.4) was added to the solution of MAX8. RPMI-1640 buffer was purchased from Life Technologies (Grand Island, NY, USA). Then the assembly

of the MAX8 peptide was triggered by raising the temperature of the solution to 37°C. A 1.25% (w/v) solution of HA of a given molecular weight (5.1 KDa, 35 KDa, 169 KDa and 419 KDa) was prepared by dissolving 1.25 mg HA in 50μL (37°C) 50mM HEPES buffer (pH 7.4). The amount of HA was fixed at 1.25 mg/ mg of peptide MAX8 since it corresponds to 1:1 charge ratio of the MAX8 peptide to the HA molecule. Once a solid hydrogel was obtained from the assembly of MAX8, it was mixed vigorously using a vortex mixer with the HA solution to yield a dispersion of precipitated solid particles. These sizes of particulate solids might be on the length scales of microns. The vigorous mixing leads to disruption of the hydrogel network due to fracture of individual fibrils. The formation of solid precipitated particles can be attributed to electrostatic complexation between the hydrogel domains formed by disruption of the hydrogel network that contain positively charged MAX8 fibrils and highly negatively charged HA molecules when the bulk MAX8 hydrogels and HA solutions are mixed and sheared uniformly using the vortex mixer. The second step involves producing a buffered solution of MAX8 peptide. A 3% (w/v) buffered solution of MAX8 is prepared by dissolving 3 mg MAX8 peptide in 50μL chilled (5°C) 50mM HEPES buffer (pH 7.4) and quickly adding 50μL chilled (5°C) Gibco® RPMI-1640 cell culture medium without Fetal Bovine Serum (FBS) (pH 7.4). This buffered solution is maintained at 5°C. Then, 100μL uniform dispersion of the particulate solids obtained in the first step is mixed uniformly with the buffered solution of MAX8 peptide and the mixture is maintained at 37°C to yield

~ 200 μL nanocomposite hydrogel. The effective concentration of the MAX8 peptide without considering the mass of peptide forming the solid precipitates in the final composite gel was thus fixed at 1.5 % (w/v). The final hydrogels are expected to have a composite morphology with the particulate solids functioning as the filler phase and the assembled fibrillar network from MAX8 as the matrix.

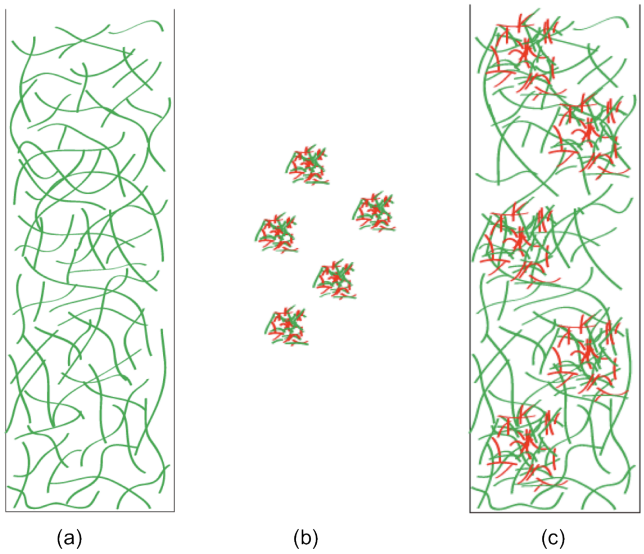

Figure 6.1. Schematic representation of (a) MAX8 hydrogel matrix with the green strings representing peptide fibrils (b) Solid precipitates of green MAX8 fibrils and red HA polymers (c) Morphology of composite hydrogels obtained using Method 1 with MAX8 fibrils being the matrix and solid precipitates being fillers.

6.2.1.2. Method 2: Composite hydrogels obtained by diffusion of hyaluronic acid molecules into solid MAX1 hydrogels

The second method of developing hybrid composite hydrogels from the β-hairpin peptide hydrogels and hyaluronic acid is allowing diffusion of HA acid molecules into a solid MAX1 hydrogel aided by electrostatic interactions and

osmotic pressure. Briefly, the experimental setup involved simply placing a solution of HA at a given concentration and charge ratio relative to the MAX1 peptide on top of a fully formed solid MAX1 hydrogel sample. Specifically for these experiments, 1mg MAX1 peptide was dissolved in 100μL chilled (5°C) de-ionized water. Buffered solution of MAX1 was prepared by adding 100μL chilled (5°C) pH 7.4 (100mM BTP, 800mM NaCl) buffer to the MAX1 solution. A solid MAX1 hydrogel at 0.5 % (w/v) concentration at solution conditions pH 7.4 (50mM BTP, 400mM NaCl) was prepared by raising the temperature of the buffered solution to 37°C. Then 0.5% (w/v) solution of 1.25 mg HA in 250μL de-ionized water at 37°C was placed on top of the solid hydrogel and allowed to diffuse for 90 minutes. The supernatant aqueous solution was removed from above the MAX1 hydrogel to yield a composite material. Many covalently and physically crosslinked hydrogels demonstrate swelling behavior when placed in contact with aqueous solutions by absorbing the aqueous solutions due to their inherent porosity and hydrophilic character[64]. A unique property displayed by MAX1/MAX8 β-hairpin hydrogels, that is very different most conventional hydrogels is that they do not swell when placed in contact with an aqueous solution and retain their original volume even though diffusion of the aqueous solution from and into the hydrogels takes place[23,24]. Thus, it is possible to place HA solution on top of a single exposed surface of a β-hairpin hydrogel of MAX1 and ensure diffusion of HA molecules into the MAX1 matrix without disrupting the original network structure of MAX1.

6.2.1.3. Method 3: Composite hydrogels obtained by mixing continuously sheared hydrogels of MAX1 and hyaluronic acid solutions

The third method used for construction of composite hydrogels from β-hairpin peptide hydrogels and HA is addition of aqueous HA solutions into continuously sheared MAX1 hydrogels. A viscoelastic material (as evidenced by oscillatory rheological measurements discussed later in the chapter) is obtained due to exclusion of a large amount of aqueous medium present in the MAX1 hydrogel (Figure 6.2). This material is optically opaque as opposed to the clear MAX1 hydrogels used to develop this material. This material is formed by electrostatic interactions between the positive charges of MAX1 and negative charges of HA and is a percolated network. This composite material is different as compared to the particulate dispersions obtained when HA solutions of comparable molecular weight are mixed with MAX8 percolated hydrogels, discussed in section 6.2.1.1. The slight excess of positive charge in case of each MAX1 molecule over that of each MAX8 molecule leads to a large excess of overall positive charge in case of MAX1 networks as compared to MAX8 networks. This large excess of positive charge can be considered accountable for many more points of electrostatic interactions functioning as physical crosslinking points between assembled fibrils and HA molecules in case of MAX1 as compared to MAX8. These extra points of physical crosslinking can be implicated in the formation of a stiff network in case of MAX1 as opposed to disconnected solid precipitates with no network like properties in case of MAX8, when mixed

with aqueous solutions of the negatively charged HA. Composite hydrogels prepared using Method 3 are constructed using MAX1 hydrogels buffered at pH 9, which is a higher pH value than pH 7.4, at which composite hydrogels are constructed using Method 1. At higher pH values, fewer peptide lysine groups are protonated as compared to lower pH values, leading to fewer positively charged and more neutral lysine groups. The fewer positively charged lysine groups can lead to fewer sites of electrostatic interactions with the HA molecules at higher pH, leading to lesser probability of solid precipitate formation and a higher probability of formation of continuous percolated network structure from peptide fibrils and HA polymers.

The preparation of these viscoelastic materials was a two-step process. In the first step, 1 mg of MAX1 peptide was dissolved in 100μL chilled (5°C) de-ionized water leading to a 1% (w/v) solution of MAX1. Buffered solution of MAX1 was prepared by adding 100μL chilled (5°C) pH 9 (250mM Boric Acid 20mM NaCl) buffer to the MAX1 solution. A magnetic stir bar was introduced into the buffered solution. Solid MAX1 hydrogels at 0.5 % (w/w) concentration were prepared by raising the temperature of the buffered solution to 37°C. Then 0.5% (w/v) solution of 1.25 mg HA in 250μL de-ionized water at 37°C was introduced at a flow rate of 5 ml/min using a syringe pump, while the MAX1 hydrogel was stirred at ~600 rpm, to yield the viscoelastic hydrogel material.

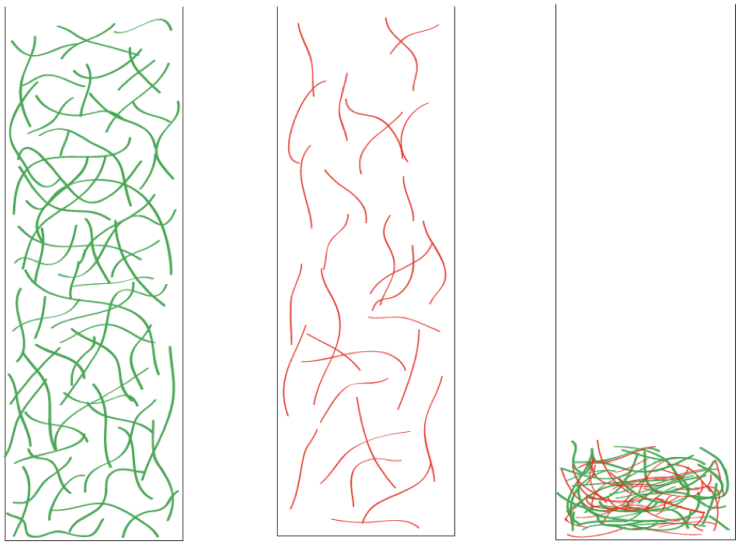

Figure 6.2. Schematic representation of (a) MAX1 hydrogel matrix with the green strings representing peptide fibrils (b) red strings representing HA polymers (c) drastic reduction in volume of solid hydrogel obtained by employing Method 3 of mixing MAX1 fibrillar hydrogel and HA polymer

6.2.2. Oscillatory Rheological Characterization

Oscillatory rheology measurements were performed on an ARG2 rheometer (TA Instruments, New Castle, DE, USA) using 20mm diameter stainless steel parallel plate geometry.

6.2.2.1. Method 1: Composite hydrogels with MAX8 fibrils as matrix and solid electrostatic complexes of MAX8 and unmodified HA as fillers

After the uniform dispersion of the particulate solids was added to the buffered solution of MAX8 maintained at 5°C, the entire mixed solution was quickly transferred to the Peltier plate of the ARG2 rheometer equilibrated at 5°C, and the upper plate was lowered to a gap height of 500 μm. The upper plate and

the Peltier plate were equilibrated to 37°C prior to carrying out the rheological experiments. Upon reaching the gap of 500 μm and ensuring uniform material distribution within the gap height, silicone oil (Sigma Aldrich, USA) was used to seal the gap to prevent solvent evaporation from the gap. The following five samples were tested using oscillatory rheological measurements. (a) MAX8 (b) Composite of MAX8 and 5 KDa HA (c) Composite of MAX8 and 35 KDa HA (d) Composite of MAX8 and 169 KDa HA (e) Composite of MAX8 and 419 KDa HA. On each sample, oscillatory time sweep measurement at fixed angular frequency 6 rad/s and oscillatory strain 1% were carried out. Oscillatory frequency sweep measurements were carried out at fixed oscillatory strain 1% while oscillatory strain sweep measurements were carried out at fixed angular frequency 6 rad/s following the oscillatory frequency sweep measurements. Oscillatory time sweep measurement steps were carried out for 90 minutes each, before and after subjecting the hydrogel networks to a steady state shear of 1000/s for 120 sec performed. Throughout these time sweep measurements the oscillatory frequency was maintained at 6 rad/s and oscillatory strain at 1%. The gap height was maintained at 500 μm for all the experiments.

6.2.2.2. Method 2: Composite hydrogels obtained by diffusion of hyaluronic acid molecules into solid MAX1 hydrogels

For rheological characterization of composite materials constructed using this method, solid MAX1 hydrogels were allowed to develop from peptide

solution on the Peltier plate of the ARG2 rheometer. A 20mm diameter stainless parallel plate was used for the measurements. 1mg MAX1 peptide was dissolved in 100μL chilled (5°C) de-ionized water. Buffered solution of MAX1 was prepared by adding 100μL chilled (5°C) pH 7.4 (100mM BTP, 800mM NaCl) buffer to the MAX1 solution. The buffered solution was placed into a specially designed cylindrical construct of 8 mm diameter. Solid MAX1 hydrogels at 0.5 % (w/v) concentration at solution conditions pH 7.4 (50mM BTP, 400mM NaCl) were prepared by raising the temperature of the buffered solution to 37°C using the Peltier plate of ARG2 rheometer. The hydrogel was allowed to equilibrate for ~ 1 hr and then 0.5% (w/v) solution of 1.25 mg HA of molecular weight (5 KDa, 169 KDa, 1 MDa) in 250μL de-ionized water at 37°C was placed on top of the solid hydrogel and allowed to diffuse for 90 minutes. The supernatant aqueous solution was removed from above the MAX1 hydrogel. The upper plate of the rheometer is lowered to a 500μm gap height. Upon reaching the gap of 500 μm and ensuring uniform material distribution within the gap height, silicone oil (Sigma Aldrich, USA) was used to seal the gap to prevent solvent evaporation from the gap. On each sample, oscillatory time sweep measurement at fixed angular frequency 6 rad/s and oscillatory strain 1% were carried out. Oscillatory frequency sweep measurements were carried out at fixed oscillatory strain 1% and oscillatory strain sweep measurements were carried out at fixed angular frequency of 6 rad/s following the oscillatory frequency sweep measurements.

6.2.2.3. Method 3: Composite hydrogels obtained by mixing continuously sheared hydrogels of MAX1 and hyaluronic acid solutions

For each molecular weight of HA, the resulting solid material obtained by mixing hyaluronic acid solution with sheared MAX1 hydrogels was placed on the Peltier plate. The geometry used was a stainless steel parallel plate 8mm in diameter. Upon reaching the gap of 500 μm and ensuring uniform material distribution within the gap height, silicone oil (Sigma Aldrich, USA) was used to seal the gap to prevent solvent evaporation from the gap. The molecular weights of HA used for producing the samples were 169KDa, 1MDa and 2MDa. On each sample, oscillatory frequency sweep measurements were carried out at fixed oscillatory strain 1% and oscillatory strain sweep measurements were carried out at fixed angular frequency of 6 rad/s following the oscillatory frequency sweep measurements.

6.2.3. Compressive Testing

The viscoelastic percolated solid networks obtained by employment of Method 3 were evaluated for their ability to withstand a compressive force. Compressive tests were performed using a Rheometrics Dynamic Mechanical Analyzer (RSA G2, TA Instruments, New Castle, DE) at 25 °C. An immersion compression fixture, an accessory that helped maintain an aqueous environment for the viscoelastic materials, was used to prevent water evaporation from the sample. A cylindrical geometry 6 mm in diameter was used for compression of

the materials. A loading gap of 1.6 mm and compression rate of 0.1 mm/sec was maintained. Three specimens were tested for each composition. MAX1 hydrogels used to develop the hybrids were constructed at 2% (w/w) concentration. Molecular weights of HA used to develop the hybrid materials were 220 KDa, 419 KDa and 1 MDa. The compressive modulus E' (kPa) was calculated as the slope of the initial linear portion of the stress-strain curve upto ~15% strain. Each sample was subject to one cycle of compression until the material fractured. The stress (σ_b) and strain (ε_b) at the breaking point were also recorded. After breaking point was attained, the samples underwent bulk fracture and could not be re-used for further characterization. Each sample was tested thrice to calculate the value of E' (KPa).

6.2.4. Negative Staining Cast Film Transmission Electron Microscopy (Cast-film TEM)

In case of Method 1, negative staining cast film TEM was carried out on the particulate solids to investigate any potentially specific nanostructure formation from the mixing and electrostatic binding of the peptide fibrils and HA polymer. The sample preparation for cast-film TEM is same as described in Chapter 2, with the specific samples in this case being a dispersion of particulate solids obtained via mixing a fully formed MAX8 hydrogel and HA solution. In the case of composites prepared using Method 2, after the supernatant HA solution is removed, a small mass of hydrogel near the top of the hybrid material

is used as the sample for imaging.

6.3. Results and Discussion

6.3.1. Method 1: Composite hydrogels with MAX8 fibrils as matrix and solid electrostatic complexes of MAX8 and unmodified HA as fillers

The first method discussed mixing in solid particulates that are electrostatic complexes of MAX8 hydrogels and HA, into a buffered MAX8 peptide solution during solution assembly process of the MAX8 peptide. The resulting composite hydrogel material is expected to have morphology with solid particulates representing the filler phase and the self-assembled fibrillar hydrogel of MAX8 representing the matrix phase. Figure 6.3 shows the oscillatory frequency sweep characterization on fully formed composite hydrogels obtained from HA polymers of different molecular weights (5 KDa, 35 KDa, 169 KDa and 419 KDa). The hydrogels show a low dependence of the storage modulus G' (Pa) to the applied angular frequency. The composite hydrogels are also stiffer than the neat MAX8 hydrogel matrix with an effective concentration of 1.5% (w/w) of MAX8 in the matrix. The stiffness values of the composite hydrogel are dependent upon the molecular weight of the HA used to prepare the composite. At higher angular frequency values, the MAX8 hydrogel matrix shows some frequency dependence of G' (Pa), (>300 rad/s) which is not shown by any other composite hydrogel sample. The morphology of the composite hydrogels discussed in this section resembles a two-phase system in which the suspended

particulate phase exhibits hydrophobic and electrostatic interactions (as explained in detail further in this section) with the fibrillar phase. Therefore, the local relaxations of the assembled peptide fibrils in the matrix phase in the HMHs can be further limited than the fibril relaxations in the pure MAX8 networks, resulting in significantly lesser angular frequency dependence of G' (Pa) in the HMHs. Oscillatory rheological measurements on all the hydrogel material obtained using this method show values of G" (loss modulus) << G' (storage modulus) demonstrating solid like properties from the hydrogels.

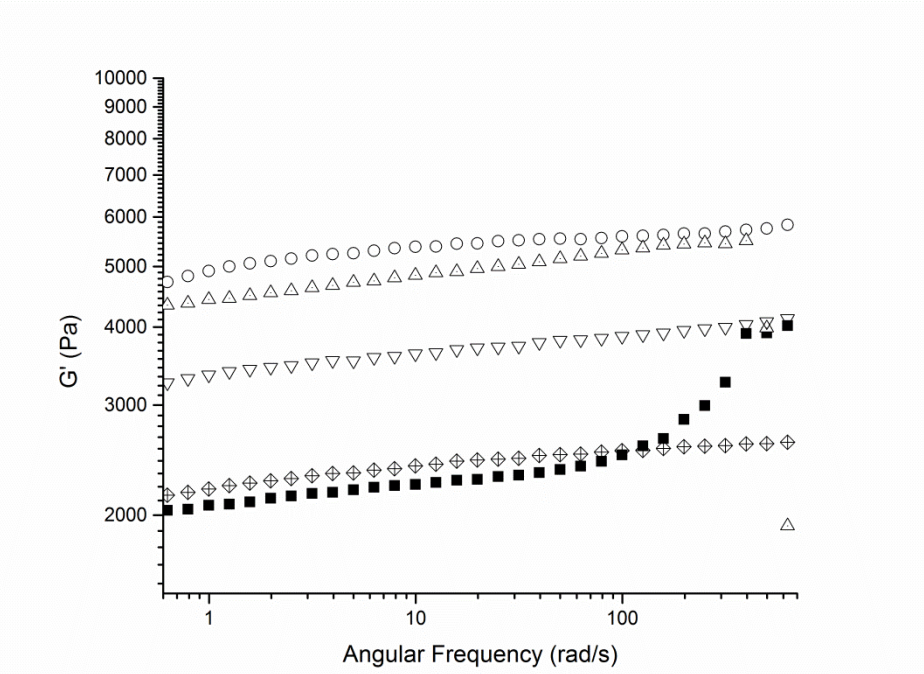

Figure 6.3. Oscillatory frequency sweep measurements on MAX8 (solid squares) and composite hydrogels developed from MAX8 using Method 1 (a) MAX8 + 5 KDa HA (open circles), (b) MAX8 + 35 KDa HA (dotted triangles) (c) MAX8 + 169 KDa HA (inverted triangles) (d) MAX8 + 419 KDa HA (marked quadrangles). The effective concentration of pure MAX8 and MAX8 matrix in the composite is 1.5% (w/w).

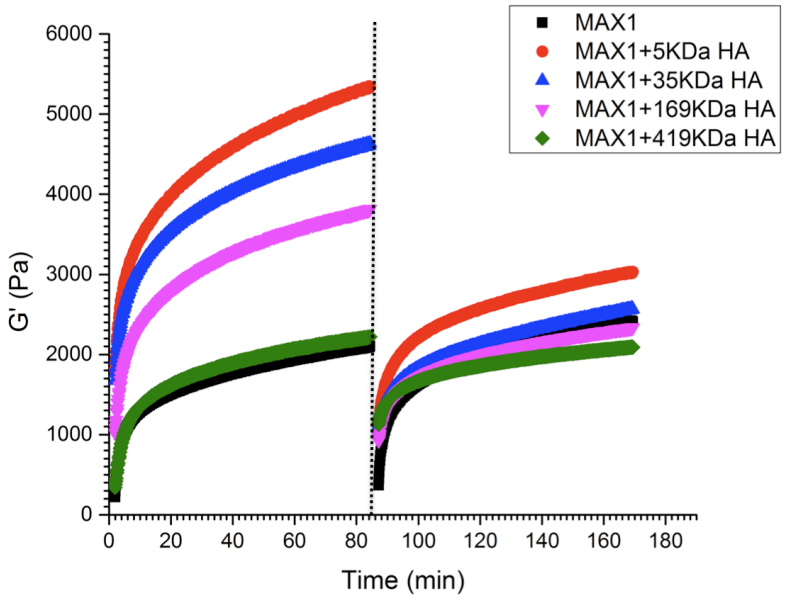

Figure 6.4. Shear thinning and rehealing behavior from hydrogels of MAX8 (Black) and composite hydrogels developed using Method 1 from MAX8 (a) MAX8 + 5 KDa HA (red), (b) MAX8 + 35 KDa HA (blue) (c) MAX8 + 169 KDa HA (pink) (d) MAX8 + 419 KDa HA (green). The black dotted line in the center at ~ 80 minutes indicates steady state shear applied at 1000/s for 2 min.

Figure 6.4 show the shear thinning and rehealing properties of the composite hydrogels as compared to those of MAX8. The blue line indicates the point in time at which a steady state shear was applied to a fully formed hydrogel MAX8 or the composite. The red, blue and pink curves to the right of the dotted lines for composites prepared using HA of molecular weight 5 KDa, 35 KDa and 169 KDa indicate a ~ 50% recovery of the stiffness values with almost 100% recovery of the composite hydrogels based on 419 KDa (green curve) and the pure MAX8 hydrogel (black curve). These data indicate that the shear thinning

and rehealing properties of MAX8 are preserved to some extent depending upon molecular weight of HA added when composite hydrogels are developed with a MAX8 network used as matrix. Figure 6.5 shows strain sweep measurements conducted on the composite materials. The stiffness modulus value (G' (Pa)) is relatively independent of the applied oscillatory strain upto a certain value of oscillatory strain, demonstrating a well-defined linear viscoelastic regime for the composite hydrogels. Oscillatory rheological measurements on all the hydrogel material obtained using this method show values of G" (loss modulus) << G' (storage modulus) demonstrating solid like properties from the hydrogels.

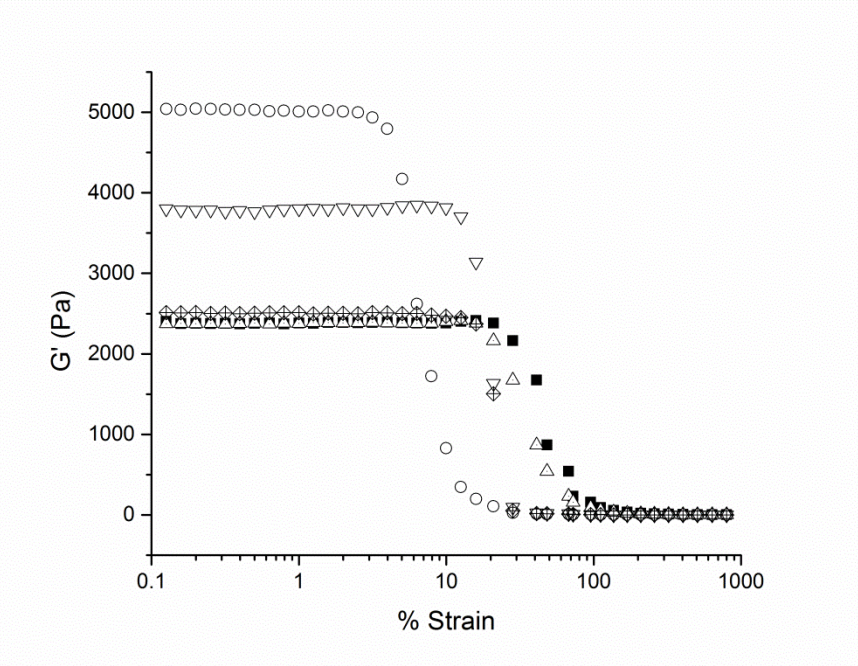

Figure 6.5. Oscillatory strain sweep data from hydrogels of MAX8 (solid squares) and composite hydrogels developed from MAX8 (a) MAX8 + 5 KDa HA (open circles), (b) MAX8 + 35 KDa HA (dotted triangles) (c) MAX8 + 169

KDa HA (inverted triangles) (d) MAX8 + 419 KDa HA (marked quadrangles). The data show a specific linear viscoelastic region for all the hydrogels.

Figure 6.6 shows that there is an acceptable variance of the stiffness values of the composite hydrogels developed, signifying a reproducible nature of the composite development process, even though the morphology of the composite hydrogels is expected to be heterogeneous at the microscale. The G' (Pa) data values obtained from composite hydrogels constructed using 5 KDa and 35 KDa HA molecules were found to be not significantly different by a statistical t-test used to compare the two sets of data with (t=15.76%). Thus, oscillatory rheological characterization demonstrates that development of composite hydrogel materials from MAX8 hydrogels and HA polymers is a useful technique for generating composites which preserve yield stress material like properties, preserving and sometimes enhancing mechanical stiffness of MAX8 hydrogels in addition to introducing biological functionality by means of HA addition. This method also offers flexibility of molecular weight of HA as desired for different biological applications.

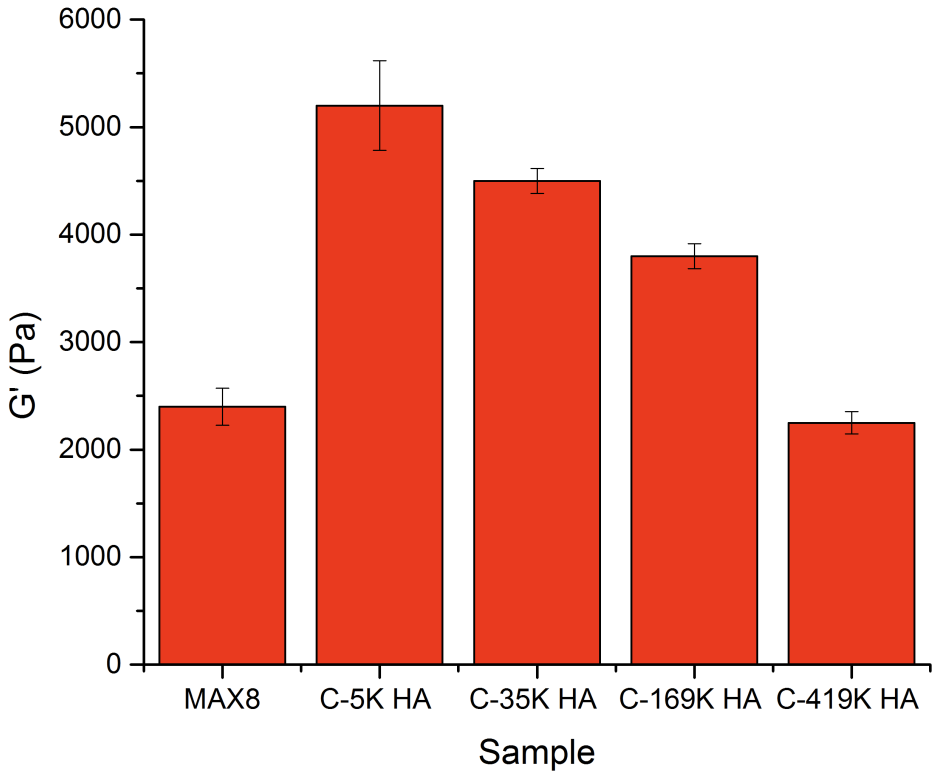

Figure 6.6. Variance in stiffness modulus values of composite hydrogels (Method 1) when performed in triplicate, is comparable to that obtained from a pure MAX8 hydrogel.

As discussed earlier, when a MAX8 hydrogel is sheared the bulk gel fractures into smaller gel domains. Electrostatic complexes that are solid precipitates are formed when a solution of hyaluronic acid molecules is mixed with the hydrogel domains. Results from the rheological measurements on the composite hydrogels demonstrate that stiffness values of the composite hydrogels are dependent on the molecular weight of the hyaluronic acid polymers used. The

solid particles can reinforce the MAX8 fibrillar networks in two ways. Each particle contains segments of peptide fibrils with a large number of amide bonds providing sites for hydrogen bonding. The growing fibrils of the MAX8 peptide in the matrix material can undergo hydrogen bonding interactions with these single particles, thus generating additional points of physical crosslinking, leading to stiffer hydrogels. The solid particles formed due to electrostatic complexation are hydrophobic in nature. This can be evidenced by the observation that they are precipitates to begin with and settle at the bottom of the vial in which they were produced at longer periods of time. These hydrophobic particles can act as points of physical crosslinking by providing hydrophobic surface for collapse of individual MAX8 β-hairpin molecules in the matrix trying to bury their hydrophobic valine side chains in the aqueous medium. These collapsed β-hairpin molecules can lead to nucleation of further matrix MAX8 fibrils. Thus, acting as anchors for fibrils of the matrix MAX8 by undergoing hydrogen bonding and hydrophobic interactions with the matrix MAX8 peptides, the particulate solids can act as reinforcement fillers in the composite materials formed.

The sizes of the solid particles formed by complexation of peptide gel domains with hyaluronic acid molecules of different molecular weight are expected to be dependent on the molecular weight. For example, solid particles formed by complexation of MAX8 with 5 KDa hyaluronic acid are expected to be much smaller in size than the particles formed by complexation of MAX8 with 419 KDa. Thus, at the same proportion by weight, the number of solid particles

formed by lower molecular weight hyaluronic acid molecules is expected to be greater than the particles formed from higher molecular weight of hyaluronic acid. Additionally, solid particles with smaller sizes are expected to form dispersions in aqueous medium that are more stable and thus more homogenous and stable as compared to the dispersions of particles with larger sizes. The greater number of particles are expected to provide correspondingly greater number of sites of physical crosslinking and thus reinforce the matrix MAX8 fibrils in a much more effective fashion.

6.3.2. Method 2: Hybrid Hydrogels obtained by diffusion of hyaluronic acid molecules into solid MAX1 hydrogels

Figure 6.7 shows the oscillatory frequency sweep characterization on hybrid networks obtained by diffusion of HA polymers of different molecular weights (5 KDa, 169 KDa and 1 MDa) into fully formed MAX1 hydrogels. This method utilizes electrostatic attraction and osmotic pressure driven diffusion of HA polymer solution into fully formed MAX1 hydrogels.

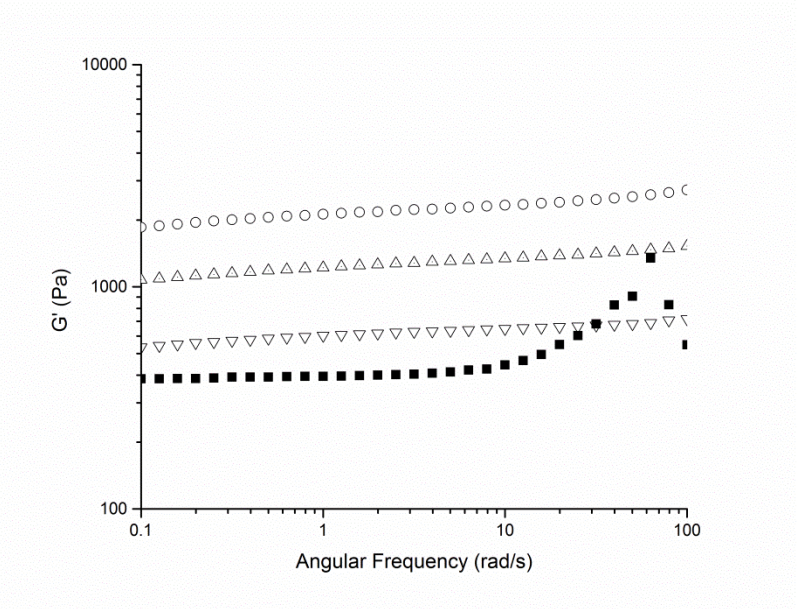

Figure 6.7. Oscillatory frequency sweep measurements on MAX1 (solid squares) and hybrid network hydrogels obtained using Method 2. Concentration of MAX1 hydrogels maintained at 0.5% (w/v) (a) MAX1 + 5 KDa HA (open circles), (b) MAX1 + 169 KDa HA (dotted triangles) (c) MAX1 + 1 MDa HA (inverted triangles).

The negatively charged HA molecules diffuse into positively charged fibrillar hydrogels and electrostatically crosslink multiple fibrils to yield overall stiffer hydrogels. It is expected that when the HA polymers diffuse into the MAX1 hydrogel due to electrostatic complexation of hyaluronic acid with the fibrils at the top of the hydrogel, they present a steric barrier or more polymers molecules to diffuse deeper into the MAX1 hydrogel matrix. Thus, the stiffening effect is expected to occur within a certain layer from the top of the solid hydrogel. Thus, when the upper plate of the ARG2 rheometer is lowered onto a hybrid hydrogel network after removal of the supernatant polymer solution, an oscillatory time

sweep measurement is performed to let the hydrogel layer equilibrate over 90 minutes. Then oscillatory frequency sweep measurements are carried out to understand solid like characteristics of the hybrid materials. The oscillatory frequency sweep measurements (Figure 6.7) demonstrate a low dependence of the storage modulus (G' (Pa)) to over three decades of applied frequency providing evidence of the solid like properties of the hybrid materials indicated by the hollow circles, hollow triangles (dotted) and hollow triangles (inverted) representing hybrid materials from diffused HA polymers with 5 KDa, 169 KDa and 1 MDa molecular weight. It is observed that the stiffness of the hybrid materials obtained by polymer diffusion varies inversely as the molecular weight of the polymer. This can be attributed to the property of shorter polymer chains with lower molecular weight, excluded volume and thus a greater availability of negatively charged side chain groups to add more points of electrostatic crosslinking to the MAX1 fibrils. The ability of polymer chains to diffuse down further into the MAX1 matrix is expected to decrease with increase in molecular weight of HA molecules as shown in Figure 6.8. Thus, the composite hydrogels obtained by diffusion of 1MDa HA are only marginally stiffer than pure MAX1 hydrogels, while the composite hydrogels obtained by diffusion of 5 KDa HA are much more stiffer then pure MAX1 hydrogels. The solid squares indicate the G' (Pa) response from the pure MAX1 solid hydrogel, which demonstrates some angular frequency response of G' (Pa) at higher frequencies (>300 rad/s), that is not shown by any other composite hydrogel sample. This angular frequency

variance of the G' (Pa) values in case of the pure MAX1 network is a result of the local fibrillar relaxations at higher frequencies. The hybrid hydrogels are constructed by using diffused HA molecules into the MAX1 matrix and contain a much higher degree of crosslinking, due to electrostatic interactions and entanglements between fibrils and HA molecules which are not observed in the pure MAX1 matrix hydrogel. As discussed in Section 6.3.1, the local relaxations of the assembled peptide fibrils in the HMHs can be further limited than the fibril relaxations in the pure MAX1 networks, resulting in significantly lesser angular frequency dependence of G' (Pa) in the HMHs as compared to the pure MAX1 sample. Oscillatory rheological measurements on all the hydrogel material obtained using this method show values of G" (loss modulus) << G' (storage modulus) demonstrating solid like properties from the hydrogels.

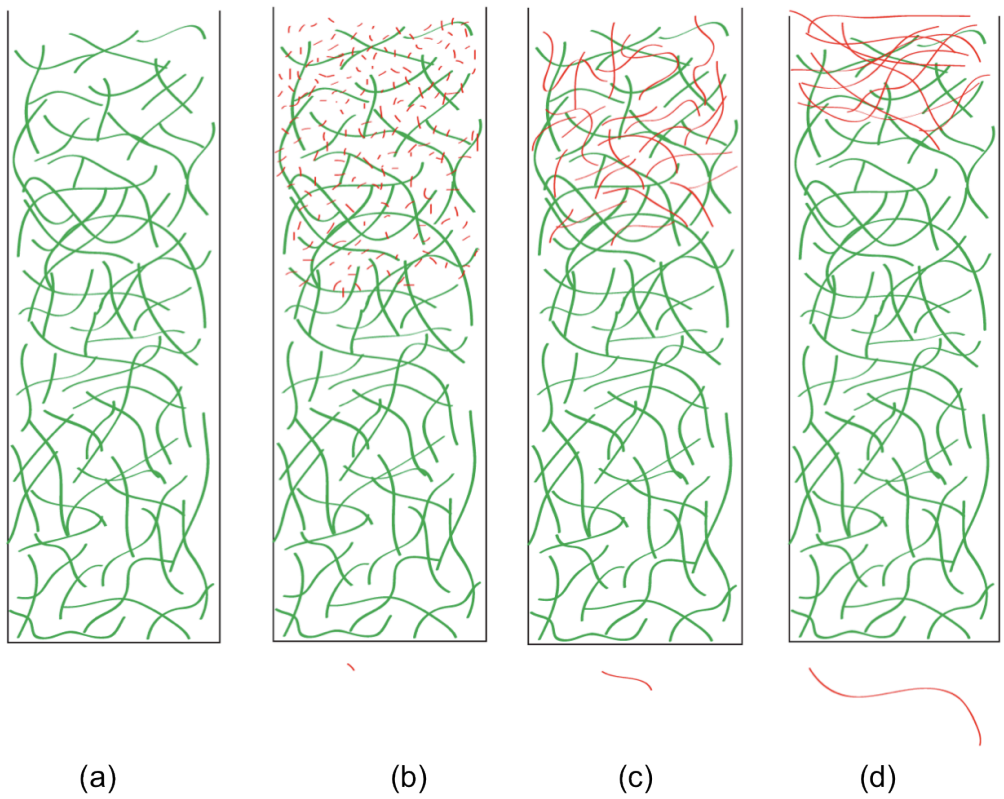

Figure 6.8. Schematic representation of (a) MAX1 hydrogel matrix with the green strings representing peptide fibrils (b) composite hydrogel with 5 KDa HA diffused into MAX1 matrix (c) composite hydrogel with 169 KDa HA diffused into MAX1 matrix (d) composite hydrogel with 1 MDa HA diffused into MAX1 matrix. The red strings represent HA molecules. The red strings at the bottom of (b), (c) and (d) indicate increasing sizes of HA molecules with increasing molecular weight.

A TEM micrograph shown in Figure 6.9b shows a difference in fibrillar nanostructure of the MAX1 hydrogel when HA with 5 KDa molecular weight is allowed to diffuse into the matrix as compared to the pure MAX1 matrix (Figure 6.9a). A network like structure is observed in case of the hybrid, but differentiating between individual fibrils of MAX1 is not possible due to electrostatic interactions of HA molecules with the MAX1 fibrils.

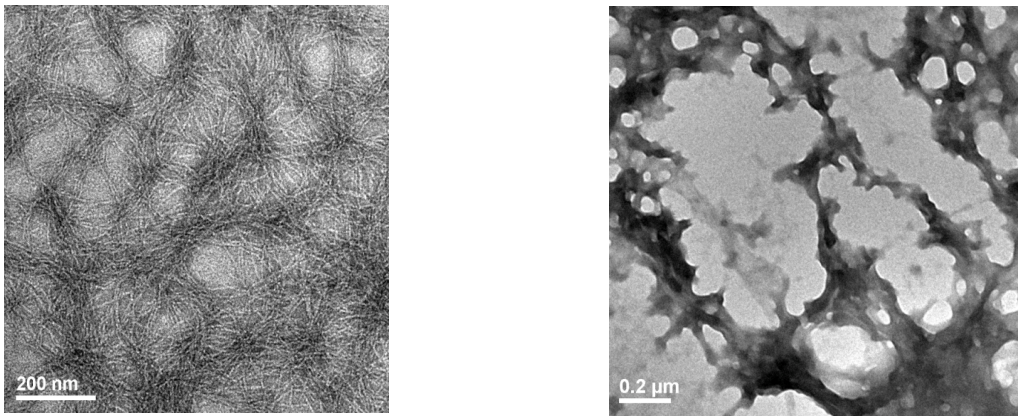

(a) (b)

Figure 6.9. Transmission Electron Micrograph of (a) pure MAX1 matrix (b) hybrid material obtained by diffusion of HA (5 KDa) molecules into MAX1.

6.3.3. Method 3: Hybrid Hydrogels obtained by mixing dynamically stirred hydrogels of MAX1 and hyaluronic acid solutions

Figure 6.10 shows the oscillatory frequency sweep measurements carried out on the continuous percolated mass obtained by employing Method 3. All the percolated materials show a relative independence of the G' (Pa) storage modulus values to the applied angular frequency over three decades of applied frequency, providing evidence of hydrogel like characteristics of the materials.

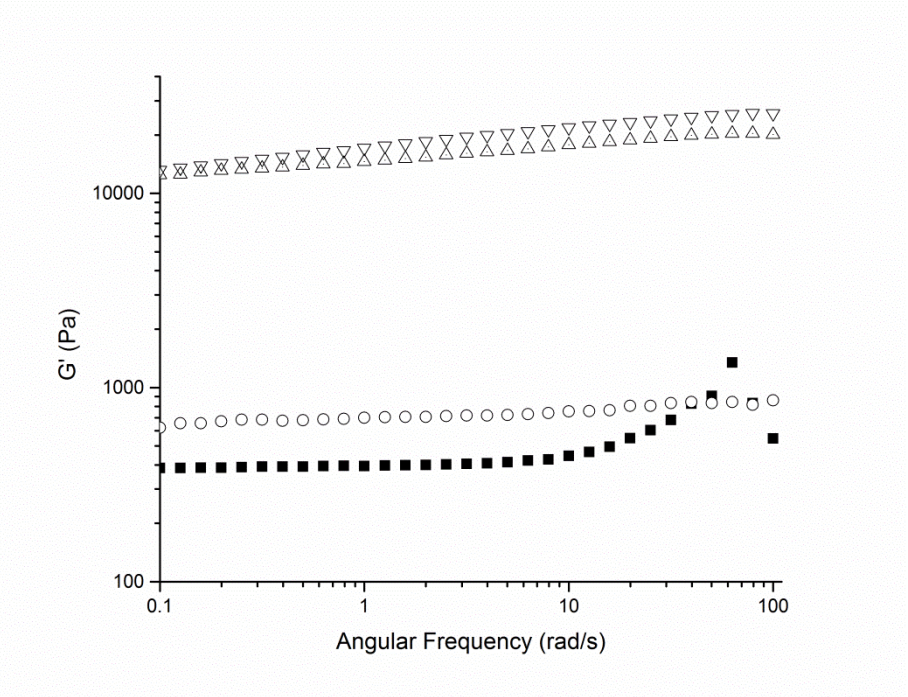

Figure 6.10. Oscillatory frequency sweep measurements on MAX1 (solid squares) and hybrid networks hydrogels obtained from vigorous mixing of HA molecules with 0.5% (w/w) MAX1 hydrogels (a) MAX1 + 169 KDa HA (open circles), (b) MAX8 + 1 MDa HA (dotted triangles) (c) MAX8 + 2 MDa HA (inverted triangles).

The dotted triangles and inverted triangles indicating hybrid materials from 1MDa and 2MDa HA show two orders of magnitude increase in the stiffness values as compared to the pure MAX1 hydrogel, while the hybrid material obtained by mixing in 169 KDa HA shows only a modest increase in stiffness. The large extent of increase in stiffness values of the hybrid materials obtained from the 1 MDa, 2 MDa and 169 KDa hydrogels can be attributed mainly to the large rise in local concentration of solids (peptide fibrils and HA polymer) due to the exclusion of aqueous medium. The oscillatory strain sweep measurements conducted on these materials show a linear viscoelastic region indicated by

relative independence of G' (Pa) to the applied oscillatory strain, upto a certain value of strain (Figure 6.11). A very negligible linear region is observed in case of the hybrid material obtained from 2 MDa HA solution due to lower stress dissipation capacity of the stiff hybrid network obtained from MAX1 and 2 MDa HA. The results from the strain sweep measurements indicate yield stress material like properties of these hybrid networks.

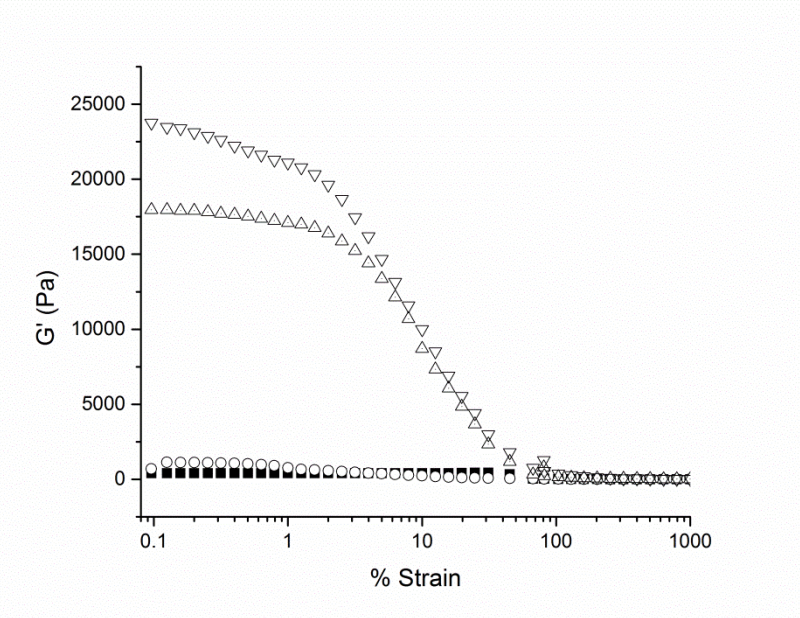

Figure 6.11. Oscillatory strain sweep data from hydrogels of MAX1 (solid squares) and hybrid hydrogels developed from MAX1 by vigorous mixing of MAX1 gels and HA solutions (a) MAX1 + 169 KDa HA (open circles), (b) MAX1 + 1 MDa HA (dotted triangles) (c) MAX8 + 2 MDa HA (inverted triangles).

Results of the compression testing demonstrate high values of compressive modulus of these hybrid materials obtained by mixing in 220 KDa, 419 KDa and 1 MDa HA solution. These values of compressive modulus are 70 KPa, 90 KPa and 10 KPa for the three molecular weights 220 KDa, 419 KDa and

1 MDa HA (Figure 6.12). The value of compressive modulus of a pure MAX1 hydrogel at 2% (w/w) obtained is ~ 6 KPa (Figure 6.12 (inverted triangles)). The compressive modulus values for the hybrid materials do not show a direct predictable dependence on the molecular weight of the hyaluronic acid used to construct the hybrid material. It is important to note that the hybrid material constructed using the highest molecular weight hyaluronic acid molecules (1MDa), exhibits the lowest value of the compressive modulus. The pendant carboxylic acid groups on the molecules of the 1MDa HA might not be completely available to the positively lysine charges on the peptide fibril due to the higher excluded volume of the large HA polymer (1 MDa) chains as compared to the 220 KDa and 419 KDa polymer chains, thus resulting into lesser points of electrostatic crosslinking and a less stiffer network.

The development of these viscoelastic materials is a first step towards developing highly compressible multicomponent hybrid hydrogel materials based completely on secondary interactions, without the need of chemical modification or crosslinking of either component. The composites obtained by employing Method 3 have bulk like characteristics with much larger solids content as compared to the composites obtained by Method 1 and Method 2. As described earlier, this can be attributed to the electrostatic interactions between the positively charged MAX1 and HA that are expected to be stronger than those between MAX8 and HA due to the higher overall positive charge of MAX1. This leads to formation of a uniform percolated bulk like network in case of MAX1

HA mixing as compared to loosely dispersed solid particles in case of MAX8 HA mixing. Thus, composites of versatile morphologies can be obtained by using peptides that are designed very slightly different from each other.

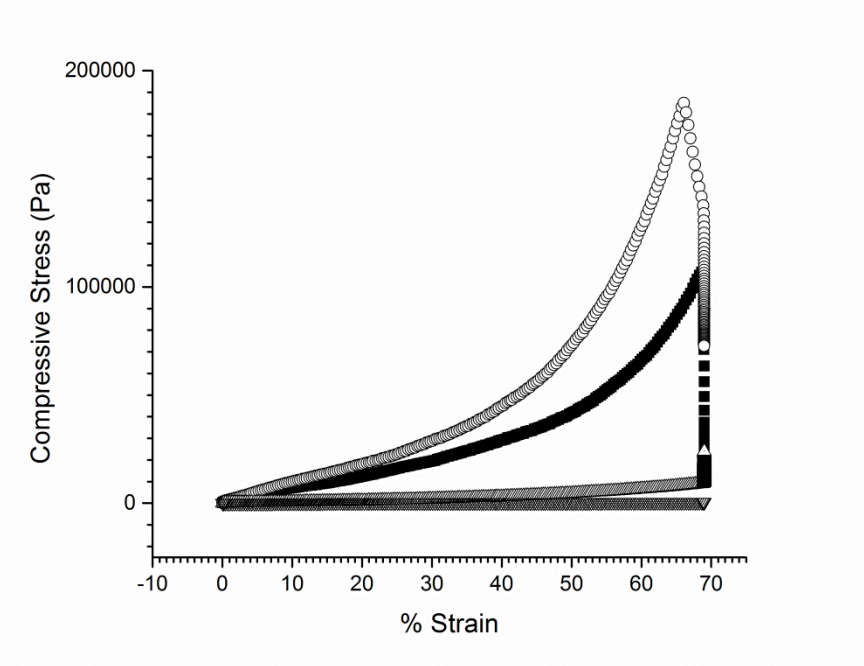

Figure 6.12. Compressive stress v/s strain data obtained from hydrogels of MAX1 (inverted traingles) and hybrid hydrogels developed from MAX1 by vigorous mixing of MAX1 gels and HA solutions (a) MAX1 + 169 KDa HA (solid squares), (b) MAX1 + 1 MDa HA (open circles) (c) MAX8 + 2 MDa HA (dotted triangles).

6.4. Conclusion

Three simple bench-top methods have been discussed for the development of hybrid multicomponent hydrogel materials hydrogels based on self-assembled β-hairpin peptides and hyaluronic acid. Method 1 is used to develop composite materials that contain a matrix of peptide fibrils and particulate domains rich in hyaluronic acid. Method 2 is used to develop composites that contain hyaluronic

acid molecules electrostatically complexed with fibrils of MAX1 peptide. Method 3 is used to develop hydrogels with high solids content and high tensile compressibility. These hybrid network hydrogels are based on electrostatic interactions and thus do not require any chemical modification of either component. Hybrid networks obtained by all three methods at least conserve the mechanical properties of the β-hairpin peptide MAX1/MAX8 hydrogels while in some cases enhance the stiffness of the hybrids. Specifically in Method 3, an increase in compressive modulus over several orders of magnitude is obtained as compared to the MAX1 hydrogels. This conservation and enhancement of mechanical properties of the β-hairpin peptide hydrogels is accompanied by introduction of potential biological activity of the hyaluronic acid polymers. Hydrogels based on hyaluronic acid similar to the ones described in this chapter have been studied as smart biomaterials that are capable of mediating cellular activities by providing biological cues[44]. Thus, the mixing methods of β-hairpin peptide hydrogels and hyaluronic acid polymers provide facile strategies to obtain biomaterials with potential utility as 3D-cell encapsulation matrices, delivery vectors for hyaluronic acid and related biopolymers, growth factors and pharmaceutical drugs.

REFERENCES

(1) Jia, X.; Kiick, K. L. *Macromolecular Bioscience* **2009**, *9*, 140.

(2) Altunbas, A.; Pochan, D. J. In *Peptide-Based Materials*; Deming, T., Ed. 2012; Vol. 310, p 135.

(3) Jonker, A. M.; Lowik, D.; van Hest, J. C. M. *Chemistry of Materials* **2012**, *24*, 759.

(4) DeVolder, R.; Kong, H. J. *Wiley Interdisciplinary Reviews-Systems Biology and Medicine* **2012**, *4*, 351.

(5) Van Vlierberghe, S.; Dubruel, P.; Schacht, E. *Biomacromolecules* **2011**, *12*, 1387.

(6) Haines-Butterick, L. A.; Rajagopal, K.; Lamm, M.; Pochan, D. J.; Schnieder, J. P. *Biopolymers* **2007**, *88*, 518.

(7) Haines-Butterick, L.; Rajagopal, K.; Branco, M.; Salick, D.; Rughani, R.; Pilarz, M.; Lamm, M. S.; Pochan, D. J.; Schneider, J. P. *Proceedings of the National Academy of Sciences of the United States of America* **2007**, *104*, 7791.

(8) Rajagopal, K.; Lamm, M. S.; Haines-Butterick, L. A.; Pochan, D. J.; Schneider, J. P. *Biomacromolecules* **2009**, *10*, 2619.

(9) Altunbas, A.; Lee, S. J.; Rajasekaran, S. A.; Schneider, J. P.; Pochan, D. J. *Biomaterials* **2011**, *32*, 5906.

(10) Haines-Butterick, L. A.; Salick, D. A.; Pochan, D. J.; Schneider, J. P. *Biomaterials* **2008**, *29*, 4164.

(11) Yan, C. Q.; Mackay, M. E.; Czymmek, K.; Nagarkar, R. P.; Schneider, J. P.; Pochan, D. J. *Langmuir* **2012**, *28*, 6076.

(12) Schneider, J. P.; Pochan, D. J.; Ozbas, B.; Rajagopal, K.; Pakstis, L.; Kretsinger, J. *J. Am. Chem. Soc.* **2002**, *124*, 15030.

(13) Hule, R. A.; Nagarkar, R. P.; Altunbas, A.; Ramay, H. R.; Branco, M. C.; Schneider, J. P.; Pochan, D. J. *Faraday Discussions* **2008**, *139*, 251.

(14) Ozbas, B.; Kretsinger, J.; Rajagopal, K.; Schneider, J. P.; Pochan, D. J. *Macromolecules* **2004**, *37*, 7331.

(15) Veerman, C.; Rajagopal, K.; Palla, C. S.; Pochan, D. J.; Schneider, J. P.; Furst, E. M. *Macromolecules* **2006**, *39*, 6608.

(16) Pochan, D. J.; Schneider, J. P.; Kretsinger, J.; Ozbas, B.; Rajagopal, K.; Haines, L. *J. Am. Chem. Soc.* **2003**, *125*, 11802.

(17) Yan, C. Q.; Pochan, D. J. *Chemical Society Reviews* **2010**, *39*, 3528.

(18) Kretsinger, J. K.; Haines, L. A.; Ozbas, B.; Pochan, D. J.; Schneider, J. P. *Biomaterials* **2005**, *26*, 5177.

(19) Kretsinger, J. K.; Pochan, D. J.; Schneider, J. P. *Biopolymers* **2003**, *71*, 319.

(20) Salick, D. A.; Kretsinger, J. K.; Pochan, D. J.; Schneider, J. P. *J. Am. Chem. Soc.* **2007**, *129*, 14793.

(21) Salick, D. A.; Pochan, D. J.; Schneider, J. P. *Advanced Materials* **2009**, *21*, 4120.
(22) Rughani, R. V.; Branco, M. C.; Pochan, D.; Schneider, J. P. *Macromolecules* **2010**, *43*, 7924.
(23) Branco, M. C.; Pochan, D. J.; Wagner, N. J.; Schneider, J. P. *Biomaterials* **2009**, *30*, 1339.
(24) Branco, M. C.; Pochan, D. J.; Wagner, N. J.; Schneider, J. P. *Biomaterials* **2010**, *31*, 9527.
(25) Necas, J.; Bartosikova, L.; Brauner, P.; Kolar, J. *Veterinarni Medicina* **2008**, *53*, 397.
(26) Hales, H. G. G. a. C. A. *Chemistry and Biology of Hyaluronan*; Elsevier Ltd.: Oxford, 2004.
(27) Prehm, P. *Biochemical Journal* **1984**, *220*, 597.
(28) Weigel, P. H.; Hascall, V. C.; Tammi, M. *Journal of Biological Chemistry* **1997**, *272*, 13997.
(29) T.C.Laurent; Fraser, J. R. E. *FASEB Journal* **1992**, *6*, 2397.
(30) West, D. C.; Kumar, S. *Ciba Foundation Symposia* **1989**, *143*, 187.
(31) Buchanan, E. P.; Longaker, M. T.; Lorenz, H. P. In *Advances in Clinical Chemistry Vol 48*; Makowski, G. S., Ed. 2009; Vol. 48, p 137.
(32) Chen, W. Y. J.; Abatangelo, G. *Wound Repair and Regeneration* **1999**, *7*, 79.
(33) Holmes, M. W. A.; Bayliss, M. T.; Muir, H. *Biochemical Journal* **1988**, *250*, 435.
(34) Meyer, K.; Palmer, J. W. *Journal of Biological Chemistry* **1934**, *107*, 629.
(35) Chan, R. W.; Titze, I. R. *Journal of the Acoustical Society of America* **1999**, *106*, 2008.
(36) Chan, R. W.; Gray, S. D.; Titze, I. R. *Otolaryngology-Head and Neck Surgery* **2001**, *124*, 607.
(37) Hammond, T. H.; Zhou, R. X.; Hammond, E. H.; Pawlak, A.; Gray, S. D. *Journal of Voice* **1997**, *11*, 59.
(38) Turley, E. A.; Austen, L.; Vandeligt, K.; Clary, C. *Journal of Cell Biology* **1991**, *112*, 1041.
(39) Turley, E. A.; Noble, P. W.; Bourguignon, L. Y. W. *Journal of Biological Chemistry* **2002**, *277*, 4589.
(40) Mascarenhas, R. M. D. a. M. M. *Chemistry and Biology of Hyaluronan*; Elsevier, Ltd., 2004.
(41) Knudson, C. B.; Knudson, W. *Faseb Journal* **1993**, *7*, 1233.
(42) Zhu, W. B.; Mow, V. C.; Rosenberg, L. C.; Tang, L. H. *Journal of Biomechanics* **1994**, *27*, 571.
(43) *Chemistry and Biology of Hyaluronan*; Hardingham, T. E., Ed.; Elsevier Ltd, 2004.

(44) Xu, X.; Jha, A. K.; Harrington, D. A.; Farach-Carson, M. C.; Jia, X. Q. *Soft Matter* **2012**, *8*, 3280.

(45) Hennink, W. E.; van Nostrum, C. F. *Advanced Drug Delivery Reviews* **2002**, *54*, 13.

(46) Giannelis, E. P. *Advanced Materials* **1996**, *8*, 29.

(47) Giannelis, E. P.; Krishnamoorti, R.; Manias, E. *Polymers in Confined Environments* **1999**, *138*, 107.

(48) LeBaron, P. C.; Wang, Z.; Pinnavaia, T. J. *Applied Clay Science* **1999**, *15*, 11.

(49) Vaia, R. A.; Price, G.; Ruth, P. N.; Nguyen, H. T.; Lichtenhan, J. *Applied Clay Science* **1999**, *15*, 67.

(50) Giannelis, E. P. *Applied Organometallic Chemistry* **1998**, *12*, 675.

(51) Yano, K.; Usuki, A.; Okada, A.; Kurauchi, T.; Kamigaito, O. *Journal of Polymer Science Part a-Polymer Chemistry* **1993**, *31*, 2493.

(52) Xu, R. J.; Manias, E.; Snyder, A. J.; Runt, J. *Macromolecules* **2001**, *34*, 337.

(53) Messersmith, P. B.; Giannelis, E. P. *Journal of Polymer Science Part a-Polymer Chemistry* **1995**, *33*, 1047.

(54) Gilman, J. W.; Kashiwagi, T.; Lichtenhan, J. D. *Sampe Journal* **1997**, *33*, 40.

(55) Gilman, J. W. *Applied Clay Science* **1999**, *15*, 31.

(56) Gilman, J. W.; Jackson, C. L.; Morgan, A. B.; Harris, R.; Manias, E.; Giannelis, E. P.; Wuthenow, M.; Hilton, D.; Phillips, S. H. *Chemistry of Materials* **2000**, *12*, 1866.

(57) Dabrowski, F.; Bourbigot, S.; Delobel, R.; Le Bras, M. *European Polymer Journal* **2000**, *36*, 273.

(58) Bourbigot, S.; Le Bras, M.; Dabrowski, F.; Gilman, J. W.; Kashiwagi, T. *Fire and Materials* **2000**, *24*, 201.

(59) Hule, R. A.; Pochan, D. J. *Journal of Polymer Science Part B-Polymer Physics* **2007**, *45*, 239.

(60) Biswas, M.; Ray, S. S. In *New Polymerization Techniques and Synthetic Methodologies*; Abe, A., Albertsson, A. C., Cantow, H. J., Dusek, K., Edwards, S., Hocker, H., Joanny, J. F., Kausch, H. H., Kobayashi, T., Lee, K. S., McGrath, J. E., Monnerie, L., Stupp, S. I., Suter, U. W., Wegner, G., Young, R. J., Eds. 2001; Vol. 155, p 167.

(61) Temenoff, J. S.; Shin, H.; Conway, D. E.; Engel, P. S.; Mikos, A. G. *Biomacromolecules* **2003**, *4*, 1605.

(62) Yucel, T.; Micklitsch, C. M.; Schneider, J. P.; Pochan, D. J. *Macromolecules* **2008**, *41*, 5763.

(63) Hoare, T. R.; Kohane, D. S. *Polymer* **2008**, *49*, 1993.

(64) R.A.Gemeinhart; Guo, C.; CRC Press, LLC: 2004.

Chapter 7

A GLIMPSE INTO AMPHIPHILIC PEPTIDE SOLUTION CO-ASSEMBLY, GLOBAL CONCLUSIONS AND FUTURE WORK

7.1. Global Conclusions

The overall aim of this dissertation is to achieve a comprehensive correlation between the molecular level changes in primary amino acid sequences of amphiphilic β-hairpin peptides and their consequent solution-assembly properties and bulk network hydrogel behavior. This has been accomplished using two broad approaches. In the first approach, amino acid substitutions were made to peptide sequence MAX1 such that the hydrophobic surfaces of the folded β-hairpins from the peptides demonstrate shape specificity in hydrophobic interactions with other β-hairpins during the assembly process, thereby causing changes to the peptide nanostructure and bulk rheological properties of hydrogels formed from the peptides. In the second approach, peptides with established differences in assembly kinetics and bulk mechanical properties of assembled peptide hydrogels are used to develop composite materials with diverse morphological and mechanical properties by blending with the biopolymer hyaluronic acid. The diverse properties of the composites have been correlated to the specific peptide hydrogels used to develop the composite and the different stages of peptide assembly at which blending with hyaluronic acid was carried out.

Before addressing these specific aims of this dissertation in Chapters 4-6, experimental evidence of the macroscopic fracture of a self-assembled MAX8 peptide hydrogel was provided in Chapter 3 as summarized here in this paragraph. The basic peptide sequence MAX1 and its derivative peptide MAX8 assemble into nanofibrillar hydrogels that demonstrate yield-stress material behavior and are based on physical crosslinking including fibrillar branching and entanglement. The MAX1/MAX8 hydrogels show a unique shear-thinning and rehealing property when subject to shear using a rheometer or via injection using a syringe or catheter. This shear thinning and rehealing behavior has been attributed to the shear-induced fracture of the bulk hydrogel into domains of smaller sizes with nanostructure identical to that of the bulk gel. As shown by Yan et al[1]., when injected through a capillary MAX8 hydrogels undergo a plug-flow with the hydrogel domains near the walls of the capillary yielding and experiencing shear while a bulk of the hydrogel away from the walls experiencing negligible shear. When subject to steady-state shear using the upper plate of a bench-top rheometer, MAX8 hydrogels undergo macroscopic fracture a distance away from the shearing upper plate that is dependent on the amplitude of steady state shear. This bulk fracture of a MAX8 hydrogel has been visually confirmed using a rheometer-confocal microscope compound assembly. The bulk fracture of the MAX8 hydrogel only within a layer of hydrogel away from the shearing upper plate in a bench top rheometer is consistent with the proposed bulk fracture behavior and also the observed plug flow behavior. Thus, a combination of a

confocal microscope and a rheometer helps in elucidation of the exact correlation between the structural changes and corresponding rheological behavior from physical hydrogels.

As a first approach to addressing the specific aims of this dissertation, Chapter 4 discussed the first molecular level design changes to the primary structure of MAX1. Steric lock and key complementary hydrophobic interactions were designed to occur between two β-hairpin molecules of the same LNK1 peptide during β–sheet fibrillar assembly. Experimentally, vast differences in the network properties of the hydrogels formed by the LNK1 peptide were observed as compared to the properties of the MAX1 peptide hydrogels. The first prominent difference was the lack of recovery of storage modulus G' (Pa) values from the LNK1 network after the brief application and cessation of in-situ steady-state shear. In addition to this, sequential, multiple syringe injections applied to the networks as a means of shear treatment were instrumental in complete elimination of network properties of the LNK1 networks. MAX1 differs from the LNK1 primarily in terms of having a sterically non-specific hydrophobic core that causes fibrils of MAX1 to be branched as well as entangled. Taken together, experimental results from circular dichroism, transmission electron microscopy and oscillatory rheology, the molecular design of the LNK1 peptide can be assigned the cause of the drastically different behavior of the networks relative to MAX1, indicating elimination or significant reduction of fibrillar branching due to steric complementarity in LNK1 that does not exist in MAX1.

As an extension of the designed steric lock and key complementarity between two β-hairpin molecules of the same peptide molecule LNK1, three new pairs of peptide molecules LP1-KP1, LP2-KP2 and LP3-KP3 that resemble complementary 'wedge' and 'trough' shapes when folded into β-hairpins were designed and studied. Chapter 5 discussed the assembly and bulk hydrogel mechanical properties of the wedge shaped hairpin peptides LP1, LP2 and LP3 and the trough shaped hairpin peptides KP1, KP2 and KP3. Shape complementary interactions among the various pairs of peptides were investigated by studying 1:1 (w/w) blends of LP1:KP1, LP2:KP2 and LP3:KP3. An overall fibrillar nanostructure as evidenced by cryo-TEM is obtained for all the individual peptides and the 1:1 (w/w) blend of shape complementary peptide pair blends. All six peptides individually and when blended with their corresponding shape complement formed fibrillar nanostructures with non-uniform thickness values. Loose packing in the assembled structures was observed in all the new peptides as compared to the uniform tight packing in MAX1 by SANS analysis. This loose packing can be attributed to the designed wedge and trough shapes of the peptides disturbing formation of a uniform bilayer type structure proposed in the case of MAX1 with each hairpin having a flat hydrophobic surface. Thus, designed changes in hydrophobic shape of the peptide nanofibril core in the new peptides were found to significantly influence the self-assembled nanostructure and network rheological behavior.

Chapter 6 discussed three simple bench-top methods for development of

hybrid composite hydrogel materials based on self-assembled β-hairpin peptides and the biopolymer hyaluronic acid. The simple mixing methods to construct the composites are based on electrostatic interactions between positively charged peptide fibrils and negatively charged hyaluronic acid biopolymer and do not require development of new derivatives of either component by chemical modification. Hybrid networks obtained by all three methods conserve and, in some cases, enhance the mechanical properties of the β-hairpin peptide MAX1/MAX8 hydrogels. This conservation and enhancement of mechanical properties of the β-hairpin peptide hydrogels is accompanied by introduction of potential biological activity of the hyaluronic acid polymers. The development of composite materials based on self-assembled β-hairpin peptide hydrogels and hyaluronic acid can act as a springboard for the development of hybrid materials from the positively charged β-hairpin peptide fibrillar hydrogels and various biologically important negatively charged species such as heparin, DNA, alginate and chondroitin sulfate.

The approach of developing composite materials using two components, e.g. the β-hairpin peptide hydrogels and hyaluronic acid, is a step towards exploring peptide assembly in the presence of a multitude of additive functional components. Co-assembly of peptides with other assembling entities such as block copolymers, functional biopolymers, peptide amphiphiles, small molecule drug compounds and other peptides or proteins is an area that deserves further exploration. A brief background of peptide co-assembly with other peptides and

some basic studies of peptide-peptide co-assembly to yield hybrid hydrogels are discussed in the next section.

7.2. Peptide Co-assembly

Synthetic peptides can undergo solution assembly into well-defined nanostructures depending on their primary amino acid structures and solution conditions. On assembly, they can also yield solid hydrogels that can be used as drug delivery vectors, tissue engineering constructs and extra-cellular matrix mimetic materials. An important direction in the study of peptide solution assembly is that of peptide co-assembly. Solution co-assembly of physical blends of multiple peptides with established assembly pathways and resulting nanostructures can potentially yield a combination of hybrid nanostructures and functionalities that cannot be obtained by the assembly of individual peptides. Physical blending as addressed in this section is defined as blending of two components without formation of covalent bonds between the two components. For example, hydrogels based on enantiomeric mixtures of self-assembling β-hairpins (MAX1 and D-MAX1) showing nonadditive, synergistic enhancement in material rigidity compared to gels prepared from either pure enantiomer, have been reported by Nagy et al[2]. The simple approach of studying solution co-assembly behavior of blends of peptides does not require any chemical modification to either peptidic component and relies purely on the secondary interactions such as electrostatic interactions, hydrophobic interactions and

hydrogen bonding between the peptides. Precisely controlled, selective co-assembly of several distinct peptide amphiphiles into multicomponent fibrils based on electrostatic interactions has begun to be explored and can be extended to a variety of peptidic architectures[3,4]. For example, solution co-assembly of blends of amphiphiles with free N-termini and free C-termini respectively into highly thermally stable β-sheet structures that are more stable than those formed by each component individually, has been reported by Behanna et al[5]. Complementary π-π interactions that are observed in blends of benzene and perfluorinated benzene have been used as a motif to design co-assembling amino acid hydrogels. The use of π-π interactions to develop fibrillar hydrogels from selectively co-assembling fluorenylmethyloxycarboxycarbonyl chloride-Phenylalanine amino acid (Fmoc-Phe) and pentafluorinated Fmoc-Phe (Fmoc-F_5-Phe) has been reported by Ryan et al[6]. Fmoc-Phe does not undergo assembly at the solution conditions at which Fmoc-F_5-Phe undergoes assembly into fibrillar hydrogels. Perfluronination of benzene, such as in Fmoc-F_5-Phe results in electronic perturbation that results in formation of a quadrupole that is equal in magnitude but opposite in sign to that of unsubstituted benzene (such as in Fmoc-Phe). Thus, when blended and allowed to solution-assemble, both components demonstrated co-assembly with the blend of the two components demonstrating expedited kinetics of assembly as compared to the individual components. The co-assembly and faster assembly kinetics of the blend of the components has been attributed to the complementary π-π interactions. Ramachandran et al.[72,73] have

reported on co-assembly of amphiphilic peptides (KAW10, KAW15, EAW10 and EAW15) into hydrogels. Peptide molecules having the same charged residue (lysine or glutamic acid) did not undergo assembly with each other but did so when blended with molecules containing an opposite charge (glutamic acid or lysine correspondingly). The assembly strategy discussed by the authors involved making hydrogels by blending pairs of peptides from the four peptides generating four pairs, two with sticky ends (with unmatched lengths of amino acids in peptide pair) and two with blunt (with exactly matched lengths of amino acids in peptide pair) ends. All four pairs were reported to undergo co-assembly as confirmed by transmission electron microscopy with different kinetics but all formed shear thinning and rehealing fibrillar hydrogels,. The KAW:EAW blunt end pair was found to form the most stable hydrogels post cessation of shear, negating the importance of the sticky ends for stiffer network formation. Thus, applying a strategy of simple blending of complementarily charged peptides, diverse kinetic pathways of assembly along with hydrogels with diverse stabilities and mechanical properties were discovered.

Peptide co-assembly can also be extended to the study of peptide assembly along with non-peptidic molecules such as biopolymers like hyaluronic acid, heparin, alginates, DNA and synthetic polymers like block copolymers and dendrimers. For example, Morfin et al[7]. have explored formation of assembled rod-like complexes from simple blends of hyaluronan and the protein lysozome. Such well-defined morphology is not demonstrated by either component

individually, and, thus, co-assembly of such individual components is an exciting future area of research. Deeper investigation of the assembly patterns, nanostructure and hydrogel formation from blends of biologically important materials like hyaluronan and comprehensively studied materials like peptides and proteins is a new direction towards development of next generation soft materials. Several parameters like assembly solution conditions, designed inter-component secondary interactions, stages of peptide assembly at which components are blended and material processing steps can be controlled in the simple blending of peptides and other co-assembling molecules to tune the co-assembly. Tuning these parameters can afford a variety of approaches to yield a rich variety of nanostructures and functionalities. This diversity is easily accessible without the need of complex chemical modification and chemical conjugation of the individual peptidic and non-peptidic molecules. The next section describes an experimental report of co-assembly of two peptides, both with different self-assembly pathways and resulting nanostructures. The co-assembly process was carried out by subjecting a physical blend of both peptides to designed solution and temperature conditions. The following discussion and preliminary results of a final peptide blending example shows a final example of the facile nature of peptide co-assembly and its utility in constructing materials with hybrid functionalities acquired from each individual component.

7.2.1. Co-assembly of branch forming (MAX1) and laminate forming (P5) peptides

In order to demonstrate the utility of the approach of simple blending of peptides, co-assembly of blends of peptides MAX1 [$(VK)_4$-V^DP^LPT-$(KV)_4$] and P5 [$(VK)_4$-V^LP^LPT-$(KV)_4$] was studied. MAX1 contains a turn sequence V^DP^LPT flanked by two amphiphilic arms consisting of alternating valine and lysine residues. This turn sequence has a high propensity to form a type-II' turn and at solution conditions of high pH and ionic strength, it is responsible for β-hairpin formation in MAX1[8]. This β-hairpin formation results into hierarchical self-assembly of MAX1 into branched nanofibrils of exact uniform thickness (~3 nm) as explained in Chapter 2, that do not form higher order assemblies such as ribbons, bundles and fibers. The peptide P5 is obtained by making a point substitution in MAX1 in the turn sequence, by replacing the ^DP with a ^LP, resulting in a turn sequence V^LP^LPT flanked by the two amphiphilic arms consisting of alternating valine and lysine residues like in MAX1[9]. This replacement of ^DP with a ^LP leads to strong disfavor of the β-turn formation and, consequently, intramolecular folding. Under the same pH and ionic strength solution conditions as MAX1 (pH 9 125mM Boric Acid, 10mM NaCl) the P5 molecule adopts an extended conformation in contrast to the MAX 1 β-hairpin conformation. Due to this extended conformation, P5 assembles into hydrogen bonded laminated fibrils with a non-twisted morphology that are morphologically different from fibrils of MAX1[9,10].

The assembly kinetics of P5 are significantly slower than those of MAX1. Under the same pH and ionic strength solution conditions as MAX1 (pH 9 125mM Boric Acid, 10mM NaCl), β-sheet fibril and higher order laminate formation results over a period of ~ 2 weeks in case of P5 as compared to several minutes in case of MAX1 at room temperature. Assembly of P5 can be expedited by incubation at elevated temperatures and can result within an hour at ~ 50°C to a few seconds at ~70°C under the same solution conditions[11]. When the temperature of an aqueous P5 solution (10 mg/mL) under the solution conditions (pH 9 125mM Boric Acid, 10mM NaCl) is increased to over 70 °C, fibril formation results, and within seconds, brittle gels are obtained. Fibrils obtained under these conditions are significantly less laminated and are more flexible thus providing for entanglement and hydrogel formation. These hydrogels demonstrate a linear viscoelastic regime (LVE) up to ~ 0.2% strain and do not reheal after undergoing shear treatment. This is in sharp contrast to hydrogels constructed using MAX1 that exhibit an LVE up to 20% strain and demonstrate unique shear thinning and rehealing abilities. Thus, MAX1 hydrogels exhibit potential for drug delivery[12-15] and cellular encapsulation applications[16-18], while the flat non-twisted morphology of the P5 fibrils can be exploited for nano-applications like nanoparticle templating[10]. Therefore, the hypothesis is that by simple blending and co-assembly of MAX1 and P5, the functionalities of hydrogel mechanical properties of MAX1 and the flat raft-like morphology of P5 can be combined into one hybrid material of MAX1 and P5 peptides.

Figure 7.1 shows the oscillatory frequency sweep data obtained for hydrogels formed from MAX1, P5 and a physical blend of MAX1 and P5 in a 1:3 (w/w) ratio. The solution conditions for preparing all the hydrogels were maintained at (pH 9 125mM Boric Acid, 10mM NaCl) and the overall peptide concentration was fixed at 1% (w/w). The temperature was fixed at 55°C to ensure the assembly of P5 to obtain comparable kinetics as MAX1 at the mM concentrations that have been maintained for both peptides. Thus for the blended sample, the individual concentrations of MAX1 and P5 were 0.25% (w/w) and 0.75% (w/w). The angular frequency sweep data shows a very weak dependence of the stiffness modulus, G' (Pa) on the applied angular frequency (rad/s) for all three samples, an indication of solid hydrogel-like characteristics from all three materials. MAX1 hydrogels have a G' (Pa) value of ~ 2800 Pa across all values of applied angular frequency whereas P5 hydrogels exhibit a higher value of ~ 4200 Pa as shown in Figure 7.1. The blend with 1:3 (w/w) ratio of MAX1 to P5 shows synergistic improvement in mechanical properties as compared to individual hydrogels that would have been prepared using MAX1 and P5 at their respective concentrations of 0.25% (w/w) and 0.75% (w/w). Figure 7.2 shows results from the oscillatory strain sweep experiments. It is important to note here that the hydrogels obtained from assembly of P5 individually are percolated networks because of fibrillar entanglement as compared to the entangled as well as branched networks of MAX1. The yield strain value indicating the LVE for the hydrogel from the 1:3 (w/w) blend of MAX1 and P5 (~10 % strain) is

intermediate to the values of the yield strain values of the pure P5 (~2 % strain) and pure MAX1 (~20 % strain) hydrogels. This value indicates an intermediate value of brittleness of the hybrid hydrogel that is less than that of the pure P5 hydrogel and more than that of the pure MAX1 hydrogel. The intermediate brittleness of the blend can be attributed the contribution from the MAX1 fibrillar network that has a high propensity towards forming a percolated network via fibrillar branching, a phenomenon not observed in pure P5 hydrogels. The results in Figure 7.1 and 7.2 help conclude that a truly hybrid mechanical properties are obtained by physically blending the two peptides with very different hydrogel mechanical properties.

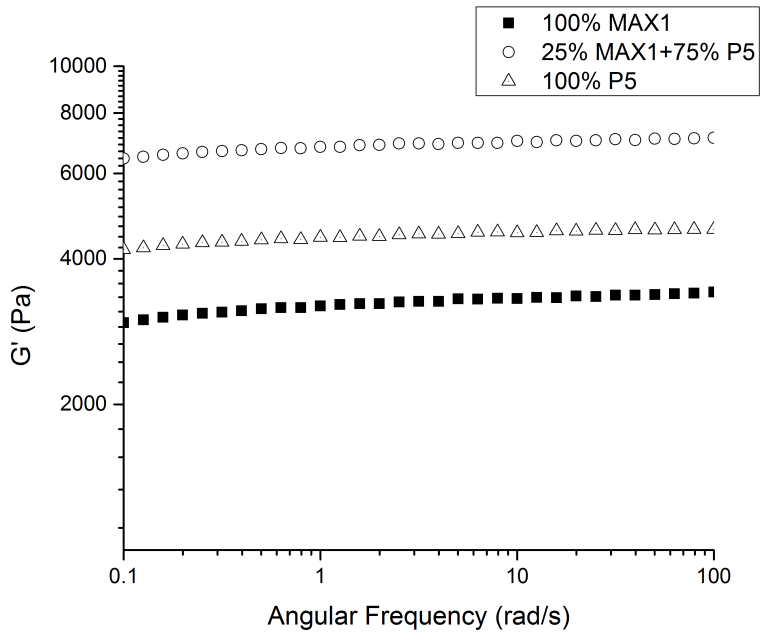

Figure 7.1. Oscillatory frequency sweep data [G' (Pa)] obtained from hydrogels

constructed using pure MAX1 (solid squares), pure P5 (hollow triangles) and a 1:3 (w/w) blend of MAX1 and P5.

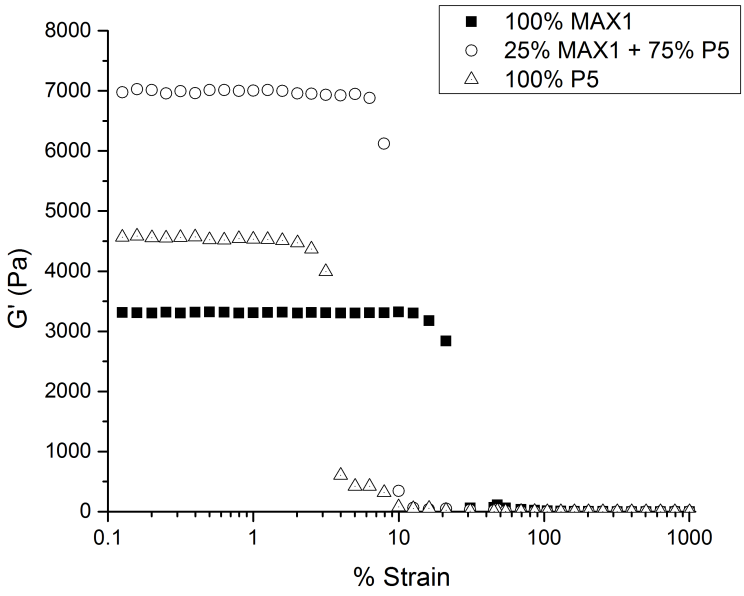

Figure 7.2. Oscillatory strain sweep data [G' (Pa)] obtained from hydrogels constructed using pure MAX1 (solid squares), pure P5 (hollow triangles) and a 1:3 (w/w) blend of MAX1 and P5. The data exhibit the extent of the linear viscoelastic region (LVE)

Figure 7.3 shows the differences in nanostructure of MAX1, P5 and the 1:3 (w/w) physical blend of MAX1 and P5 as studied using Transmission Electron Microscopy (TEM). The histogram in Figure 7.4 shows the ranges of thickness values of the nanostructure obtained from pure MAX1 (black column), 1:3 (w/w) blend (red column) and pure P5 (blue column). MAX1 exhibits a fibrillar structure with fibrils of uniform thickness ~3 nm (Figure 7.3a, Figure 7.4) while P5 exhibits a non-twisted tape-like laminated morphology with width values ~24-34 nm (Figure 7.3c, Figure 7.4). The assembled nanostructure of P5 depends on the kinetics of the assembly process as stated before. When a buffered

solution of P5 is heated quickly at temperatures ~ 70°C, laminated structures are formed that are laminated to a much lesser extent as the structures obtained by room temperature assembly of P5 peptides over ~ 2 weeks. Samples for TEM measurements discussed in this section were prepared by heating a buffered solution of P5 quickly to 70° C. Thus, nanostructure showing alesser degree of lamination is obtained as compared to the nanostructure obtained by room temperature assembly of P5 that can have width values of ~ 100 nm[9]. The nanostructure obtained after assembly of 1:3 (w/w) ratio blend of MAX1 and P5 is characterized by flat laminated morphology (Figure 7.3b) in contrast to the uniformly thick fibrils obtained after MAX1 assembly (Figure 7.3a). The laminates exhibit smaller widths as compared to the quickly assembled pure P5 laminates in a range of 10-20 nm (Figure 7.3b, Figure 7.4). Thus, the nanostructure of the 1:3 (w/w) blend also shows truly hybrid properties of MAX1 and P5, with laminates formed that are thinner than pure P5 laminates but thicker than pure MAX1 fibrils.

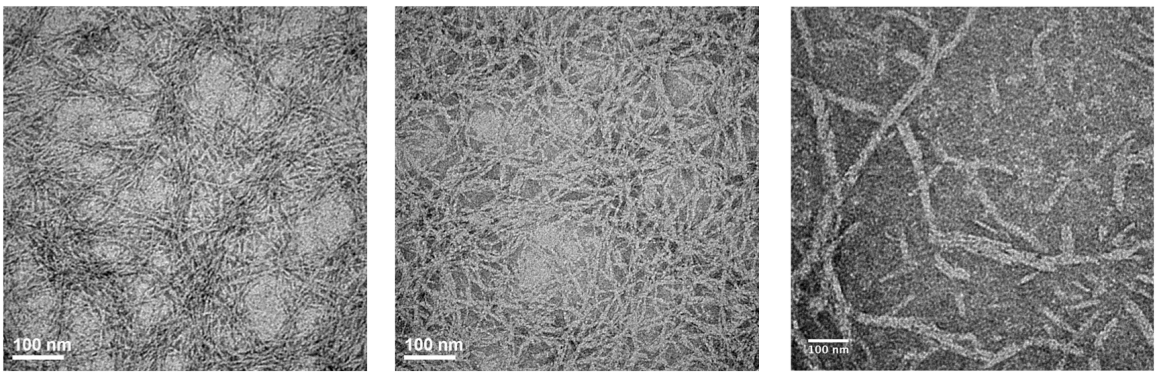

Figure 7.3. Transmission Electron Microscopy data acquired using samples made from (a) pure MAX1, (b) 1:3 (w/w) blend of MAX1and P5 (c) pure P5

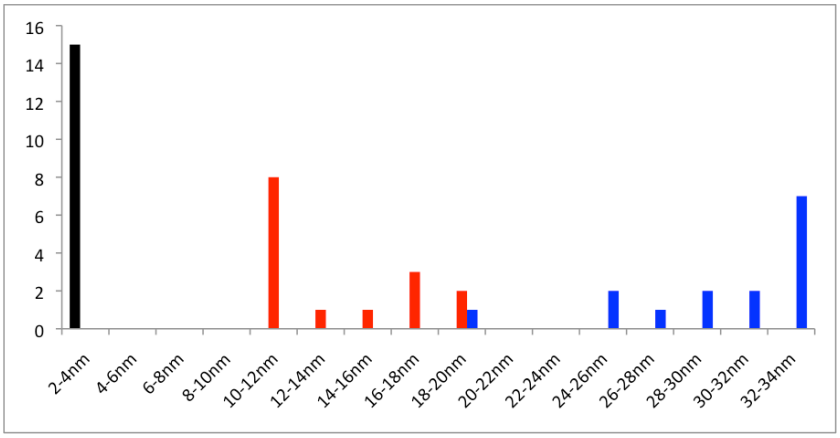

Figure 7.4. Histogram showing ranges of nanostructure thickness obtained from samples made from pure MAX1 (black column), 1:3 (w/w) blend of MAX1and P5 (red column) pure P5 (blue column)

The experimental report on co-assembly of MAX1 and P5 demonstrates the facile approach of co-assembly of blends of peptides with diverse assembled nanostructures and bulk mechanical properties towards obtaining hybrid

properties of the blended materials in a single material. The experimental approaches discussed in this thesis involved studying assembly patterns and hydrogel characteristics of blends of various peptide-peptide systems (LP1-KP1, LP2-KP2, LP3-KP3) and peptide-polymer systems (MAX1/MAX8-Hyaluronic acid). These approaches serve as a springboard for experiments studying assembly of physically blended multicomponent peptide, polypeptide and protein systems towards development of hybrid multifunctional materials. The final section describes some of the specific experimental ideas and peptide designs associated with the blending strategy that can be undertaken as projects in the future.

7.3. Future Work

An immediate experimental idea that could follow the research described in this dissertation is tuning the primary structures of the wedge and trough shaped peptides described in Chapter 5. As discussed in Chapter 5, non-specific hydrophobic interactions between peptides due to the large hydrophobic side chains used in the peptide design and the exposure of these hydrophobic side chains to the solution during the folding and assembly of the peptides causing non-specific aggregation, leading to irregular and non-uniform nanostructure from the new peptides. Therefore, the design of new peptides incorporating a new set of hydrophobic side chain amino acids assembly of which can ensure proper shielding of hydrophobic side chains along the fibrillar edges to so as limit non-

specific aggregation of peptides during solution assembly can be explored as a next step.

Co-assembly of β-hairpin peptides with biopolymers in order to yield hybrid materials with the favorable mechanical properties of the peptide hydrogels (in particular the unique shear thinning and rehealing properties) and established biologically relevant properties of the biopolymers is an immediate step forward. This proposed area of work follows the development of hybrid materials using β-hairpin peptide hydrogels and the biopolymer hyaluronic acid. Section 7.3.1 discusses some of the potential biopolymers that can be used in hybrid material development with the β-hairpin peptide hydrogels. And while blends and simple mixing are exciting strategies for new hydrogel material development, there also is plenty of opportunity in new peptide primary strucure designs for new material properties. Section 7.3.2 discusses some peptide designs that incorporate new chemical functionality in order to facilitate covalent crosslinking at the hydrophobic surface of the assembling β-hairpin peptides, potentially producing hydrogels much stiffer in comparison to the existing hydrogels for various biomedical applications.

7.3.1. Hybrid Materials from electrostatic complexation of MAX1/MAX8 hydrogels and anionic biopolymers

Biopolymeric materials like heparin, alginate, chondroitin sulfate and DNA that contain negative charges and have been studied extensively towards

biomaterial development are potential candidates for construction of hybrid multicomponent hydrogels with MAX1/MAX8 fibrils. Taking advantage of the electrostatic interactions between the positively charged peptide fibrils and negatively charged biopolymers, smart biomaterials can be developed without the need of complex chemical modification of either component. Chondroitin sulfate possesses biocharacteristics like receptor binding and modulation of certain growth factors[19]. It is readily water-soluble and thus requires chemical crosslinking for any in-vitro or in-vivo hydrogel application. Electrostatic complexation with positively charged, percolated hydrogels of MAX1/MAX8 could offer physically crosslinked, hybrid biomaterials that combine the favorable functionalities of both peptide hydrogels and chondroitin sulfate. Alginate is well known to be mucoadhesive, biocompatible and non-immunogenic[20] and is also often processed into microcarriers for cell-encapsulation[21]. Alginate has also shown the potential to be electrostatically complexed using Ca^{+2} ions[19]. Heparin is a highly sulfated glycosaminoglycan that is used widely as an anticoagulant in subcutaneous and intravenous therapies[22]. The anionic character of heparin is responsible for protein binding by heparin thus leading to indirect mediation of many processes such as cell proliferation, differentiation and control of chemokine signaling by heparin[23,24]. Therefore, designed blends of MAX1 or MAX8 and heparin may impart excellent biological properties in addition to mechanical properties to the final hybrid hydrogel material. DNA delivery systems are necessary in the field of gene therapy to introduce foreign DNA

encoding therapeutic protein sequences into cells. Non-viral vectors used in DNA delivery are constructed using the association of DNA with cationic lipids and polymers. To prevent the degradation of the administered DNA by DNAse enzymes, the DNA molecules are condensed using cationic molecules[25]. MAX1/MAX8 peptides demonstrate a highly controllable assembly process and form nanofibrils such that the fibril-DNA complexes could be potentially favorably sized for cellular penetration through endocytosis. Construction of electrostatically complexed DNA and MAX1/MAX8 hydrogels may afford highly efficient DNA delivery systems, and their development deserves further investigation. Thus, a rich diversity of biological functionality can be imparted to hybrid materials constructed using MAX1/MAX8 hydrogels and any of the above discussed biopolymers.

7.3.2. Covalently crosslinked hydrophobic surfaces of β-hairpin peptides

Load bearing capacities of scaffolding hydrogels until formation of extracellular matrix (ECM) by cells in hydrogels are important for applications of hydrogels as tissue engineering or 3-D cell culturing scaffolds[26,27]. For applications of hydrogels as therapeutic cell delivery vectors, cellular efficacy depends upon hydrogel mechanical properties. As discussed by Discher et al[28]., when hydrogels are used as substrates for tissue engineering, many properties including cellular differentiation, proliferation and migration are influenced by hydrogel mechanical properties[29]. A seminal report from the Discher group[30]

discusses the influence of hydrogel matrix elasticity on stem cell lineage specification. Thus, control over mechanical properties of hydrogels is a very important parameter for biomedical applications of hydrogels

Hydrogels constructed from β-hairpin peptides MAX1, MAX8 and other related sequences are based completely on physical crosslinking including fibrillar entanglement and fibrillar branching. Covalent crosslinking is a great strategy to impart more stiffness to the peptide networks. The functionality of covalent crosslinking has been imparted onto a derivative of MAX1 by substituting lysine residues on the hydrophilic face with the residue lysyl sorbamide[31]. Lysyl sorbamide is a derivative of lysine with unsaturated double bonds. Irradiation of the assembled fibrillar network containing sorbamide moieties resulted in polymerization of the sorbamide moieties, leading to intrafibrillar covalent crosslinking, in turn leading to stiffer overall hydrogels. The lateral and facial hydrophobic interactions between individual β-hairpin peptides are dominant secondary interactions that anchor the self-assembled fibrillar nanostructure[8,32]. Introduction of chemical functionality onto the hydrophobic face of the folded β-hairpin is an excellent opportunity for new peptide design that should be pursued. Functionalization of the fibril hydrophobic core would allow covalent crosslinking to be carried out at the *hydrophobic* surface within the core of each self-assembled fibril post-fibril assembly. This strategy potentially could generate much stiffer gels than the gels containing covalently crosslinked *hydrophilic* faces. Perhaps more importantly, this strategy could allow for

covalent crosslinking without any perturbation of the hydrophilic environment or the existing gel moprhology. Thus, covalent crosslinking of the hydrophobic face is a step forward in developing smarter biomaterials from these hydrogels. The facial and lateral hydrophobic interactions as shown in Figure 7.5a and Figure 7.5b potentially can be reinforced with covalent crosslinking leading to stiffer individual fibrils and thus, stiffer overall hydrogels. For example, the hydrophobic side chain valine residues in MAX1 or MAX8 can be replaced by non-natural amino acids like dehydrovaline (Scheme 7.1a), which is capable of covalent crosslinking. The extent of valine substitution by dehydrovaline can help control the extent of chemical crosslinking and, thus, ultimate mechanical properties of the assembled and crosslinked hydrogel. This covalent crosslinking can be carried out post self-assembly when an already percolated fibrillar hydrogel network is present. Such covalent crosslinking can provide an additional degree of control over the mechanical properties of the solution-assembled peptide hydrogels. Scheme 7.1 shows three candidate amino acid residues that can be used to substitute valine to various degrees and confer covalent crosslinking ability onto the resulting peptide sequence. A preliminary attempt at peptide fibril covalent crosslinking was attempted by using the peptide design derivative of MAX8 with all its hydrophobic valine groups replaced by allylglycine. This peptide (AA-MAX8) underwent conformational change from a random coil to β-sheet under solution conditions pH 7 (50mM BTP 150mM NaCl) i.e. the same conditions at which MAX8 undergoes folding and self-assembly at room

temperature (~20°C). Figure 7.6 shows the circular dichroism data from a 150μM buffered solution of AA-MAX8 at pH 7 (50mM BTP 150mM NaCl). The mean residual ellipticity (MRE) was measured at the wavelength (λ= 218 nm), which is the signature wavelength for a β-sheet structure to exhibit a minimum in MRE values. The data in Figure 7.6 show that AA-MAX8 undergoes a random coil to β-sheet structure conformational change at the temperature of ~ 55°C, which is higher than the folding temperature of MAX8. These preliminary data show that the allylglycine derivative of MAX8 forms β-sheet structures and is a viable candidate design that can be explored immediately.

7.4. Conclusion

The research described in this dissertation focuses on solution assembly of amphiphilic β-hairpin peptides into physically crosslinked fibrillar hydrogels that demonstrate significant potential as biomaterials in areas such as tissue engineering and drug delivery. In addition to functioning as biomaterials, hydrogels constructed using solution-assembling peptides with diverse molecular architectures and blends of peptides as discussed in Section 7.2.1., can act as model systems for the study of fundamental solution assembly pathways. Results from these studies can be potentially correlated to the peptide molecular architectures to understand advanced structure-property relationships in assembling peptides.

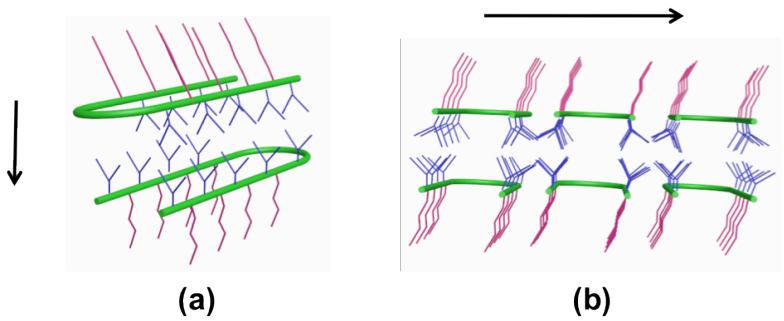

Figure 7.5. (a) Facial hydrophobic interactions (b) Lateral Hydrophobic Interactions. Arrows indicate directions of potential covalent crosslinking that can be designed into new peptide sequences, resulting in reinforcement of hydrophobic interactions and stiffening of individual fibrils and thus, the overall hydrogel networks.

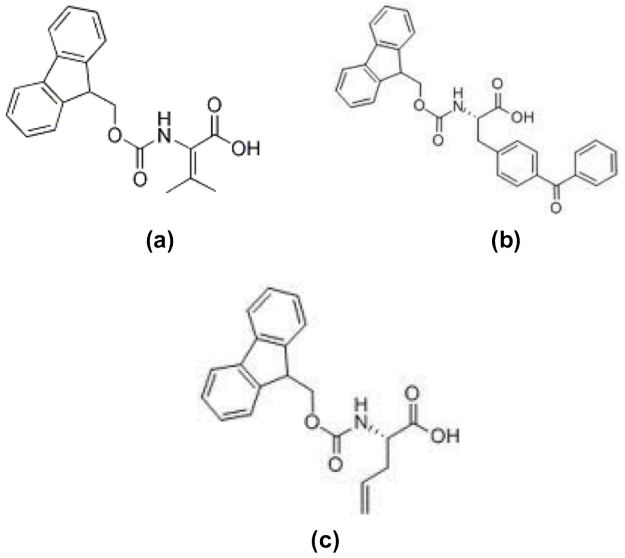

Scheme 7.1. Amino acid candidates (a) 2,3-Dehydrovaline (b) Benzoyl-phenylalanine (c) Allyl-glycine with the Fmoc protecting group. These residues can be potentially substituted for valine in MAX1/MAX8 peptide sequence and can confer the ability of covalent crosslinking upon the newly designed peptide sequences.

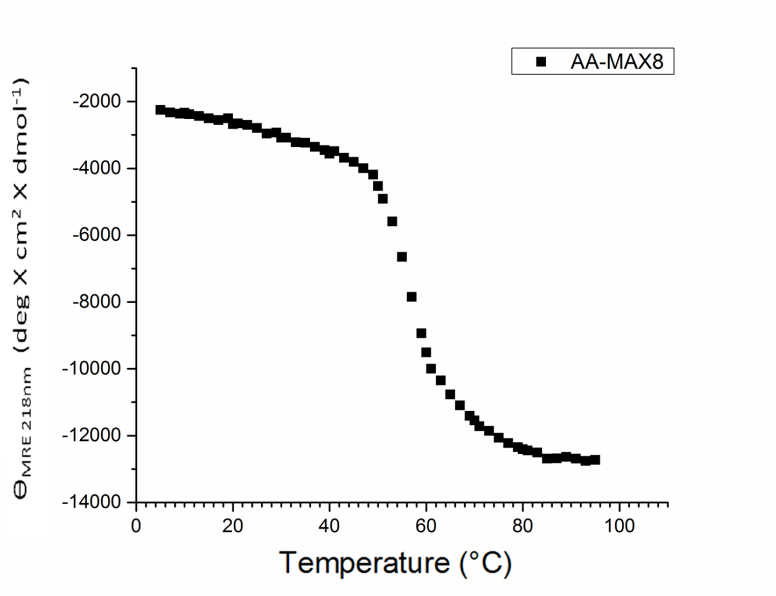

Figure 7.6. Circular dichroism data showing dependence of mean residual ellipticity (MRE) value from a buffered solution (pH 7 50mM BTP 150mM NaCl) of AA-MAX8 at λ = 218 nm on temperature.

REFERENCES

(1) Yan, C. Q.; Pochan, D. J. *Chemical Society Reviews* **2010**, *39*, 3528.

(2) Nagy, K. J.; Giano, M. C.; Jin, A.; Pochan, D. J.; Schneider, J. P. *J. Am. Chem. Soc.* **2011**, *133*, 14975.

(3) Bothner, B.; Aubin, Y.; Kriwacki, R. W. *J. Am. Chem. Soc.* **2003**, *125*, 3200.

(4) Behanna, H. A.; Rajangam, K.; Stupp, S. I. *J. Am. Chem. Soc.* **2007**, *129*, 321.

(5) Behanna, H. A.; Donners, J.; Gordon, A. C.; Stupp, S. I. *J. Am. Chem. Soc.* **2005**, *127*, 1193.

(6) Ryan, D. M.; Doran, T. M.; Nilsson, B. L. *Langmuir* **2011**, *27*, 11145.

(7) Morfin, I.; Buhler, E.; Cousin, F.; Grillo, I.; Boue, F. *Biomacromolecules* **2011**, *12*, 859.

(8) Schneider, J. P.; Pochan, D. J.; Ozbas, B.; Rajagopal, K.; Pakstis, L.; Kretsinger, J. *J. Am. Chem. Soc.* **2002**, *124*, 15030.

(9) Lamm, M. S.; Rajagopal, K.; Schneider, J. P.; Pochan, D. J. *J. Am. Chem. Soc.* **2005**, *127*, 16692.

(10) Lamm, M. S.; Sharma, N.; Rajagopal, K.; Beyer, F. L.; Schneider, J. P.; Pochan, D. J. *Advanced Materials* **2008**, *20*, 447.

(11) Lamm, M. S., University of Delaware, 2007.

(12) Branco, M. C.; Pochan, D. J.; Wagner, N. J.; Schneider, J. P. *Biomaterials* **2009**, *30*, 1339.

(13) Branco, M. C.; Nettesheim, F.; Pochan, D. J.; Schneider, J. P.; Wagner, N. J. *Biomacromolecules* **2009**, *10*, 1374.

(14) Branco, M. C.; Pochan, D. J.; Wagner, N. J.; Schneider, J. P. *Biomaterials* **2010**, *31*, 9527.

(15) Altunbas, A.; Lee, S. J.; Rajasekaran, S. A.; Schneider, J. P.; Pochan, D. J. *Biomaterials* **2011**, *32*, 5906.

(16) Haines-Butterick, L.; Rajagopal, K.; Branco, M.; Salick, D.; Rughani, R.; Pilarz, M.; Lamm, M. S.; Pochan, D. J.; Schneider, J. P. *Proceedings of the National Academy of Sciences of the United States of America* **2007**, *104*, 7791.

(17) Yan, C. Q.; Mackay, M. E.; Czymmek, K.; Nagarkar, R. P.; Schneider, J. P.; Pochan, D. J. *Langmuir* **2012**, *28*, 6076.

(18) Kretsinger, J. K.; Pochan, D. J.; Schneider, J. P. *Biopolymers* **2003**, *71*, 319.

(19) Van Vlierberghe, S.; Dubruel, P.; Schacht, E. *Biomacromolecules* **2011**, *12*, 1387.

(20) Sundar, S.; Kundu, J.; Kundu, S. C. *Science and Technology of Advanced Materials* **2010**, *11*.
(21) Grellier, M.; Granja, P. L.; Fricain, J.-C.; Bidarra, S. J.; Renard, M.; Bareille, R.; Bourget, C.; Amedee, J.; Barbosa, M. A. *Biomaterials* **2009**, *30*, 3271.
(22) Hirsh, J.; Warkentin, T. E.; Raschke, R.; Granger, C.; Ohman, E. M.; Dalen, J. E. *Chest* **1998**, *114*, 489S.
(23) Park, P. W.; Reizes, O.; Bernfield, M. *Journal of Biological Chemistry* **2000**, *275*, 29923.
(24) Lever, R.; Page, C. R. *Nature Reviews Drug Discovery* **2002**, *1*, 140.
(25) Saltzman, D. L. a. W. M. *Synthetic DNA Delivery Systems* New York, USA, 2003.
(26) Sundelacruz, S.; Kaplan, D. L. *Seminars in Cell & Developmental Biology* **2009**, *20*, 646.
(27) Martins, A. M.; Alves, C. M.; Kasper, F. K.; Mikos, A. G.; Reis, R. L. *Journal of Materials Chemistry* **2010**, *20*, 1638.
(28) Discher, D. E.; Janmey, P.; Wang, Y. L. *Science* **2005**, *310*, 1139.
(29) Schmidt, J. J.; Rowley, J.; Kong, H. J. *Journal of Biomedical Materials Research Part A* **2008**, *87A*, 1113.
(30) Engler, A. J.; Sen, S.; Sweeney, H. L.; Discher, D. E. *Cell* **2006**, *126*, 677.
(31) Rughani, R. V.; Branco, M. C.; Pochan, D.; Schneider, J. P. *Macromolecules* **2010**, *43*, 7924.
(32) Rajagopal, K.; Ozbas, B.; Pochan, D. J.; Schneider, J. P. *European Biophysics Journal with Biophysics Letters* **2006**, *35*, 162.